UNIVERSIDADE FEDERAL DO RIO GRANDE DO SUL
INSTITUTO DE GEOCIÊNCIAS
PROGRAMA DE PÓS-GRADUAÇÃO EM GEOCIÊNCIAS

LITOESTRATIGRAFIA E GEOQUÍMICA DA PROVINCIA ÍGNEA DO PARANÁ-ETENDEKA E CARACTERIZAÇÃO DOS ASPECTOS PETROFÍSICOS DE SEQUÊNCIAS VULCANO-SEDIMENTARES

LUCAS DE MAGALHÃES MAY ROSSETTI

Porto Alegre, 2018

UNIVERSIDADE FEDERAL DO RIO GRANDE DO SUL
INSTITUTO DE GEOCIÊNCIAS
PROGRAMA DE PÓS-GRADUAÇÃO EM GEOCIÊNCIAS

LITOESTRATIGRAFIA E GEOQUÍMICA DA PROVINCIA ÍGNEA DO PARANÁ-ETENDEKA E CARACTERIZAÇÃO DOS ASPECTOS PETROFÍSICOS DE SEQUÊNCIAS VULCANO-SEDIMENTARES

LUCAS DE MAGALHÃES MAY ROSSETTI

ORIENTADORES

Prof. Dr. Evandro Fernandes de Lima

Prof. Dr. Malcolm J. Hole

BANCA EXAMINADORA

Dra. Isabela de Oliveira Carmo – Centro de Pesquisa Leopoldo - CENPES, Petrobras

Prof. Dr. Valdecir de Assis Janasi – Instituto de Geociências, Universidade de São Paulo

Prof. Dr. Lauro Valentim Stoll Nardi – Instituto de Geociências, Universidade Federal do Rio Grande do Sul

Tese de doutorado apresentada como requisito parcial para obtenção do Título de Doutor em Ciências pela Universidade Federal do Rio Grande do Sul

Porto Alegre, 2018

Agradecimentos

Esta tese de doutorado faz parte do Programa “Sistemas Sedimentares” desenvolvido na Universidade Federal do Rio Grande do Sul e na Universidade de Aberdeen recebeu o apoio financeiro da Shell Brasil e do CNPq com apoio da ANP através da lei de P&D. Aos Programas de Pós-Graduação em Geociências da Universidade Federal do Rio Grande do Sul e ao PGR da University of Aberdeen pelo suporte durante o desenvolvimento desta tese os meus agradecimentos. A Karen, Luciane e Juliana pelo apoio dedicação e coordenação deste projeto.

Agradeço a minha família por ter fornecido a base para que eu pudesse escolher e trilhar meu próprio caminho, e por apoiar as minhas decisões. Agradeço o amor e carinho durante toda essa vida. Vocês são especiais e me fazem bem!

Ao orientador Evandro, por ter aberto para mim as portas do mundo da vulcanologia a muitos anos atrás. Pelo companheirismo e paciência, por todas as viagens de campo, pelos sábios conselhos e elucidações e por todo conhecimento passado. Agradeço ao carinho e amizada que ao longo destes anos só cresceu. Agradeço principalmente por ter me inspirado atravez da tua impolgação e dedicação a pesquisa e ao ensino, com certeza foste e ainda és meu melhor professor. Aguardando para abrir o JURA!

Aos queridos amigos Eduardo e Matheus por todos os bons momentos durante esses anos, por mais que exista uma distancia física a amizade prevalece. Aos queridos amigos que partilharam durante muitos anos a sala e participaram ativamente desta tese auxiliando durante as atividades de campo Fernando, Matheus e Marcos.

Agradeço aos Professores e Amigos Carlos Sommer e Claiton Scherer por todas as conversas e discussões nas quais sempre sai beneficiado pela grandeza de pensamento de vocês. Carlão por todas as discussões vulcânicas e plutonicas espero que muitas ainda estejam por vir! Aos Professores Lauro Nardi e Juliano Kulche pelas suggestões durante a qualificação desta tese.

Agradeço em especial a minha esposa e melhor amiga Thaiza, presente em todos os momentos durante estes anos. Companheira para todas as horas e principal incentivadora do meu trabalho. Obrigado pela compreensão, tua presença ao meu lado durante estes anos tornou esta caminhada muito mais agradável, não teria sido o mesmo sem você perto de mim.

Resumo

A Província Ígnea do Paraná-Etendeka, formou-se no Cretáceo Inferior e está diretamente associada ao rifteamento da porção ocidental do supercontinente Gondwana. Na porção sul do brasil a sequência de lavas é composta por pacotes de lava heterogêneos formados durante estágios evolutivos distintos do magmatismo. A expressão em superfície e composição geoquímica das lavas reflete diretamente a influência dos processos magmáticos profundos que ocorrem durante estes estágios eruptivos. A sequência de lavas pode ser dividida em quarto unidades distintas com base na morfologia e estrutura interna das lavas padrões de empilhamento e posição estratigráfica. A Formação Torres representa os estágios iniciais do magmatismo e é composta por basaltos e andesitos basálticos que ocorrem como derrames lobados pahoehoe e espessas unidades confinadas nos espaços interdune, formadas durante erupções de pequeno volume. Estas lavas interagiram e competiram por espaço com o sistema sedimentar existente e estratigraficamente são formadas por um empilhamento complexo de lobos de lava pontuadas pela ocorrência de unidades sedimentares intercaladas. As lavas da Formação Torres foram formadas por fusões da astenosfera (30 – 40 kbar) e estes magmas assimilaram materiais do manto continental litosférico e evoluíram a partir de processos de cristalização fracionada polibárica, assimilando diferentes proporções de materiais crustais. A Formação Vale do Sol sucede os derrames da Formação Torres e é caracterizada por lavas espessas regionalmente espalhadas de composição andesito basáltica que formam camadas tabulares empilhadas verticalmente. Estas lavas são formadas durante erupções de grande volume e são caracterizadas por topos fragmentados típicos de lavas do tipo rubbly pahoehoe. A evolução dos magmas parentais da Formação Torres para composições evoluídas da formação Vale do Sol é caracterizada por um razeamento das câmaras magmáticas durante a evolução do sistema de alimentação resultando em graus de fracionamento e assimilação avançados em porções meso a supra crustais. Durante a fase principal do magmatismo as rochas ácidas da Formação Palmas foram formadas a partir de condições extremas de AFC. A Formação Palmas recobre as lavas da unidade anterior na área central e leste da província e está colocada diretamente sobre os derrames da Formação Torres no Oeste. A unidade é composta por dacitos e riolítios na forma de domos de lava e derrames tabulares. A Formação Esmeralda ocorre no topo da estratigrafia e caracteriza os estágios de

declínio da atividade magmática e é formada por derrames pahoehoe compostos. Um afinamento litosférico significativo ocorreu concomitante ao magmatismo e os magmas da Formação Esmeralda foram gerados a partir da fusão parcial da astenosfera na zona de estabilidade do espinélio a pressões relativamente mais baixas, sem contribuição de fontes enriquecidas da litosfera. Unidades sedimentares ocorrem ao longo de toda sequencia vulcânica e representam importantes marcadores estratigráficos formados durante períodos de quietude do magmatismo.

Sequencias Vulcano-sedimentares como as do Paraná-Etendeka representam fronteiras para a exploração de hidrocarbonetos em bacias offshore nas margens continentais do Atlântico Norte e Sul. A compreensão entre os processos primários e secundários na geração de porosidade destes sistemas é de suma importância na definição do potencial e propriedades de reservatório para estas rochas. Nas sequencias vulcânicas as características petrofísicas variam de forma cíclica e as porções externas vesiculares são tipicamente mais porosas (> 10%) enquanto as porções maciças de núcleo têm porosidades baixas (< 5%) e consequentemente tem consequentemente, velocidades acústicas 0.5-1.0 kms^{-1} mais rápidas. As maiores porosidades foram encontradas nas brechas de topo de derrames rubbly pahoehoe (c. 28.3%) e topos vesiculares de derrames pahoehoe (c. 26.6%). Permeabilidades são tipicamente baixas para todas as facies vulcânicas analisadas. As rochas sedimentares que ocorrem intercaladas as vulcânicas preservam características primárias com porosidades altas (>15%) e permeabilidades de em média 450mD e representam as melhores fácies de reservatório para a Província do Paraná-Etendeka. As propriedades petrofísicas em lavas são controladas por processos primários (p.e. inflação, degaseificação, fragmentação) e podem ser posteriormente modificadas por processos de alteração hidrotermal e diagênese.

Abstract

The Paraná-Etendeka Large Igneous Province in southern Brazil (the Serra Geral Group) that is associated with the fragmentation of the western Gondwana during the Early Cretaceous is formed of heterogenous packages of lava flows emplaced during different evolutive phases of the province. The surface expression and geochemical compositions of the lava flows reflect deep magmatic process within the evolving province. The lava pile can be subdivided into four main lava formations based on their flow geometry, internal structures and stratigraphic position, and these units reflect the evolutive stages of the magmatism.

Torres Formation that represent the onset of magmatism in the area, is formed of basalt and basaltic andesite lavas, that occur as compound Hawaiian-like pahoehoe lavas, and thick ponded units formed during low volume eruptions. These lavas covered and competed with the existing sedimentary environment, and stratigraphically are characterized by a complex stacking of compound lava lobes punctuated by sedimentary interbeds. Torres Formation lavas have been formed by melting in the asthenosphere (30 and 40 kbar) with contributions of SCLM melts and have fractionated polybaric and assimilated variable amounts of enriched materials in the crust prior eruption. The Vale do Sol Formation succeeded Torres Formation lavas and it is composed of formed thick and widespread basaltic andesites and subordinate basalts lavas with fragmented rubbly tops, formed during high volume eruptions. These lavas are vertically stacked and attribute a classic tabular architecture to the unit. The evolution of Torres parental melts to more evolved compositions of Vale do Sol Formation is marked by the progressive shallowing of magma chambers during plumbing system development, resulting in advanced fractionation and assimilation at mid to upper crustal levels. At the main phase of magmatism silicic rocks of Palmas Formation were formed by extensive AFC of the parental basaltic melts. Palmas Formation overlay the Vale do Sol Formation lavas in the central and eastern outcrop area and rest directly upon Torres Formation lavas in the west. The unit is characterized by dacites and rhyolite lava domes and tabular widespread flow units. Esmeralda Formation is the upper stratigraphic unit and it is formed of basaltic pahoehoe flow fields emplaced during the waning phase of volcanic activity in the area Significant lithospheric thinning occur concomitant to magmatism and Esmeralda Formation lavas were formed by partial melting of asthenosphere at shallow depths in

the spinel stability field of the upper mantle, with no significant contribution from enriched lithospheric melts. Sedimentary interbeds are preserved throughout the whole lava pile and were deposited during quiescence periods of volcanic activity, representing important stratigraphic markers.

Volcano-sedimentary sequences, such as the one in the Paraná-Etendeka Province, represent frontier targets for exploration in hydrocarbon rich basins offshore the South and North Atlantic margins and uunderstanding the interplay between primary and secondary processes on the final petrophysical characteristics of these rocks is key on defining reservoir properties. Petrophysical properties vary cyclic, as a response to the internal structure, within the lavas. Lava upper and lower crust have relatively high porosity (> 10%) and low acoustic velocities, whilst lava flow cores have low porosity (< 5%) velocities typically 0.5-1.0 kms^{-1} higher than lava crust. The highest porosities are found in the upper crust of rubbly pahoehoe (c. 28.3%) and pahoehoe lavas (c. 26.6%) and vesicles account for most of the pore space. Permeability is relatively low in all volcanic facies (< 1 mD). The sedimentary interbeds preserve relatively high porosity (>15%) and permeability (avg. 450 mD) and have the best reservoir quality in the Paraná-Etendeka Province. The petrophysical properties of volcanic rocks are controlled primarily by lava emplacement mechanisms (e.g. inflation, degassing and flow fragmentation), and secondarily by bulk mineral composition and petrophysical properties can be further modified by diagenetic and/or hydrothermal alteration processes

SUMÁRIO

MATERIAL SUPLEMENTAR E ANEXOS

Anexo I - *Lithostratigraphy and volcanology of the Serra Geral Group, Paraná-Etendeka Igneous Province in Southern Brazil: Towards a Formal Stratigraphical Framework*

Anexo II - *Evaluating petrophysical properties of Volcano-sedimentary sequences: A case study in the Paraná-Etendeka Large Igneous Province*

Anexo III - *Geochemical stratigraphy and Magmatic evolution of the Paraná-Etendeka Large Igneous Province: Insights from shallow crystallization magmatic processes and magma genesis*

Anexo IV – Apresentações de Trabalhos resumos publicados em anais de eventos

Anexo V - Análises petrofísicas das rochas vulcânicas e sedimentares da Província do Paraná-Etendeka

Anexo VI – Litogeoquímica e Isótopos de Sr-Nd-Pb

CAPÍTULO 1 - INTRODUÇÃO

Províncias Basálticas Continentais (PBCs) representam eventos geológicos de magnitudes extraordinárias que produziram as maiores erupções conhecidas na história geológica da Terra (magnitudes >M8; Bryan *et al*. 2011), formando campos de lavas que excedem 0,1 Mkm^2 em cobertura areal e produzem volumes de magmas superiores a 0,1 Mkm^3 (Bryan e Ernest, 2008). O magmatismo de PBC, em muitos casos, antecede a fragmentação e rifteamento de áreas continentais (Courtillot *et al*., 1999) e estão associadas a importantes anomalias térmicas no manto superior capazes de produzirem quantidades imensas de magma de afinidade dominantemente toleítica (Ernst and Buchan, 2003). A estratigrafia e a evolução de Províncias Basálticas Continentais fornecem importantes informações sobre a dinâmica e os estilos eruptivos atuantes durante a construção destes imensos volumes de lavas, e do impacto e interação destes eventos magmáticos com o paleoambiente.

O presente trabalho tem como objetivo principal uma proposta formal de estratigrafia para as lavas da porção sul da Bacia do Paraná no Brasil, e uma avaliação das características geoquímicas dentro deste novo arcabouço estratigráfico. Esta integração busca compreender a variação temporal do magmatismo e os principais processos petrológicos atuantes durante a construção da sequência vulcânica. Adicionalmente, propõe-se a definição dos padrões petrofísicos, incluindo porosidade e permeabilidade, velocidades ultrassônicas (ondas p e s) e densidades das principais litofacies que compõem a sequência vulcânica. A integração destas informações permitirá a construção de modelos estratigráficos que poderão ser utilizados como comparativos para áreas *offshore,* onde as informações são obtidas de maneira indireta por meio de métodos geofísicos e dados de poço.

1.1 JUSTIFICATIVA

A Província Ígnea do Paraná-Etendeka (PIPE) representa um evento magmático do Cretáceo Inferior que precedeu a fragmentação da porção sul do Supercontinente Gondwana e a abertura do oceano Atlântico Sul. Quando

comparada com outras províncias similares, como o Deccan, o Columbia River, a Província Ígnea do Atlântico Norte ou até mesmo a sua margem conjugada no leste africano (A província do Etendeka) o arcabouço estratigráfico da PIPE no Brasil é pouco detalhada. Este fato dificulta principalmente a correlação estratigráfica e o entendimento da dinâmica atuante durante o vulcanismo, tanto na geração de magmas como na colocação dos mesmos em superfície. A carência de uma estratigrafia apropriada, que possa ser correlacionada e sirva como um guia temporal (sucessão de derrames no tempo/estratigrafia) para discussões geoquímicas, geocronológicas, e paleomagnéticas, é o principal motivador do presente trabalho.

1.2 OBJETIVOS

Objetiva-se identificar os tipos de lavas, a estratigrafia e a arquitetura de fácies dos depósitos vulcânicos na província Ígnea do Paraná-Etendeka na porção sul do Brasil. Em um arcabouço estratigráfico detalhado definir os padrões petrofísicos das diferentes litofácies vulcânicas e das rochas sedimentares associadas, assim como os padrões petrográficos e geoquímicos de cada unidade estratigráfica. A integração destas informações permite a construção de modelos estratigráficos que poderão ser utilizados como comparativos para áreas de magmatismo *offshore* (e.g. Bacias da margem passiva brasileira) onde as informações são limitadas, em geral, obtidas de maneira indireta por meio de métodos geofísicos e dados de poço.

1.2.1 Objetivos Específicos

- Definição de um arcabouço litoestratigráfico para a porção sul da Província Paraná-Etendeka, na calha de Torres, baseado em características vulcanológicas petrográficas e padrões de empilhamento das lavas;
- Identificação de aspectos petrofísicos das rochas vulcânicas da Província Paraná-Etendeka e a variação destas propriedades em escala regional;

- Construção de modelos petrofísicos em escala de afloramento para avaliar heterogeneidades relacionadas às variações laterais e verticais de fácies;
- Compreensão da gênese e evolução das diferentes unidades do ponto de vista geoquímico;

1.3 HIPÓTESE

A Província Ígnea do Paraná-Etendeka foi construída por diferentes episódios vulcânicos que envolveram estilos eruptivos e volumes de magma distintos, e representaram diferentes momentos da geração/evolução de magmas e sistemas de alimentação (básico-ácido) durante um ciclo evolutivo caracterizado por uma fase inicial, um clímax, e um estágio de declínio da atividade vulcânica.

1.4 ESTRUTURA DA TESE

A presente tese está inserida no Programa de dupla diplomação de Doutorado e cotutela firmado entre a Universidade Federal do Rio Grande do Sul (UFRGS) - Brasil, e a *University of Aberdeen* (UoA) – Escócia, Reino Unido. No referido programa o aluno proponente apresenta dois volumes distintos a serem defendidos nas respectivas universidades. Este volume é apresentado como requisito para a obtenção do título de doutor perante ao Programa de Pós-Graduação em Geociências da Universidade Federal do Rio Grande do Sul e difere em estrutura do volume apresentado a *University of Aberdeen*. As principais distinções, além do idioma da tese, são relacionadas a estrutura. Enquanto a tese na universidade estrangeira segue um formato clássico, composto por capítulos contínuos, a presente tese é estruturada na forma de artigos científicos.

O capítulo inicial apresenta os objetivos e hipóteses que nortearam esta pesquisa e é seguido da apresentação dos métodos utilizados durante as investigações aqui apresentadas (capítulo 2). No capítulo 3 são apresentados o contexto geológico regional da Província Ígnea do Paraná-Etendeka e os conceitos básicos associados ao magmatismo das grandes províncias ígneas.

São apresentadas também as características principais e a estratigrafia das Províncias do *Columbia River* e do Atlântico Norte que foram visitadas durante este projeto de doutorado e servem como análogos no estudo das rochas vulcânicas do Paraná-Etendeka.

Os capítulos 4, 5 e 6 apresentam uma breve introdução aos assuntos abordados nos artigos científicos correspondentes, que são apresentados como anexos ao final deste volume.

O capítulo 4 apresenta os principais resultados do estudo dos aspectos estratigráficos e vulcanológicos da porção sul da Província Ígnea do Paraná-Etendeka e resultou na formalização de uma proposta litoestratigráfica para divisão das diferentes unidades vulcânicas que compõe a área. O artigo intitulado "*Lithostratigraphy and volcanology of the Serra Geral Group, Paraná-Etendeka Igneous Province in Southern Brazil: Towards a Formal Stratigraphical Framework*" publicado no volume especial dedicado ao magmatismo da província do Paraná-Etendeka do *Journal of Volcanology and Geothermal Research*, é apresentado na forma de publicação no Anexo I.

O capítulo 5 introduz brevemente os resultados obtidos durante o estudo das características petrofísicas das rochas vulcânicas e sedimentares associadas que ocorrem na área de estudo. Os resultados da pesquisa são apresentados no artigo "*Evaluating petrophysical properties of Volcano-sedimentary sequences: A case study in the Paraná-Etendeka Large Igneous Province*" que submetido para publicação na revista Marine and Petroleum Geology, e encontra-se atualmente em revisão. Este é apresentado na forma de manuscrito, acrescido das figuras no Anexo II.

O capítulo 6 apresenta brevemente os aspectos gerais da geoquímica das rochas que compõe a porção sul do Paraná-Etendeka e os resultados e modelos geoquímicos propostos são apresentados no Anexo III no qual consta o artigo científico submetido ao Gondwana Research intitulado "*Geochemical stratigraphy and Magmatic evolution of the Paraná-Etendeka Large Igneous Province: Insights from shallow crystallization magmatic processes and magma genesis".*

O capítulo 7 apresenta um sumário e síntese dos principais resultados alcançados durante este projeto de doutorado.

CAPÍTULO 2 - METODOLOGIA

Nesta capítulo são descritos de forma sucinta os métodos utilizados até aqui no desenvolvimento da tese e na obtenção de amostras em campo e dados de laboratório.

2.1 REVISÃO BIBLIOGRÁFICA

A etapa de revisão bibliográfica objetiva a organização e definição dos conceitos clássicos definidos para as Províncias Basálticas Continentais, e a construção de um estado da arte para este contexto geológico. A revisão de conceitos fundamentais da vulcanologia física aplicados na definição dos diferentes tipos de derrames, e da utilização destes para a definição da arquitetura de fácies.

2.2 ATIVIDADES DE CAMPO

Ao longo do doutorado foram realizadas diversas etapas de campo na porção sul da PIPE, no estado do Rio Grande do Sul, uma etapa de campo no oeste dos Estados Unidos na Província Basáltica do Columbia River (PBCR) (novembro de 2016), e quatro visitas aos afloramentos da Província Ígnea do Atlântico Norte (NAIP) (Maio e Setembro de 2015; Julho e Setembro de 2016). O foco principal do trabalho foi o detalhamento do Grupo Serra Geral no estado do Rio Grande do Sul. Durante as etapas de campo foram descritas em afloramento as estruturas vulcânicas, visando a classificação dos diferentes tipos morfológicos de derrames e o levantamento de seções colunares individuais e compostas de perfis aflorantes, visando à identificação das diferentes litofácies, associações de fácies, arquitetura das rochas vulcânicas e superfícies limítrofes entre unidades. Nestas etapas também foram coletadas amostras de rocha para estudos petrográficos, geoquímicos e petrofísicos.

As atividades de campo na NAIP e PBCR tiveram como objetivo principal a comparação entre os depósitos formados nestas províncias e os da PIPE. O excelente grau de exposição permitiu o reconhecimento de estruturas vulcânicas

primárias e uma visão geral das unidades vulcânicas formadas durante os diferentes estágios de evolução da NAIP e da PBCR.

2.3 AMOSTRAGEM

Durante duas etapas de campo foram coletadas amostras de testemunhos de rocha fresca utilizando uma perfuratriz rotativa. A perfuratriz permite a aquisição de testemunhos de rocha cilíndricos com até 1” (polegada) de diâmetro e 8” de comprimento. Os testemunhos foram utilizados para a confecção de lâminas delgadas e para a realização dos ensaios petrofísicos. Na segunda etapa de campo optou-se pela coleta de amostras de blocos de rocha orientados, perfurados posteriormente no laboratório de preparação de amostras da Universidade de Aberdeen.

2.4 PETROGRAFIA

A partir das amostras e testemunhos coletados nas etapas de campo, um total de 100 amostras foram selecionadas para a confecção de lâminas petrográficas impregnadas com resina de azul (Fig. 1). Esta resina destaca os padrões de microvesiculações e fraturas. O estudo petrográfico destas lâminas permite a caracterização das microtexturas e estruturas das rochas, além da distinção mineralógica. Esta etapa contempla a contagem modal e caracterização dos padrões de vesiculação e porosidade (primária e secundária). A Investigação petrográfica das unidades efusivas e vulcanossedimentares permite a distinção entre diferentes tipos de porosidade e fornece informações importantes sobre a gênese dos poros.

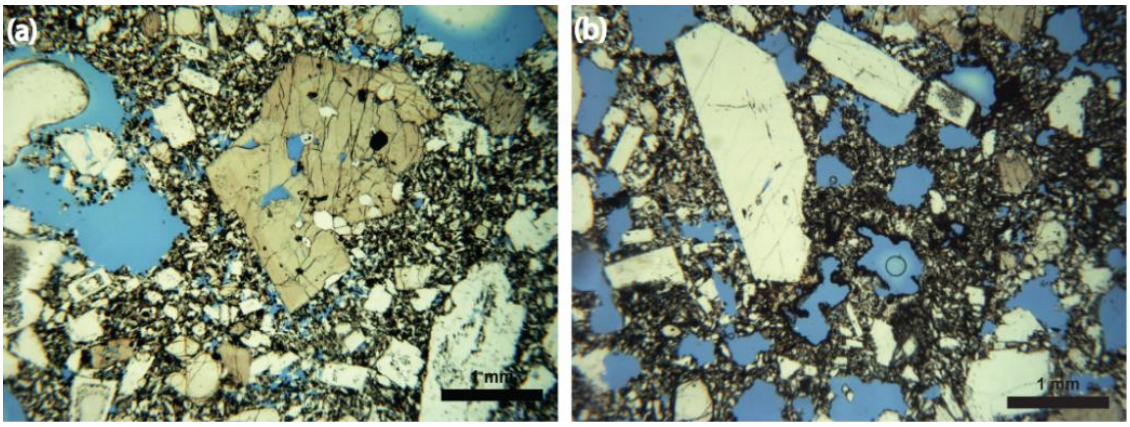

Figura 1 - Fotomicrografias em lâminas impregnadas, porosidade em azul. a) basalto porfirítico, com destaque para a porosidade intracristalina e em vesícula realçado pela resina; b) porosidade primária em vesiculas irregulares (azul) em basalto vesicular.

2.5 GEOQUÍMICA DE ROCHA TOTAL

Os dados de geoquímica de rocha total foram utilizados como uma ferramenta auxiliar na compreensão das variações composicionais identificadas nas sequências vulcânicas e durante a evolução dos episódios vulcânicos. As análises químicas expressam as concentrações de elementos maiores, menores e terras raras das rochas e foram analisadas até o momento 167 amostras representativas das diferentes unidades vulcânicas. Os critérios de seleção das amostras levaram em conta a distribuição estratigráfica e geográfica das amostras, visando uma representatividade das diferentes unidades vulcânicas e critérios petrográficos como grau de alteração e composição mineralógica.

As análises foram realizadas no ACME ANALYTICAL LABORATORIES LTD., Vancouver, Canadá. A concentração de elementos maiores e elementos traço foram medidos por ICP-AES(*Inductively Coupled Plasma atomic emission spectroscopy*) e os elementos terras raras e elementos refratários por ICP-MS (*Inductively Coupled Plasma Mass Spectrometer*). Em ambas rotinas de análise foram analisados 0,2g de pó de rocha. Elementos maiores e menores são expressos na forma de oxido e o limite de detecção foi de 0.01%, com exceção da abundância de Fe_2O_3, na qual os limites de detecção foram de 0,04%. Para elementos traço e terras raras, expressos em concentração em peso na forma de partes por milhão (ppm) os limites de detecção foram de 1ppm. Estas técnicas são baseada na utilização da indução de plasma acoplado como forma de produção de íons (ionização) e um espectrômetro de massa para detecção e

separação de íons. Com isso o espectrômetro de massa, ICP-MS, é capaz de analisar os componentes das amostras ionizadas por meio da detecção e separação dos componentes através de suas razões massa *versus* carga (m/z).

2.6 ENSAIOS PETROFÍSICOS

Os estudos petrofísicos como os de porosidade e permeabilidade foram baseados em um conjunto de ensaios e técnicas analíticas tais como: estimativa de poros em lâmina petrográfica impregnada; ensaios de porosimetria por injeção de hélio; ensaios de permeametria; e ensaios de velocidades ultrassônicas. Foram analisadas 245 amostras de rochas vulcânicas, e sedimentares intercaladas as unidades vulcânicas. O banco de amostras incluiu 162 amostras da PIPE, 45 amostras dos basaltos do *Columbia River* e 38 amostras da Ilha de São Jorge (Açores Central), sendo estes dois últimos grupos de amostras utilizados de forma comparativa.

As medidas de porosidade e permeabilidade foram realizadas utilizando o equipamento *Jones Porosimeter/Permeameter* (FRANK JONES AND ASSOCIATES, INC.). Este equipamento combina o porosímetro de *Coberly-Stevens Boyle's Law* com um permeâmetro a gás, situado no mesmo painel. A porosidade foi obtida pelo método de injeção de He (hélio), o qual fornece a porosidade efetiva, ou seja, o volume de poros da amostra que estão interconectados. A medida se dá pela admissão de gás (He) a uma pressão de 100 Psig em uma célula de referência (volume conhecido). Utilizando um manômetro eletrônico de alta precisão, mede-se a pressão inicial, a seguir libera-se o gás para a célula contendo a amostra, e lendo-se a menor pressão resultante. A razão entre a pressão inicial e a pressão final permite calcular o volume de grãos da amostra usando uma expressão derivada da Lei de Boyle. O volume de poros é obtido pela subtração do volume de grãos do volume total calculado da amostra (Fig. 2).

Para a obtenção de dados de permeabilidade foram realizados ensaios de permeametria. A medida de permeabilidade foi obtida a partir de um minipermeâmetro a gás. O permeâmetro usa a pressão diferencial de fluxo de ar por uma amostra, a uma pressão de até 60 Psig para medir as taxas de fluxo (*flow rate*). O equipamento estima taxas de fluxo de 0.00001ml/s até 3.5 ml/s,

equivalente a permeabilidades de 0.1 microdarcys a 2500 millidarcys. A permeabilidade é calculada a partir dos parâmetros estipulados por Goggin *et al*. (1988).

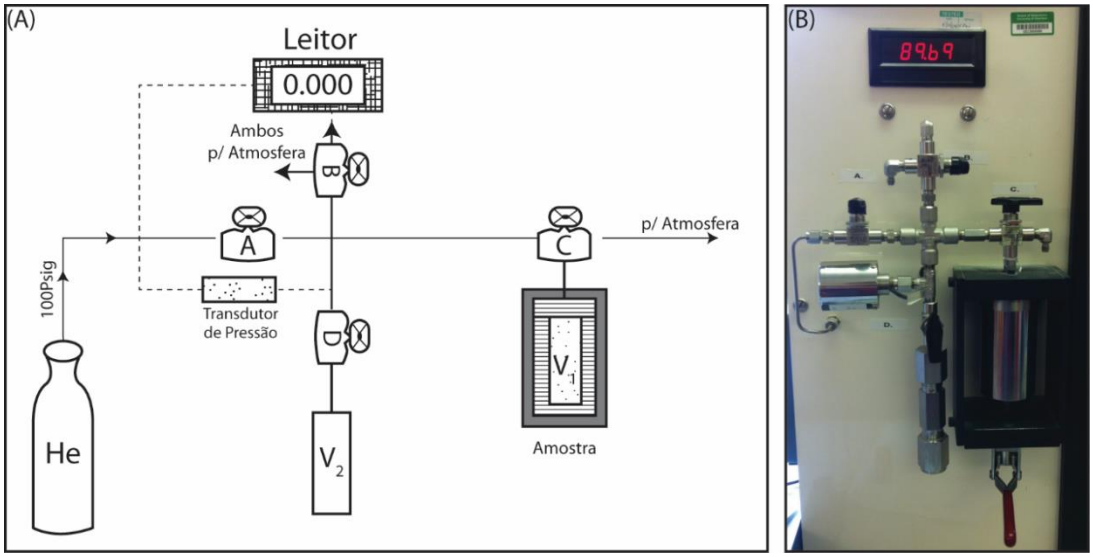

Figura 2 - A) Fluxograma representativo do processo de análise no porosímetro. B) fotografia do porosímetro Jones utilizado durante as análises.

Foram obtidos dados velocidades de onda P e S. A técnica fundamenta-se no princípio de propagação de ondas sísmicas, onde as ondas P, primárias, são compressivas e propagam-se em meios sólidos e líquidos. Diferentemente, as ondas S, também chamadas de secundárias ou cisalhantes, se propagam ao longo do eixo da onda de forma transversal, propagam-se apenas em meios sólidos com velocidades relativamente menores quando comparadas as das ondas P. Estes dados foram obtidos pela técnica de transmissão de pulso (*Pulse Trasmition Tecnic*). As medidas foram obtidas em amostras secas e em condições de pressão e temperatura ambientes. As velocidades foram medidas por um pulsor/receptor ultrassônico em modo de transmissão (Fig. 4), utilizando dois transmissores e receptores separados, um em cada extremo da amostra. O pulsor/receptor é conectado a um osciloscópio digital para a visualização da forma da onda. As velocidades foram medidas com voltagem de 900 V e ganho de 60dB. Para obtenção de um sinal claro os lados da amostra devem ser retos e paralelos entre si.

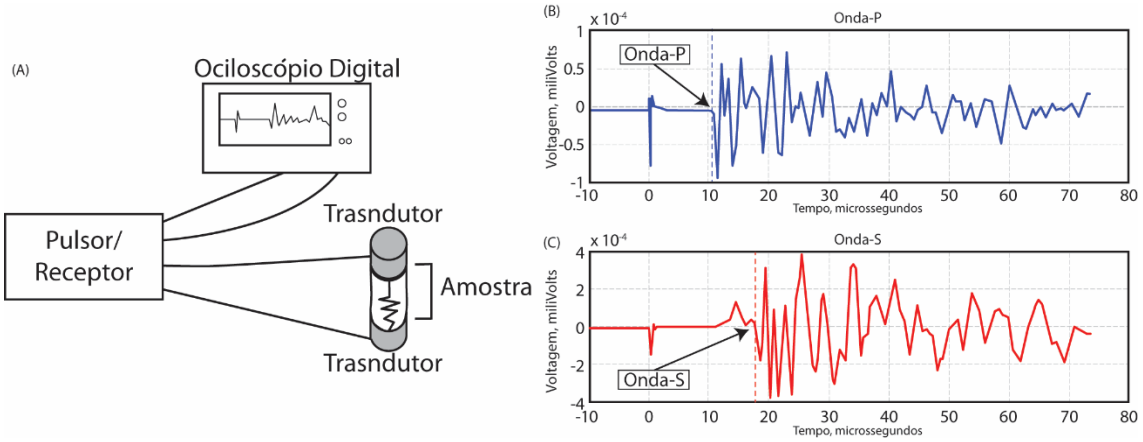

Figura 3 - Fluxograma simplificado de aquisição de velocidades ultrassônicas utilizadas. A) O pulsor gera um sinal para um dos transdutores, o qual é transmitido através da amostra de rocha e detectado após o tempo de atraso medido (delay time) no outro transdutor. B) Exemplo da morfologia da onda P no osciloscópio digital (após linha azul tracejada), o sinal gerado no pulsor está plotado no tempo 0. C) Exemplo da morfologia da onda S captada no osciloscópio digital (após linha tracejada vermelha), o sinal gerado no pulsor está plotado no tempo 0, primeira quebra (~tempo 15 mili segundos) detecção da onda P, segunda quebra (~19mili segundos) detecção da onda S.

CAPÍTULO 3 - CONTEXTO GEOLÓGICO

Este capítulo apresenta de forma sintética a revisão dos principais conceitos associados ao magmatismo em Províncias Basálticas Continentais e a estruturação física destes imensos campos de derrames, utilizados como base das discussões propostas durante a tese de doutorado.

3.1 AS GRANDES PROVÍNCIAS ÍGNEAS - *"LARGE IGNEOUS PROVINCES"*

Grandes Províncias Ígneas (*Large Igneous Provinces – LIP's*) foram originalmente definidas como "qualquer atividade magmática anômala, onde grandes volumes de magmas, dominantemente basálticos, foram produzidos por mecanismos diferentes daquele responsável pela geração e espalhamento do assoalho oceânico" (Coffin and Eldholm, 1994). Esta atividade magmática é responsável pela acreção de grandes quantidades de material rochoso às porções intraplaca da crosta continental e oceânica e é comumente associada à presença de anomalias térmicas nas porções superiores do manto. Grandes Províncias Ígneas ocorrem em todos os continentes e oceanos, e estão presentes no registro geológico desde o arqueano até o cenozoico. *LIPs* são formadas por grandes volumes de lavas e intrusões associadas que caracterizam as maiores erupções da história geológica da Terra (Bryan *et al.* 2010; Bryan & Ferrari 2013). No entanto, a maior parte dos dados relacionados a estes ambientes está associada ao estudo de províncias mesozoicas e cenozoicas (Fig. 1) onde o volume e a extensão areal são próximos dos originais e as estruturas primárias estão preservadas. Províncias proterozóicas e arqueanas são muitas vezes identificadas por restos de basaltos continentais ou enxames de diques associados ao sistema de alimentação destas erupções. A intensa erosão modifica as características originais destas LIPs, que são referidas como "remanescentes" ou "fragmentos" de Grandes Províncias Ígneas (Ernst *et al*., 2005).

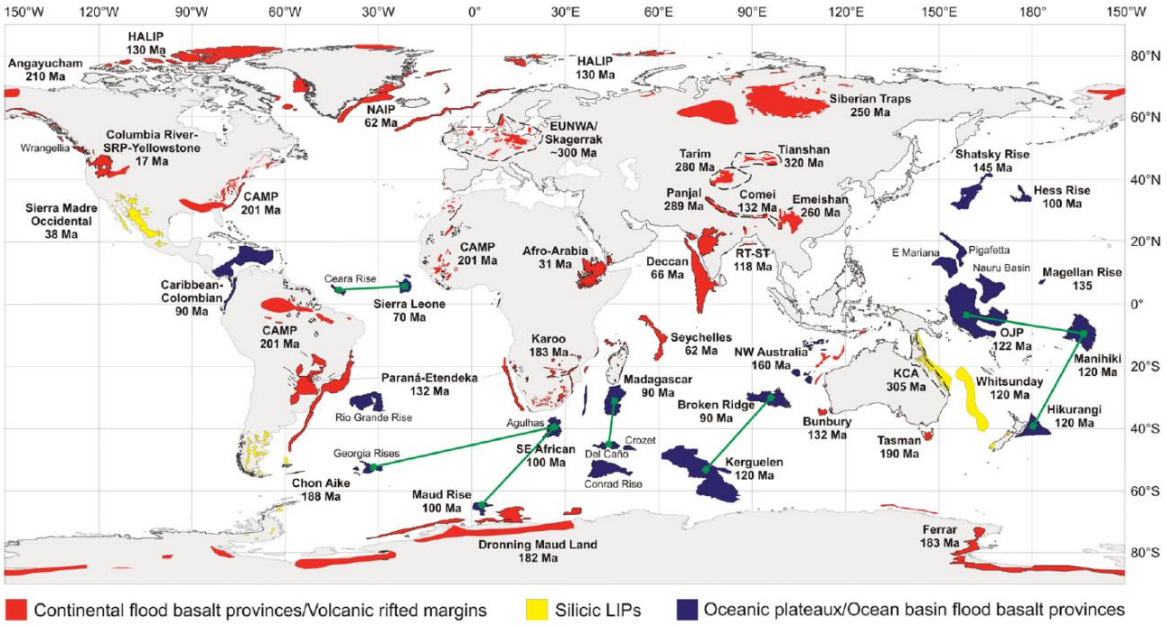

Figura 4 - Distribuição global de Grandes Províncias Ígneas com idades inferiores a 320 Ma. Incluindo idades do inicio da atividade principal do magmatismo. Abreveações: CAMP-Central Atlantic magmatic province; EUNWA-European, northwest Africa; ALIP-High Arctic large igneous province; NAIP-North Atlantic igneous province; OJP-Ontong Java Plateau; RT-ST-Rajmahal Traps–Sylhet Traps; SRP—Snake River Plain; KCA-Kennedy-Connors-Auburn (modificado de Bryan and Ernst, 2008).

Trabalhos recentes consideram que a definição original de *LIPs* de Coffin and Eldholm (1994) é muito abrangente, e recentemente novas definições foram propostas por diversos autores (Seth, 2007; Bryan & Ernst, 2008; Cañón-Tapia, 2010; Bryan & Ferrari, 2013). Bryan and Ernest (2008) sugerem que LIPs sejam definidas como "*províncias magmáticas dominantemente máficas (+ultramáficas) intraplaca com extensão areal >0,1 Mkm^2, e volumes >0,1 Mkm^3, onde a maior parte do volume de magma foi produzido durante pulsos magmáticos de curta duração (1-5 Ma) e o evento como um todo não excedeu um tempo máximo de ~50 Ma*". *LIP's* podem ser agrupadas em LIPs continentais e LIPs oceânicas (Coffin e Eldholm, 1994). Bryan e Ernest sugerem também uma subdivisão destas duas grandes categorias, na qual: 1) *LIP's* oceânicas, possam ser divididas em platôs oceânicos e basaltos de fundo oceânico; 2) *LIP's* continentais, possam ser subdivididas em províncias basálticas continentais, margens vulcânicas rifteadas, *greenstone belts* arqueanos, enxames de dikes gigantes e complexos intrusivos máfico- ultramáficos, e grandes províncias ígneas ácidas (ou silicosas – do inglês *Silicic LIPs*) (Fig. 2).

Esta tese tem como foco principal as Províncias Basálticas Continentais/ Margens vulcânicas Rifteadas, em especial a Província Ígnea do Paraná-Etendeka, que dentro deste contexto, representa um episódio magmático do Cretáceo Inferior que antecedeu a fragmentação da porção sul do supercontinente Gondwana formando uma Província basáltica continental com volumes expressivos de produtos ácidos associados ao magmatismo, e que evoluiu posteriormente com a abertura do Oceano Atlântico Sul para uma margem rifteada.

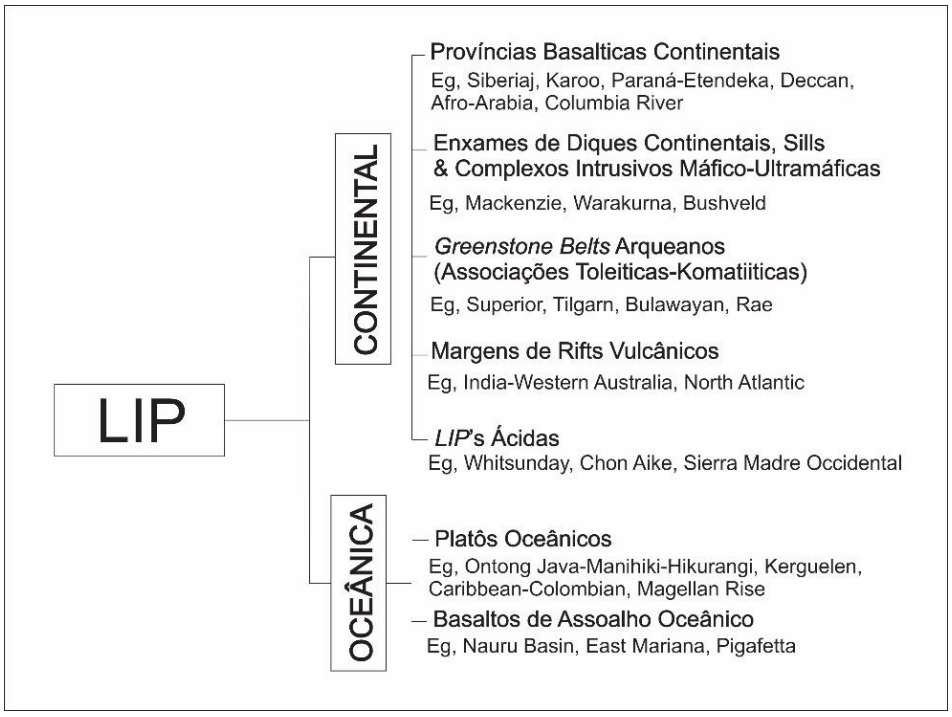

Figura 5 – Classificação de Grandes Províncias Ígneas, modificado de Bryan e Ernst (2008)

3.2 PROVÍNCIAS BASÁLTICAS CONTINENTAIS

Províncias Basálticas Continentais (PBCs), em especial PBCs Mesozoicas e Cenozoicas, são a principal fonte de informações geológicas no estudo de Grandes Províncias Ígneas permitindo a observação direta dos aspectos vulcanológicos e arquiteturais destes imensos campos de lavas. As PBCs estão geralmente associadas com anomalias termais localizadas no manto superior (Ernst and Buchan, 2003). Estas são capazes de produzir um extraordinário grau de fusão (pluma?), que uma vez iniciado é fixado em um período de tempo, independentemente dos processos tectônicos ou outros movimentos que possam estar operando dentro da litosfera (Jerram and Widdowson, 2005). Estas províncias

estão comumente associadas à processos de extensão e afinamento crustal, e em muitos casos apresentam uma correlação direta com a fragmentação de supercontinentes onde o magmatismo antecede em alguns milhões de anos a fase principal de rifteamento e a formação de nova crosta oceânica, evoluindo para Margens Vulcânicas Rifteadas (Bryan and Ernst, 2008; Courtillot et al., 1999).

Províncias basálticas continentais são caracterizadas principalmente por um imenso volume de lavas colocado sobre crosta continental em um intervalo relativamente curto de tempo (1-10 Ma) (Bryan and Ernst, 2008). O magmatismo em PBC tem afinidade dominantemente toleítica e composições basálticas, com a ocorrência de composições ácidas e/ou alcalinas em algumas províncias (e.g. riolitos e dacitos do Paraná-Etendeka - Bellieni *et al.* 1984; Milner *et al.* 1992).

3.3 ANATOMIA DE PROVÍNCIAS BASÁLTICAS CONTINENTAIS

A estruturação interna dos depósitos gerados durante o magmatismo em PBCs é fundamental na construção de um arcabouço estratigráfico e evolutivo para estes megaeventos. Variações nos estilos eruptivos, volumes das erupções, padrões de empilhamento e assinaturas geoquímicas são classicamente associados a diferentes estágios evolutivos destas províncias. Para a definição da arquitetura e anatomia das PBCs é importante entender a distribuição espacial dos depósitos vulcânicos e a organização interna dos pacotes de lavas que formam o edifício vulcânico. Nesta seção serão definidas a terminologia utilizada na descrição das lavas em PBCs, as ferramentas utilizadas na identificação de um evento eruptivo e a organização interna dos depósitos vulcânicos em PBCs.

3.3.1 Terminologia Utilizada no Estudo de Províncias Basálticas Continentais

Self *et al.* (1998) propuseram a uniformização de uma terminologia para o estudo de PBCs com base na hierarquia e escala dos produtos vulcânicos formados durante uma erupção ou um evento eruptivo continuo, ou seja, mais de uma erupção ocorrendo ao longo de um intervalo de tempo, associadas a uma mesma fonte de magma ou uma mesma fissura. Foram definidos os seguintes termos descritivos: 1) *Campo de derrames (lava flow fields)* são os produtos agregados de

um evento eruptivo e são constituídos por um ou mais derrames. Campos de derrames são identificados e distinguidos com base na composição química das lavas, e/ou pela presença de paleossolos ou depósitos sedimentares e vulcanoclásticos que indiquem uma quebra na atividade vulcânica (Fig. 3A); 2) *Derrame (lava flow)* é o produto de uma única e continua efusão, tipicamente de curta duração e com características homogênias (químicas e petrográficas), e são os principais constituintes dos campos de derrames; 3) *Lobos* são corpos de lava com geometrias lobulares, com espessuras variadas, (comumente entre 0,5 a 5 m – Fig. 3B) delimitados por margens resfriadas e são identificados com base na sua estrutura interna (crosta basal, núcleo, crosta superior). Lobos espessos (dezenas de metros) e extensos (quilômetros) com geometria tabular são denominados *sheet lobes* (derrames em lençol). Estruturas lobulares menores (<0,5 m) associadas a porções distais dos campos de lava são chamados de *dedos* (*lava toes)* (Fig. 3C).

3.3.2 Erupções em Províncias Basálticas Continentais

Um dos maiores desafios no estudo de PBCs é definir e reconhecer quais são os produtos de uma única erupção e correlacioná-los lateralmente. Dada a grande extensão areal destas províncias e o fato de que muitas vezes a continuidade lateral é comprometida pela falta de exposição (cobertura vegetal), erosão, soterramento/ soerguimento, ou falhamentos tectônicos posteriores a formação dos campos de derrames. A sobreposição estratigráfica; presença de marcadores estratigráficos como paleossolos e níveis de rochas sedimentares e/ou vulcanoclásticas; as características petrográficas e geoquímicas; e características paleomagnéticas são ferramentas fundamentais no reconhecimento e correlação de erupções individuais (Bryan *et al.* 2010). O reconhecimento destes produtos é fundamental para a construção da estratigrafia em PBCs e a combinação de diferentes métodos é demonstradamente a forma mais eficiente de correlacionar unidades dentro de PBCs (Jay *et al*., 2009) e foi amplamente aplicada na construção da estratigrafia dos basaltos do Columbia River (Tolan *et al.*, 1989; Reidel *et al.*, 1989, 2013, e outras referências).

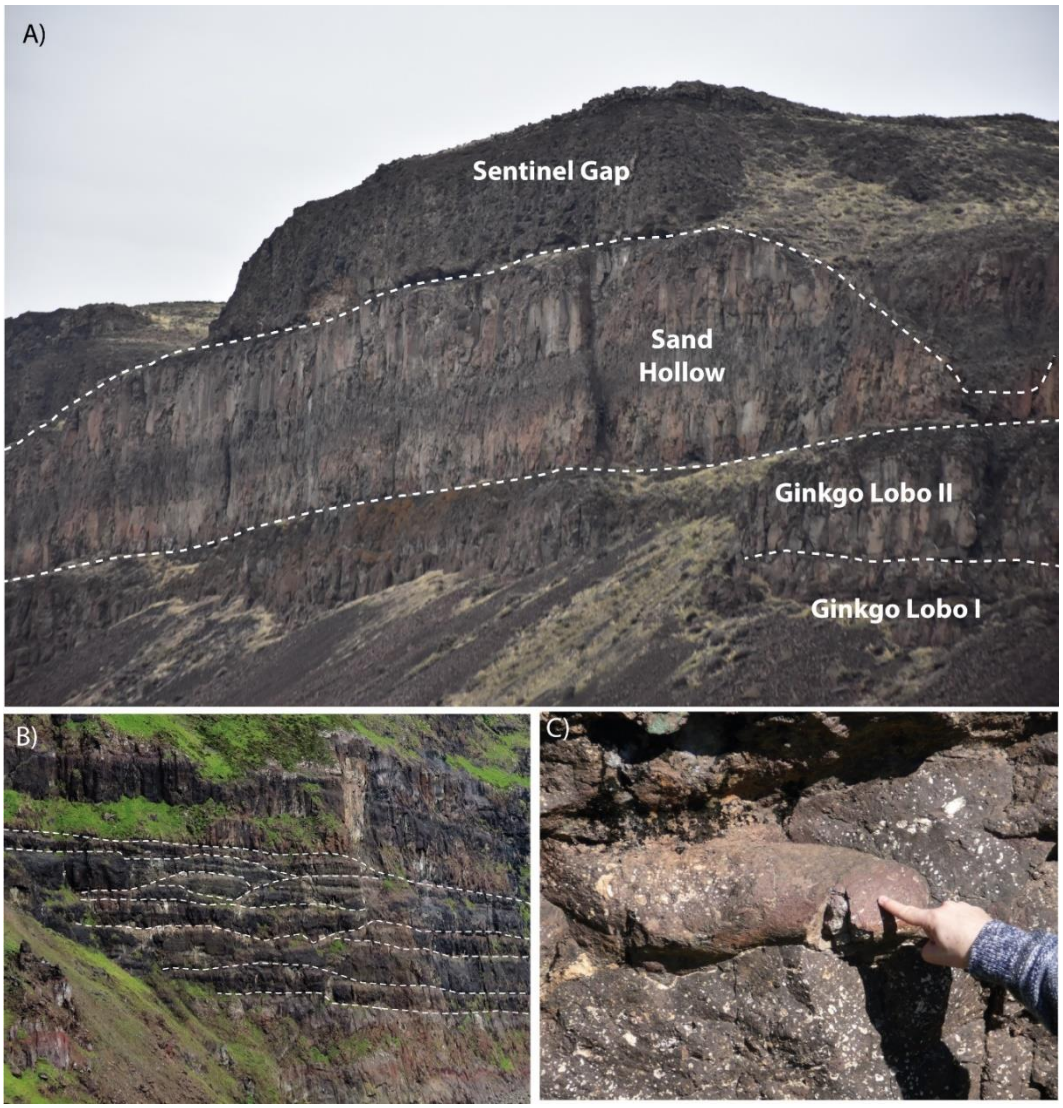

Figura 6 – Hierarquia de unidades vulcânicas e exemplos. A) campos de derrames (Sand Hollow, Sentinel Gap e Ginko) do Membro Frenchmann Springs no Columbia River, escala vertical ~50m. B) Lobos de lava em unidade composta da Província do Atlântico Norte em Skye, escala vertical ~30m. C) dedo de lava no Grupo Serra Geral do Paraná-Etendeka na região de Lajeado, no sul do Brasil.

3.3.2 Erupções em Províncias Basálticas Continentais

Um dos maiores desafios no estudo de PBCs é definir e reconhecer quais são os produtos de uma única erupção e correlacioná-los lateralmente. Dada a grande extensão areal destas províncias e o fato de que muitas vezes a continuidade lateral é comprometida pela falta de exposição (cobertura vegetal), erosão, soterramento/ soerguimento, ou falhamentos tectônicos posteriores a formação dos campos de derrames. A sobreposição estratigráfica; presença de marcadores estratigráficos como paleossolos e níveis de rochas sedimentares e/ou

vulcanoclásticas; as características petrográficas e geoquímicas; e características paleomagnéticas são ferramentas fundamentais no reconhecimento e correlação de erupções individuais (Bryan *et al.* 2010). O reconhecimento destes produtos é fundamental para a construção da estratigrafia em PBCs e a combinação de diferentes métodos é demonstradamente a forma mais eficiente de correlacionar unidades dentro de PBCs (Jay *et al*., 2009) e foi amplamente aplicada na construção da estratigrafia dos basaltos do Columbia River (Tolan *et al.*, 1989; Reidel *et al.*, 1989, 2013, e outras referências).

Erupções Basálticas - Derrames basálticos subaéreos são classicamente classificados de acordo com suas feições de superfície em *pahoehoe* e ***a'ā*** (Macdonald, 1953). Derrames *pahoehoe* são caracterizados por superfícies lisas, onduladas ou em corda. Estes são formados pela colocação de uma lava pouco espessa na forma de lobo que imediatamente resfria a porção externa, isolando o núcleo ainda quente da lava e evitando a perda rápida de calor. A contínua alimentação interna provoca o intumescimento da crosta externa da lava, inflação e crescimento endógeno, que aliada a ruptura da frente resfriada promove o avanço na forma de um novo lobo (Hon *et al*., 1994). Derrames ***a'ā*** são caracterizados por uma carapaça fragmentada e um núcleo coerente. A porção externa da lava rompe e fragmenta continuamente devido à grande deformação do fluxo, causada em geral pela declividade do terreno, ou por altas taxas de efusão. Os fragmentos são continuamente transportados na frente do derrames para as porções basais em um movimento análogo ao de uma esteira (Pinkerton and Sparks, 1976; Rowland and Walker, 1990).

Províncias Basálticas Continentais são constituídas principalmente por extensos campos de derrames *pahoehoe* e *rubbly pahoehoe* (um derrame *pahoehoe* com a superfície fragmentada), que tipicamente excedem volumes de 1000 km³ (Reidel *et al*., 2013; Tolan *et al*., 1989), e podem se estender por distâncias de até 1000 km (Self *et al*., 2008). Estes campos de derrames são formados durante eventos eruptivos contínuos, que podem durar de alguns anos a algumas décadas, nos quais as lavas são alimentadas ao longo de extensos sistemas fissurais, com a atividade vulcânica migrando em diferentes segmentos de fissuras ao longo do tempo, o que promove, assim, o crescimento e migração lateral destes campos de derrames, conforme figura 4 (Swanson 1979; Self et al.

1996; Self et al. 1997; Thordarson e Self 1998). As taxas de erupção destas lavas seriam similares as maiores taxas registradas por erupções históricas como a de Laki na Islândia (4000 m³s-1 - Thordarson e Self, 1993). Os principais constituintes destes campos de derrames são derrames tabulares (sheet flows), com espessuras de em média 20-30 m, equivalentes aos derrames simples (sensu Walker, 1971) e representam a maior parte do volume produzido durante uma única erupção. Internamente, estas lavas são formadas por uma estrutura simples, que se desenvolve durante alimentação e o crescimento endógeno, típica de derrames pahoehoe (Fig. 5). Esta estrutura pode ser dividida em: crosta inferior, núcleo, e crosta superior, e impreterivelmente apresentam estruturas de alimentação interna e inflação (Hon et al. 1994; White, et al., 2009). Nas lavas do tipo pahoehoe as porções de crosta inferior e superior são ricas em vesículas enquanto o núcleo da lava é maciço e pobremente vesicular (Self et al., 1998).

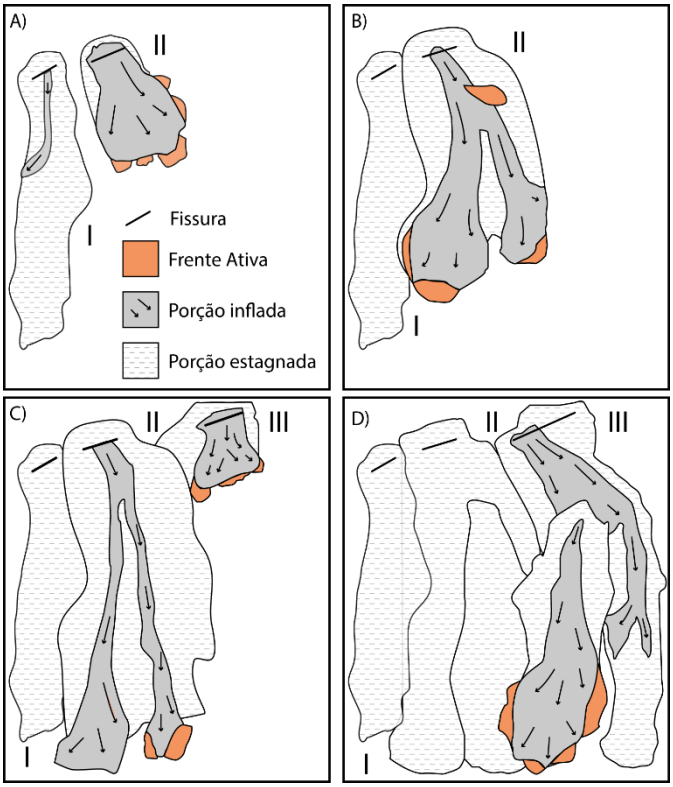

Figura 7 – Desenho esquemático da evolução de um campo de derrames. Atividade vulcânica migra ao longo de fissuras com diferentes segmentos ativos em diferentes momentos, promovendo o crescimento lateral dos campos de lava (modificado de Self et al., 1996).

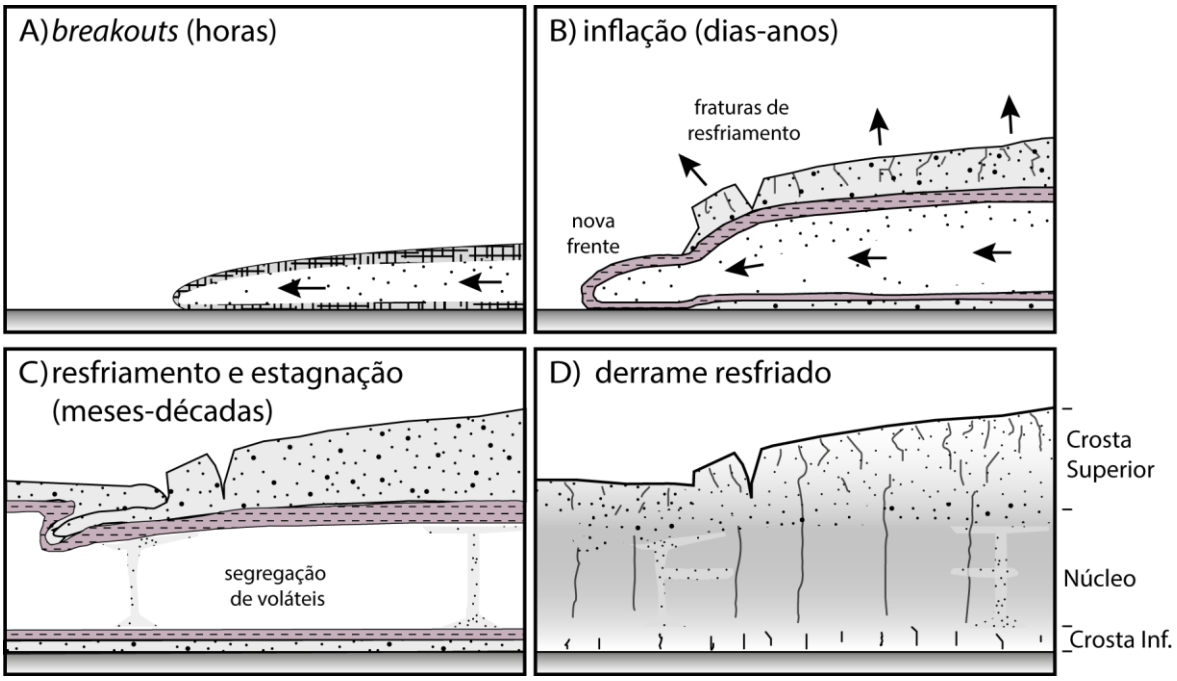

Figure 8– Modelo genérico de colocação de derrames pahoehoe inflados. A) lobo de lava pouco espesso se coloca na superfície, imediatamente a porção externa da lava resfria formando uma crosta isolante; B) a alimentação interna continua da lava promove a inflação e espessamento e o lobo de lava avança por uma nova frente de lava (lava breakout); C) com a parada no suprimento de lava, o derrame estagna e resfria, neste estágio ocorre a segregação de voláteis aprisionados nas porções internas da lava; D) derrame solidificado e resfriado (modificado de Thordarson & Self 1998).

Morfologias do tipo rubbly pahoehoe são comuns, e em muitos casos compõem uma porção importante da estratigrafia, formando cerca de 30 % das lavas na província do Columbia River (Keszthelyi et al., 2004); boa parte da estratigrafia na porção superior da província do Deccan (Duraiswami et al., 2008); e espessas camadas tabulares de lavas na Formação Vale do Sol no Paraná-Etendeka (Rossetti et al 2014, 2017). Estes derrames são caracterizados por uma estrutura interna que pode ser dividida em quatro partes: uma base coerente vesicular, um núcleo maciço, uma porção vesicular coerente e uma superfície autobrechada. As brechas são constituídas por fragmentos de diferentes tamanhos, vesiculados e oxidados que aparentemente são derivados de uma antiga crosta pahoehoe rompida. Derrames rubbly pahoehoe são geralmente mais espessos e extensos que lobos individuais de derrames pahoehoe. O melhor análogo para erupções do tipo rubbly pahoehoe é a erupção histórica de 1783-1784 ocorrida em Laki, Islândia. A erupção produziu um campo de lava de ~600 km² dominantemente do tipo rubbly pahoehoe (Guilbaud et al., 2005). Essas lavas são colocadas inicialmente como um derrame em lençol pahoehoe (sheet flow), que sofre uma

intensa inflação e variações nas taxas de efusão que causam um aumento na pressão interna, e por consequência, resultando na ruptura da crosta externa da lava e degassing das porções de núcleo (Fig. 6 - Keszthelyi et al., 2004, 2006; Guilbaud et al., 2005; Duraiswami et al., 2008). A fragmentação episódica das porções externas da lava promove a formação de uma superfície externa relativamente estável que evita a perda excessiva de calor. Keszthelyi et al. (2006) demonstraram que apesar da superfície fragmentada, derrames rubbly pahoehoe são termicamente tão eficientes quanto lavas pahoehoe, perdendo apenas 0.1°C a cada quilômetro percorrido, considerando uma espessura média entre 20-30 m. Esse fato é importante para explicar as longas distâncias percorridas por essas lavas em algumas PBCs, como por exemplo na Formação Vale do Sol da Província Ígnea do Paraná-Etendeka (Rossetti, et al. 2017).

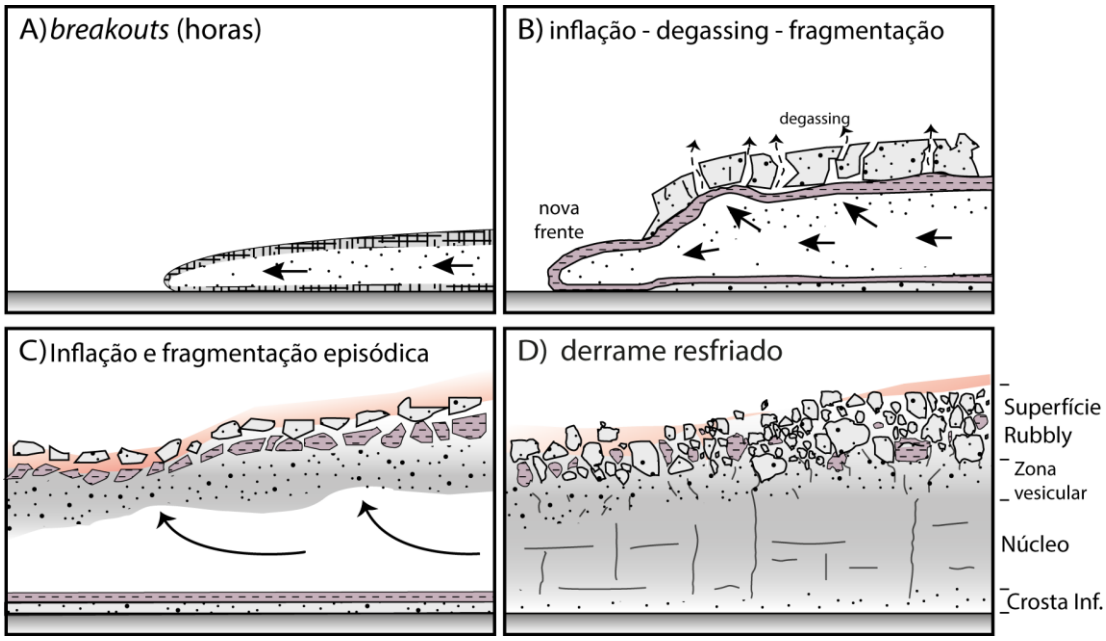

Figure 9 - Modelo genérico de colocação de derrames rubbly pahoehoe. A) lobo de lava pouco espesso se coloca na superfície, imediatamente a porção externa da lava resfria formando uma crosta isolante; B) a alimentação interna continua da lava promove a inflação e o aumento da pressão interna provoca o degassing e fragmentação da crosta pahoehoe previamente formada; C) a superfície da lava estabiliza e é episodicamente fragmentada por sucessivos pulsos de inflação e overpressure; D) estrutura interna de derrame solidificado e resfriado (baseado no modelo de Thordarson & Self 1998 para derrames pahoehoe e nos dados de Guilbaldi et al. 2005)

Erupções Ácidas - Grandes volumes de rochas ácidas podem ocorrer de forma intercalada ao vulcanismo basáltico, como é o caso da Província do Paraná-Etendeka (Peate, 1997), ou ocorrer isolado geograficamente da PBC, como é o caso do *Snake River Plain*, uma província evoluída (dominantemente riolítica)

cronocorrelata aos basaltos do Columbia River (Branney *et al*., 2008). Os principais produtos formados por erupções ácidas em LIP's continentais são: 1) depósitos piroclásticos de queda; 2) ignimbritos; 3) domos de lava; 4) erupções de grande volume de reoignimbritos fortemente soldados fortemente soldados; 5) extensos derrames de lavas ácidas.

Destacam-se em LIP's, depósitos com grandes volumes de material, que em geral se colocam na forma de camadas tabulares e apresentam uma homogeneidade composicional e petrográfica (monótonos), e uma grande extensão lateral em comparação a suas espessuras totais (low-aspect ratio), diferente dos produtos típicos de erupções ácidas. Estes depósitos são em geral associados a erupções de muito alta temperatura (>1000º C) e foram nomeados riolítos do tipo SR, por terem sidos descritos na Província do *Snake River* (Branney *et al.*, 2008). As unidades vulcânicas ácidas (riolíticas e dacíticas) da Província Ígnea do Paraná-Etendeka apresentam características similares as dos extensos derrames de lava descritos no *Snake River*.

Os extensos derrames de lavas riolíticas são caracterizados por *low aspect ratios,* ou seja, grande distribuição horizontal em comparação a espessura. A estrutura interna é marcada por níveis de autobrechas basais e núcleos maciços granulares (litoidais), por vezes bandados, disjunções tabulares apertadas que por vezes se cruzam formando estruturas do tipo "*pencil type*" (Bonnichsen, 1982) e terminações lobadas. Nas porções inferiores dos núcleos são comuns esferulítos e litofises (Fig. 7 – Branney *et al.*, 2008). Na Província do *Snake River*, extensas lavas riolíticas apresentam volumes superiores a 200 km³ (e.g. *Creek Rhyolite* – Bonnichsen, 1982), e nas porções proximais algumas lavas apresentam texturas de aglutinados indicando uma origem clastogênica associada a algum tipo de *fire fountain* riolítico (Manley e McIntosh, 2002). Texturas similares foram recentemente reconhecidas na província do Paraná-Etendeka (Luchetti *et al.*, 2017).

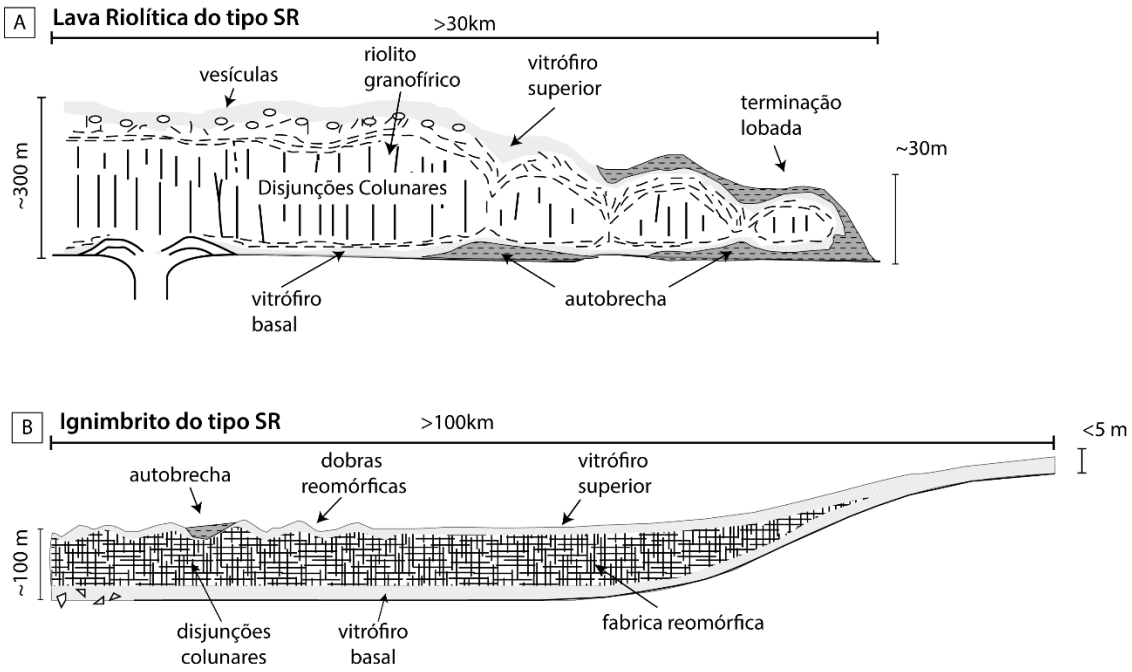

Figure 10 – Estrutura de depósitos riolíticos do tipo SR e características distintivas entre lavas e ignimbritos. A) extensos derrames riolíticos caracterizados por uma pequena razão de aspecto (low aspect ratio), autobrechas basal, e terminações lobadas; B) Ignimbritos do tipo SR, depósitos extensos formados por rochas fortemente soldadas (modificado de Branney et al., 2008).

3.4 GEOMETRIA E ARQUITETURA DE PROVÍNCIAS BASÁLTICAS CONTINENTAIS

Walker (1971) cunhou os termos “simples” e “composto” para a descrição das lavas presentes em províncias basálticas continentais (Fig. 8A). Lavas compostas são aquelas que podem ser subdivididas em unidades de fluxo/resfriamento menores, marcadas por diversas superfícies de resfriamento. Estas são caracterizadas principalmente por campos de derrames formados por múltiplos lobos de lava de pequena espessura (compostos). A sucessão destes lobos de lava define um empilhamento vertical complexo semelhante ao de um vulcão de baixa declividade em escudo e estão relacionadas a erupções de pequenos volumes de magma. Em diversas províncias, derrames compostos representam um importante componente da estratigrafia, especialmente durante as fases de início e declínio da atividade magmática (p.ex. Formações Torres e Esmeralda no Paraná-Etendeka - Rossetti et al., 2017; Steens basalts no Columbia River - Camp et al., 2013; Kalsubai Subgroup no Deccan - Bondre et al., 2004).

Lavas *simples* (Fig. 8B) são caracterizadas por uma unidade única de resfriamento, geralmente com geometria tabular, não divisível (ausência de lobos menores de lava) e são tipicamente associadas a erupções de grandes volumes de magma que “inundam” uma bacia (*Flood Basalts*). Estas erupções constituem grande parte dos depósitos formados durante o estágio principal do magmatismo em muitas províncias ígneas. O empilhamento destas lavas tabulares constitui a chamada estratigrafia do tipo layer-cake, que quando erodida atribuem a geomorfologia da província um aspecto de escada (*Trapp* – em sânscrito significa escada ou escadaria formada por sucessões de lavas).

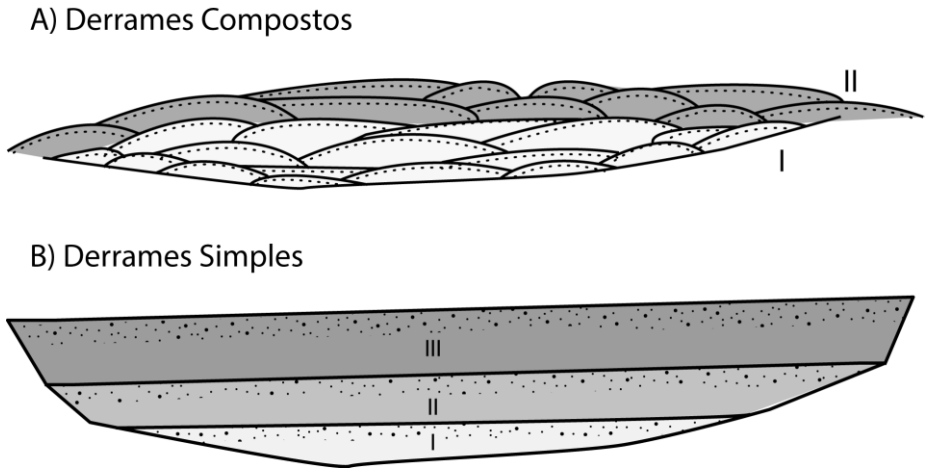

Figura 11 – Desenho esquemático de campos de derrames em vista transversal A) compostos, I e II; e B) derrames simples I, II e III. (Adaptado de Walker, 1973)

Jerram (2002) propôs uma classificação dos produtos eruptivos de *LIPs* com base na arquitetura geral e distribuição das principais facies vulcânicas (Tabela 1). De uma maneira geral, facies em PBCs foram definidas com base na arquitetura, distribuição lateral e empilhamento das lavas. A arquitetura de facies composta anastomosada, e tabular clássica, propostas por Jerram (2002) correspondem de uma forma geral aos termos composto e simples de Walker (1971), respectivamente. Adicionalmente, Jerram (2002) sugeriu uma arquitetura de facies para deltas de lava/hialoclastitos, uma para corpos intrusivos e uma para unidades sedimentares/vulcanoclásticas que ocorrem intercaladas as rochas vulcânicas. Deltas de hialoclastitos são importantes marcadores da transição do regime subaéreo para subaquoso, e estão comumente associados a progradação de lavas em ambientes costeiros (Watton *et al*., 2013). A intercalação de unidades

sedimentares e depósitos vulcânicos em PBCs é comum (Ross *et al*., 2005; Scherer, 2002). Camadas sedimentares são, em muitos casos, importantes marcadores estratigráficos (Jolley and Bell, 2002; Passey and Jolley, 2008) e podem fornecer informações importantes relacionadas a dinâmica da bacia e impacto do magmatismo nas condições paleoclimáticas e paleoambientais (Jolley *et al.* 2012; Ebinghaus *et al.* 2014).

Tabela 1 – Arquitetura de Facies em Províncias Basálticas Continentais (adaptado de Jerram 2002, e Millett 2014).

Arquitetura de Facies	Estrutura Esquemática	Examplo	Descrição
Tabular clássica	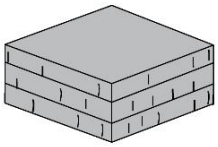		Derrames espessos (20-50m) empilhados verticalmente definindo uma morfologia em degraus. Formados por erupções contínuas e de grande volume.
Composta Anastomosada	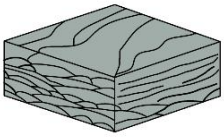	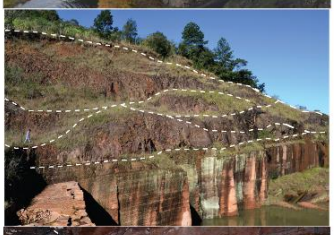	Lobos de lava pouco espessos (0.1 to 15m) empilhados de forma complexa formando um padrão anastomosado. Associados a erupções de pequeno volume e baixa efusão.
Corpos Intrusivos	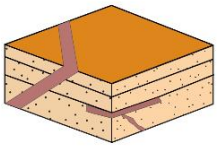		Corpos intrusivos concordantes ou discordantes ao acamamento. Representam o *plumbing system* das lavas.
Unidades Sedimentares Intervulcânicos	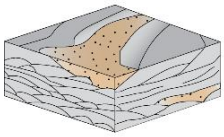		Unidades sedimentares ou vulcanoclásticas depositadas entre lavas. Representam quebras na atividade vulcânica.

A descrição de variações litológicas internas aos pacotes de lava ou a um único derrame foram denominadas intrafacies por Single e Jerram (2004). Hierarquicamente, intrafacies são equivalentes a litofácies utilizadas na estratigrafia de sistemas sedimentares e também em sistemas vulcânicos. O uso de litofácies é comum em ambientes vulcânicos atuais onde a variação e heterogeneidade dos depósitos é mais frequente do que a de PBCs e a intercalação entre depósitos piroclásticos e extrusivos é comum (Brown and Branney, 2013; Watton et al., 2013). O uso de litofácies na descrição de rochas vulcânicas segue a proposta de McPhie

(1993) utilizando uma combinação de características petrográficas, estruturais e texturais. Litofácies vulcânicas são subdivididas em dois grupos principais: 1) coerentes; e 2) vulcanoclásticos. O primeiro agrupa principalmente derrames e intrusões, sendo estes classificados com base em seus aspectos texturais (p.ex. basalto vesicular). Rochas vulcanoclásticas podem ser descritas de forma análoga a rochas sedimentares, sendo classificadas pelo tamanho das partículas, estruturas deposicionais, e composição. A nomenclatura tipicamente utiliza uma combinação de litologia e estrutura, como por exemplo, sLT é utilizado para caracterizar um lapili-tufo estratificado, ou seja, uma camada de rocha formada por fragmentos piroclásticos com tamanhos variando entre 0,5 mm (cinza – do termo tufo - T) e 2 mm (lapili - L), que possuí estratificação cruzada (s).

A figura 9 apresenta um exemplo de seção colunar em uma sequência de depósitos vulcânicos do Vulcão Central na Ilha da Graciosa nos Açores. A intercalação de litofácies vulcanoclásticas e coerentes caracterizam as diferentes associações de fácies (depósitos geneticamente relacionados).

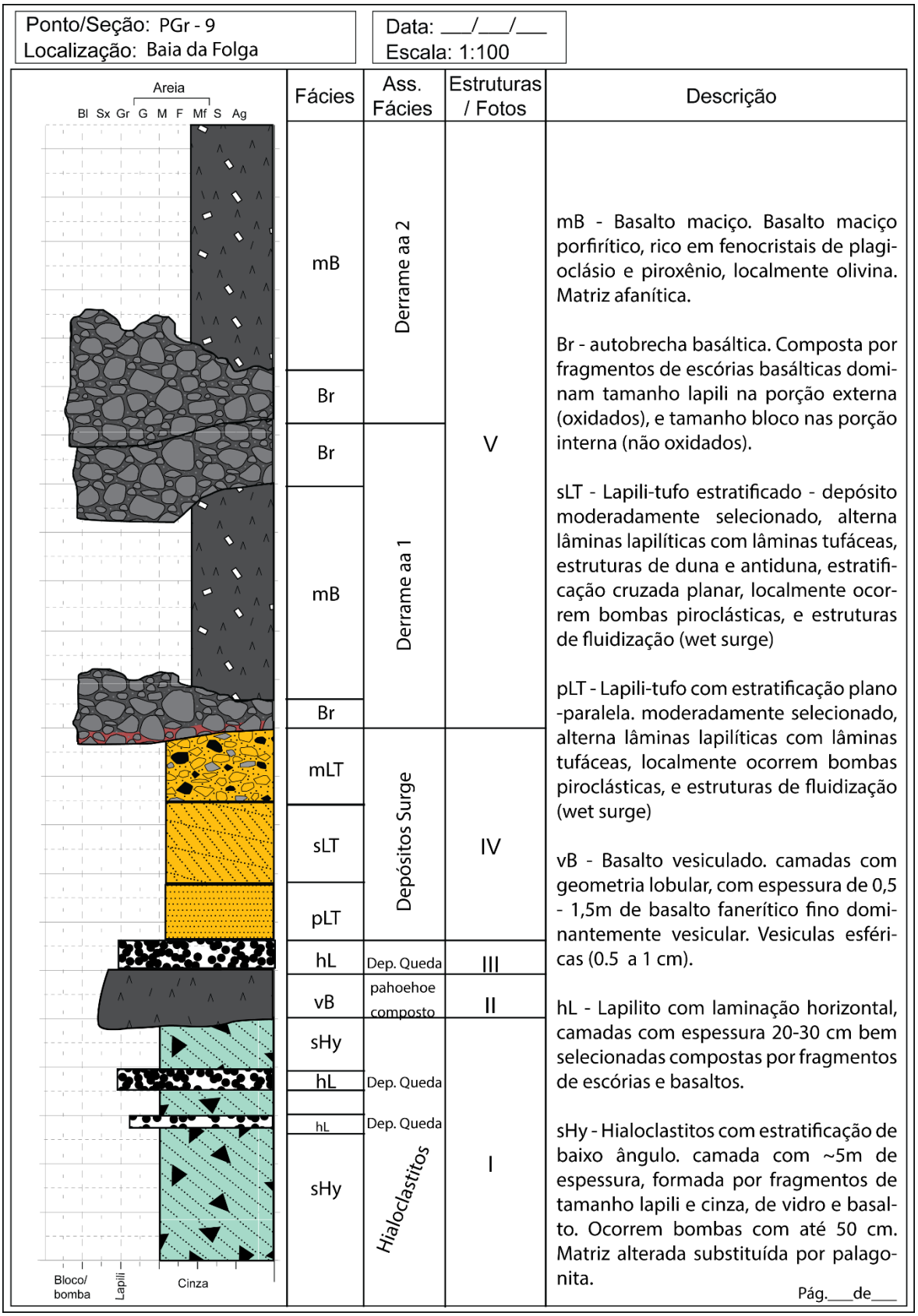

Figure 12 – Exemplo da aplicação de litofácies na descrição de rochas vulcânicas, seção colunar dos depósitos vulcânicos da Baia da Folga, na Ilha da Graciosa, Arquipélago dos Açores.

3.5 ESTRATIGRAFIA DE PROVÍNCIAS BASÁLTICAS CONTINENTAIS

Províncias Basálticas Continentais são em geral formadas durante pulsos de magmatismo (0.1-5 Ma) que podem ser divididos em três etapas eruptivas/evolutivas principais: 1) um estágio inicial, no qual são colocados pequenos volumes de magma basáltico, em geral de afinidade transicional alcalina (olivina toleítos), formando derrames compostos com múltiplos lobos pouco espessos; 2) uma fase principal, na qual a maior parte da estratigrafia é construída, sendo formada por sucessivas erupções de grande volume de basaltos toleíticos e, em alguns casos, erupções ácidas intercaladas; e 3) uma fase de declínio da atividade magmática na qual a produção de magmas decresce rapidamente, tornando-se espalhada espacialmente, ou concentrada em zonas de rifte (Bryan and Ernst, 2008; Jerram and Widdowson, 2005). A construção de uma estratigrafia detalhada permite a compreensão dos diferentes estágios evolutivos. Na seção 4.1 serão apresentadas a estratigrafia e uma síntese dos estágios evolutivos das Províncias do Columbia River; Atlântico Norte e Paraná-Etendeka.

3.5.1 Província Basáltica Continental do Columbia River (CR)

Os basaltos do Columbia River formaram-se no Mioceno, recobrindo ~234.000 km2 em parte do território dos estados de Oregon, Washington e Idaho, no oeste dos Estados Unidos (Fig.10 - Barry et al., 2013; Reidel et al., 2013). O vulcanismo como um todo produziu um volume de ~200.000 km³ de lavas ao longo de um intervalo de 11 Ma (entre 16.7 e 5.5 Ma - Barry et al., 2013). A província apresenta uma estratigrafia detalhada, construída ao longo das últimas décadas com base em uma combinação de mapeamento geológico detalhado e uma compreensiva (com controle estratigráfico) amostragem geoquímica, geocronológica e paleomagnética (Wright, 1973; Swanson, 1979; Hooper, 1982; Wright, 1973; Tolan et al., 1989; Reidel et al., 2013). A província foi subdividida em 7 unidades equivalentes a formações (Fig. 10), mas referidas na literatura como basaltos, são elas: Steens basalt; Imnaha basalt; Grande

Ronde Basalt; Picture Gorge basalt; Prineville basalt; Wanapum Basalt; e Saddle Mountain basalt (Tolan et al., 1989; Reidel et al., 1989, 2013).

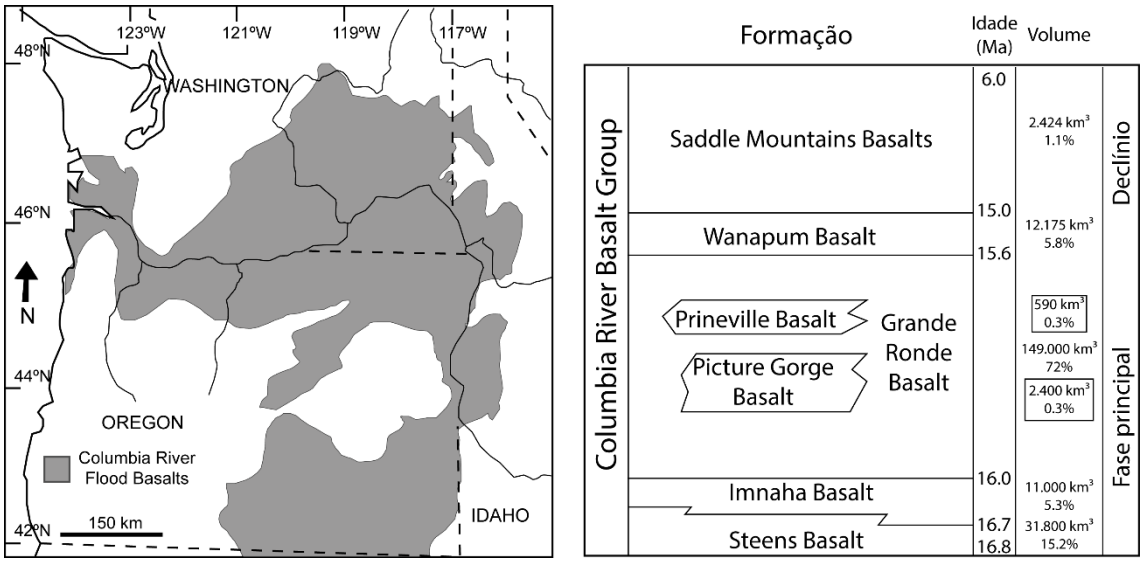

Figura 13– Mapa simplificado da ocorrência dos basaltos do Columbia River, oeste do Estados Unidos e coluna estratigráfica simplificada (modificado de Reidel et al., 2013).

Os estágios iniciais do magmatismo, (Steens Basalt) são caracterizados principalmente por campos de derrames formados por múltiplos lobos alongados de lavas pahoehoe que ocorrem na porção sul da província. Esta unidade é composta de dois campos principais de lavas, uma unidade basal toleítica de composição mais primitiva, e uma unidade superior formada por basaltos toleíticos e alcalinos, e traquiandesitos (Camp et al., 2013). Durante o clímax do magmatismo, a atividade vulcânica migrou de sul para norte/noroeste concentrando-se ao longo do enxame de diques do Chief Joseph, próximo ao limite entre os estados de Washington e Idaho. O pico principal da atividade magmática produziu ~93% do volume total em um intervalo de ~1 Ma (Reidel et al., 2013). Esta fase contém os basaltos do Grande Ronde, Picture Gorge, Prineville e Wanapum e é caracterizada principalmente por derrames tabulares, com volumes tipicamente excedendo 1000 km³ e se estendendo por algumas centenas de quilômetros de distância (Fig. 11A - Tolan et al., 1989; Reidel et al., 1989; Reidel, 2005; Reidel e Tolan, 2013). O declínio da atividade magmática é marcado pela colocação localizada de lavas ao longo de um intervalo de ~9 Ma (Saddle Mountain basalt). A porção superior da estratigrafia é caracterizada por intervalos erosivos e de sedimentação, durante os períodos de quiescência e pausa na atividade vulcânica. O volume das lavas é significativamente menor, e

derrames comumente ocupam os vales incisos dos sistemas fluviais, formando lavas *intracanyon* (Tolan *et al.*, 1989; Reidel *et al.*, 2013).

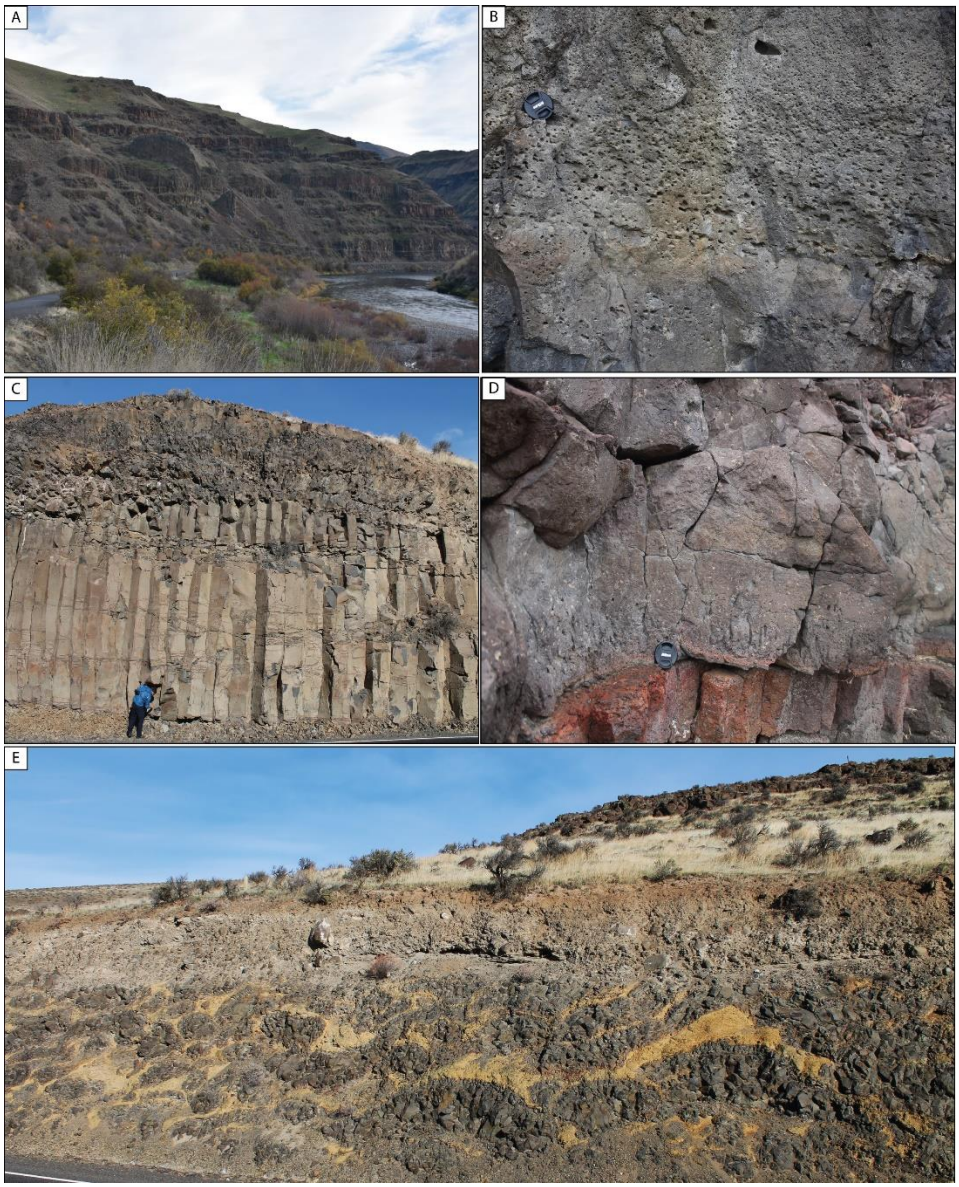

Figura 14 – Aspectos de Campo das Lavas do Columbia River. A) Sucessão de derrames tabulares do Grande Ronde Basalts, na margem do rio Grande Ronde, Oregon; B) topo vesicular; C) disjunções colunares e zona de entablatura na porção de núcleo de lava do membro Frenchmen Springs, da Formação Wanapum; D) zona de base de derrame com vesículas em pipe do membro Sentinel Gap, Formação Wanapum; E) foresets de pillow lavas com matriz palagonizada, base de um derrame, em Vantage.

Um campo de lavas da Província do *Columbia River* (durante a fase principal de magmatismo) é tipicamente caracterizado por uma porção basal que pode conter *foresets* de *pillow* lavas e hialoclastitos (Fig. 11E), quando esta se avança sobre ambientes com água, ou uma base subaérea vesicular pouco espessa em condições normais (Fig. 11D). A porção interna da lava é maciça,

pobre em vesículas, que tipicamente desenvolve disjunções colunares bem formadas (Spry, 1962 -Fig. 11C). O topo das lavas é vesicular ou escoriáceo, ocupando entre 10- 20% da espessura total da lava (Fig. 11B).

3.5.2 Província Ígnea do Atlântico Norte (NAIP)

A Província Ígnea do Atlântico Norte (Fig. 12) representa um evento anômalo que produziu cerca de 1.3 x 106 km³ durante a fragmentação e abertura do oceano Atlântico Norte entre 60.5 e 54.5 Ma (Jolley and Bell, 2002). O desenvolvimento da província está associado a dois pulsos principais de magmatismo relacionados a uma anomalia térmica do manto superior (Saunders 1997). O magmatismo ocorreu de forma diácrona em diferentes porções geográficas da província (p.ex. Oeste e leste da Groelândia, Ilhas Faroe, e na Província Ígnea do Paleogeno Britânico BPIP – Hole e Millett, 2016). No oeste da Groelândia o magmatismo foi continuo entre 62 e 58 Ma com um hiato significativo entre 58 e 56 Ma, seguido por um novo pulso contínuo de magmatismo entre 56 e 53 Ma (Larsen et al., 2015). Nas ilhas do oeste britânico (chamada British Paleogene Igneous Provínce – BPIP), o magmatismo ocorre agrupado em diferentes unidades estratigráficas como o grupo de lavas de Antrim, o Platô de Mull, e a série principal de lavas de Skye (Jolley and Bell, 2002). As idades variam entre 61,32 Ma para riolítos na Irlanda do Norte à 58,12 Ma para o platô de lavas de Mull (Chambers & Pringle, 2001). Nas Ilhas Faroe e na porção leste da Groelândia, o magmatismo coincide com o máximo termal do Paleoceno-Eoceno (PETM – 55,8Ma - Larsen et al., 1999; Larsen e Pedersen, 2009; Passey e Jolley, 2008).

A fase inicial do magmatismo é marcada por um soerguimento regional e subsidências localizadas em algumas porções da província (Jerram and Widdowson, 2005). A atividade vulcânica é parcialmente caracterizada por espessos pacotes de hialoclastitos colocados em ambiente subaquoso, como por exemplo, no oeste da Groelândia e nas Ilhas Faroe (Ellis et al., 2002). Sincronicamente, em outras porções da província como nas áreas do BPIP, lavas foram colocadas em ambiente subaéreo (Ellis et al., 2002). As primeiras manifestações vulcânicas são caracterizadas por composições primitivas, formando lavas picríticas principalmente no oeste da Groelândia (Larsen and

Pedersen, 2009). As sequências vulcânicas preservadas na Ilha de Mull, no oeste da Escócia, representam um bom exemplo da evolução local da província do Atlântico Norte. As primeiras manifestações vulcânicas (Formação Staffa) ocorrem associadas as sequências sedimentares e são confinadas a grabens de orientação NW (Williamson and Bell, 2012). Os depósitos vulcânicos da Formação Staffa são caracterizados por uma variação lateral complexa de litofacies 1) coerentes: basaltos com disjunções colunares e entablados (Fig. 13A); 2) vulcanoclásticas: hialoclatitos, e brechas vulcânicas; e 3) unidades sedimentares intercaladas (Williamson e Bell, 2012). Os derrames da Formação Staffa são correlatos aos basaltos da calçada dos gigantes (membro Antrim) na Irlanda do Norte. do Atlântico Norte.

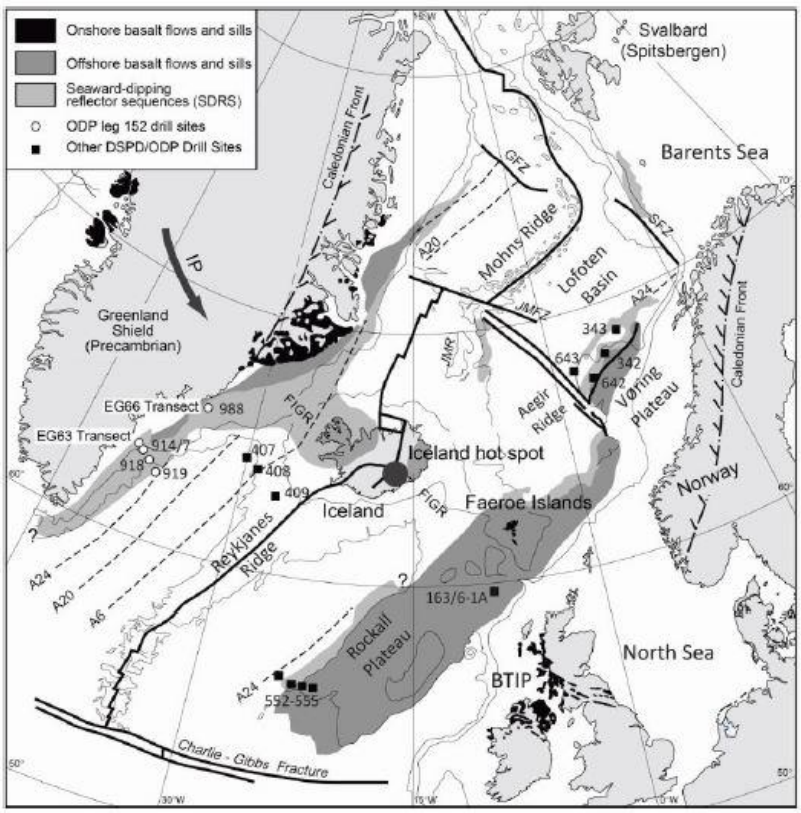

Figure 25 - Mapa de localização da Província Ígnea do Atlântico Norte (Fitton et al., 1998).

As primeiras manifestações vulcânicas (Formação Staffa) ocorrem associadas as sequências sedimentares e são confinadas a grabens de orientação NW (Williamson and Bell, 2012). Os depósitos vulcânicos da Formação Staffa são caracterizados por uma variação lateral complexa de litofacies 1) coerentes: basaltos com disjunções colunares e entablados (Fig.

13A); 2) vulcanoclásticas: hialoclatitos, e brechas vulcânicas; e 3) unidades sedimentares intercaladas (Williamson e Bell, 2012). Os derrames da Formação Staffa são correlatos aos basaltos da calçada dos gigantes (membro Antrim) na Irlanda do Norte. Esta unidade é sucedida na estratigrafia pela Formação Mull (*Plateau Formation*). As lavas do Platô de Mull, formam derrames tabulares lateralmente extensos (s*heet pahoehoe*) e se colocam em uma paleotopografia relativamente plana (Fig. 13B). A passagem de uma unidade para a outra é marcada pelo desenvolvimento e formação de depósitos fluviais, e por uma importante variação na composição geoquímica das lavas. As lavas da Fm. Staffa são dominantemente toleíticos enquanto as lavas do Platô são olivina basaltos com composições transicionais alcalinas (Kerr, 1995). Os estágios finais do magmatismo da NAIP na ilha de Mull são caracterizados pela intrusão de gabros, granitos e benmoreitos agrupados no complexo central de Mull (Kerr, 1995; Kerr *et al*., 1999).

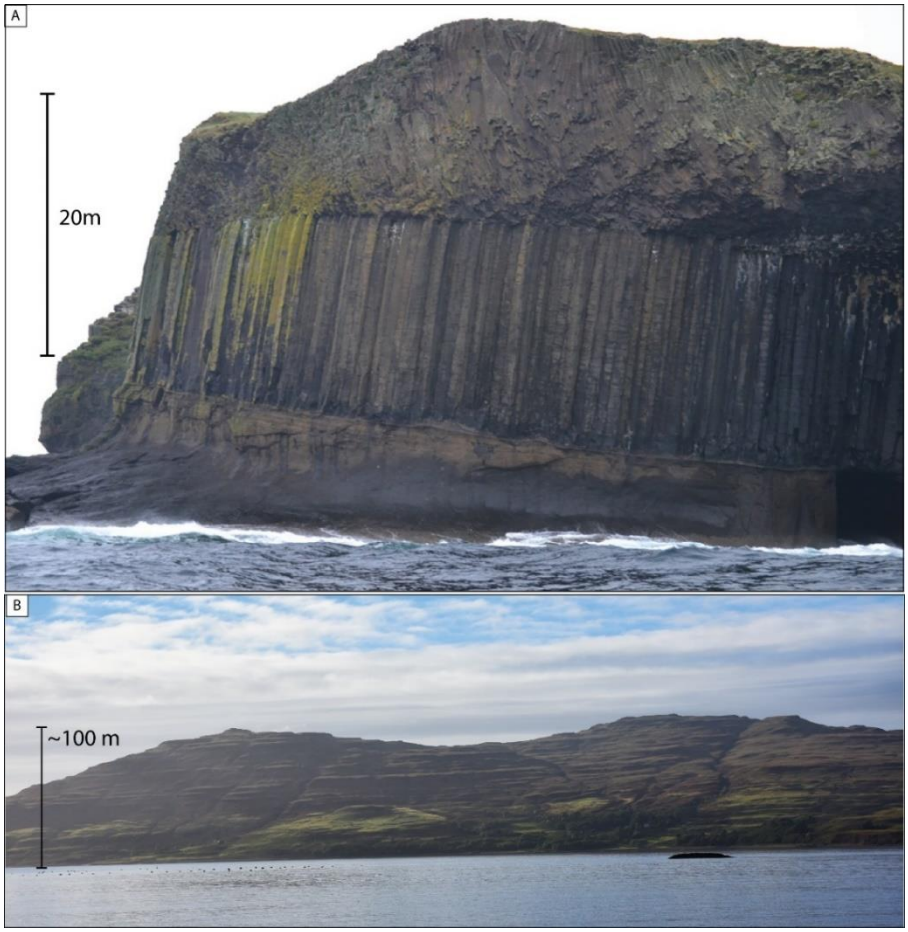

Figure 16 – A) Formação Staffa, derrame espesso com disjunções colunares na porção basal e núcleo entablado recobrindo nível epiclástico. B) Platô de lavas de Mull, formados por derrames tabulares extensos empilhados verticalmente.

3.5.3 A Província Ígnea do Paraná-Etendeka

A Província Ígnea do Paraná-Etendeka (PIPE – Fig. 14) representa um megaevento vulcânico formado por um grande volume de lavas subaéreas de afinidade toleítica. As rochas vulcânicas são em grande maioria (90%) basálticas e subordinadamente ácidas. O vulcanismo está preservado em uma área de $1.2x10^6$ km^2 sobre a plataforma Sul-Americana (Brasil, Paraguai, Uruguai e Argentina) e uma menor área na África, Angola e Namíbia (Cordani e Vandoros, 1967). No Brasil as rochas vulcânicas recobrem a Bacia do Paraná em uma área de 917.000 km^2 e atualmente o volume estimado é de no mínimo 450.000 km^3 (Frank *et al*., 2009). A bacia do Paraná é uma bacia intracratônica que acumula um total de 7000 m de sedimentos e rochas vulcânicas, com uma história deposicional que engloba desde o Devoniano até o Neocretáceo. Pode ser dividida em seis supersequências deposicionais: Rio Ivaí (Ordoviciano-Siluriano), Paraná (Devoniano), Gondwana I (Carbonífero-Eotriássico), Gondwana II (Meso a Neotriássico), Gondwana III (Neojurássico-Eocretáceo) e Bauru (Neocretáceo) (Milani et al., 2007). O magmatismo do Paraná-Etendeka, juntamente com a Formação Botucatu, representa a supersequência deposicional Gondwana III. As primeiras lavas recobriram e interagiram com sedimentos eólicos inconsolidados da Formação Botucatu (Scherer, 2002; Waichel et al., 2008). A pilha vulcânica tem em média 700 metros de espessura atingindo uma espessura máxima de 1800 m na porção central da bacia (Piccirillo and Melfi, 1988). A fração intrusiva do magmatismo é representada por quatro grandes enxames de diques, relacionados as porções preservadas do sistema de alimentação das lavas em superfície (Raposo et al., 1998; Florisbal et al., 2014).

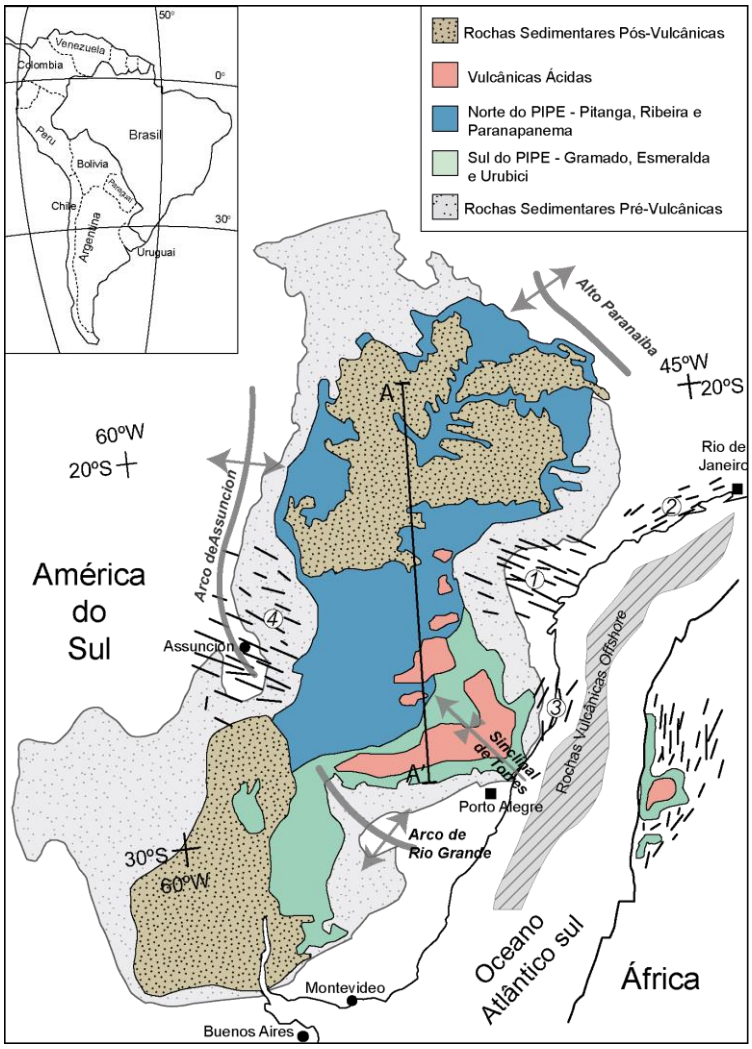

Figura 37 - Mapa geológico simplificado da PMPE na América do Sul. Lineamentos Tectônicos: PR- Rio Piquiri, UR – Rio Uruguai, TP-Torres Possadas; Enxames de diques: PG-Ponta Grossa; F- Florianópolis; SRJ-Santos Rio de Janeiro; PA – Paraguai. (Modificado de Peate et al. 1992, Janasi et al 2011).

Um modelo “estratigráfico” regional (Fig. 15) foi construído com base em um conjunto de características químicas de diferentes magma-tipo, apresentados de forma simplificada na tabela 1 (Peate *et al*., 1992). Na porção sul, uma província de baixo-Ti/Y (<300) caracterizada por magmas do tipo Gramado na base, recobertos por dacitos e riolitos do tipo Palmas que são sucedidos por basaltos do tipo esmeralda. Lavas basálticas alto-TiO_2 do tipo Urubici ocorrem como uma faixa alongada (~100 km X 350 km) no limite nordeste da escarpa no sul do Brasil, essas lavas são contemporâneas e estão intercaladas aos magmas do tipo Gramado (Peate *et al*., 1999). Ao Norte, uma província vulcânica de alto-Ti/Y (>300) é formada por uma pequena quantidade

de rochas ácidas do tipo Chapecó, e basaltos do tipo Ribeira, Pitanga e Paranapanema (Peate, 1997).

Tabela 2 – Tipos de magma tipo para os basaltos da Formação Serra Geral. (Modificado de Peate, 1997).

Magma Tipo	Características	Sub Província	TiO_2	Ti/Y	Ti/Zr
Gramado	Baixo Ti/Y & TiO_2	Sul	0.7-1.9	<310	<70
Esmeralda	Baixo Ti/Y & TiO_2	Sul	1.1-2.3	<310	>60
Ribeira	Alto Ti/Y & baixo TiO_2	Norte	1.5-2.3	>310	>65
Paranapanema	Alto Ti/Y & TiO_2	Norte	1.7-3.2	>330	>65
Pitanga	Alto Ti/Y &TiO_2	Norte	>2.9	>350	>60
Urubici	Alto Ti/Y &TiO_2	Sul	>3.3	>500	>57

Datações isotópicas sugerem que a maior parte do magmatismo ocorreu num intervalo relativamente curto (<4 Ma) durante o Cretáceo Inferior, entre 135Ma e 131Ma. Estratigraficamente mais antiga, a província baixo-Ti/Y a sul, apresenta idades 40Ar/39Ar step-heating recalculadas agrupadas entre 134.1-134.8 Ma (Renne et al., 1992; Thiede and Vasconcelos, 2010). Ao Norte, idades relativamente mais novas variando entre 131.5-133.6 Ma foram obtidas para os basaltos de alto-Ti/Y (40Ar/39Ar step-heating - Ernesto et al., 1999). Recentemente Janasi et al. (2011), obtiveram para dacito do tipo Chapecó, uma idade de 134±0.8 (U-Pb em badeleíta). Essas lavas recobrem o embasamento ao norte da bacia, e são recobertas pelos basaltos alto-Ti/Y mais jovens, representando um importante marco estratigráfico na bacia.

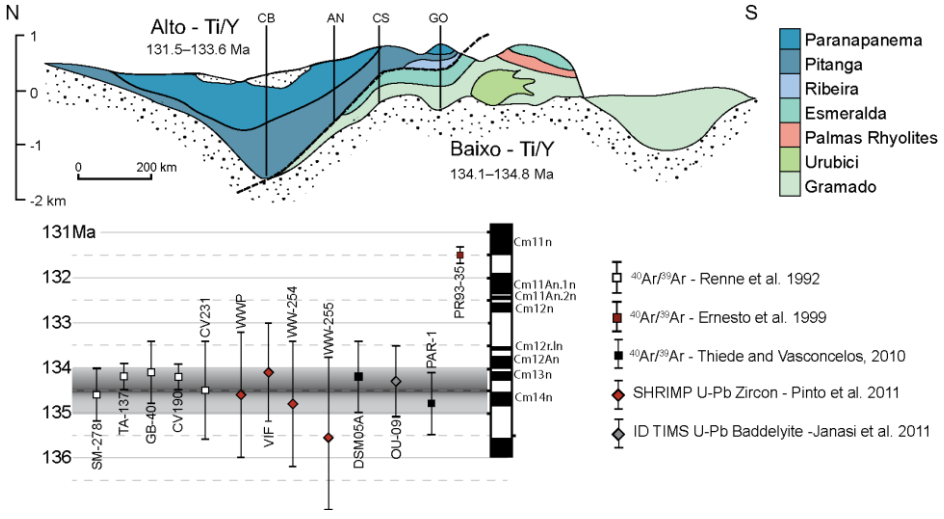

Figura 18 – Distribuição regional de magma tipos segundo Peate et al. (1992) e Peate (1997). Principais datações radiométricas e intervalo temporal das rochas da Província Ígnea do Paraná-Etendeka, referencias na figura.

A porção sul da Província Ígnea do Paraná-Etendeka aflora ao longo das escarpas da Serra Geral, no sul do Brasil, na calha de Torres. As escarpas sul e sudeste são cortadas por diversas rodovias que expõem a estratigrafia das rochas vulcânicas desde a base no contato com os arenitos da Formação Botucatu. Esses perfis foram intensamente estudados nas décadas de 80 e 90 com foco principalmente nas características geoquímicas, geocronológicas e paleomagnéticas (Belliene *et al.* 1984; Peate *et al.*,1992, Peate,1997; Ernesto *et al*., 1990). Estudos recentes sobre a vulcanológica de PBCs deslocaram a pesquisa tradicionalmente geoquímica para o desenvolvimento e compreensão dos modelos *emplacement,* geração de fácies, associação e arquitetura de fácies. Esta nova abordagem permitiu recentemente a divisão na porção sul da bacia em cinco episódios vulcânicos principais (Waichel *et al*., 2012). Estudos em detalhe mostraram variações vulcanológicas e geoquímicas associadas às diferentes unidades vulcânicas (Lima *et al*., 2012; Barreto *et al*., 2014; Rossetti *et al*., 2014) e que os episódios vulcânicos propostos por Waichel *et al. (*2012) poderiam representar unidades estratigráficas correlacionáveis regionalmente (Rossetti *et al*., 2018).

Na Namíbia, a Província do Paraná-Etendeka recobre uma área de 0.8 × 10^5 km^2 (Erlank *et al*., 1984). A sequência vulcânica é caracterizada por um estágio inicial de magmatismo formado por magmas primitivos, algumas vezes com composições picríticas (Gibson *et al*., 2000; Jerram *et al*., 1999), caracterizado por derrames compostos do tipo *pahoehoe* intercalados a camadas sedimentares agrupados no membro Tafelkop (Jerram *et al*., 1999). A fase principal do magmatismo é caracterizada por uma espessa sequência de lavas de composições andesito-basálticas (Membro Tafelberg, Jerram *et al*., 1999). Estas lavas têm geometrias tabulares, e formaram derrames espessos e com grandes extensões laterais. Nas porções superiores da estratigrafia unidades tabulares de composição ácida (reoignimbritos?) ocorrem intercaladas as lavas do Membro Tafelberg (Milner *et al*., 1992).

CAPÍTULO 4 - ESTRATIGRAFIA DA PORÇÃO SUL DA PROVÍNCIA ÍGNEA DO PARANÁ-ETENDEKA

Nesta seção são sintetizados os dados apresentados no artigo intitulado “Lithostratigraphy and volcanology of the Serra Geral Group, Paraná-Etendeka Igneous Province in Southern Brazil: Towards a formal stratigraphical framework”, publicado na edição especial do Journal of Volcanology and Geothermal Research dedicada ao magmatismo da Província Ígnea do Paraná-Etendeka (Anexo I). A publicação propoe a formalização da estratigrafia na porção sul da Província Ígnea do Paraná-Etendeka, elevando a Formação Serra Geral ao status de Grupo e dividindo a pilha vulcânica na área de estudo em quatro unidades, equivalentes a formações. As lavas da porção norte da província não foram incluídas nesta proposta de estratigrafia por não terem sido estudadas no presente trabalho, então são aqui apresentadas como uma unidade indivisa.

Na área de estudo, 29°35’ – 27°00’ S e 55°06’ – 49°31’ W, a sequência de lavas é limitada a norte e noroeste por derrames alto-TiO_2, a leste pelo limite erosional da abertura do oceano Atlântico sul e soerguimento da Serra do Mar e a sul pelo Arco de Rio Grande (Fig. 5). A sucessão vulcânica pôde ser dividida em quatro grupos principais de lavas, estratigraficamente equivalentes a Formações definidas neste trabalho como: Formação Torres (FT), Formação Vale do Sol (FVS), Formação Palmas (FP) e Formação Esmeralda (FE) (Fig. 6).

Esta proposta difere da estratigrafia geoquímica de Peate et al. (1992) e Peate (1997) por utilizar como base aspectos vulcanológicos como morfologia e arquitetura dos derrames, além dos limites físicos mapeáveis (contatos inferior e superior de cada unidade) integrado as características petrográficas e geoquímicas de cada grupo de lavas. A proposta de Waichel et al. (2012) definiu diferentes episódios vulcânicos com base em variações na arquitetura vulcânica dos depósitos, porém não leva em consideração os limites das unidades, sua distribuição regional e características geoquímicas.

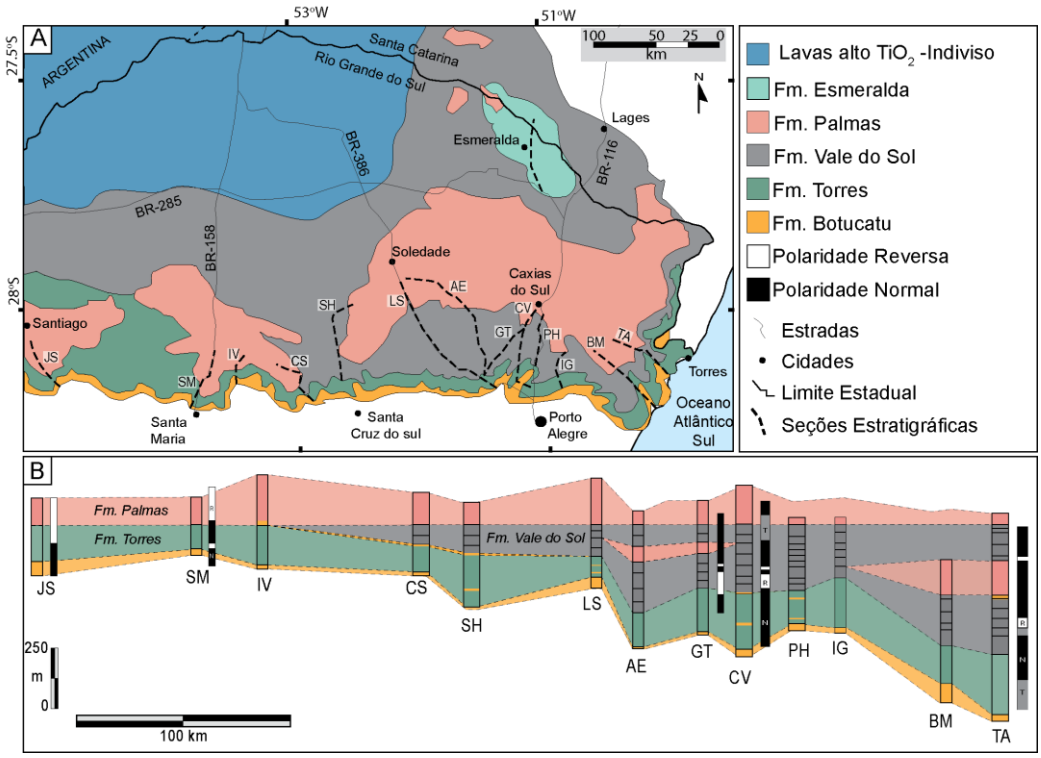

Figura 19 – Mapa geológico simplificado da área de estudo, porção sul da Província Paraná-Etendeka. Em destaque as principais seções que expõem a variação da estratigrafia. B) empilhamento estratigráfico das seções geológicas.

A base da sequência vulcânica é formada por basaltos e basaltos andesíticos que ocorrem na forma de derrames pahoehoe com uma arquitetura composta anastomosada, agrupados na Formação Torres. O segundo grupo de lavas, Formação Vale do Sol, é caracterizado por sucessivos derrames tabulares (sheet like) de andesitos basálticos com morfologias do tipo rubbly pahoehoe. Estas lavas recobrem parcialmente a Formação Torres e o contato entre as duas unidades é caracterizado localmente pela presença de camadas, em geral pouco espessas, de arenitos, que podem atingir até 2m de espessura (Fig. 6B e C). Esse contato representa uma mudança no estilo eruptivo e uma parada da atividade vulcânica (tempo suficiente para deposição dos arenitos) representando um marcador regional importante. A porção superior da sequência vulcânica é formada por derrames tabulares dacíticos e riolíticos agrupados na Formação Palmas. Essas lavas recobrem principalmente a Formação Vale do Sol (Fig. 6D e E), com exceção da porção oeste na qual as rochas acidas estão depositadas diretamente sobre os basaltos da Formação

Torres. A Formação Esmeralda é formada por basaltos na forma derrames pahoehoe similares aos da Formação Torres.

Figura 20 - A) Contato entre dois derrames basálticos, separados por arenito, Formação Torres; B) Contato entre Formação Torres e Formação Vale do Sol na região de candelária, contato marcado por camada de arenito silicificada; C) Contato entre Formação Torres e Formação Vale do Sol na região de Herveiras, camada pouco espessa de arenito entre as unidades; D) Contato entre Formações Vale do Sol e Palmas na região de São Marcos; E) Contato entre as Formações Vale do sol e Palmas na região de Herveiras.

CAPÍTULO 5 - PROPRIEDADES PETROFÍSICAS DE SEQUENCIAS VULCANO-SEDIMENTARES E UM ESTUDO DE CASO DA PROVÍNCIA ÍGNEA DO PARANÁ-ETENDEKA

Dados petrofísicos foram obtidos em ensaios descritos na seção 2.6 do capítulo de metodologia. Foram analisadas 245 amostras secas, em condições de pressão e temperatura ambiente. Destas, 162 análises são do Grupo Serra Geral na Bacia do Paraná; 45 analises de basaltos do *Columbia River (CR)*, no oeste dos Estados Unidos; e 38 amostras da Ilha de São Jorge no arquipélago dos Açores. A amostragem em diferentes áreas permiti a comparação e correlação das condições de formação e modificação destas rochas (diagênese, alteração, preenchimento da vesicularidade original).

Na tabela 2 são apresentados os resultados obtidos em análise das rochas vulcânicas da PIPE, CR e São Jorge. Dados de porosidade, permeabilidade e velocidades acústicas em rochas vulcânicas são relativamente raros e em geral restritos a campanhas de perfuração do assoalho oceânico realizadas pelo *International Ocean Drilling Program* (IODP). Os resultados apresentados representam um banco de dados inédito para as rochas vulcânicas da PIPE e tendo uma grande importância para a manutenção dos aquíferos associados a estas rochas e para comparações futuras com as rochas vulcânicas presentes nas bacias marginais brasileiras.

Durante a coleta de amostras e realização dos ensaios foram testadas as diferentes litofácies que compõem as diferentes morfologias. A variação das características petrofísicas nestas fácies permite avaliar os fatores controladores destas mudanças. Além das litofácies vulcânicas foram analisadas amostras de arenitos eólicos e fluviais que ocorrem entre derrames na PIPE, além de hialoclastitos e pillow-breccias que ocorrem entre derrames no *Columbia River*.

De uma maneira geral a porosidade das amostras varia de 0,03% a 62,23%, com uma porosidade média de 13% (±12%). A permeabilidade em geral varia de muito baixa a média ($1*10^{-3}$ mD a 2792 mD) com permeabilidade média de 45 mD. Em geral, os sedimentos e os hialoclastitos apresentam os maiores valores de porosidade e permeabilidade, seguidos pelas fácies de brechas de

topo dos derrames, topos vesiculares, sendo os menores valores de porosidade encontrados nos núcleos maciços dos derrames.

De forma geral as velocidades ultrassônicas variam de 1955 ms^{-1} a 5941 ms^{-1} para ondas P e de 1178 ms^{-1} a 4550 ms^{-1} para ondas S. As menores velocidades das ondas S, quando comparada as ondas P, devem-se ao tipo de propagação e trajetória percorrida pela onda. As velocidades são inversamente proporcionais à porosidade, sendo as menores velocidades encontradas nos arenitos (3250ms^{-1} Vp; 2100ms^{-1} Vs), brechas de topo dos derrames *rubbly pahoehoe* (3500 ms^{-1} Vp; 2100ms^{-1} Vs), zonas vesiculares de derrames *pahoehoe* (4300ms^{-1} Vp; 2500ms^{-1} Vs), zonas vesiculares em derrames ácidos (4478ms^{-1} Vp; 2505ms^{-1} Vs), núcleos maciços de derrames básicos e ácidos (5500ms^{-1} Vp; 3500ms^{-1} Vs). Nas amostras do Columbia River as velocidades são tipicamente maiores para qualquer litofácies. Este fato está relacionado as composições das rochas, e principalmente ao grau de alteração (precipitação de minerais secundários) mais elevado em amostras da PIPE.

Tabela 2 – Resultados obtidos nos ensaios petrofísicos para as rochas vulcânicas da Província Magmática do Paraná-Etendeka, Columbia River e São Jorge.

Paraná-Etendeka	N	Variação Por. (%)		Por. Média (%)	Perm. (mD)		Perm. Média (mD)	N	Vp (m/s)		Vp (m/s) Média	Vs (m/s)		Vs (m/s) Média
Riolito/Dacito	14	1.1	9.38	4.02	0.0003	0.0141	0.0022	28	4448	5866	4847	2672	3321	2980
Basaltos	62	0.41	26.60	5.68	0.0003	415.68	7.08	124	3214	5937	4828	1856	3776	2868
And-Basaltos	51	0.03	28.28	6.76	0.0001	0.7268	0.0227	102	2934	5898	4818	1809	3417	2799
Arenitos	33	3.5	34.18	19.18	0.0029	1115.3	225.5	66	1955	5365	3310	1178	4098	2139
Columbia River														
Basaltos	39	0.87	35.72	17.28	0.0001	25.57	2.17	78	3944	5863	5174	2217	4551	3085
Hialoclastitos	6	21.28	36.70	27.14	0.859	69.766	17.98	12	2492	3571	3090	1349	2084	1595
São Jorge														
Basaltos	38	5.96	62.23	25.37	0.0289	2792	80	76	2566	5172	3402	1331	3188	1957

3.4.1 Tipos de Poros e Origem

Uma síntese dos tipos de poros primários e secundários e processos formadores de porosidade foram apresentados por Sruoga e Rubinstein (2007). A comparação dos resultados destes autores com os encontrados nas rochas da PMPE, CR e São Jorge permitiram classificar os processos em:

- Processos primários: decorrentes de processos de degaseificação das lavas *pre* e *sin emplacement,* principalmente representados por vesículas e bolhas (Fig. 15 A, B, D) formadas durante a colocação das lavas em superfície. Os diferentes tipos de derrames desenvolvem diferentes padrões de vesiculação (Fig. 15 A e C - derrames *rubbly pahoehoe* da FVS e derrames *pahoehoe* FT e FE). Grande parte da microporosidade está relacionada a uma fase de degaseificação tardia que gera textura do tipo *diktytaxitic*, caracterizada pela presença de poros irregulares, em geral microscópicos, entre cristais de plagioclásio e piroxênio (Fig.15 E, F). Texturas em peneira, decorrentes do desequilíbrio entre fenocristais e líquido, são também importantes geradoras de porosidade primária.
- Porosidade secundária: está associada a processos que ocorrem após o resfriamento das lavas ou em estágios finais de resfriamento. São principalmente representadas por fraturas decorrentes de relaxamento térmico das lavas, ou fraturas e falhas tectônicas. A alteração/precipitação de fases minerais também tem um papel importante na modificação da porosidade primária podendo gerar porosidade por dissolução e alteração de cristais, ou diminuir a porosidade pela precipitação de minerais secundários nos poros (ex.: zeólitas).

Figura 214 - Exemplo de tipos de poros nas rochas vulcânicas da PMPE. A) porosidade primária representada por vesículas irregulares na porção de topo de derrame pahoehoe; B) porosidade primaria e secundária representadas por vesículas e fraturas respectivamente, porção de topo de derrame pahoehoe; C) brecha de topo de derrame rubbly formada por fragmentos vesiculares, porosidade primária intra e entre fragmentos, parcialmente preenchidos por zeólitas e quartzo; D) porosidade primária em megavesículas no núcleo de derrame rubbly pahoehoe; E) Fotomicrografia de porção superior de núcleo de lobo pahoehoe. Trastejado em laranja vesículas/amígdalas preenchidas por zeólitas. Textura diktytaxitic destacada por setas vermelhas. F) porosidade intracristalina em fenocristal de plagioclásio.

3.4.2 Características Petrofísicas da Província Ígnea do Paraná-Etendeka

As características petrofísicas da Província Ígnea do Paraná-Etendeka são apresentadas no anexo II e são apresentadas de forma resumida a seguir.

As diferentes morfologias de lavas são caracterizadas por diferente estruturação interna e variações de fácies, que implicam em diferentes características petrofísicas. Na área de estudo existem dois principais tipos de derrames básicos: *pahoehoe* e *rubbly pahoehoe*. Derrames *pahoehoe* compõem as unidades basal e superior, Formação Torres e Formação Esmeralda, respectivamente. Estes são caracterizados por bases vesiculares (Fig.16 C), em geral com vesículas alongadas, nas quais a porosidade é em média ~7%; núcleos maciços a micro vesiculares, ou com cilindros e níveis horizontais de vesículas, apresentam uma porosidade variando entre 1.4% a 5.8% (Fig.16 B). As zonas de topo vesicular são caracterizadas por vesículas esféricas que decrescem em tamanho em direção ao topo, nestas porções a porosidade varia de 3% a 18% (Fig. 16 A).

Nos derrames do tipo *rubbly pahoehoe*, que compõem a FVS, a estrutura interna é caracterizada por uma base afanítica vesicular, com vesículas estiradas ou esparsas, onde a porosidade é de 15.11% (Fig. 16G); um núcleo maciço afanítico, em geral sem vesículas, com porosidades variando de 2% a 8% (Fig. 16F); e uma zona superior grossamente vesicular, com vesículas esféricas a irregulares com diâmetros de 1 a 3 centímetros (Fig. 16E) e localmente com megavesículas. A superfície brechada é constituída de fragmentos fortemente vesiculares com em média 5-10cm de diâmetro, onde valores de porosidade variam entre 15% e 20% (Fig. 16D). As rochas ácidas ocorrem dominantemente na forma de vitrófiros e granófiros maciços sem vesículas onde a porosidade varia entre 3.38%-4.86%. As fácies muito vesiculadas associadas a domos e lobos ácidos coletadas em campo, apresentaram problemas nas etapas de preparação em laboratório. Devido à grande quantidade de vesículas as amostras fraturaram durante a perfuração, apenas uma amostra foi analisada nesta fácies, apresentando uma porosidade de ~10%.

Figura 225 - Exemplo da heterogeneidade de texturas e estruturas nos derrames basálticos. A) zona vesicular de topo em derrame pahoehoe, FT; B) Núcleo maciço de derrame com níveis horizontais de vesículas, FT; c) base de derrame pahoehoe com vesículas em pipe, FT; D) Brecha de topo que forma a superfície do derrame rubbly pahoehoe, FVS; E) Zona vesicular superior em derrame rubbly pahoehoe, FVS; F) Núcleo de derrame rubbly pahoehoe com disjunções tabulares irregulares, FVS; G) zona vesicular basal em derrame rubbly pahoehoe, FVS.

A permeabilidade das amostras varia de 0.0001 a 1000 mD. A maioria das amostras tem baixa permeabilidade (<1mD). Do ponto de vista de reservatórios, as amostras podem ser classificadas como apertadas (*tight*), com a maioria das amostras acima do *cut off* para reservatórios de gás, ocupando o campo de *tight gas reservoirs* (> 1 microdarcy). A precipitação de minerais secundários, em especial zeólitas, é um dos principais fatores que contribuem para os baixos valores de permeabilidade. A precipitação desta fase mineral sela a conexão entre os poros, reduzindo a permeabilidade à valores muito baixos, mesmo em amostras com alta porosidade. Os valores de permeabilidade mais elevados são encontrados nos arenitos depositados entre os derrames. Nestes a permeabilidade é controlada principalmente pelo empacotamento dos grãos sendo maior nas fácies eólicas, e menor nas fácies fluviais (Fig. 17D).

As velocidades de ondas P e S têm comportamentos similares e uma forte correlação linear positiva (Fig. 17C). As razões entre ondas P e S são importantes principalmente em ensaios onde as amostras estão saturadas, possibilitando estimativas indiretas de porosidade. Tendo em vista que as ondas S não se propagam em fluídos, quanto maior as razões de Vp/Vs maior a porosidade efetiva. Para o conjunto de amostras analisadas em condições não saturadas as razões de Vp/Vs (Fig. 17C) variam entre 1.5 e 2.0, e apresentam um agrupamento em torno de 1.6, valor comum para rochas vulcânicas não saturadas (Saunders *et al*., 1998). Variações de Vp/Vs estão associadas neste caso ao grau de alteração das amostras, com valores maiores para amostras com alteração avançada. Existe também uma forte correlação positiva entre as velocidades e a densidade das rochas, e uma correlação negativa entre velocidade e porosidade (Fig. 17A e B).

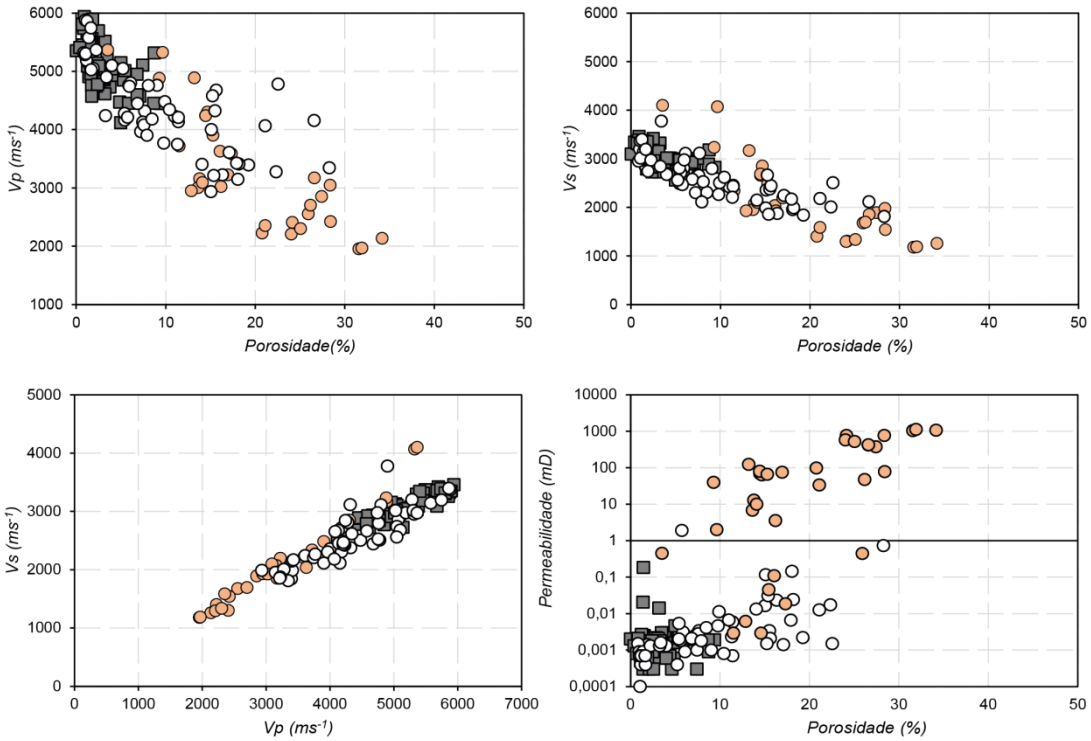

Figura 23 – Diagramas de variação dos padrões petrofísicos nas diferentes litofácies investigadas. A) Porosidade x Vp (ms^{-1}); B) Porosidade x Vs (ms^{-1}); C) Vp (ms^{-1}) x Vs (ms^{-1}); D) Porosidade (%) x Permeabilidade (mD). Quadrados Cinza representam facies de núcleo das lavas; círculos brancos representam facies vesiculares / brechadas; círculos laranja representam arenitos inter-derrames.

As velocidades variam de acordo com a fácies ao longo de um derrame. As menores velocidades ocorrem nas porções basais e superiores das lavas, ~4200ms^{-1} para derrames *pahoehoe* e ~3600ms^{-1} nos derrames *rubbly pahoehoe*, onde ocorrem as maiores concentrações de vesículas e uma maior intensidade de fraturas. As velocidades são significativamente maiores nas porções de núcleo (~5500ms^{-1}), onde as litofácies são maciças e mais compactas com uma menor quantidade de vesículas e fraturas (Fig. 18).

Outro parâmetro importante é o grau de alteração das rochas que modifica os valores de velocidade absoluta. A substituição dos minerais máficos (olivina e piroxênio) por argilominerais (esmectitas) causa uma atenuação nas velocidades de ondas P e S. Para uma mesma litofácies e porosidade a velocidade pode diminuir em até 1000 ms^{-1} em amostras alteradas. Essa atenuação está associada a estrutura cristalina dos minerais do grupo das argilas, os quais possuem coeficientes de compressibilidade (*bulk modulus*) e cisalhamento (*shear modulus*) menores do que os minerais máficos (piroxênios e olivinas). A precipitação de minerais secundários, principalmente zeólitas e

quartzo, tem um efeito importante na diminuição da porosidade e consequente aumento na Vp e Vs. Grande parte das amostras analisadas tem pelo menos parte da sua porosidade primária preenchida por minerais secundários. A diminuição da porosidade por precipitação destas fases minerais gera um suave aumento nas velocidades, tendo em vista que a densidade destes minerais é maior que a densidade do poro vazio (ar).

A presença de fraturas primárias (de resfriamento) ou tectônicas causa uma atenuação nas velocidades de onda P e S. A difícil obtenção de amostras de cilindros de rocha em porções fraturadas dificulta a quantificação e uma melhor avaliação do efeito destas fraturas a partir de ensaios de petrofísicas convencional.

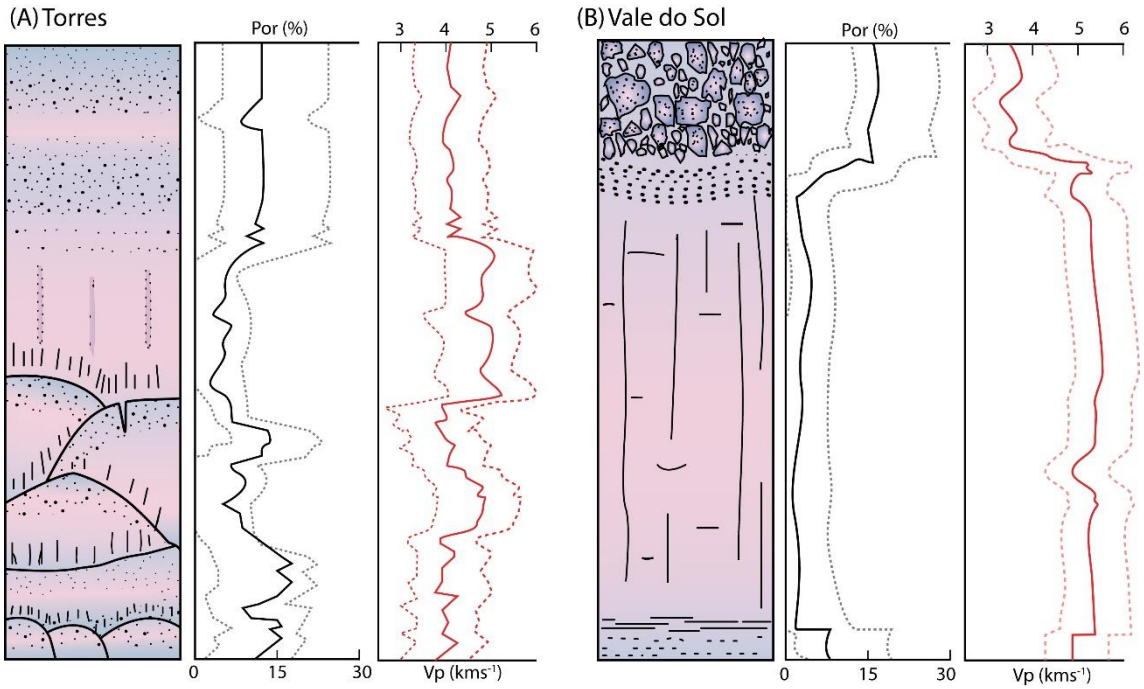

Figura 24 - Variação vertical de fácies, estruturação interna das lavas;, variação de porosidade (%) e velocidades de onda compressiva (Vp – kms^{-1}) em: a) campo de derrames pahoehoe; b) derrame rubbly pahoehoe. Escala vertical ~25m. Fácies de acordo com legenda da Figura 11. CI – Crosta Inferior; CS – Crosta Superior.

CAPÍTULO 6 - ESTRATIGRAFIA GEOQUÍMICA E EVOLUÇÃO MAGMÁTICA DA PROVÍNCIA ÍGNEA DO PARANÁ-ETENDEKA

Os resultados das investigações geoquímicas são apresentados no anexo III, no manuscrito intitulado "*Geochemical stratigraphy and Magmatic evolution of the Paraná-Etendeka Large Igneous Province: Insights from shallow crystallization magmatic processes and magma genesis"* e brevemente introduzidas aqui.

As amostras para estudos geoquímicos foram coletadas ao longo do limite sul do platô de lavas, onde a descontinuidade entre unidades vulcânicas e unidades sedimentares formam uma abrupta escarpa com face sul. Rodovias federais e estaduais cortam a escarpa com orientação dominantemente N-S expondo a estratigrafia das unidades vulcânicas desde o contato com os arenitos da Fm. Botucatu ao topo onde unidades ácidas estão capeando os basaltos. A distribuição lateral das estradas permite, também, investigar variações laterais na distribuição destas lavas e suas variações geoquímicas.

Foram analisadas 190 amostras de rocha total de acordo com a metodologia descrita na seção 2.5. A amostragem visou contemplar unidades vulcânicas representativas da estratigrafia, e o maior número de derrames. A figura 10 apresenta de forma esquemática a variação de facies ao longo da estratigrafia no perfil de Terra de Areia- Aratinga e a distribuição e localização das amostras analisadas.

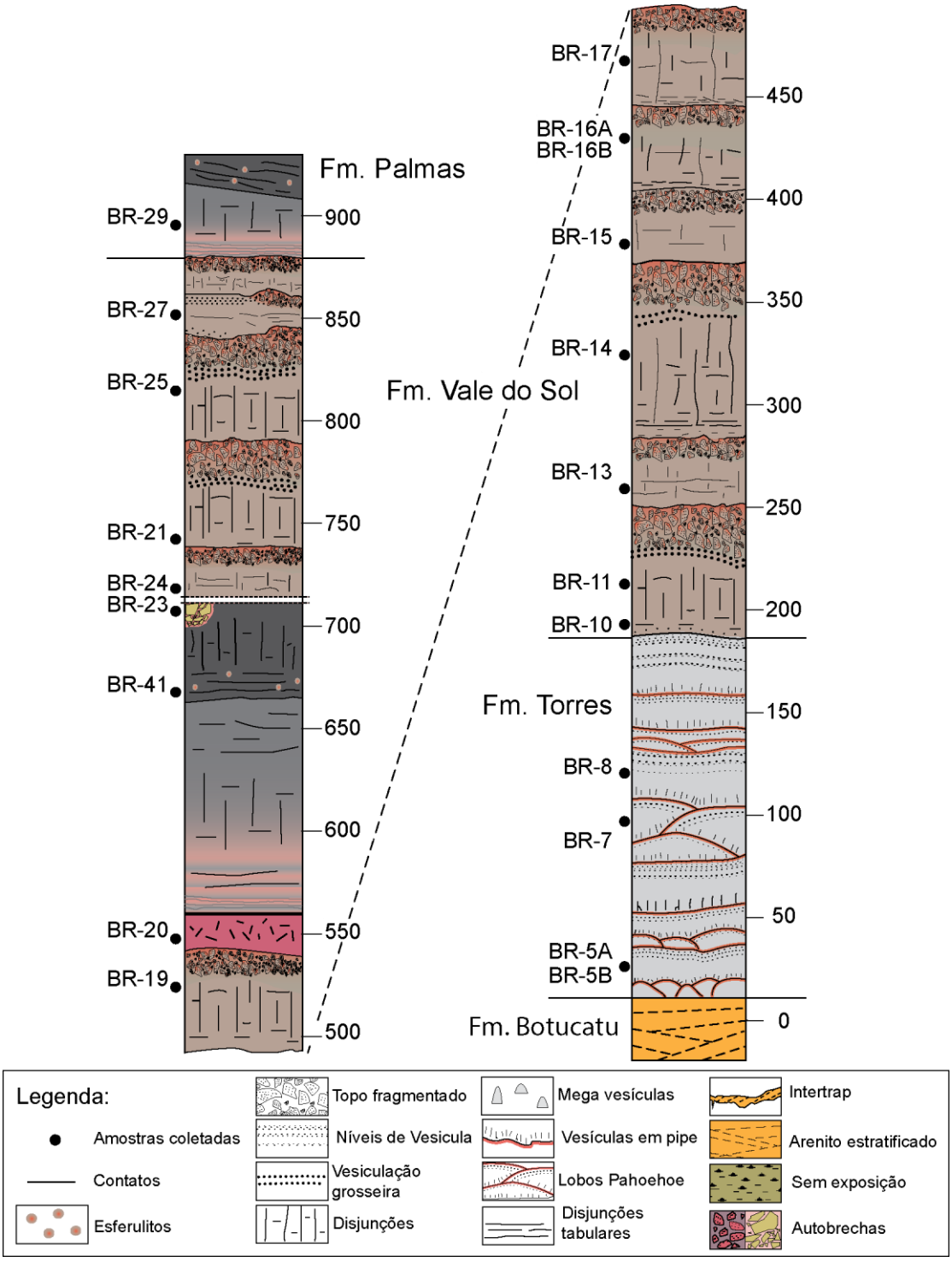

Figura 25 - Facies vulcânicas e distribuição estratigráfica das lavas da PMPE no perfil de Terra de Areia – Aratinga. Pontos representam a localização estratigráfica das amostras.

A maioria das amostras de rochas máficas ocupa o campo dos basaltos-andesíticos, e subordinadamente o campo dos basaltos (Fig. 11). As rochas ácidas ocupam os campos dos riolitos e dacitos, com os dacitos representando a porção basal da estratigrafia (membro Caxias do Sul - Peate, 1997; Nardy *et*

al. 2008) mais comum nas porções leste da area aflorante, enquanto riolitos (membro Santa Maria - Peate, 1997; Nardy *et al*. 2008) representam a porção superior das unidades ácidas, comumente preservada na porção oeste da área de estudo. As rochas da Fm. Torres ocupam dominantemente o campo dos basaltos com algumas amostras espalhadas nos campos dos basaltos andesiticos e andesitos. Em geral as lavas compostas são quimicamente mais primitivas, enquanto os derrames espessos que ocupam o espaço interduna têm composições mais evoluídas. Na Fm. Vale do Sol conteúdos de SiO_2 variam de 52,43 a 60,91 % com a maioria das composições restrita entre 52 e 57 %, plotando no campo dos basaltos-andesiticos. Amostras da Fm. Esmeralda ocupam o campo dos basaltos com conteúdos de SiO_2 ~50%.

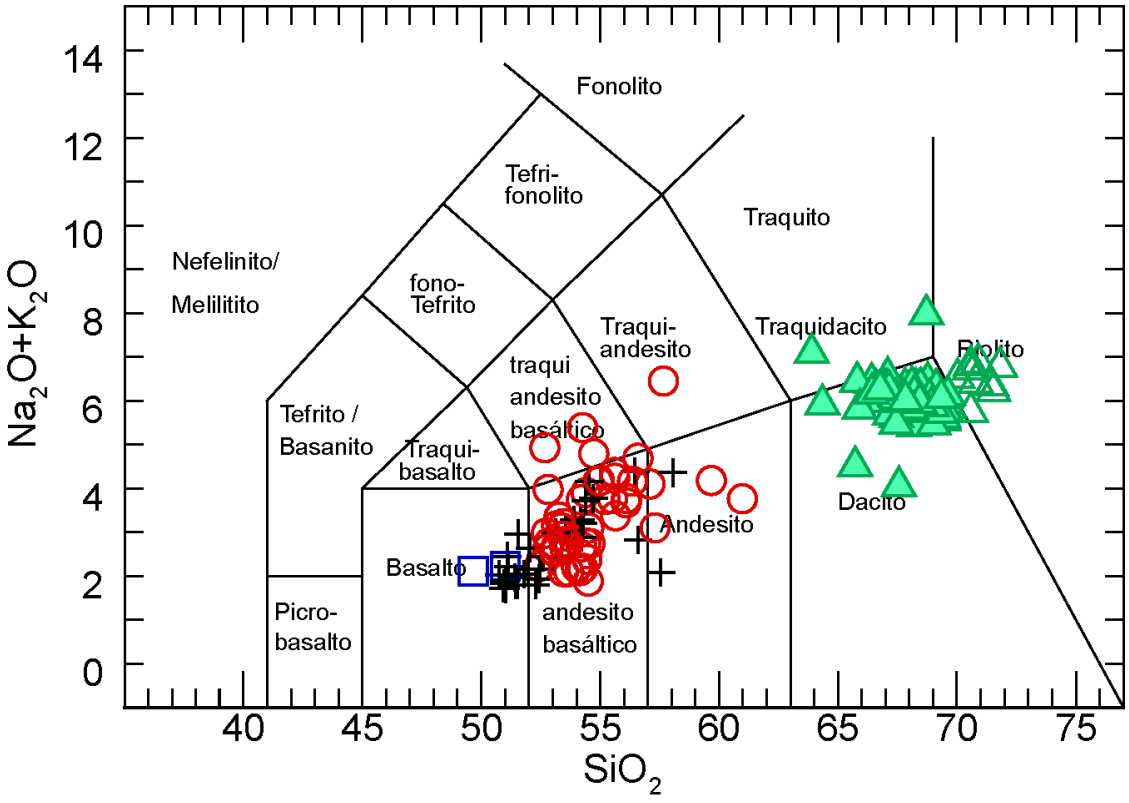

Figura 26 - Distribuição das composições em diagrama de classificação de SiO_2 versus álcalis (TAS – Le Maitre, 1989). Cruzes pretas = Fm. Torres; Círculos Vermelhos = Fm. Vale do Sol; Triângulos verdes = Fm. Palmas, símbolos preenchidos (Membro Santa Maria), e símbolos abertos (Membro Caxias do Sul); Quadrados azuis = Fm. Esmeralda.

As rochas são toleíticas com baixa concentração de álcalis nos membros menos diferenciados (basaltos a andesitos), Na2O+K2O <5 % e com um aumento gradativo nas razões de FeO*/MgO com o aumento no conteúdo de

sílica (Fig. 12A). A evolução geral das rochas segue o trend de cristalização de Fenner (1929), com um acentuado enriquecimento na concentração de FeO* nas composições intermediárias (com decréscimo de MgO) e sem um significativo aumento no conteúdo de álcalis. Essa evolução é típica de magmas que cristalizaram fases ricas em MgO (p.e. olivina e piroxênios), comum em rochas toleíticas (Fig. 12B). Composições normativas são tipicamente saturadas a supersaturadas em sílica. As lavas da Fm. Torres são dominantemente toleítos com quartzo-normativo e subordinadamente olivina-toleítos. As lavas da Fm. Vale do Sol são toleítos com quartzo normativo e as rochas da Fm. Esmeralda são toleítos com olivina-normativa. Em diagrama pseudoternário de composições normativas as linhas de cotéticos representam o equilíbrio entre ol + plag + cpx + líquido basáltico a pressões de 1 atm, 0,2 , 0,7, 0,8 e 0,9 GPa (Thompson 1982, Grove et al.,1992; Villiger et al. 2007). As linhas cotéticas apresentam uma migração consistente a partir do vértice Di com o aumento gradativo das pressões de equilíbrio. As amostras da PIPE estão distribuídas próximas ao cotética experimental para a cristalização de toleítos de 0,7 GPa de Villiger et al. (2007) (Fig13C), indicando que estas rochas cristalizaram em pressões relativamente maiores, equivalentes a porções mais profundas da crosta (meso-crustais, ~20 -25 km), e não a baixas pressões (~1atm) e próximos a superfície como sugerido por Peate (1997).

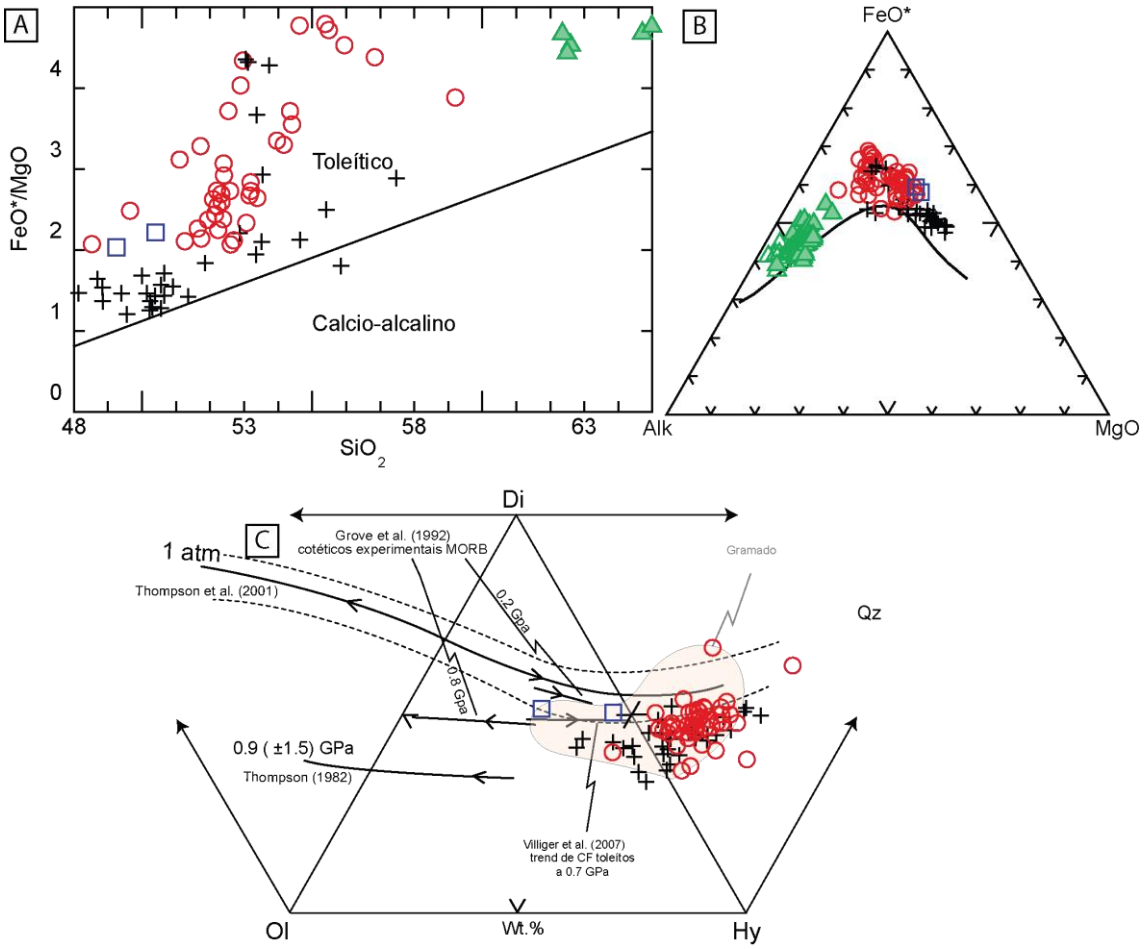

Figura 27- Diagrama de classificação FeO*/MgO versus SiO2 (Miyashiro, 1974); B) Diagrama AFM com trend evolutivo das rochas da PMPE (modificado de Irvine e Baragar, 1971); C) Diagrama pseudoternário de componentes normativos Ol-Hy-Di-Qtz, amostras distribuídas abaixo da trajetória de 1 atm definida por Thompson (1982). Cruzes pretas = Fm. Torres; Círculos Vermelhos = Fm. Vale do Sol; Triângulos verdes = Fm. Palmas, símbolos preenchidos (Membro Santa Maria), e símbolos abertos (Membro Caxias do Sul); Quadrados azuis = Fm. Esmeralda.

A distribuição de elementos maiores apresenta uma grande variação nos conteúdos de MgO de 0,34 a 8,8 %. Lavas da Fm. Torres são as mais primitivas com composições, em geral, > 6% MgO, rochas da FVS estão dispersas entre 2 e 6 % MgO e rochas ácidas agrupadas entre 0,34 e 1,7 % MgO. Concentrações de SiO2 apresentam correlação negativa com MgO, apresentando um aumento progressivo em direção aos termos mais diferenciados, com concentrações agrupadas em três grupos, de 50-52, 52-56 e 65-72 % SiO2, que representam aproximadamente as três formações principais. Abundâncias de TiO2 são menores que 2 % e variam entre 0,68 e 1,95 %. Duas trajetórias principais são observadas, a primeira tem valores de TiO_2 >1 % em composições primitivas e

evolui na porção superior do *plot* para composições de ~2 % TiO_2; já a segunda trajetória evolui na porção basal do gráfico com valores iniciais menores que 1 % TiO_2. CaO e Al_2O_3 apresentam um comportamento similar, com um enriquecimento inicial de 9,8 a 11,2 e 14 a 16% respectivamente para valores de MgO > 7,5%, seguidos de um rápido decréscimo em suas concentrações com o consumo progressivo de MgO (<7,5%). FeO* apresenta correlação positiva com MgO para valores de MgO maiores que 8 %. Para MgO <8 % FeO* apresenta uma correlação negativa, com o aumento progressivo com o decréscimo de MgO. Dois *trends* se destacam na distribuição de concentrações de FeO*, um primeiro, que apresenta enriquecimento contínuo em direção as menores concentrações de MgO; e um segundo com um acentuado decréscimo nas concentrações de FeO* a partir de composições intermediárias (MgO 3-6 %). Essa variação representa a entrada de titanomagnetita na cristalização dos magmas consumindo grandes quantidades de FeO*. Na_2O, K_2O e P_2O_5 têm uma distribuição similar com um aumento nas concentrações com a redução de MgO. Para a Formação Esmeralda, as amostras têm SiO_2 49,25-50,4 % e MgO entre 6,15 e 6,56 %. Quando comparadas com as lavas da FT, em valores de MgO similares, as amostras da FE são relativamente enriquecidas em FeO*, CaO e TiO_2. As variações na distribuição de elementos maiores são típicas de uma cristalização controlada pelo fracionamento de olivina nos termos menos diferenciados (MgO >7.5%), seguida pelo ingresso de augita e plagioclásio, causando o decréscimo em Al_2O_3 e CaO.

Elementos traços são apresentados em diagramas binários plotados contra concentrações de Zr (ppm). Abundâncias de Zr variam de 80 a 344 ppm com os menores valores nos basaltos da FT e concentrações mais elevadas nos riolitos. Ni se comporta de forma antipatética com relação a Zr com as concentrações sofrendo um rápido decréscimo com o aumento de Zr. Os maiores valores de Ni são dos basaltos da FT (~165 ppm). As rochas intermediarias da FT e FVS apresentam concentrações tipicamente menores do que 60 ppm. Rochas ácidas têm Ni tipicamente <10ppm com no máximo 25 ppm.

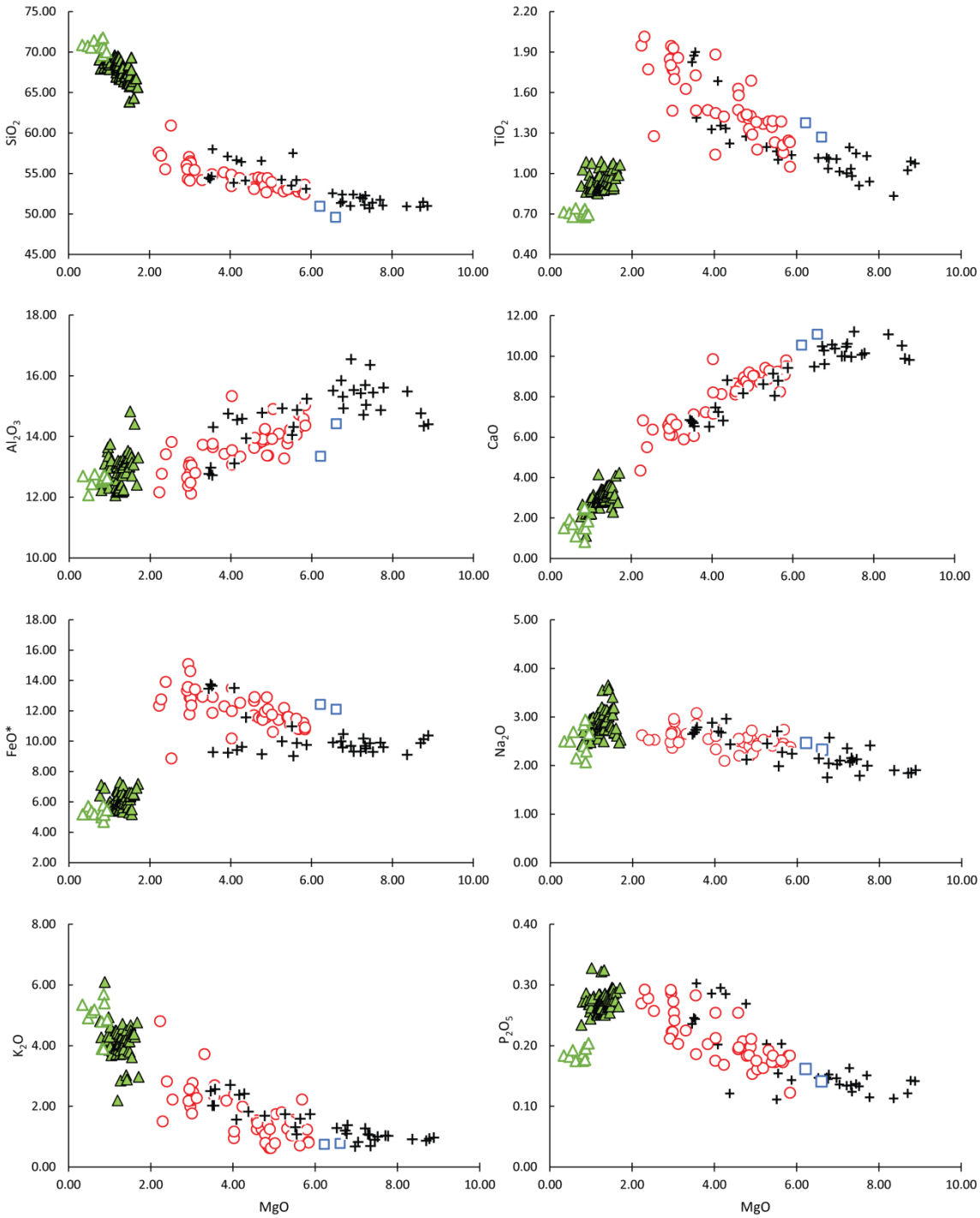

Figura 286 - Elementos maiores na forma de óxidos (%) versus MgO (%) para lavas de baixo-TiO₂ da porção sul da PMPE. Cruzes pretas = Fm. Torres; Círculos Vermelhos = Fm. Vale do Sol; Triângulos verdes = Fm. Palmas, símbolos preenchidos (Membro Santa Maria), e símbolos abertos (Membro Caxias do Sul); Quadrados azuis = Fm. Esmeralda.

Large Ion Litophile Elements (LILE) como Ba, Rb, Pb, apresentam um comportamento similar com uma forte correlação positiva com Zr concentrando-se nos líquidos resíduais com o avanço da cristalização. LILE são facilmente

dissolvidos e remobilizados durante alteração intempérica e metamorfismo (Gill, 1996). Entretanto, a forte correlação positiva entre estes elementos e Zr (HFSe) demonstra que a redistribuição associada a processos de alteração é negligenciável. As abundâncias aumentam gradativamente dos basaltos da FT até os riolitos da FP. Sr apresenta uma distribuição irregular com concentrações variando desde 40 até 500 ppm. As rochas ácidas da FP apresentam as menores variações composicionais e as menores concentrações de Sr (85 - 200 ppm). Nas rochas máficas as variações são de até 150 ppm para uma determinada concentração de Zr. Os conteúdos de Nb apresentam uma forte correlação positiva com Zr, com concentrações variando deste 5 até 30 ppm.

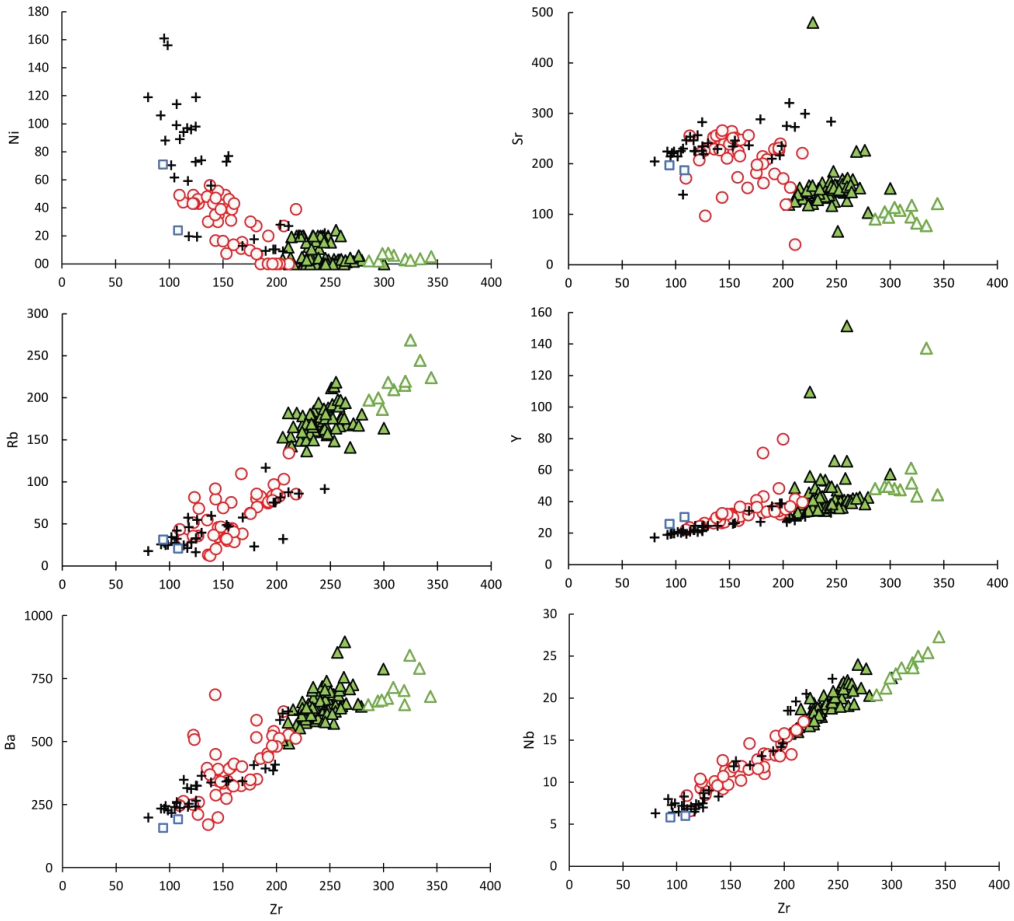

Figura 29 - Concentração de elementos traço (ppm) versus concentrações de Zr (ppm) das lavas da porção sul da* PIPE*. Cruzes pretas = Fm. Torres; Círculos Vermelhos = Fm. Vale do Sol; Triângulos verdes = Fm. Palmas, símbolos preenchidos (Membro Santa Maria), e símbolos abertos (Membro Caxias do Sul); Quadrados azuis = Fm. Esmeralda.

CAPÍTULO 7 - SÍNTESE E CONCLUSÕES

O estudo detalhado da estratigrafia da porção sul da Província Ígnea do Paraná-Etendeka revelou que o Grupo Serra Geral é formado por pacotes heterogêneos de lavas com morfologias, estruturas internas e padrões de empilhamento distintos. Essas variações podem ser mapeadas e fornecem informações diretas sobre a dinâmica de colocação destas lavas em superfície e refletem processos magmáticos associados ao sistema de alimentação das lavas em sub-superficie. Dentre os principais resultados desta presente tese, destacam-se:

- A estratigrafía da porção sul do Paraná-Etendeka no Brasil pode ser dividida em 4 unidades vulcânicas: Formação Torres; Formação Vale do Sol; Formação Palmas; e Formação Esmeralda.
- As diferentes unidades vulcânicas foram formadas durande condições de colocação (*emplacement*) distintos com as fases de ínicio e declínio sendo caracterizadas por derrames compostos do tipo pahoehoe e a fase principal de magmatismo por derrames tabulares espessos de composições mais evoluidas intermediárias e ácidas.
- As sequencias vulcano-sedimentares da Província do Paraná-Etendeka têm porosidades relativamente altas e estas são controladas pelas fácies vulcânicas e alteração hidrotermal/diagenética. As permeabilidades são baixas e refletem tipicamente o preenchimento entre conexões de poros pela precipitação de minerais secundários (p.e. zeólitas)
- A expressão das lavas em superfície refletem processos petrológicos atuantes em subsuperfície e as variações na arquitetura e na pressão de cristalização e fracionamento dos magmas está diretamente relacionada a composição e volume de lavas que atingem a superfície.
- As variações geoquímicas encontradas nas unidades estratigráficas fornecem uma ferramenta importante na correlação de erupções ou eventos eruptivos e estas variações podem ser explicadas por dinamicas de fracionamento distintas.

- A partir de modelos geoquímicos sugere-se que os magmas parentais da Formação Torres foram formados a partir da fusão parcial de um manto astenosférico, em condições de temperatura potencial elevada em relação a temperaturas ambientes do manto. Esses magmas incorporaram porções litosféricas e crustais ao longo de sua evolução. A evolução destes magmas primários poderia originar, a partir de fracionamento e assimilação as rochas da Formação Vale do Sol e Palmas.
- O magmatismo Esmeralda foi Formado por fusão parcial do manto astenosférico em condições relativamente rasas na zona de estabilidade do espinélio no manto superior (< 80km) e estes magmas não sofreram grandes quantidades de contaminação na litosféra.

REFERÊNCIAS

Barreto, C.J.S.C.J.S., de Lima, E.F.E.F., Scherer, C.M.C.M., Rossetti, L. de M.M.L.D.M.M., 2014. Lithofacies analysis of basic lava flows of the Paraná igneous province in the south hinge of Torres Syncline, Southern Brazil. J. Volcanol. Geotherm. Res. 285, 81–99. doi:10.1016/j.jvolgeores.2014.08.008

Barry, T.L., Kelley, S.P., Camp, V., Self, S., Jarboe, N., Duncan, R., 2013. Eruption chronology of the Columbia River Basalt Group. Geol. Soc. Am. Spec. Pap. 2497, 45–66. doi:10.1130/2013.2497(02).

Bellieni, G., Brotzu, P., Comin-Chiaramonti, P., Ernesto, M., Melfi, A., Pacca, I.G., Piccirillo, E.M., 1984. Flood Basalt to Rhyolite Suites in the Southern Paraná, Plateau (Brazil): Palaeomagnetism, Petrogenesis and Geodynamic Implications. J. Petrol. 25, 579–618. doi:10.1093/petrology/25.3.579

Bondre, N.R., Duraiswami, R. a., Dole, G., 2004. Morphology and emplacement of flows from the Deccan Volcanic Province, India. Bull. Volcanol. 66, 29–45. doi:10.1007/s00445-003-0294-x

Branney, M.J., Bonnichsen, B., Andrews, G.D.M., Ellis, B., Barry, T.L., McCurry, M., 2008. “Snake River (SR)-type” volcanism at the Yellowstone hotspot track: distinctive products from unusual, high-temperature silicic super-eruptions. Bull. Volcanol. 70, 293–314. doi:10.1007/s00445-007-0140-7

Brown, R.J., Branney, M.J., 2013. Internal flow variations and diachronous sedimentation within extensive, sustained, density-stratified pyroclastic density currents flowing down gentle slopes, as revealed by the internal architectures of ignimbrites on Tenerife. Bull. Volcanol. 75, 727. doi:10.1007/s00445-013-0727-0

Bryan, S.E., Ernst, R.E., 2008. Revised definition of Large Igneous Provinces (LIPs). Earth-Science Rev. 86, 175–202. doi:10.1016/j.earscirev.2007.08.008

Bryan, S.E., Ferrari, L., 2013. Large igneous provinces and silicic large igneous provinces: Progress in our understanding over the last 25 years. Bull. Geol. Soc. Am. 125, 1053–1078. doi:10.1130/B30820.1

Bryan, S.E., Peate, I.U., Peate, D.W., Self, S., Jerram, D.A., Mawby, M.R., Marsh, J.S. (Goonie), Miller, J.A., 2010. The largest volcanic eruptions on Earth. Earth-Science Rev. 102, 207–229. doi:10.1016/j.earscirev.2010.07.001

Camp, V., Ross, M., Duncan, R.A., Jarboe, N.A., Coe, R.., Hanan, B.B., Johnson, J.A., 2013. The Steens basalt: Earliest lavas of the Columbia River basalt group, in: The Columbia River Flood Basalt Province: Geological Society of America Special Paper 497. p. 87–116. doi:10.1130/2013.2497(04).

Cañón-Tapia, E., 2010. Origin of Large Igneous Provinces: The importance of a definition. What Is a Volcano? 470, 77. doi:10.1130/2010.2470(06)

Chambers, L.M. e Pringle,M. S. (2001). Age and duration of ac- tivity at the Isle ofMull Tertiary igneous centre, Scotland, and confirmation of the existence of subchrons during Anomaly 26r. Earth and Planetary Science Letters 193,333–345

Coffin, M.F., Eldholm, O., 1994. Large igneous provinces: Crustal structure, dimensions, and external

consequences. Rev. Geophys. 32, 1. doi:10.1029/93RG02508

Courtillot, V., Jaupart, C., Manighetti, I., Tapponnier, P., Besse, J., 1999. On casual links between flood basalts and continental breakup. Earth Planet. Sci. Lett. 166, 177–195.

Duraiswami, R.A., Bondre, N.R., Managave, S., 2008. Morphology of rubbly pahoehoe (simple) flows from the Deccan Volcanic Province: Implications for style of emplacement. J. Volcanol. Geotherm. Res. 177, 822–836. doi:10.1016/j.jvolgeores.2008.01.048

Duraiswami, R.A., Gadpallu, P., Shaikh, T.N., Cardin, N., 2014. Pahoehoe-a'a transitions in the lava flow fields of the western Deccan Traps, India-implications for emplacement dynamics, flood basalt architecture and volcanic stratigraphy. J. Asian Earth Sci. 84, 146–166. doi:10.1016/j.jseaes.2013.08.025

Ebinghaus, A., Hartley, A.J., Jolley, D.W., Hole, M., Millett, J., 2014. Lava-Sediment Interaction and Drainage-System Development In A Large Igneous Province: Columbia River Flood Basalt Province, Washington State, U.S.A. J. Sediment. Res. 84, 1041–1063. doi:10.2110/jsr.2014.85

Ellis, D., Bell, B.R., Jolley, D.W., O'Callaghan, M., 2002. The stratigraphy, environment of eruption and age of the Faroes Lava Group, NE Atlantic Ocean. Geol. Soc. London, Spec. Publ. 197, 253–269. doi:10.1144/GSL.SP.2002.197.01.10

Ernesto, M., Pacca, I.G., Hiodo, F.Y., Nardy, a. J.R., 1990. Palaeomagnetism of the Mesozoic Serra Geral Formation, southern Brazil. Phys. Earth Planet. Inter. 64, 153–175. doi:10.1016/0031-9201(90)90035-V

Ernesto, M., Raposo, M.I.B., Marques, L.S., Renne, P.R., Diogo, L. a., De Min, a., 1999. Paleomagnetism, geochemistry and 40Ar/39Ar dating of the North-eastern Parana Magmatic Province: Tectonic implications. J. Geodyn. 28, 321–340. doi:10.1016/S0264-3707(99)00013-7

Ernst, R.E., Buchan, K.L., 2003. Recongnizing mantle plumes in the geological record. Annu. Rev. Earth Planet. Sci. 31, 469–523. doi:10.1146/annurev.earth.31.100901.145500

Ernst, R.E., Buchan, K.L., Campbell, I.H., 2005. Frontiers in Large Igneous Province research. Lithos 79, 271–297. doi:10.1016/j.lithos.2004.09.004

Fitton, J.G., Saunders, A.D., Larsen, L.M., Hardarson, B.S., Norry, M.J., 1998. Volcanic Rocks from the Southeast Greenland Margin at 63°N: Composition, Petrogenisis and Mantle Sources. Proc. Ocean Drill. Program, Sci. Results 152, 331–350. doi:10.2973/odp.proc.sr.152.233.1998

Florisbal, L.M., Heaman, L.M., de Assis Janasi, V., de Fatima Bitencourt, M., 2014. Tectonic significance of the Florianópolis Dyke Swarm, Paraná–Etendeka Magmatic Province: A reappraisal based on precise U–Pb dating. J. Volcanol. Geotherm. Res. 289, 140–150. doi:10.1016/j.jvolgeores.2014.11.007

Frank, H.T., Elisa, M., Gomes, B., Luiz, M., Formoso, L., 2009. Review of the areal extent and the volume of the Serra Geral Formation , Paraná Basin , South America. Pesqui. em Geociencias 36, 49–57.

Gibson, S.A., Thompson, R.N., Dickin, A.P., 2000. Ferropicrites: geochemical evidence for Fe-rich streaks in upwelling mantle plumes. Earth Planet. Sci. Lett. 174, 355–374. doi:10.1016/S0012-821X(99)00274-5

Guilbaud, M.-N., Siebe, C., Layer, P., Salinas, S., Castro-Govea, R., Garduño-Monroy, V.H., Le Corvec,

N., 2011. Geology, geochronology, and tectonic setting of the Jorullo Volcano region, Michoacán, México. J. Volcanol. Geotherm. Res. 201, 97–112. doi:10.1016/j.jvolgeores.2010.09.005

Guilbaud, M., Self, S., Thordarson, T., Blake, S., 2005. Morphology, surface structures, and emplacement of lavas produced by Laki, AD 1783–1784. Geol. Soc. Am. Spec. Pap. 396, 81–102. doi:10.1130/2005.2396(07).

Hole, M.J., Millett, J.M., 2016. Controls of Mantle Potential Temperature and Lithospheric Thickness on Magmatism in the North Atlantic Igneous Province. J. Petrol. 57, 417–436. doi:10.1093/petrology/egw014

Hon, K., Kauahikaua, J., Denlinger, R., Mackay, K., 1994. Emplacement and inflation of pahoehoe sheet flows: observations and measurements of active lava flows on Kilauea volcano, Hawaii. Geol. Soc. Am. Bull. 106, 351–370. doi:10.1130/0016-7606(1994)106<0351:EAIOPS>2.3.CO;2

Hooper, P., 1982. The Columbia river basalts. Science (80-.). 215, 1463–1468.

Janasi, V.D.A., de Freitas, V.A., Heaman, L.H., 2011. The onset of flood basalt volcanism, Northern Paraná Basin, Brazil: A precise U–Pb baddeleyite/zircon age for a Chapecó-type dacite. Earth Planet. Sci. Lett. 302, 147–153. doi:10.1016/j.epsl.2010.12.005

Jay, A.E., Niocaill, C. Mac, Widdowson, M., Self, S., Turner, W., 2009. New palaeomagnetic data from the Mahabaleshwar Plateau, Deccan Flood Basalt Province, India: implications for the volcanostratigraphic architecture of continental flood basalt provinces. J. Geol. Soc. London. 166, 13–24. doi:10.1144/0016-76492007-150

Jerram, D.A., 2002. Volcanology and facies architecture of flood basalts, in: Special Paper 362: Volcanic Rifted Margins. Geological Society of America, p. 119–132. doi:10.1130/0-8137-2362-0.119

Jerram, D. a., Widdowson, M., 2005. The anatomy of Continental Flood Basalt Provinces: geological constraints on the processes and products of flood volcanism. Lithos 79, 385–405. doi:10.1016/j.lithos.2004.09.009

Jerram, D., Mountney, N., Holzförster, F., Stollhofen, H., 1999. Internal stratigraphic relationships in the Etendeka group in the Huab Basin, NW Namibia: understanding the onset of flood volcanism. J. Geodyn. 28, 393–418. doi:10.1016/S0264-3707(99)00018-6

Jolley, D.W., Bell, B.R., 2002. The evolution of the North Atlantic Igneous Province and the opening of the NE Atlantic rift. Geol. Soc. London, Spec. Publ. 197, 1–13. doi:10.1144/GSL.SP.2002.197.01.01

Jolley, D.W., Passey, S.R., Hole, M., Millett, J., 2012. Large-scale magmatic pulses drive plant ecosystem dynamics. J. Geol. Soc. London. 169, 703–711. doi:10.1144/jgs2012-012

Kerr, A.C., 1995. The Geochemical Stratigraphy, Field Relations and Temporal Variation of the Mull-Morvern Tertiary Lava Succession, Nw Scotland. Trans. R. Soc. Edinburgh-Earth Sci. 86, 35–47. doi:doi:10.1017/S0263593300002145

Kerr, A.C., Kent, R.W., Thomson, B.A., Seedhouse, J.K., Donaldson, C.H., 1999. Geochemical Evolution of the Tertiary Mull Volcano, Western Scotland. J. Petrol. 40, 873–908. doi:10.1093/petroj/40.6.873

Keszthelyi, L., Self, S., Thordarson, T., 2006. Flood lavas on Earth, Io and Mars. J. Geol. Soc. London. 163, 253–264. doi:10.1144/0016-764904-503

Keszthelyi, L., Thordarson, T., McEwen, A., Haack, H., Guilbaud, M.-N., Self, S., Rossi, M.J., 2004. Icelandic analogs to Martian flood lavas. Geochemistry, Geophys. Geosystems 5, 1–32. doi:10.1029/2004GC000758

Larsen, L.M., Pedersen, A.K., 2009. Petrology of the paleocene picrites and flood basalts on disko and nuussuaq, West Greenland. J. Petrol. 50, 1667–1711. doi:10.1093/petrology/egp048

Larsen, L. M., Pedersen, A. K., Tegners, C., Duncan, R. A., Hald, N. & Larsen, J. G. (2015). Age of Tertiary volcanic rocks on the West Greenland continental margin: volcanic evolution and event correlation to other parts of the North Atlantic Igneous Province. Geological Magazine doi:10.1017/S0016756815000515.

Larsen, L.M., Waagstein, R., Pedersen, A.K., M., S., 1999. Trans-Atlantic correlation of the Palaeogene volcanic successions in the Faeroe Islands and East Greenland. J. Geol. Soc. London. 156, 1081–1095. doi:10.1144/gsjgs.156.6.1081

Lima, E.F. De, Waichel, B.L.B.L., Rossetti, L.D.M.M., Viana, A.R., Scherer, C.M.C.M., Bueno, G.V.G. V., Dutra, G., De Lima, E.F., Waichel, B.L.B.L., De Magalhães May Rossetti, L., Viana, A.R., Scherer, C.M.C.M., Bueno, G.V.G. V., Dutra, G., 2012. Morphological and petrographic patterns of the pahoehoe and “a”ā flows of the Serra Geral Formation in the Torres Syncline (Rio Grande do Sul state, Brazil). Brazilian J. … 42, 744–753. doi:10.5327/Z0375-75362012000400007

Luchetti, A.C.F., Gravley, D.M.,Gualda, G.A.R.,Nardy, A.J.R.,2017. Textural evidence for high-grade ignimbrites formed by low-explosivity eruptions, Paraná Magmatic Province, southern Brazil. J. Volcanol. Geotherm. Res. in press.

Macdonald G.A., (1953) Pahoehoe, a'a, and block lava. Am J Sci 251:169-191

Manley CR, McIntosh WC (2002) The Juniper Mountain Volcanic Center, Owyhee County, Southwestern Idaho: age relations and physical volcanology. In: Bonnichsen B, White CM, McCurry M (eds) Tectonic and magmatic evolution of the Snake River Plain Volcanic Province. Idaho Geol Surv Bull 30:205–227

McPhie, J., 1993. Volcanic Textures: a Guide to the Interpretation of Textures in Volcanic Rocks. Hobart, CODES Key Centre, University of Tasmania, p. 196.

Milani, E.J., Henrique, J., Melo, G. De, Souza, P.A. De, Fernandes, L.A., França, A.B., 2007. Bacia do Paraná. Bol. Geociências da Petrobras 15, 265–287.

Milner, S.C., Duncan, A.R., Ewart, A., 1992. Quartz latite rheoignimbrite flows of the Etendeka Formation, north-western Namibia. Bull. Volcanol. 54, 200–219. doi:10.1007/BF00278389

Passey, S.R., Jolley, D.W., 2008. A revised lithostratigraphic nomenclature for the Palaeogene Faroe Islands Basalt Group, NE Atlantic Ocean. Earth Environ. Sci. Trans. R. Soc. Edinburgh 99, 127–158. doi:10.1017/S1755691009008044

Peate, D., 1997. The Paraná-Etendeka Province. Large igneous Prov. Cont. Ocean. Planet. flood Volcanism 100, 217–245.

Peate, D., Hawkesworth, C., Mantovani, M., 1992. Chemical stratigraphy of the Paraná lavas (South America): classification of magma types and their spatial distribution. Bull. Volcanol. 55, 119–139.

Peate, D., Hawkesworth, C., Mantovani, M., Rogers, N.W., Turner, S., 1999. Petrogenesis and stratigraphy of the high-Ti/Y Urubici magma type in the Paraná flood basalt province and

implications for the nature of “Dupal”-type mantle in the. J. Petrol. 40, 451–473.

Piccirillo, E.M., Melfi, A.J., 1988. The Mesozoic flood volcanism from the Paraná Basin (Brazil): petrogenetic and geophysical aspects. Universidade de São Paulo, São Paulo.

Pinkerton, H., Sparks, R.S.J., 1976. The 1975 sub-terminal lavas, mount etna: a case history of the formation of a compound lava field. J. Volcanol. Geotherm. Res. 1, 167–182. doi:10.1016/0377-0273(76)90005-6

Raposo, M.I.B., Ernesto, M., Renne, P.R., 1998. Paleomagnetism and 40Ar/39Ar dating of the early Cretaceous Florianópolis dike swarm (Santa Catarina Island), Southern Brazil. Phys. Earth Planet. Inter. 108, 275–290. doi:http://dx.doi.org/10.1016/S0031-9201(98)00102-2

Reidel, S., 2005. A lava flow without a source: The Cohassett flow and its compositional components, Sentinel Bluffs Member, Columbia River Basalt Group. J. Geol. 113, 1–21.

Reidel, S., Tolan, T., 1992. Eruption and emplacement of flood basalt: An example from the large-volume Teepee Butte Member, Columbia River Basalt Group. Geol. Soc. Am. … 1650–1671.

Reidel, S.P., Camp, V.E., Tolan, T.L., Martin, B.S., 2013. The Columbia River flood basalt province: Stratigraphy, areal extent, volume, and physical volcanology. Geol. Soc. Am. Spec. Pap. 497, 1–43. doi:10.1130/2013.2497(01).

Reidel, S.P., Fecht, K.R., Hagood, M.C., Tolan, T.L., 1989. The geologic evolution of the central Columbia Plateau. Volcanism Tectonism Columbia River Flood-Basalt Prov. 247–264. doi:10.1130/SPE239-p247

Reidel, S.P., Tolan, T.L., 2013. The late Cenozoic evolution of the Columbia River system in the Columbia River flood basalt province. Geol. Soc. Am. Spec. Pap. 497, 201–230. doi:10.1130/2013.2497(08)

Reidel, S.P.S., 1982. Stratigraphy of the Grande Ronde Basalt , Columbia River Basalt Group , From the Lower Salmon River and Northern Hells Canyon Area, Idaho, Oregon and Washington, in: Bonnichsen, B., Breckenridge, R.M. (Orgs.), Cenozoic Geology of Idaho: Idaho Bureau of Mines and Geology Bulletin 26. Idaho Bureau of Mines and Geology, p. 77–101.

Renne, P.R., Ernesto, M., Pacca, I.G., Coe, R.S., Glen, J.M.G., Prevot, M., Perrin, M., 1992. The Age of Parana Flood Volcanism, Rifting of Gondwanaland, and the Jurassic-Cretaceous Boundary. Science (80-.). 258, 975–979. doi:10.1126/science.258.5084.975

Ross, P.-S., Ukstins Peate, I., McClintock, M.K., Xu, Y.G., Skilling, I.P., White, J.D.L., Houghton, B.F., 2005. Mafic volcaniclastic deposits in flood basalt provinces: A review. J. Volcanol. Geotherm. Res. 145, 281–314. doi:10.1016/j.jvolgeores.2005.02.003

Rossetti, L., Lima, E.F., Waichel, B.L., Hole, M.J., Simões, M.S., Scherer, C.M.S., 2017. Lithostratigraphy and volcanology of the Serra Geral Group, Paraná-Etendeka Igneous Province in Southern Brazil: Towards a formal stratigraphical framework. J. Volcanol. Geotherm. Res. in press. doi:10.1016/j.jvolgeores.2017.05.008

Rossetti, L.M.L.M., Lima, E.F.E.F., Waichel, B.L.B.L., Scherer, C.M.C.M., Barreto, C.J.C.J., 2014. Stratigraphical framework of basaltic lavas in Torres Syncline main valley, southern Parana-Etendeka Volcanic Province. J. South Am. Earth Sci. 56, 409–421. doi:10.1016/j.jsames.2014.09.025

Rowland, S.K., Walker, G.P., 1990. Pahoehoe and aa in Hawaii: volumetric flow rate controls the lava structure. Bull. Volcanol. 52, 615–628. doi:10.1007/BF00301212

Scherer, C.M.S., 2002. Preservation of aeolian genetic units by lava flows in the Lower Cretaceous of the Paran Basin, southern Brazil. Sedimentology 49, 97–116. doi:10.1046/j.1365-3091.2002.00434.x

Self, S., Jay, A., Widdowson, M., Keszthelyi, L., 2008. Correlation of the Deccan and Rajahmundry Trap lavas: Are these the longest and largest lava flows on Earth? J. Volcanol. Geotherm. Res. 172, 3–19. doi:10.1016/j.jvolgeores.2006.11.012

Self, S., Keszthelyi, L., Thordarson, T., 1998. The Importance of Pahoehoe. Annu. Rev. Earth Planet. Sci. 26, 81–110. doi:10.1146/annurev.earth.26.1.81

Self, S., Thordarson, T., Keszthelyi, L., 1997. Emplacement of Continental Flood Basalt Lava Flows, Large igneous provinces: Continental, oceanic, and Planetary Flood Volcanism, Geophysical Monograph Series. American Geophysical Union, Washington, D. C. doi:10.1029/GM100

Self, S., Thordarson, T., Keszthelyi, L., Walker, G.P.L., Hon, K., Murphy, M.T., Long, P., Finnemore, S., 1996. A new model for the emplacement of Columbia River basalts as large, inflated Pahoehoe Lava Flow Fields. Geophys. Res. Lett. 23, 2689–2692. doi:10.1029/96GL02450

Sheth, H.C., 2007. 'Large Igneous Provinces (LIPs)': definition, rec- ommended terminology, and a hierarchical classification. Earth- Sci Rev 85:117–124

Single, R., Jerram, D., 2004. The 3D facies architecture of flood basalt provinces and their internal heterogeneity: examples from the Palaeogene Skye Lava Field. J. Geol. Soc. London. 161, 911–926.

Swanson, D., 1979. Revisions in stratigraphic nomenclature of the Columbia River Basalt Group. Geol. Surv. Bull.

Thiede, D., Vasconcelos, P., 2010. Paraná flood basalts: Rapid extrusion hypothesis confirmed by new 40Ar/39Ar results. Geology 747–750. doi:10.1130/G30919.1

Thordarson, T., Self, S., 1993. The Laki (Skaftar Fires) and Grimsvotn eruptions in 1783– 1785. Bulletin of Volcanology 55, 233–263. doi:10.1007/BF00624353

Thordarson, T., Self, S., 1998. The Roza Member, Columbia River Basalt Group: A gigantic pahoehoe lava flow field formed by endogenous processes? J. Geophys. Res. Solid Earth 103, 27411–27445. doi:10.1029/98JB01355

Tolan, T.L., Reidel, S.P., Beeson, M., Anderson, J.L., Fecht, K., Swanson, D.A., 1989. Revisions to the estimates of the areal extent and volume of the Columbia River Basalt Group. Geol. Soc. Am. Spec. Pap. 239, 1–20.

Waichel, B., Scherer, C., Frank, H., 2008. Basaltic lava flows covering active aeolian dunes in the Paraná Basin in southern Brazil: Features and emplacement aspects. J. Volcanol. Geotherm. Res. 171, 59–72. doi:10.1016/j.jvolgeores.2007.11.004

Waichel, B.L., de Lima, E.F., Lubachesky, R., Sommer, C.A., 2006. Pahoehoe flows from the central Paraná Continental Flood Basalts. Bull. Volcanol. 68, 599–610. doi:10.1007/s00445-005-0034-5

Waichel, B.L., de Lima, E.F., Viana, A.R., Scherer, C.M., Bueno, G. V., Dutra, G., 2012. Stratigraphy and volcanic facies architecture of the Torres Syncline, Southern Brazil, and its role in

understanding the Paraná–Etendeka Continental Flood Basalt Province. J. Volcanol. Geotherm. Res. 215–216, 74–82. doi:10.1016/j.jvolgeores.2011.12.004

Walker, G.P.L., 1971. Compound and simple lava flows and flood basalts. Bull. Volcanol. 35, 579–590. doi:10.1007/BF02596829

Watton, T.J., Jerram, D. a., Thordarson, T., Davies, R.J., 2013. Three-dimensional lithofacies variations in hyaloclastite deposits. J. Volcanol. Geotherm. Res. 250, 19–33. doi:10.1016/j.jvolgeores.2012.10.011

White, J., Bryan, S., Ross, P., 2009. Physical volcanology of continental large igneous provinces: update and review, in: Thordarson, T., Self, S., Larsen, G., Rowland, S.K., Hoskuldsson, A. (Org.), Studies in Volcanology: The Legacy of George Walker. Special Publications of IAVCEI, 2. Geological Society, London. p. 291–321.

Williamson, I.T., Bell, B.R., 2012. The Staffa Lava Formation: graben-related volcanism, associated sedimentation and landscape character during the early development of the Palaeogene Mull Lava Field, NW Scotland. Scottish J. Geol. 48, 1–46. doi:10.1144/0036-9276/01-439

Wright, T., 1973. Chemical variation related to the stratigraphy of the Columbia River basalt. Geol. Soc. Am. Bull. 371–385.

Zou, C. (2013). Volcanic reservoirs. Elsevier, USA.

Anexo I

Lithostratigraphy and volcanology of the Serra Geral Group, Paraná-Etendeka Igneous Province in Southern Brazil: Towards a Formal Stratigraphical Framework"

Journal of Volcanology and Geothermal Research 355 (2018) 98–114

Contents lists available at ScienceDirect

Journal of Volcanology and Geothermal Research

journal homepage: www.elsevier.com/locate/jvolgeores

Lithostratigraphy and volcanology of the Serra Geral Group, Paraná-Etendeka Igneous Province in Southern Brazil: Towards a formal stratigraphical framework

Lucas Rossetti [a,b,*], Evandro F. Lima [b], Breno L. Waichel [c], Malcolm J. Hole [a], Matheus S. Simões [b,d], Claiton M.S. Scherer [b]

[a] Department of Geology and Petroleum Geology, University of Aberdeen, AB24 3UE Aberdeen, United Kingdom
[b] Instituto de Geociências, Universidade Federal do Rio Grande do Sul, Av. Bento Gonçalves, 9500, Prédio 43136, Caixa Postal 15001, Agronomia, 91501-970 Porto Alegre, RS, Brazil
[c] Universidade Federal de Santa Catarina e UFSC, Campus Universitário Trindade, 88.040-900 Florianópolis, SC, Brazil
[d] CPRM – Serviço Geológico do Brasil (Geological Survey of Brazil) – Manaus, Av. André Araújo, 2160, 69060-000, AM, Brazil

ARTICLE INFO

Article history:
Received 29 July 2016
Received in revised form 21 April 2017
Accepted 8 May 2017
Available online 13 May 2017

Keywords:
Paraná-Etendeka Igneous Province
Stratigraphy of LIP
Basalt
Volcanology
Lava emplacement

ABSTRACT

The volcanic rocks of the Lower Cretaceous Paraná-Etendeka Igneous Province, in Brazil, are grouped in the Serra Geral Group. The province can be chemically divided into low-TiO_2, and high-TiO_2. In southern Brazil, the low-TiO_2 lava pile reaches a thickness of ~1 km and is formed of heterogeneous lava packages here divided into four lava formations. Torres Formation (TF) is characterized by chemically more primitive basaltic (>5 wt% MgO) compound pahoehoe flow fields; these lavas stratigraphically overly aeolian sandstones of Botucatu Formation and represent the onset of the volcanic activity. Vale do Sol Formation (VSF) groups vertically stacked sheet-like rubbly pahoehoe basaltic andesites (SiO_2 > 51 wt%; MgO < 5 wt%). These lavas covered the former basalts in the Torres Syncline axis and pinch out towards southwest and represent the most voluminous mafic lava flows. Dacites and rhyolites of Palmas Formation (PF) overlay VSF flows in the central and eastern outcrop area and rest directly upon TF lavas in the west. The acidic units were emplaced as lava domes and widespread tabular lava flows. Esmeralda Formation (EF) is the upper stratigraphic unit and it is formed by a basaltic pahoehoe flow field emplaced during the waning phase of volcanic activity of the low-TiO_2 lava sequence. Sedimentary interbeds are preserved throughout the whole lava pile and were deposited during quiescence periods of volcanic activity, and represent important stratigraphic markers (e.g. TF-VSF contact). The newly proposed stratigraphy provides promptly recognized stratigraphic units in a regional framework of fundamental importance for future correlations and provide vital information in the understanding of how the Paraná-Etendeka Igneous Province evolved through time.

1. Introduction

The Paraná-Etendeka Igneous Province (PEIP) represents a major magmatic event of the Lower Cretaceous and precedes the fragmentation of southern Gondwana and opening of the South Atlantic Ocean. The province covers 1.2 × 10^6 km^2 mostly over South America continent, and in its counterparts in Africa (Cordani and Vandoros, 1967; Peate, 1997). The lava pile is formed mainly of basalts and basaltic andesites (97.5%) with minor quantities of acidic rocks (2.5%). The volcanic succession can be roughly divided into two major sectors (1) in the south, low-TiO_2 (also called low-Ti/Y) lava field and (2) a north, high-TiO_2 (also called high-Ti/Y) lava field (Bellieni et al., 1984b; Peate, 1997). A stratigraphy based on magma types and their spatial distribution provides a regional framework suggesting that the volcanic activity migrated northwards (Peate et al., 1992). Recently, a volcanological approach provided important evidence that the lava packages changed their morphologies and architecture throughout the different phases of volcanic evolution (Waichel et al., 2012; Rossetti et al., 2014). Nonetheless, the stratigraphical position and its correlation with the existing chemical stratigraphy is not well documented.

When compared with other LIP's such as Deccan, Columbia River, NAIP, and with its conjugated margin in Namibia, the stratigraphy of Paraná-Etendeka LIP in Brazil is poorly understood. The short time duration (135 to 131 Ma) allied to the dry climate during the lower Cretaceous inhibited the formation of paleosoil horizons, resulting in an absence of ubiquitous stratigraphic markers.

To better define the stratigraphy of LIP events it is important to (1) delimit products of single eruptions, eruptive events or lava packages

* Corresponding author at: Department of Geology and Petroleum Geology, University of Aberdeen, AB24 3UE Aberdeen, United Kingdom.
E-mail address: l.rossetti@abdn.ac.uk (L. Rossetti).

http://dx.doi.org/10.1016/j.jvolgeores.2017.05.008
0377-0273/

(e.g. Roza Member Columbia River Flood Basalts - Thordarson and Self, 1998); (2) recognize and map stratigraphical horizons such as volcanic unconformities and sedimentary beds (Jerram et al., 1999; Passey and Bell, 2007; Passey and Jolley, 2008); (3) understand chemical variations within the lava pile (Cox and Hawkeshworth, 1985; Peate et al., 1992; Hooper, 2000) and its paleomagnetic characteristics (Jay et al., 2009). The greatest success is achieved where a combination of approaches is used (Bryan et al., 2010).

The absence of a formal stratigraphy and a proper delimitation of the lava units difficult the correlation of existing data in the PEIP, in special the correlation of paleomagnetic, chemical and volcanological units. This work proposes a formal lithostratigraphy following the recommendations of the *International Stratigraphic Code* (Salvador, 1994). The units were divided based on their volcanic architecture, lava morphologies, petrographic characteristics, stratigraphical position, and distribution, together with a proper delimitation of unit boundaries and stratigraphical markers. We also present a correlation of the new stratigraphy with existing paleomagnetic data (Ernesto et al., 1990; Ernesto and Pacca, 1988) and the chemical stratigraphy (Peate et al., 1992; Peate, 1997) and its implications for the volcanic evolution of southern PEIP. The main goal is to define the characteristics of each lava unit, promptly identifiable in field basis, providing a refined stratigraphy with local and regional stratigraphic markers (key surfaces) to be used as a guide to future correlations.

1.1. Terminology and nomenclature

The majority of LIP's in special Continental Flood Basalts (CFB's) lavas are described based on their facies architecture. According to Jerram (2002), the lava packages are grouped in two major facies: (1) a tabular classic facies, where tabular 'sheet-like' lava flows are vertically stacked, giving a step-like morphology to the deposits; and (2) compound braided facies formed by a series of anastomosing small flow lobes. This classification scheme is based on the classic terms 'simple' and 'compound' introduced by Walker (1971) to describe the flood basalts of the Deccan Province. Other descriptive terms adopted from Self et al. (1997) are here used to describe internal features within the lava units and lava packages, those are flow fields, lava flows, and flow lobes. *Flow fields* are aggregate products of a single eruption and are formed by one or more lava flows; *lava flow* is the product of a single and continuous outpouring of lava, and *flow lobe* is a single set of lava surrounded by chilled margins.

2. The Paraná-Etendeka Igneous Province

The Lower Cretaceous (Valanginian - Hauterivian) Paraná-Etendeka Igneous Province (PEIP, Fig. 1) represents a large volume of subaerial lavas, dike swarms, and other intrusive igneous rocks, which are mainly of tholeiitic affinity. The volcanic pile is distributed over central South America (Brazil, Argentina, Uruguay, and Paraguay) and a small part of southwestern Africa, in Namibia and Angola. In Brazil, the volcanic rocks are stratigraphically referred as Serra Geral Formation. The lava pile is in average 700 m thick reaching 1.750 m in the central north portion of the basin (Piccirillo and Melfi, 1988), covers an area of 917,000 km^2 over Paraná basin sediments and reach volumes, including intrusive bodies, of at least 600,000 km^3 (Frank et al., 2009). In Namibia, the Etendeka Lava group spreads over an area of 0.8×10^5 km^2 (Erlank et al., 1984) and in Kwanza basin, Angola, a similar area is also covered by Cretaceous volcanic rocks associated with PEIP (Marzoli et al., 1999). The volcano-stratigraphy of the main Etendeka succession is composed of two major units separated by a regional disconformity the Awahab and the Tafelberg Formations (Milner et al., 1995; Jerram et al., 1999). The Awahab Formation is formed of olivine-phyric pahoehoe lavas, covered by thick, tabular basaltic-andesites. The Tafelberg formation is formed of tabular basaltic-andesites and thick silicic units (Jerram et al., 1999) that can be correlated with acidic units in the Parana (Milner et al., 1995). Extensive dike swarms occur along the coastal areas of Brazil, Angola, and Namibia and represent the preserved plumbing systems that fed the flood basalts (Raposo et al., 1998; Florisbal et al., 2014).

In the Parana, a regional stratigraphy has been built based on the succession and regional distribution of magma types. In the south a low-TiO_2 (Ti/Y < 310) succession of lavas is characterized by Gramado magma type basalts overlaid by Palmas dacites and rhyolites. At the top of the lava sequence basalt lavas of Esmeralda magma type (Peate et al., 1992; Peate, 1997). High-TiO_2 lavas (Urubici type) occur as a small strip (~100 km × 350 km) along the northeast limit of the lava escarpment in the south of Brazil and are contemporaneous and interbedded with Gramado lava flows (Peate et al., 1999). The northern high-TiO_2 (Ti/Y > 310) lavas are characterized by Ribeira, Pitanga and Paranapanema magma type basalts, respectively (Peate, 1997), covering the low-TiO_2 sequence towards north and west. Acidic volcanics occur in the lower portion of the high-TiO_2 lava pile covering the basement in the north or covering the top low-TiO_2 lavas in the central Paraná (Piccirillo et al., 1987; Peate et al., 1990; Janasi et al., 2007). The volcanic pile as a whole shows a northward migration with younger magma types thicker in the north and thinning southwards (Peate et al., 1992) (Fig. 2).

Isotopic ages constrain the majority of the magmatic activity to a 4 Ma interval during Lower Cretaceous, from 135 to 131 Ma (recalculated $^{40}Ar/^{39}Ar$ ages from Janasi et al., 2011). The volcanic activity started in the southern portion of the province and the ages are clustered between 134.1 and 134.8 Ma ($^{40}Ar/^{39}Ar$ step-heating - Renne et al., 1992; Thiede and Vasconcelos, 2010). In the northern province high-TiO_2 lavas and associated intrusive bodies have slightly younger ages, ranging 131.5–133.6 Ma ($^{40}Ar/^{39}Ar$ step-heating - Ernesto et al., 1999). A precise age of 134 ± 0.8 (U-Pb in baddeleyite) was obtained in a Chapecó dacite, this lava unit occurs covering the low-TiO_2 lavas, and was later covered by the younger high-TiO_2 basalts (Janasi et al., 2011). This new age represents an important stratigraphical marker and confirms a relatively rapid formation for the southern lava pile (~1 Ma). Paleomagnetic data from Namibia, based on the number of reversions in the magnetic field (16 individual polarity intervals), also points to a duration of at least 4 Ma for the emplacement of the entire lava pile (Dodd et al., 2015).

Waichel et al. (2012) divided the southern low-TiO_2 sequence in the Torres Syncline area into five volcanic episodes based on the architecture and volcanic structures of the lava fields. The first lavas are compound pahoehoe flows grouped in the Basaltic Volcanic Event I (BVEI), the flows tend to be thicker and extensive towards the top of the lava succession and were then grouped in the Basaltic Volcanic Event (BVEII). The contact of BVEI and BVEII is arbitrary and the occurrence of compound flows is not restricted to the first unit, and it seems likely that the thicker flows are larger lobes and not necessarily 'simple' flows (individual cooling units). The Basaltic Volcanic Event III comprise aa/rubbly pahoehoe lava units. Waichel et al. (2012) also recognized two different acidic volcanic episodes, the first formed of dome-like flows and the second formed of extensive tabular flow units. On a more local geographical scale, geochemical and volcanological data reveal that the volcanic succession was heterogeneous and that the volcanic episodes described by Waichel et al. (2012) were not well constrained stratigraphically (Barreto et al., 2014; Rossetti et al., 2014). Consequently, here it is considered necessary to review and redefined the stratigraphical units. (See Table 1.)

3. Lithostratigraphy of the Serra Geral Group in southern Brazil

The outcrop area is located in the south limit of the Paraná-Etendeka Igneous Province in southern Brazil (29°35′–27°00′S and, 55°6′–49°31′ W – Fig.3). Data collection and logged sections were mainly focused in the south escarpment of the lava field. The escarpment is cut by several road profiles that expose great part of the volcanic stratigraphy, and it

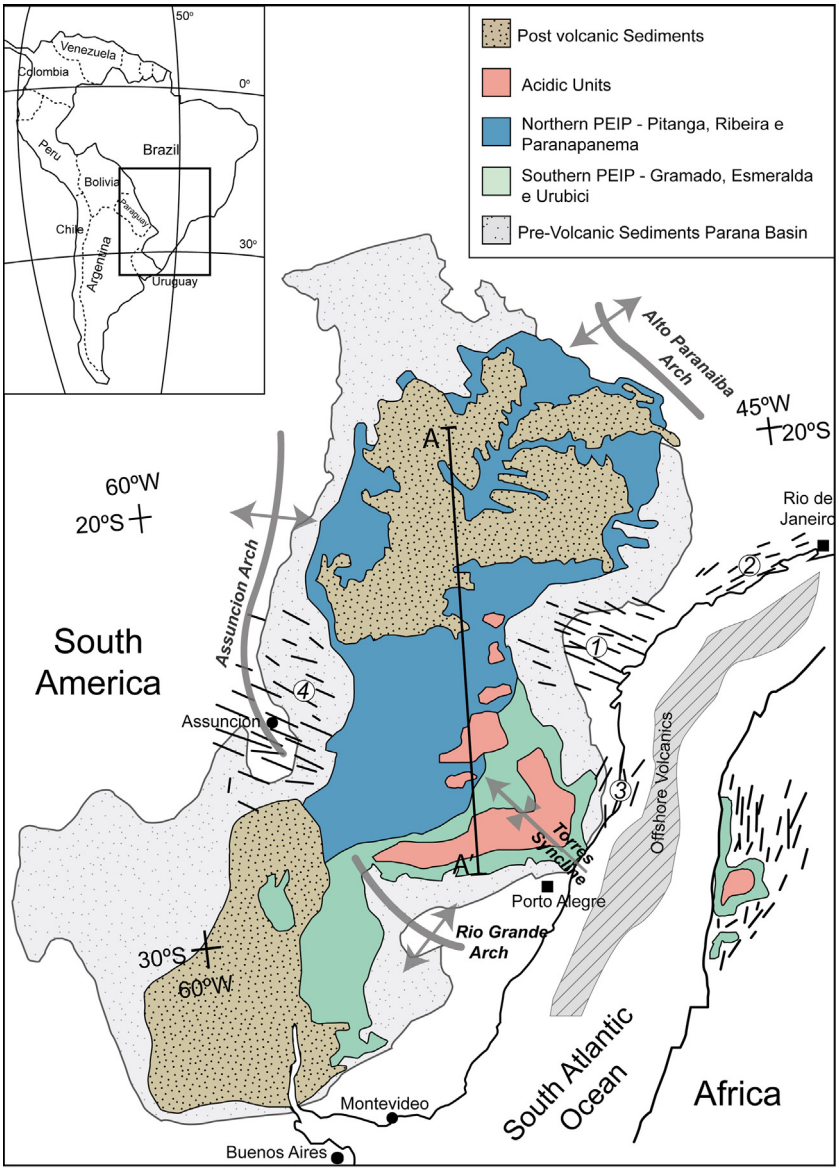

Fig. 1. Distribution of the Paraná-Etendeka Igneous Province and main tectonic structures in a pre-drift reconstruction (modified after Peate et al., 1992; Stewart et al., 1996; Hawkesworth et al., 2000). Dike swarms: 1 - Ponta Grossa; 2 – Santos-Rio de Janeiro; 3 – Florianopolis; 4 – Paraguay.

was at these locations that a comprehensive set of geochemical, mineral chemical and paleomagnetic data were generated in the 80's and 90's (Bellieni et al., 1984a, 1986; Ernesto and Pacca, 1988; Mantovani et al., 1988; Peate et al., 1992). The area is limited at north and northwest by the overlaying high-TiO_2 volcanic sequence, at east and southeast by an erosional limit associated with the Serra do Mar and Rio Grande Arc uplifts, respectively. A simplified stratigraphic distribution of the logged sections is presented in Fig. 3B.

The lithostratigraphy was built following the recommendations of the International Subcommission on Stratigraphic Classification and the published International Stratigraphical Guide (Salvador, 1994). The proposed formations were also named according to these recommendations, i.e. when a given formation is the unique correspondent of an existing magma type, the name of the latter was kept (e.g. Palmas and Esmeralda). Conversely, the Gramado magma type does not represent a single stratigraphic unit; therefore new names (Torres and Vale do Sol) were proposed to avoid further uncertainty and misinterpretation. The lava pile can be divided into four different lava packages, which was deposited on top of the Botucatu Formation sandstones. The volcanic units differ in architecture, internal flow field structure, textures and composition, and the main characteristics are highlighted in Table 2. The proposed stratigraphical nomenclature is Torres, Vale do Sol, Palmas, and Esmeralda formations. It is further recommended that the former Serra Geral Formation should be upgraded to Serra Geral Group (a term already informally used - Comin-Chiaramonti et al., 2010; Pinto and Hartmann, 2011; Arena et al., 2014).

Torres Formation (TF) lavas are chemically more primitive compound pahoehoe flow fields; these lavas generally stratigraphically overly aeolian sandstones of Botucatu Formation (Fig. 4A). The Vale do Sol Formation (VSF) is characterized by the stacking of tabular sheet-like rubbly pahoehoe lavas dominantly basaltic andesitic in composition that covered the pahoehoe flow fields of Torres Formation (Fig. 4B). The upper part of the lava pile is characterized by tabular flows of dacitic to rhyolitic composition here defined as the Palmas Formation (PF). These lavas mainly overly VSF flows (Fig. 4C and D); although in the western limit of the lava pile they are deposited directly over the pahoehoe flow fields of TF. Esmeralda Formation (EF) is a pahoehoe flow field that covers the acidic flows of the Palmas Formation, and locally the basaltic rocks of VSF in the north portion of the area. The occurrence and

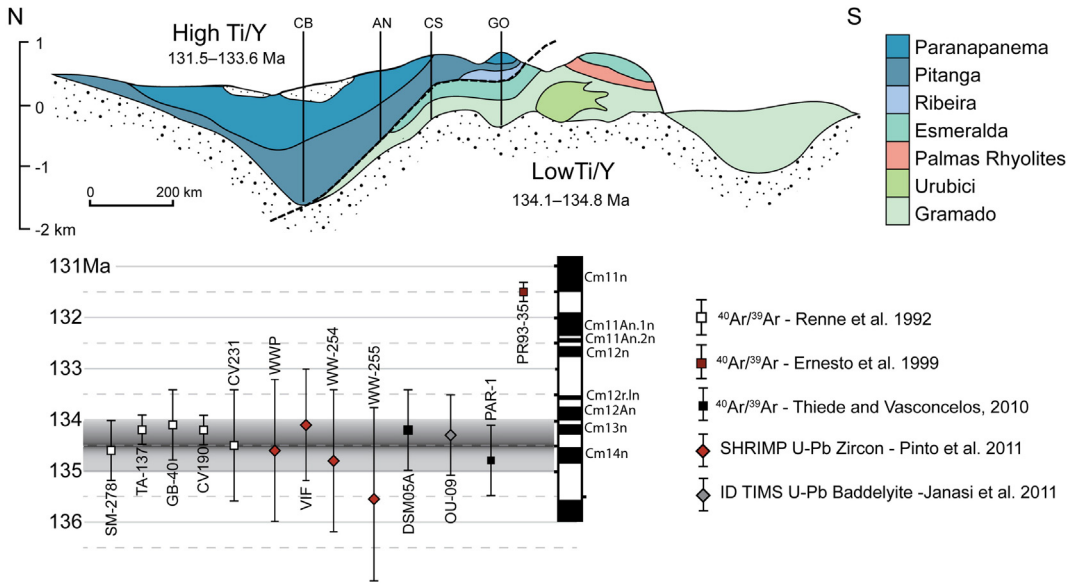

Fig. 2. Chemical stratigraphy and distribution of magma types based on well data (CB, AN, CS, and GO). Southern sub-province: Gramado, Esmeralda, Urubici magma types; Northern sub-province: Ribeira, Pitanga and Paranapanema magma types (modified after Peate, 1997); and distribution of radiometric ages with majority of samples constrained in the 134.5 ± 0.5 Ma (Renne et al., 1992; Ernesto et al., 1999; Thiede and Vasconcelos, 2010; Pinto et al., 2011; Janasi et al., 2011).

main characteristics of each volcanic package are presented in Table 2 and described in detail in the following sections.

3.1. Torres Formation (TF)

Torres Formation is here named after the coastal exposures that occur in the cliffs of Torres beach, in the northeast Rio Grande do Sul state. The basalts of TF are equivalent to the tholeiitic basalts described by Bellieni et al. (1984a), lower portion of Gramado magma type lavas (Peate et al., 1992), compound lavas from *Basic Volcanic Episode I* and part of the tabular flows in the *Basic Volcanic Episode II* (Waichel et al., 2012). This unit has been mapped in detail in two distinct areas and referred as early compound pahoehoe flows by Barreto et al. (2014) and Unit I (Rossetti et al., 2014).

The formation represents the lower portion of the volcanic succession and it is widespread along the south limit of the outcrop area. The basal boundary of the TF is a sharp contact between basalt and sandstone generally controlled by the topography of the paleo-dune fields. Preserved ripple marks and scours, formed by the advance of lava lobe on the dune surface, have been identified by Waichel et al. (2008), and features of lava-sediment interaction, such as peperites, are also preserved close to the contact of the formations (Jerram and Stollhofen, 2002; Petry et al., 2007).

Individual flow fields are formed by lava toes (<0.5 m), lobes (0.5–2.5 m) and thicker sheet-like lobes (Fig. 5A) with a complex vertical stacking that define a compound braided facies architecture (Fig. 4A). The internal structure typically displays (1) a lower crust with pipe vesicles (<1 m in thickness – Fig. 6D); (2) a massive core, with segregation structures such as vesicle cylinders and vesicle sheets (lobes >5 m thick); (3) a vesicular upper crust with gradual decrease in vesicle sizes towards the flow top (Fig. 6E). The contacts of lobes are marked by chilled and oxidized margins (Fig. 6A and B) and lobe surface is generally smooth or ropey (Fig. 6C). Sheet lobes are characterized by widespread (10–100's of meters) flow lobes with a thickness varying from 5 to 12 m, in general, and reaching 18 m. Inflation clefts are found within the flow fields and are mainly 0.5–1 m deep and filled with sandstone or by the overlying lava flow (Fig. 6F). Flow field limits are usually highlighted by the presence of aeolian sandstones occurring as discontinuous inter-basaltic beds (Fig. 7A and B).

Within the lava pile cross-bedded laminated sandstones are interbedded with the lavas. The thicker sedimentary units are preserved in

Table 1
The new lithostratigraphic framework for the southern Paraná-Etendeka volcanic rocks, and previous stratigraphical sub-divisions.

Bellieni et al. 1984		Peate et al. 1992		Waichel et al. 2012		This study	
Parana Plateau		Serra Geral Formation	Esmeralda	Serra Geral Formation		Serra Geral Group	Esmeralda Formation
	Rhyolites and Rhyodacites		Palmas		Acidic Volcanic Episode II Acidic Volcanic Episode I		Palmas Formation
	Tholeitic Andesites		Gramado		Basic Volcanic Episode III		Vale do Sol Formation
	Tholeitic Basaltic Andesites Tholeitic Basalts				Basic Volcanic Episode II		
					Basic Volcanic Episode I		Torres Formation
Botucatu Formation							

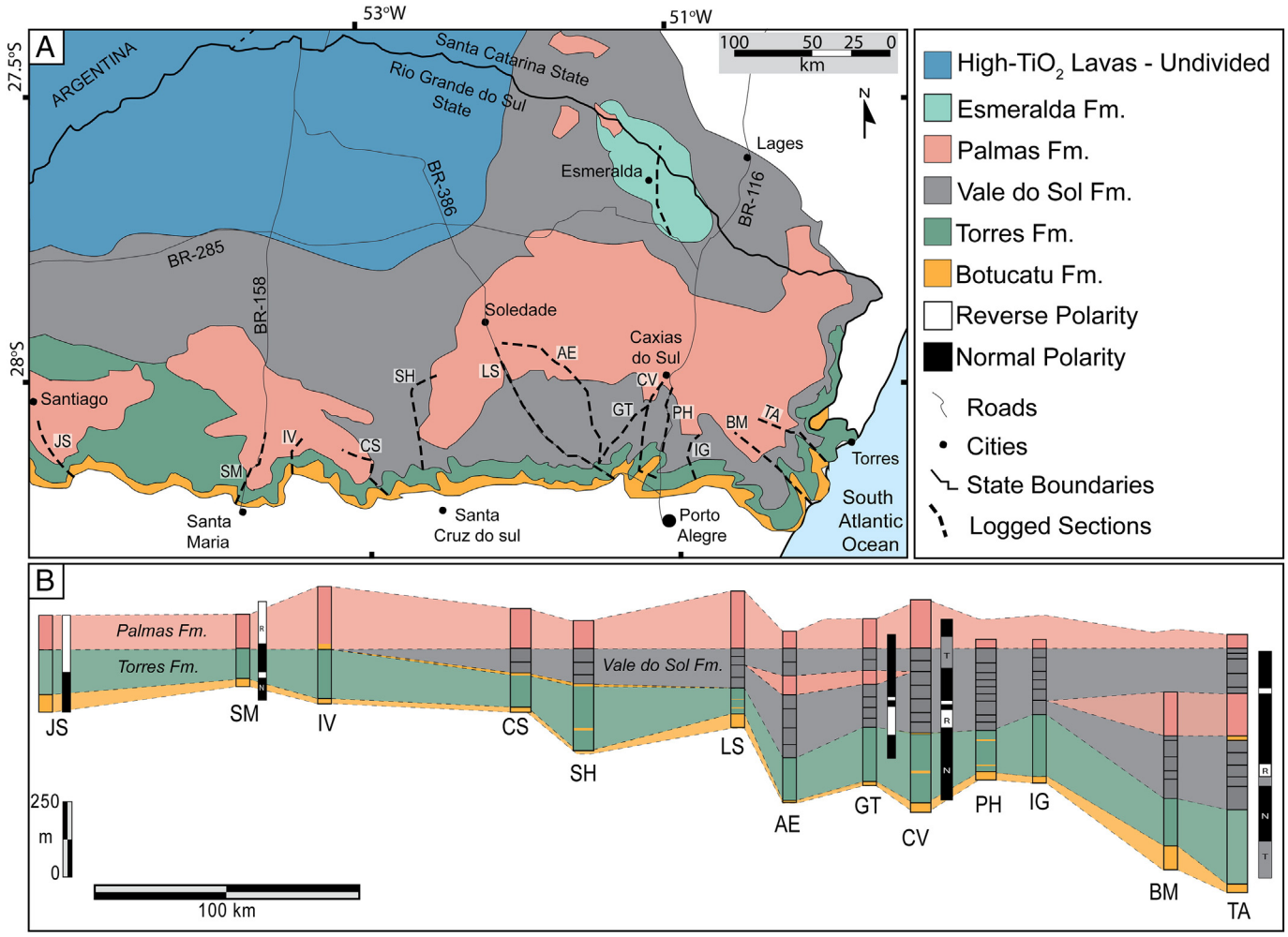

Fig. 3. A) Map showing the distribution of lava formations in the southern Paraná-Etendeka Igneous Province, and logged sections. B) Stratigraphic distribution of lava formations in the logged sections, and correlation with existing paleomagnetic data (from Ernesto and Pacca, 1988). JS = Jaguari–Santiago; SM = Santa Maria; IV = Ivorá; CS = Candelária–Sobradinho; SH = Santa Cruz do Sul-Herveiras; LS = Lajeado–Soledade; AE = Arvorizinha–Encantado; GT = Garibaldi-Teotônia; CV = São Sebastião do Caí–Caxias do Sul; PH = Picada Café Nova Petrópolis; IG = Igrejinha - Gramado; BM = Barra do Ouro - Morrinhos; TA = Terra de Areia - Aratinga.

the lower portions of the succession, and in the western margin of the outcrop area, decreasing in frequency and thickness in the central portion of the lava pile and in the upper portion of the formation (Fig. 7A and B). The aeolian deposits formed thin sand lenses (<3 m thick) made by aeolian sand sheets and cross-stratified thick sand lenses (3–15 m thick) formed by the migration of sand dunes (Scherer, 2002). The accumulation of the sand deposits is controlled by the topography of the lava field. Isolated sand bodies (e.g. barchans dunes) which migrate across the barren lava surface can be trapped by the next advancing lava flows and also be preserved as aeolian interbeds (Jerram et al., 2000; Scherer, 2002; Waichel et al., 2008).

Petrographically (Fig. 9A and B), the majority of the lava flows are fine to medium-grained aphyric or plagioclase-phyric basalts (1–4 mm, ≤5% modal volume) comprising a holocrystalline groundmass of plagioclase (~An_{60}), augite (~$En_{46}Wo_{34}$ Fs_{20}), and iron oxides (Ti-magnetite and magnetite) ± olivine (in most cases replaced by secondary mineralogy). Augite forms subhedral plates intergranular to plagioclase crystals, although ophitic and sub-ophitic textures are also

Table 2
Flow facies, main physical and petrographic characteristics of the lava Formations from the Serra Geral Group.

Formation	Unit Thickness/Flow Thickness	Lava Facies	Main Physical Characteristics	Petrographic Features
Esmeralda	25–300 m 0.2–3 m	Compound braided	Metric lava lobes with typical pahoehoe structure: basal vesicular crust, massive core and vesicular upper crust	Aphyric and aphanitic black basalts. Acicular to skeletal plagioclase microlites, augite and Fe-oxides. Glassy matrix
Palmas	40–400 m ?	Tabular classic	Tabular wide spread dacite, rhyolites and obsidian flows. Lobate terminations, flow foliation autobreccia pockets, vesicle layers and megavesicles	Vitrophyric texture, plagioclase and augite phenocrysts, commonly granophyric texture with K-feldspar and quartz overgrowth
Vale do Sol	40–500 m 20–60 m	Tabular classic	Simple tabular geometry rubbly pahoehoe lavas. Four part structure: basal vesicular crust; massive core; coherent vesicular crust; rubbly surface	Aphanitic to fine grained basaltic-andesites, rarely plagioclase-phyric. Fine grained plagioclase with intergranular augite and Fe-oxides
Torres	100,290 m 0.2–18 m	Compound braided	Lava lobes, toes, and sheet-like lobes. Typical pahoehoe structure with: basal crust with pipe vesicles, massive core, and upper vesicular crust	Olivine or plagioclase-phyric medium grained basalts. Porphyritic and glomeroporphyritic, with plagioclase, augite, Fe-oxides ± olivine

Fig. 4. A) Outcrop cross-section of contact between sandstones of Botucatu Formation and first compound lava of Torres Formation. Location: 29° 52.652′S, 50° 23.688′W; B) Light grey compound pahoehoe lava of Torres Fm. covered by thick tabular lava of Vale do Sol Fm. Location: 29° 31.364′S, 52° 38.511′W; C) Highly altered rubbly flow top overlain by dacite flow of Palmas Fm. Location: 28°58′5.07″S, 51° 6′53.54″W; D) Contact of Vale do Sol and Palmas Formations in Herveiras. Rubbly flow top in reddish brown, covered by massive grey dacite. Location: 29° 30.790′S, 52° 39.075′W.

identified. Plagioclase phenocrysts occur as euhedral tabular labradorite (~An_{56}), with bytownite cores (up to ~An_{80}). Olivine-phyric basalts are restricted to the lowermost portions of the lava pile, typically occurring in the first few flows of the formation, olivine phenocrysts are equant, euhedral (~2 mm) and completely replaced by bowlingite, smectite, and iddingsite (Fig. 9A). The upper and lower crust facies are aphanitic with glassy matrix surrounding plagioclase microphenocrysts (0.01 mm), commonly oxidized. Vesicles are present in the flow crust and subordinately in the core as late degassing phases, generating diktytaxitic textures where plagioclase surrounds micro-cavities.

3.2. Vale do Sol Formation (VSF)

The VSF is characterized by the vertically stacked sheet-like lava flows of rubbly pahoehoe morphology (Fig. 5 B), with an average thickness of 35–45 m. The formation reaches a maximum thickness of 500 m in the Terra de Areia - Aratinga profile (TA) where the unit is formed of ~11 flows, and the number of lavas gradually decreases to west/southwest towards the basin limits. In the SM profile, no lavas from VSF are preserved, and the rhyolites from Palmas Formation are sitting directly on top of Torres Formation basalts. The type section crops out in the RST-153 (SH profile) road between elevations of 370 and 500 m a.s.l. near Vale do Sol county, where three rubbly pahoehoe flows are well exposed and the internal architecture is easily identified.

The contact of Vale do Sol Formation (VSF) with the underlying lavas of Torres Formation is a non-erosional sharp surface, usually highlighted by the presence of a sandstone bed. The contact is well exposed in the Santa Cruz-Herveiras (SH) and Candelaria-Sobradinho (CS) profiles where the sandstone bed is up to 2 m thick, with fine to medium grain sand with a locally preserved pin-stripe lamination (Fig. 7C). In other areas, the bed is intensely silicified and zeolite-rich, due to post-emplacement alteration (Fig. 4B). The surface represents a regional marker of the internal volcanic stratigraphy highlighted by the change of volcanic architecture and morphology together with a shift in the

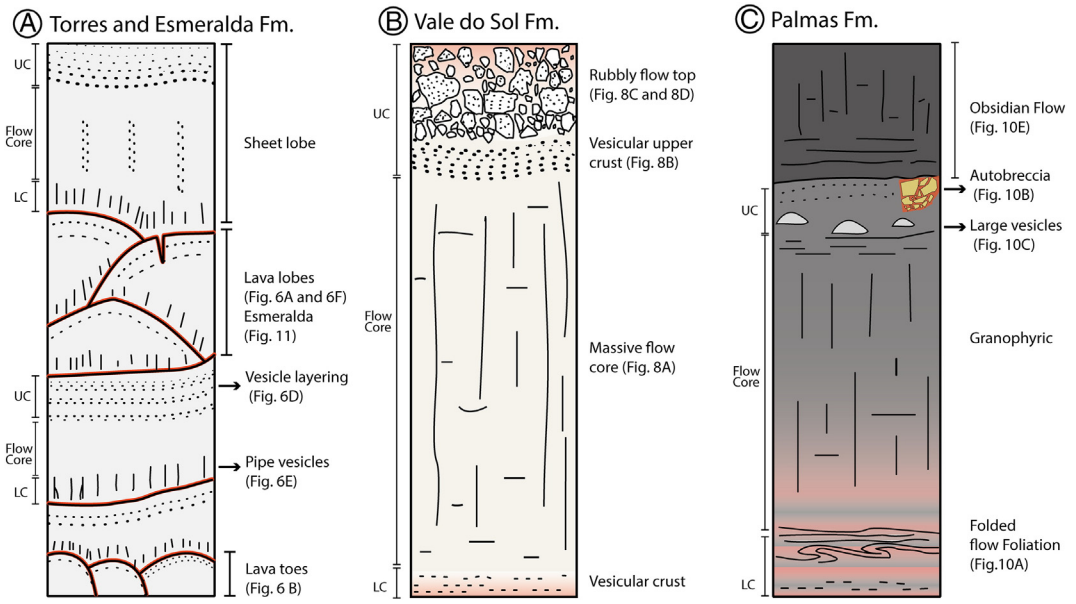

Fig. 5. Schematic logged section through lava flow fields. A) Torres and Esmeralda Formations. Compound pahoehoe flow field formed small lava lobes, toes and thicker sheet lobes. Three-part structure with vesicular lower crust, massive flow core, and vesicular upper crust; B) Vale do Sol Formation. Rubbly pahoehoe lava with thin vesicular lower crust, massive flow core, coarsely vesicular upper crust and rubble surface. C) Palmas Formation. Tabular dacitic lava with vesicle-poor lower crust with flow foliation, massive granophyric flow core, vesicular and autobrecciated upper crust, covered by obsidian flow. LC – lower crust; UC – upper crust.

chemical compositions from relatively more primitive basaltic lavas of TF to more evolved basaltic andesites of VSF.

Individual lava flows are characterized by a tabular sheet-like geometry and an internal structure that can be divided into four parts: (1) a smooth vesicular base (<1 m thick); (2) aphanitic massive cores with irregular joints; (3) upper vesicular crust and (4) a rubbly flow top (disrupted to brecciated). The basal crust is vesicular and aphanitic, ranging from 0.2–1 m in thickness, with spherical (2–5 mm) or stretched vesicles. Flow basal boundary is commonly glassy and oxidized. Lava core is massive aphyric basalt and in some portions develop irregular columnar joints (Fig. 4 B). The coherent portion of the upper crust is a 1–3 m thick coarsely vesicular or amygdaloidal layer (vesicles with 1 to 6 cm in diameter). Locally vesicles are distributed in vertical trails similar to a convection structures (Fig. 8B). The flow surface is brecciated and forms a rubble layer with irregular geometry and thickness varying from 3 to 7 m (Fig. 8A). This crust is formed by vesicular basalt fragments of previously formed pahoehoe crust. The fragments vary from 5 to 25 cm diameter and are generally sub-angular to sub-rounded. The rubble surface gradually changes from a lava cemented inner portion to a porous external portion where the fragments are loose or cemented by zeolite (Fig. 8C).

The occurrence and preservation of interbedded sedimentary rocks is restricted to infilled space among fragments and as very thin beds on the upper portion of the rubbly flow tops (Fig. 8D). Those sediments are generally poorly sorted and finely laminated with grain size variation from silt to medium sand, composed mainly of quartz with a minor contribution of volcaniclastic material (Fig. 7E) reflecting a water-related deposition. Immediately before the first acidic flow in the Torres-Aratinga profile (elev. ~550 m) a small depression on top of a rubbly pahoehoe flow is infilled with volcaniclastic material. The bed has a maximum thickness of 2 m, massive and is formed by lapilli size sub-rounded fragments of plagioclase phyric basalt in a fine-grained size matrix. The material is cemented by zeolites possible due to later diagenesis (Fig. 8D).

Flow cores are aphyric to plagioclase-phyric basaltic-andesites with a microcrystalline groundmass texture (<0.1 mm) formed of plagioclase (An_{58}), two pyroxenes, augite (En_{45} Wo_{32} Fs_{25}) and pigeonite (En_{42} Wo_{11} Fs_{47}), and Ti-magnetite. The pyroxene crystals are in general subhedral with augite cores surrounded by pigeonite rims, micro phenocrysts are 0.3 mm in average and <0.1 mm in the groundmass. Grouped phenocrysts into glomeroporphyritic texture can reach 2.5 mm, and occur as sparse clusters in the flow cores (Fig. 9C). The upper portion of the flow core is aphanitic/hypocrystalline and rich in plagioclase microlites, the matrix commonly presents a disrupted to partially brecciated pattern. The vesicles have irregular shapes and sometimes are elongated.

3.3. Palmas Formation (PF)

Palmas Formation groups the acidic rocks from southern PEIP. The Formation comprises tabular flow units, lava domes, and complex conduit systems. The acidic units rest upon the upper portions of the volcanic pile, although intercalations of acidic units with basaltic-andesites lavas of Vale do Sol Formation occur locally (Terra de Areia-Aratinga, Arvorizinha-Encantado profiles); such intercalations are also reported from other stratigraphical sections and boreholes (Bellieni et al., 1986; Peate et al., 1992). The total estimated area occupied by acidic rocks in the Serra Geral Group is 64,000 km^2, with a volume of at least 15,300 km^3, of which Palmas Formation represents 95% of the area and 80% volume (Nardy et al., 2008). The combined units' thickness can reach 400 m in the eastern portions decreasing towards the west and north. The Palmas type rocks were described by Bellieni et al. (1986) as generally aphyric to poorly porphyritic dacites and rhyolites that occur associated with the low-TiO_2 basalts. Based on chemical composition and trace elements abundances, these rocks were further subdivided into five subgroups: (1) Caxias do Sul, in general, dacitic and occurring in the eastern outcrop area, with contents of TiO_2 > 0.85 wt% and P_2O_5 > 0.25 wt%; (2) Santa Maria, rhyolites concentrated on the western side of the lava field, with TiO_2 < 0.75 wt% and P_2O_4 < 0.2 wt%; (3) Anita Garibaldi, (4) Jacuí and (5) Clevelândia (Peate et al., 1992; Nardy et al., 2008).

The acidic units cover the rubbly pahoehoe lavas from VSF in the majority of the outcrop area, especially in the central and eastern portions, while in the west it overlays pahoehoe flow fields (see Fig. 3). In general, the contact with the VSF is easily recognizable. The lithological contrast of the rubble of the former formation with the vitric acidic lavas highlights the basal boundary of PF. In several localities, the surface is

Fig. 6. Volcanic features of Torres Formation and different lava facies. A) Metric flow lobes in compound pahoehoe lava, contact of lobes marked by oxidized chilled margins. Location: 29° 30.917′S, 51° 56.414′W, hammer for scale; B) Lava lobes covering sandstone of Botucatu Fm. Location: see Fig. 4A, hammer for scale; C) ropey surface of pahoehoe lava lobe. Location: 29° 22.031′S, 52° 3.752′W, pencil for scale; D) layered vesicular upper crust, and oxidized chilled margin close to flow contact. Location: 29° 22.031′S, 52° 3.752′W, GPS for scale; E) pipe amygdales in vesicular lower crust, Location: 29° 30.917′S, 51° 56.414′W, lens cap for scale; F) inflation cleft filled by sand (left-hand side) and by overlying lava flow (centre of picture). Location: see Fig. 4A.

preserved as small caves formed by differential erosion which "excavate" the soft rubbly flow tops (Fig. 4C and D).

Dacites from the Caxias do Sul sub-group are generally characterized by a basal banded portion with horizontally elongated vesicles, grading upwards to flow-folded zones (Fig. 5C–Fig. 10A). The flow core is fine grained granophyric, massive or with horizontal and columnar joints. Autobreccias are found locally, usually forming pockets of angular vitric fragments in a fine altered matrix in the extremities of the flows (Fig. 10B). Large gas cavities (10–20 cm in diameter) occur in the upper portions of flow core (Fig. 10C). The flow extremities are lobate, varying from 2 to 10 m thick lobe units formed of an altered external portion, a vesicular upper crust, and a massive core (Fig. 10D). Obsidian flows commonly cover the massive core portions of the dacites (Fig. 10E). Lava domes are well exposed in the BR-471 road close to Soledade and have been documented by Polo and Janasi (2014). The area exposes both dacitic and rhyolitic units. Dacitic lava domes show circular structures with typical dimensions from 5 to 8 m in height and up to 30 m in length at the base. They occur individually or are coalescent with other domes, and are covered by rhyolitic lavas from Santa Maria subgroup, showing a clear stratigraphical relation between the two subunits of PF.

Within PF the occurrence of sediments is very restricted. Isolated aeolian dunes are preserved in the western limit of the outcrop area and between different acidic units (Dacites and Rhyolites) in the central portion (see Fig. 8 - Polo and Janasi, 2014). Volcaniclastic and epiclastic sediments were recently identified by Riccomini et al. (2016). These deposits are formed of reworked pyroclastic material sitting on top of the acidic rocks of Santa Maria Sub-group in the SM area and were deposited synchronously with the acidic magmatic activity.

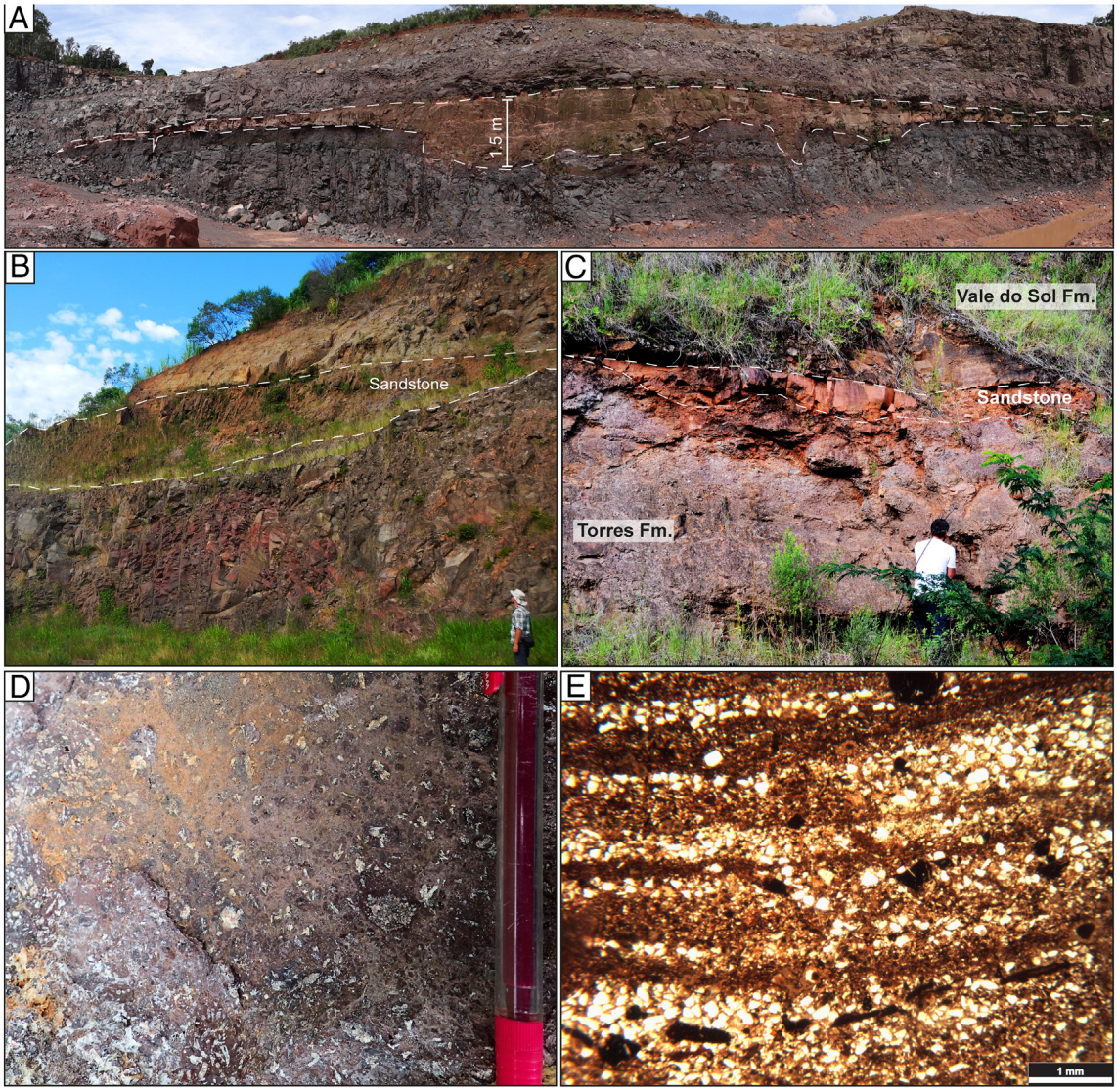

Fig. 7. Sedimentary interbeds. A) Sandstone interbed preserved between lavas of TF, note that the sedimentary rock infills the topographic low in the flow surface. Location: 29° 37.848′S, 51° 8.823′W, outcrop ~5 m high; B) Interbedded sandstone between two basalt lavas from Torres Fm. Location: 29° 33.179′S, 52° 38.083′W; C) Sandstone bed in the contact of Torres and Vale do Sol formations. Location: 29° 34.074′S, 52° 49.683′W; D) plagioclase-phyric volcaniclastic material in altered fine-grained matrix, Location: 29°22.445′S, 50°10.867′W, pen for scale; E) photomicrography of thinly laminated sandstone, with sparse basaltic andesite fragments. Sample from rubbly flow top (Fig. 7D), parallel polarisers.

The lavas are in general aphyric to poorly porphyritic with phenocrysts (2–3 mm) and micro phenocrysts (0.1–0.5 mm) of plagioclase feldspar ($An_{55–65}$) and Pigeonite (En_{45} Wo_{10} Fs_{45}) as the most common phases, locally clustered in glomerocrysts forming glomeroporphyritic textures (Fig. 8E). The matrix is formed of glass and quartz + K-feldspar overgrowth textures, K-feldspar rarely occurs as phenocryst, and is usually altered and replaced by albite (Fig. 8F). Iron oxides in special Ti-magnetite occur as an accessory phase. Flow banding is marked by millimetric (2–5 mm) bands with different crystallinity and oxides content.

3.4. Esmeralda Formation (EF)

The Esmeralda Formation (EF) is the uppermost unit of the low-TiO_2 volcanic succession. It comprises the Esmeralda magma-type basalts (Peate et al., 1992). The flow field is mainly exposed in the northeast border of Rio Grande do Sul and Santa Catarina states and has a smaller areal extent than other volcanic units. The lavas are not commonly preserved in road sections and their occurrence is restricted to inland shallow outcrops, where these lavas partially overlie Palmas dacites. The formation thickness varies from 25 to 150 m in the field. Well data reports the occurrence of Esmeralda magma type samples in several wells including the central Paraná area (Peate et al., 1992) and according to these authors, the units can reach 300 m thickness and it is always preserved in the upper portion of the low-TiO_2 sequence. The basal contact of the Formation is not well exposed in the studied profiles but stratigraphic relations indicate that these lavas overly the acidic units of Palmas Formation.

The lava flow fields are of pahoehoe nature with a compound braided facies architecture. The flow structure and distribution are very similar to those from Torres Formation. Flow fields are generally characterized by small pahoehoe lava lobes (<2 m) of the s-type (*spongy*- Wilmoth and Walker, 1993) with a vesicular upper crust and massive cores. The vesicular lower crust is formed of spherical vesicles, and no pipe vesicles have been identified in this lava units. The flows are aphanitic to vitric with a characteristic black colour, commonly altered to reddish clay-rich materials. Plagioclase is essentially acicular to skeletal micro phenocrysts, involved in a glass rich to aphanitic matrix. These characteristics contrast with the lavas from TF that generally have intergranular textures and fine-grained augite plus plagioclase matrix. The two units are also distinct chemically, as described in the next section.

Fig. 8. Volcanic features of the Vale do Sol Fm. lavas. A) Contact of rubbly top and overlain flow base of two flows. Location: 29° 20.999′S, 50° 10.358′W, rucksack for scale; B) Coarsely vesicular layer in flow upper crust. Location: 28° 56.684′S, 51° 11.102′W, hammer for scale; C) Rubbly flow surface formed of vesicular oxidized fragments. Location: 29° 31.226′S, 52° 39.071′W; D) Rubbly flow surface filled with space among fragments occupied by sandstone. Location: 29° 31.226′S, 52° 39.071′W, pen for scale.

4. Correlation with the Paraná-Etendeka geochemical groups

Representative chemical compositions of each lava formation are presented as supplementary data (electronic Supplementary material), further analyses were compiled from Rossetti et al. (2014) and Simões et al. (2014). The different rocks in the studied sections range chemically from basalts to rhyolites (Fig. 12A – Le Maitre, 1989). When compared with the existing chemical stratigraphy, the two first lava formations have trace elements ratios (Ti/Zr < 70 and Ti/Y < 330) equivalent to those of the Gramado magma type (Peate et al., 1992) and the LTZ.Z magma type from the Etendeka (Erlank et al., 1984) (Fig. 12B). REE profiles are also similar to the average signature of Gramado magma type (Fig. 12D). TF lavas are compositionally basalts and basaltic andesites, with TiO_2 wt% < 1.5, concentration of MgO in general >5 wt% (3.5–8.7 wt%) and SiO_2 48.69–55.9 wt%. The lavas of VSF are compositionally basaltic-andesites with SiO_2 51.1 to 56.8 wt%, MgO 2.5 to 5.7 wt% (usually <5 wt%). The rocks have high FeO* (10.43–13.23 wt%) and TiO_2 (1.17–1.83 wt%) and lower CaO and Al_2O_3 when compared with TF lavas. These values are in agreement with the most differentiated end of a continuous evolution trend from primitive TF lavas. Trace element diagrams show enrichment in large-ion-lithophile elements (LIL) in relation to high field strength (HFS) and rare earth elements (REE) with marked negative anomalies of Nb, P, and Ti. Normalized (chondrite – Sun and McDonough, 1989) REE profile show an enrichment in LREE ($[La / Yb]_N$ = 4.9–8.9) in relation to HREE ($[Dy / Yb]_N$ = 1.2–1.4). In VSF normalized trace elements distribution is parallel to those of TF with higher absolute concentrations in the differentiated terms (Fig. 12E). The variations in composition of the two formations can be explained by simple trends of fractional crystallization of olivine, augite, and plagioclase, common in tholeiitic basaltic magmas.

Esmeralda Formation samples have low SiO_2, 49.25–50.40 wt%, and MgO values of 6.15 and 6.56 wt%. For a given MgO value Esmeralda samples are enriched in FeO* (~12 wt%) and CaO (~10.5 wt%) showing slightly higher values of TiO_2 (0.2 wt%) when compared with TF lavas. The most significant difference is in the REE distribution. EF has a flat REE profile with subtle enriched LREE $[La / Yb]_N$ ~2.85, while Gramado magmas have a strong enrichment in the LREE and incompatible elements in general $[La / Yb]_N$ > 4.5 (Fig. 12D). These different features were firstly noticed by Peate et al. (1992). The acidic rocks (PF) sit on the dacite and rhyolite fields in the TAS diagram (Le Maitre, 1989), are equivalent to Palmas type acidic rocks, and Caxias do Sul and Santa Maria sub-group respectively (see Fig. 12C). The content of SiO_2 varies from 65.5 to 69.4 wt%, MgO <1.6 wt%, Al_2O_3 ~12 wt%. The two distinct sub-groups are separated by TiO_2 wt% and P_2O_5 wt% contents, with lower values in the Santa Maria subgroup, 0.65–0.72 and 0.17–0.19 respectively, and 0.85–0.97 and 0.26–0.28 in the Caxias do Sul sub-group.

5. Discussion

According to Bryan et al. (2010), Continental Flood Basalts are in general formed by extensive flow fields of pahoehoe and rubbly pahoehoe lavas (Self et al., 1998; Jerram et al., 1999; Bondre et al., 2004; Waichel et al., 2006; Passey and Bell, 2007). The lavas are emplaced during long-lived eruptions lasting years to decades, fed by long fissure systems, where the volcanic activity migrates along different segments of the fissure system through time, promoting the flow field growth and migration (Swanson et al., 1975; Self et al., 1996, 1997, 1998; Thordarson and Self, 1998). Major sheet lobes are the building blocks of CFB, with 20–30 m of thickness and several kilometers long, and represent the bulk volume produced by one typical eruption,

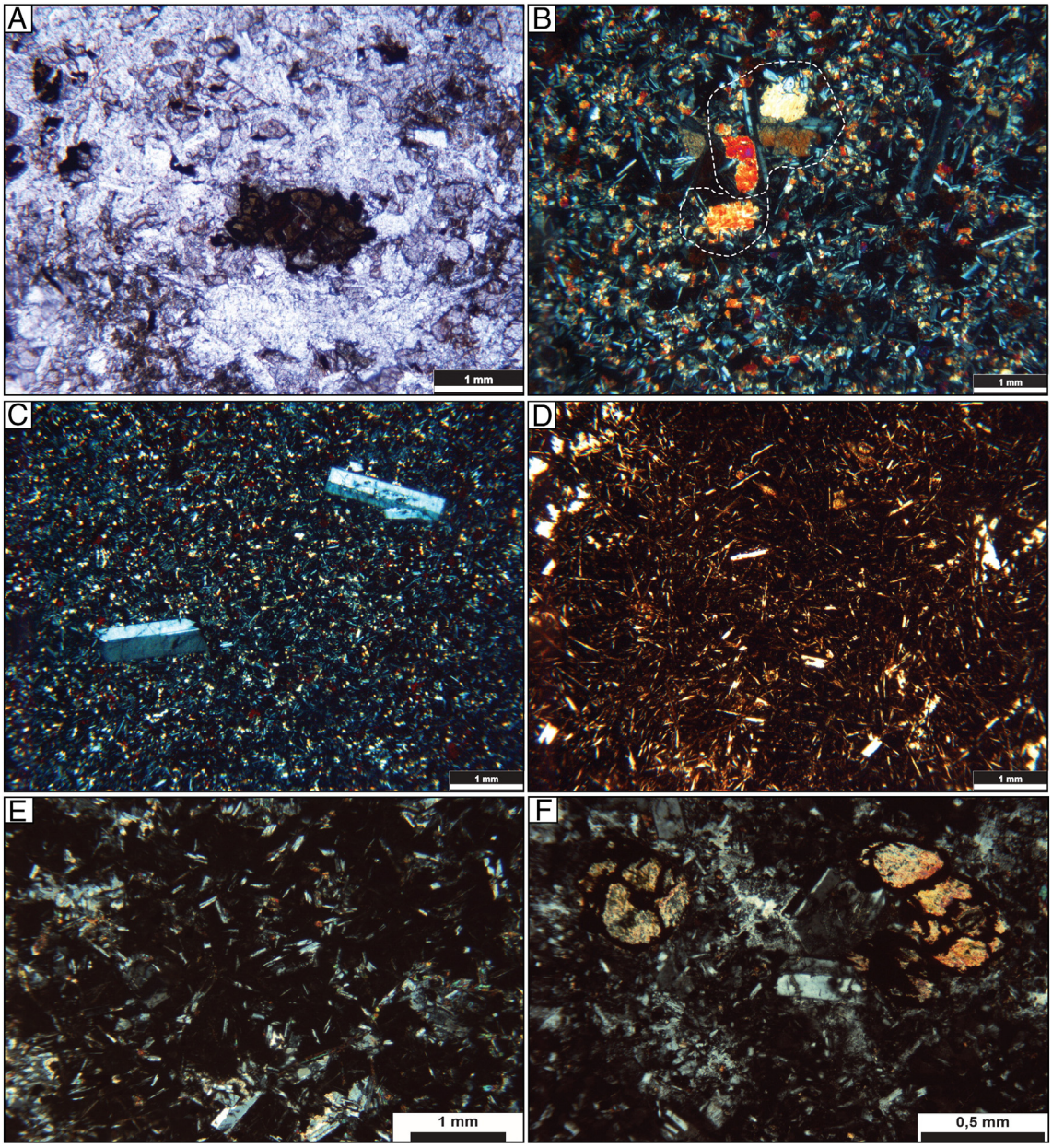

Fig. 9. Photomicrography of the different lava units. A) Olivine phenocryst altered to iddingsite in an olivine-phyric basalt from TF, parallel polarisers; B) fine-grained basalt with augite intergranular to plagioclase crystals and sub-ophitic texture (dashed lines) in a basalt flow core TF, crossed polarisers; C) plagioclase phyric basaltic andesite of VSF, crossed polarisers; D) acicular plagioclase crystals in a oxidized hyaline matrix in basalt from EF, parallel polarisers; E) Plagioclase micro phenocrysts in a glassy matrix in dacite from Palmas Formation, cross polarisers; F) altered pyroxene phenocrysts, graphic K-feldspar and quartz overgrowth texture (red dashed line) in dacite from Palmas Formation, cross polarisers.

usually presenting features of endogenous growth (Hon et al., 1994; White et al., 2009). A close analysis of the volcanic facies that are found in many CFB can be shown to have distinct internal characteristics that help to define the 3D architecture of the units (e.g. the facies types of Jerram, 2002). These features are also useful as they can be recognized in core data where limited outcrop information is available (e.g. Nelson et al., 2009), and may also extend the interpretation of the volcanics into the offshore areas (e.g. Jerram et al., 2009).

5.1. Emplacement mechanisms of the Torres and Esmeralda Formations

The lower Torres and upper Esmeralda basalts are formed of multiple small lobes and do not form a classical Continental Flood Basalts step-like morphology. Both formations are made of compound pahoehoe lavas <15 m thick, with common features that indicate endogenous growth and inflation (e.g. inflation clefts and vesicle layering). These features are commonly associated with Hawaiian-like eruptions and were also identified in pahoehoe lavas from Hawaii and in other CBP's (Hon et al., 1994; Self et al., 1998; Bondre et al., 2004; Single and Jerram, 2004). The transition from small (1 m thick) lobes in the bottom to significantly thicker, 12–15 m, lavas on the top of Torres Formation might reflect a gradual increase in magma supply, or longer sustained eruptions where inflation processes were more active and promote in situ thickening and development of the lava field.

One other important distinction between the two units is the type of lobes. According to Wilmoth and Walker (1993), p-type lobes (lobes with pipe vesicles) have longer residence time and suffer intense vesicle lost throughout emplacement. P-type lobes form thicker flow units and have considerably lower cooling rates experimenting more intense

Fig. 10. Lava facies and structures of Palmas Fm. rocks. A) The base of dacitic lava with flow foliation, locally folded. Location: 28°58′5.07″S, 51°6′53.54″W; B) Autobreccia with jig-saw fit texture. Location: 29°18.536′S, 52°38.604′W, a compass for scale; C) large gas cavities in the upper portion of lava core. Location: 29°5.441′S, 51°59.351′W, hammer for scale; D) Lobe termination in flow margin covered by massive dacite lava. Location: 28°50.597′S, 51°50.137′W, photograph taken from northeast to southwest; E) Contact of a massive granophyre and obsidian. Location: 28°50.955′S, 51°50.042′W, photograph taken from northeast to southwest, road board (~1 m) for scale.

inflation and degassing processes than in s-type lobes (spongy lobes). Torres Formation is composed dominantly of p-type lobes, and the flow fields are widespread and thicker than Esmeralda Formation lavas. This fact is compatible with a longer residence time and slower cooling rates. The thin, and glassy s-type lobes of Esmeralda Formation indicate relatively higher cooling rates and less efficient inflation processes. The occurrence of these lavas in the central Paraná was reported in boreholes (RO well) ~350 km north of the outcrop area (see Fig. 11 - Peate et al., 1992). The small surface extension of Esmeralda Formation might be related to intense erosion and tectonic uplift post-dating the volcanic activity (Gallagher et al., 1994).

5.2. Emplacement mechanisms of the Vale do Sol Formation

The bulk volcanic succession is marked by a step-like morphology formed of vertically stacked sheet-like rubbly pahoehoe flows from the Vale do Sol Formation. These lavas are significantly thicker than any other flow field of Torres and Esmeralda formations, and internal flow structure is formed of a thin vesicular lower crust, massive core, vesicular upper crust and rubbly flow surface. Similar rubbly pahoehoe lavas make up to 30% of the Columbia River lavas (Keszthelyi et al., 2004), part of the Deccan lava succession (Duraiswami et al., 2008), and are also described in the Kalkarindji continental flood basalt in

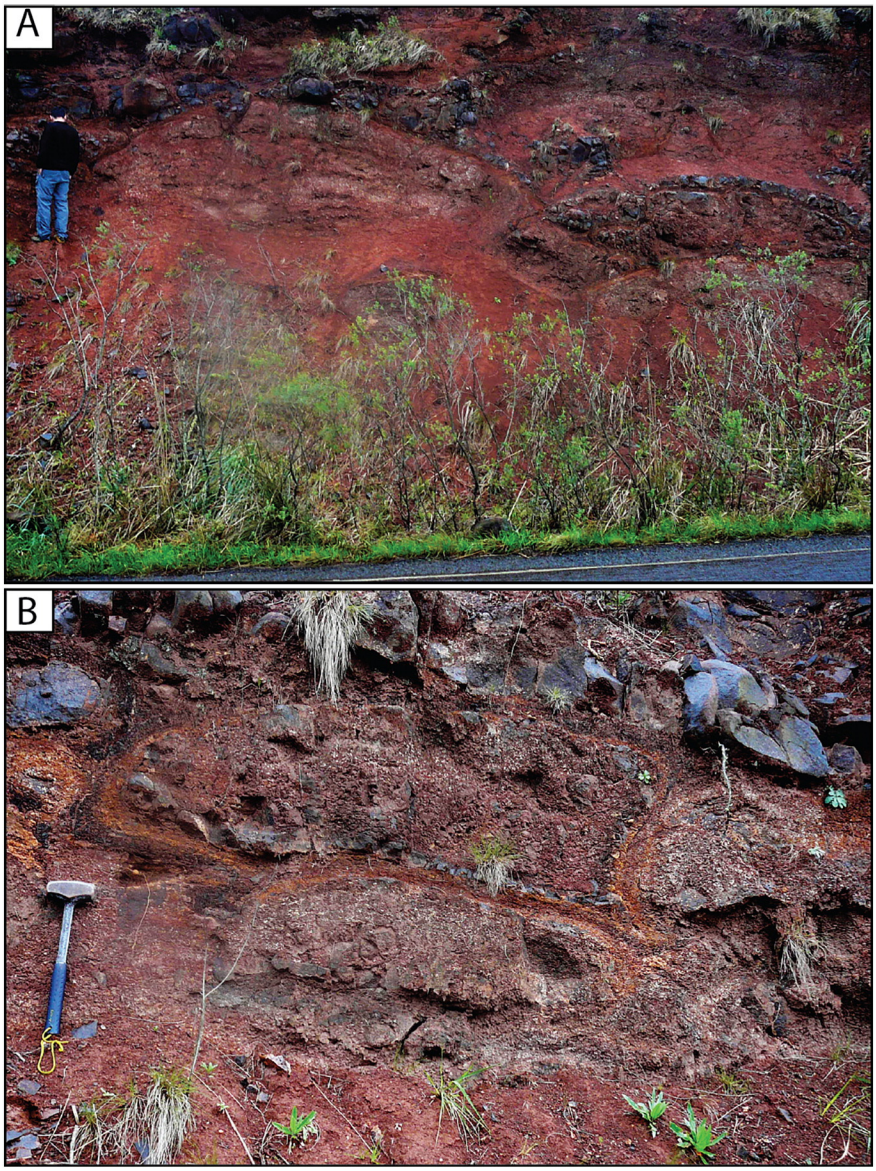

Fig. 11. Lava facies of Esmeralda Formation. A) Metric lava lobes with vesicular upper and lower crusts and massive cores, flow contact marked by chilled margins. Location: 28° 15.148′S, 51° 5.525′W; B) Small lava lobes with altered chilled margins; Location: 28° 15.605′S, 51° 5.721′W, hammer for scale.

Australia (Marshall et al., 2016) and eastern Iceland (Óskarsson and Riishuus, 2014).

The best modern analogue to rubbly pahoehoe eruptions is the 1783–1784 Laki eruption in Iceland. The Laki flow field extends along ~600 km^2 and is dominated by rubbly pahoehoe surfaces (Guilbaud et al., 2005). It is generally considered that the mode of emplacement is firstly as pahoehoe sheet-lobes with inflation processes and surges in effusion rate increasing the internal pressure and promoting episodic degassing and disruption of the flow crust resulting in subsequent brecciation of the flow extremities (Guilbaud et al., 2005; Keszthelyi et al., 2004, 2006; Duraiswami et al., 2008). Keszthelyi et al. (2006) demonstrate mathematically that rubbly pahoehoe eruptions can be as thermally effective and insulated as classic pahoehoe lavas, losing only 0.1 °C km^{-1} for 20–30 m thick lavas. This fact is important to explain the apparent long length of this flows in the VSF. The episodic fragmentation of the flow crust promotes the formation of a partially stable flow surface where no significant heat loss would take place. Additionally, Óskarsson and Riishuus (2014) argued that fast moving flow front would promote continuous tearing and brecciation in the contact of previously formed crust with the fluid core, this fact would explain a formation of a uniform fragment size thick and continuous rubble surface.

In the Vale do Sol Formation lavas, the relatively uniform size of the fragments and the absence of large platy fragments are suggestive of disruption of a relatively thin pahoehoe crust, and the presence of heterogeneous fragments with different vesicularity and crystallinity might indicate episodic disruption of the external crust. The presence of thick (1–3 m) vesicular layer in the upper core (just beneath the rubbly surface) indicate continuous inflation and degassing during the whole emplacement, and possibly a more stable emplacement in the final stages of the eruption, with no significant brecciation.

5.3. Emplacement mechanisms of the Palmas formation

The acidic lavas of Palmas Formation have been emplaced in anomalous high crystallization temperatures (~1000 °C - Bellieni et al., 1986; Garland et al., 1995; Simões et al., 2014). The flow units are characterized by a low aspect ratio when compared to classic rhyolitic eruptions. These facts allied to the presence of central complexes which resemble caldera structures (e.g. Messum Complex – Etendeka, Namibia)

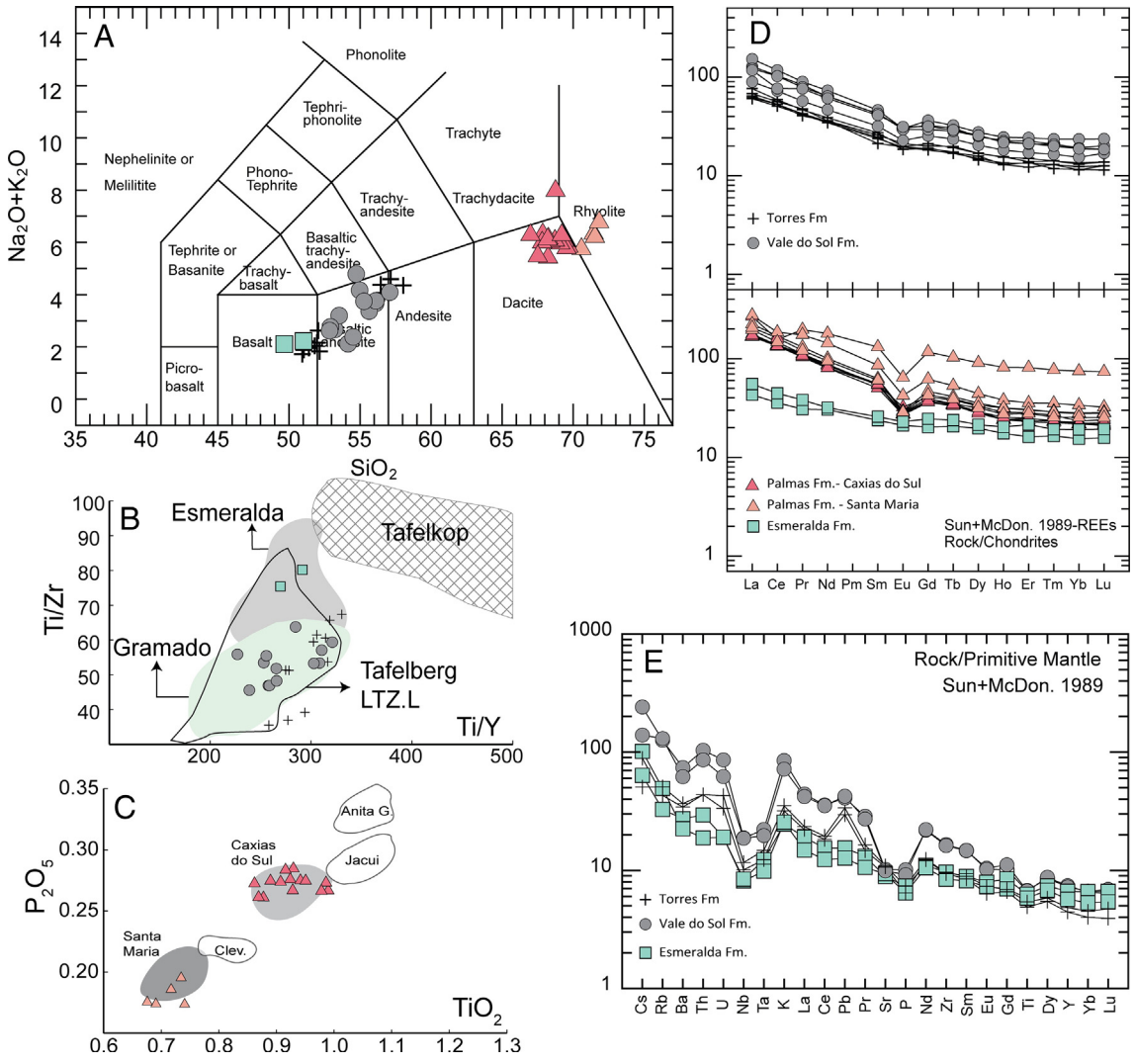

Fig. 12. Geochemical data distribution. A) Samples distribution in TAS diagram (after Le Maitre, 1989); B) Ti/Zr vs Ti/Y plot with classification fields of Paraná magma types from Peate et al. (1992) and Etendeka from Erlank et al., 1984 and Jerram et al., 1999; C) P_2O_5 vs TiO_2 classification diagram for the Palmas lavas, samples plotting in both Caxias do Sul and Santa Maria subgroups (fields from Nardy et al., 2008); D) REE profiles (normalized by Primitive mantle - Sun and McDonough, 1989); Trace element plot of representative samples of the different basaltic units (normalized by Primitive mantle - Sun and McDonough, 1989). Geochemical data from Rossetti et al., 2014; Simões et al., 2014 and this study (see Supplementary data). Crosses – Torres Fm.; grey circles – Vale do Sol Fm.; light pink triangles – Rhyolites Palmas Fm.; dark pink triangles Dacites Palmas Fm.; green squares – Esmeralda Fm.

encouraged several authors to assume a pyroclastic origin to these rocks and an emplacement as highly welded ignimbrites and rheoignimbrites (Milner et al., 1992, 1995; Garland et al., 1995; Bryan et al., 2010). As an alternative, the high temperatures associated with low viscosity values could inhibit the explosivity of this systems and promote the emplacement as lava flows (Bellieni et al., 1986; Henry and Wolff, 1992; Uman et al., 2001; Waichel et al., 2012; Polo and Janasi, 2014; Simões et al., 2014).

The acidic units preserved in Palmas formation are characterized by low aspect ratio flows with lobate terminations, internal thick lithoidal core and external autobreccias and are similar to the large-volume, low-aspect-ratio rhyolite lavas described in the central Snake River Plain area, USA (Branney et al., 2008). These rhyolite units commonly exceed 10 km^3, and in some cases can reach volumes of 200 km^3 (e.g. Creek Rhyolite – Bonnichsen, 1982).

Restricted explosive activity is preserved as reworked volcaniclastic deposits and could represent local explosive activity in proximal vent areas (Riccomini et al., 2016). Alternatively, hot state shear and annealing of pumiceous autobreccias during the emplacement of lava flows could generate vitroclastic textures that resemble welded pyroclastic textures (Manley and Fink, 1987; Branney et al., 2008).

5.4. Time duration and volcanic evolution

Available radiometric ages place the PEIP in the lower Cretaceous with a suggested time duration of ~3 Ma (Janasi et al., 2011 and references therein), nevertheless, these ages are not conclusive on the time duration of individual stratigraphic units. As an alternative, paleomagnetic surveys sampled several complete vertical sections throughout the volcanic pile (Ernesto and Pacca, 1988) and part of the data can be correlated with the new lithostratigraphy providing important indications on the relative time constraint of volcanic activity (Fig. 2).

Torres Formation is the oldest unit and the bulk volume of lavas was formed during a normal polarity period. Only a small portion of the formation have reversed polarity (e.g. PH and GT profiles), this fact points to a relatively short time interval for the construction of Torres Formation lavas. The later Vale do Sol Formation occurrence is tectonically restricted to the central portions of Torres Syncline and pinches out towards the border of the basin. Several changes of polarity are present in Vale do Sol Formation: 4 in the CV, PH, and GT profiles and 5 in the TA profile (including an interval of acidic lavas). In all profiles, the first lava flow has reversed polarity with the exception of the TA area. This fact

allied to the thickness variations and its distribution are suggestive of a progressive infill of Torres syncline structure starting in the deepest portions (TA profile) with latter flows being more equally spread and not restricted only to the main axis. Using an average value of 0.2 Ma (with some short duration intervals) for the polarity inversion in the Early Cretaceous between 133.5 and 135 Ma (GPT-Gee and Kent, 2007) it is possible to estimate a time interval of ~0.8 to 1 Ma for the emplacement of the whole Vale do Sol Formation. The acidic units are in general constrained in a normal polarity interval that coincides with the end of VSF, and no paleomagnetic data is available to the Esmeralda Formation lavas. Considering the low-TiO_2 pile as a whole, the estimation of ~1 Ma is coherent with the paleomagnetic data and existing ages (Renne et al., 1992; Thiede and Vasconcelos, 2010; Janasi et al., 2011) with the bulk time interval developed during the formation of VSF lava pile.

6. Summary and conclusions

The Paraná-Etendeka Igneous Province in south Brazil is formed of heterogeneous lava packages with distinct architecture, morphology, and chemistry. The lavas are grouped in the Serra Geral Group, and four lava formations were recognized for the southern low-TiO_2 series: Torres, Vale do Sol, Palmas, and Esmeralda. Sedimentary beds are preserved throughout the stratigraphy and are important markers of quiescence periods in the volcanic activity, and in some cases, as in the contact of Torres and Vale do Sol formations, of important changes in the dynamic of the volcanism. The base stratigraphy is made of compound lavas from the Torres Formation formed by Hawaiian-like eruptions on the early stages of volcanic activity and passively covered the sandstones of Botucatu Formation These lavas represent the most chemically primitive basalts in the whole sequence. Thick tabular basaltic andesite lavas from Vale do Sol Formation represent an increase in the volume of individual eruptions and the climax of volcanic activity in southern Paraná-Etendeka. The lavas are voluminous and widespread in the Torres Syncline area. The peak of the volcanism culminates with the emplacement of extensive acidic lavas. Esmeralda formation lavas are formed during the waning phase of volcanic activity.

The new lithostratigraphy provides an important framework of the Serra Geral Group in the southern Paraná-Etendeka Igneous Province. It is the first contribution to consider the variations in the volcanology of the lava pile and not solely the geochemistry. It also opens the possibility to improve the existing geochemical and geochronological data, understanding the time duration, emplacement rates and chemical variations within the lava formations and should be considered in future correlations and detailed works.

Acknowledgements

The research is part of Lucas Ph.D. thesis and was carried out with the financial support of CNPq (Conselho Nacional de Desenvolvimento Científico e Tecnológico -Brazil) and BG-Brazil/Shell. The University of Aberdeen and the Federal University of Rio Grande do Sul are acknowledged for additional support. Evandro is thankful for research grants from CNPq (project - 479784/2012-4), FAPERGS (100713) and FAPESP (2012/06082-6). M. Rossetti and F. Luz are acknowledged for their support during fieldwork and samples collection. We acknowledge Dougal Jerram and Pablo D. Harris for their constructive reviews and Edgardo Cañón-Tapia for editorship.

Appendix A. Supplementary data

Supplementary data to this article can be found online at http://dx.doi.org/10.1016/j.jvolgeores.2017.05.008.

References

Arena, K.R., Hartmann, L.A., Baggio, S.B., 2014. Geological controls of copper, gold and silver in the Serra Geral Group, Realeza region, Paraná, Brazil. Ore Geol. Rev. 63: 178–200. http://dx.doi.org/10.1016/j.oregeorev.2014.05.005.

Barreto, C.J.S., de Lima, E.F., Scherer, C.M., Rossetti, L.D.M.M., 2014. Lithofacies analysis of basic lava flows of the Paraná igneous province in the south hinge of Torres Syncline, Southern Brazil. J. Volcanol. Geotherm. Res. 285:81–99. http://dx.doi.org/10.1016/j.jvolgeores.2014.08.008.

Bellieni, G., Brotzu, P., Comin-Chiaramonti, P., Ernesto, M., Melfi, A., Pacca, I.G., Piccirillo, E.M., 1984a. Flood basalt to rhyolite suites in the Southern Paraná, Plateau (Brazil): palaeomagnetism, petrogenesis and geodynamic implications. J. Petrol. 25:579–618. http://dx.doi.org/10.1093/petrology/25.3.579.

Bellieni, G., Comin-Chiaramonti, P., Marques, L.S., Melfi, A.J., Piccirillo, E.M., Nardy, A.J.R., Roisen, 1984b. High- and low-TiO_2 flood basalts from the Parana plateau (Brazil): petrology and geochemical aspects bearing on their mantle origin. N. Jb. Mineral. (Abh.) 150, 273–306.

Bellieni, G., Comin-chiaramonti, P., Marques, L.S., Melfi, A.J., Nardy, A.J.R., Papatrechas, C., Piccirillo, E.M., Roisenberg, A., Stolfa, D., 1986. Petrogenetic aspects of acid and basaltic lavas from the paraná plateau (Brazil): geological, mineralogical and petrochemical relationships. J. Petrol. 27:915–944. http://dx.doi.org/10.1093/petrology/27.4.915.

Bondre, N.R., Duraiswami, A., Dole, G., 2004. Morphology and emplacement of flows from the Deccan Volcanic Province. India. Bull. Volcanol. 66, 29–45.

Bonnichsen, B., 1982. Rhyolite lava flows in the Bruneau-Jarbidge Eruptive Centre, southwestern Idaho. In: Bonnichsen, B., Breckenridge, R.M. (Eds.), Cenozoic Geology of Idaho. 26. Idaho Bur Mines Geol Bull, pp. 283–320.

Branney, M.J., Bonnichsen, B., Andrews, G.D.M., Ellis, B., Barry, T.L., McCurry, M., 2008. "Snake River (SR)-type" volcanism at the Yellowstone hotspot track: distinctive products from unusual, high-temperature silicic super-eruptions. Bull. Volcanol. 70: 293–314. http://dx.doi.org/10.1007/s00445-007-0140-7.

Bryan, S.E., Peate, I.U., Peate, D.W., Self, S., Jerram, D.A., Mawby, M.R., Marsh, J.S. (Goonie), Miller, J.A., 2010. The largest volcanic eruptions on Earth. Earth Sci. Rev. 102:207–229. http://dx.doi.org/10.1016/j.earscirev.2010.07.001.

Comin-Chiaramonti, P., Riccomini, C., Slejko, F., De Min, A., Ruberti, E., Gomes, C.B., 2010. Cordierite-bearing lavas from Jaguarão, southern Brazil: petrological evidence for crustal melts during early rifting of Gondwana. Gondwana Res. 18:514–527. http://dx.doi.org/10.1016/j.gr.2009.12.007.

Cordani, U.G., Vandoros, P., 1967. Basaltic rocks of the Parani basin. In: Bigarella, J.J., Becker, R.D., Pinto, J.D. (Eds.), Problems in Brazilian Gondwana Geology, pp. 207–231.

Cox, K.G., Hawkeshworth, C.J., 1985. Geochemical stratigraphy of the Deccan Traps at Mahabaleshwar, Western Ghats, India,with implications for open system magmatic processes. J. Petrol. 26, 355–377.

Dodd, S.C., Mac Niocaill, C., Muxworthy, A.R., 2015. Long duration (>4 Ma) and steady-state volcanic activity in the early Cretaceous Paraná–Etendeka Large Igneous Province: new palaeomagnetic data from Namibia. Earth Planet. Sci. Lett. 414:16–29. http://dx.doi.org/10.1016/j.epsl.2015.01.009.

Duraiswami, R.A., Bondre, N.R., Managave, S., 2008. Morphology of rubbly pahoehoe (simple) flows from the Deccan Volcanic Province: implications for style of emplacement. J. Volcanol. Geotherm. Res. 177:822–836. http://dx.doi.org/10.1016/j.jvolgeores.2008.01.048.

Erlank, A.J., Marsh, J.S., Duncan, A.R., Miller, R.McG, Hawkesworth, C.H., Betton, P.J., Rex, D.C., 1984. Geochemistry and petrogenesis of the Etendeka volcanic rocks from SWA/Namibia, 195–247. In: Erlank, A.J. (Ed.), Petrogenesis of Volcanic Rocks of the Karoo Province. 13. Special Publication of the Geological Society of South Africa, p. 395.

Ernesto, M., Pacca, I.G., 1988. Paleomagnetism of the Parana Basin Flood Volcanism, Southern Brazil. In: Piccirillo, E., Melfi, A.J. (Eds.), The Mesozoic Flood Volcanism of The Parana Basin. Universidade de São Paulo, pp. 229–255.

Ernesto, M., Pacca, I.G., Hiodo, F.Y., Nardy, A.J.R., 1990. Palaeomagnetism of the Mesozoic Serra Geral Formation, southern Brazil. Phys. Earth Planet. Inter. 64:153–175. http://dx.doi.org/10.1016/0031-9201(90)90035-V.

Ernesto, M., Raposo, M.I.B., Marques, L.S., Renne, P.R., Diogo, L.A., De Min, A., 1999. Paleomagnetism, geochemistry and $^{40}Ar/^{39}Ar$ dating of the North-eastern Parana Magmatic Province: tectonic implications. J. Geodyn. 28:321–340. http://dx.doi.org/10.1016/S0264-3707(99)00013-7.

Florisbal, L.M., Heaman, L.M., de Assis Janasi, V., de Fatima Bitencourt, M., 2014. Tectonic significance of the Florianópolis Dyke Swarm, Paraná–Etendeka Magmatic Province: a reappraisal based on precise U–Pb dating. J. Volcanol. Geotherm. Res. 289: 140–150. http://dx.doi.org/10.1016/j.jvolgeores.2014.11.007.

Frank, H.T., Elisa, M., Gomes, B., Luiz, M., Formoso, L., 2009. Review of the areal extent and the volume of the Serra Geral Formation, Paraná Basin, South America. Pesqui. em Geosci. 36, 49–57.

Gallagher, K., Hawkesworth, C.J., Mantovani, M.S.M., 1994. The denudation history of the onshore continental-margin of SE Brazil inferred from apatite fission-track data. J. Geophys. Res. Earth 99, 18117–18145.

Garland, F., Hawkesworth, C.J., Manto, 1995. Description and Petrogenesys of the Parana Rzhyolites Southern Brazil. J. Petrol. 36, 1193–1227.

Gee, J.S., Kent, D.V., 2007. Source of Oceanic Magnetic Anomalies and the Geomag-netic Polarity Time Scale, Geomagnetism. Elsevier, Amsterdam, pp. 455–507.

Guilbaud, M., Self, S., Thordarson, T., Blake, S., 2005. Morphology, surface structures, and emplacement of lavas produced by Laki, AD 1783–1784. Geol. Soc. Am. Spec. Pap. 396:81–102. http://dx.doi.org/10.1130/2005.2396(07).

Hawkesworth, C., Gallagher, K., Kirstein, L., Mantovani, M.S.M., Peate, D.W., Turner, S.P., 2000. Tectonic controls on magmatism associated with continental break-up: an example from the Paraná–Etendeka Province. Earth Planet. Sci. Lett. 179:335–349. http://dx.doi.org/10.1016/S0012-821X(00)00114-X.

Henry, C.D., Wolff, J.A., 1992. Distinguishing strongly rheomorphic tuffs from extensive silicic lavas. Bull. Volcanol. 54:171–186. http://dx.doi.org/10.1007/BF00278387.

Hon, K., Kauahikaua, J., Denlinger, R., Mackay, K., 1994. Emplacement and inflation of pahoehoe sheet flows: observations and measurements of active lava flows on Kilauea volcano, Hawaii. Geol. Soc. Am. Bull. 106, 351–370 (doi:10.1130/0016-7606(1994)106<0351:EAIOPS>2.3.CO;2).

Hooper, P.R., 2000. Chemical discrimination of Columbia River basalt flows. Geochem. Geophys. Geosyst. 1:1–14. http://dx.doi.org/10.1029/2000GC000040.

Janasi, V. de A., Montanheiro, T.J., Azor de Freitas, V., Reis, P.M., de Assis Negri, F., Dantas, F.A., 2007. Geology, petrography and geochemistry of the acid volcanism of the Parana magmatic province in the Piraju-Ourinhos region, SE Brazil. Rev. Bras. Geosci. 37, 745–759.

Janasi, V.D.A., de Freitas, V.A., Heaman, L.H., 2011. The onset of flood basalt volcanism, Northern Paraná Basin, Brazil: a precise U–Pb baddeleyite/zircon age for a Chapecó-type dacite. Earth Planet. Sci. Lett. 302:147–153. http://dx.doi.org/10.1016/j.epsl.2010.12.005.

Jay, A.E., Niocaill, C. Mac, Widdowson, M., Self, S., Turner, W., 2009. New palaeomagnetic data from the Mahabaleshwar Plateau, Deccan Flood Basalt Province, India: implications for the volcanostratigraphic architecture of continental flood basalt provinces. J. Geol. Soc. Lond. 166:13–24. http://dx.doi.org/10.1144/0016-76492007-150.

Jerram, D.A., 2002. Volcanology and Facies Architecture of Flood Basalts. Special Paper 362: Volcanic Rifted MarginsGeological Society of America:pp. 119–132. http://dx.doi.org/10.1130/0-8137-2362-0.119.

Jerram, D.A., Stollhofen, H., 2002. Lava–sediment interaction in desert settings; are all peperite-like textures the result of magma–water interaction? J. Volcanol. Geotherm. Res. 114:231–249. http://dx.doi.org/10.1016/S0377-0273(01)00279-7.

Jerram, D., Mountney, N., Holzförster, F., Stollhofen, H., 1999. Internal stratigraphic relationships in the Etendeka group in the Huab Basin, NW Namibia: understanding the onset of flood volcanism. J. Geodyn. 28:393–418. http://dx.doi.org/10.1016/S0264-3707(99)00018-6.

Jerram, D.A., Moutney, N.P., Howell, J.A., Long, D., Stolhofen, H., 2000. Death of a sand sea: an active aeolian erg systematically buried by the Etendeka flood basalts of NW Namibia. J. Geol. Soc. Lond. 157:513–516. http://dx.doi.org/10.1144/jgs.157.3.513.

Jerram, D.A., Single, R.T., Hobbs, R.W., Nelson, C.E., 2009. Understanding the offshore flood basalt sequence using onshore volcanic facies analogues: an example from the Faroe–Shetland basin. Geol. Mag. 146:353. http://dx.doi.org/10.1017/S0016756809005974.

Keszthelyi, L., Thordarson, T., McEwen, A., Haack, H., Guilbaud, M.-N., Self, S., Rossi, M.J., 2004. Icelandic analogs to Martian flood lavas. Geochem. Geophys. Geosyst. 5:1–32. http://dx.doi.org/10.1029/2004GC000758.

Keszthelyi, L., Self, S., Thordarson, T., 2006. Flood lavas on Earth, Io and Mars. J. Geol. Soc. Lond. 163:253–264. http://dx.doi.org/10.1144/0016-764904-503.

Le Maitre, R.W., 1989. A Classification of Igneous Rocks and Glossary of Terms. Blackwell, Oxford (193 pp).

Manley, C.R., Fink, J.H., 1987. Internal textures of rhyolite flows as revealed by research drilling. Geology 15, 549–552 (doi:10.1130/0091-7613(1987)15<549:ITORFA>2.0.CO;2).

Mantovani, S.M., Peate, D.W., Hawkesworth, C.J., 1988. Geochemical stratigraphy of Parana continental flood basalts: a contribution from boreholes samples. In: Melfi, A.J. (Ed.), Piccirillo, E.M. The Mesozoic Flood Volcanism of The Parana Basin, São Paulo, pp. 15–24.

Marshall, P.E., Widdowson, M., Murphy, D.T., 2016. The Giant Lavas of Kalkarindji: rubbly pāhoehoe lava in an ancient continental flood basalt province. Palaeogeogr. Palaeoclimatol. Palaeoecol. 441:22–37. http://dx.doi.org/10.1016/j.palaeo.2015.05.006.

Marzoli, A., Melluso, L., Morra, V., Renne, P.R., Sgrosso, I., D'Antonio, M., Duarte Morais, L., Morais, E.A.A., Ricci, G., 1999. Geochronology and petrology of Cretaceous basaltic magmatism in the Kwanza basin (western Angola), and relationships with the Paranà-Etendeka continental flood basalt province. J. Geodyn. 28:341–356. http://dx.doi.org/10.1016/S0264-3707(99)00014-9.

Milner, S.C., Duncan, A.R., Ewart, A., 1992. Quartz latite rheoignimbrite flows of the Etendeka Formation, north-western Namibia. Bull. Volcanol. 54:200–219. http://dx.doi.org/10.1007/BF00278389.

Milner, S.C., Duncan, A.R., Whittingham, A.M., Ewart, A., 1995. Trans-Atlantic correlation of eruptive sequences and individual silicic volcanic units within the Paraná-Etendeka igneous province. J. Volcanol. Geotherm. Res. 69:137–157. http://dx.doi.org/10.1016/0377-0273(95)00040-2.

Nardy, A., Machado, F., Oliveira, M., 2008. As rochas vulcânicas mesozóicas ácidas da Bacia do Paraná: litoestratigrafia e considerações geoquímico-estratigráficas. Rev. Bras. Geosci. 38, 178–195.

Nelson, C.E., Jerram, D.A., Hobbs, R.W.R., 2009. Flood basalt facies from borehole data: implications for prospectivity and volcanology in volcanic rifted margins. Pet. Geosci. 15:313–324. http://dx.doi.org/10.1144/1354-079309-842.

Óskarsson, B.V., Riishuus, M.S., 2014. The mode of emplacement of Neogene flood basalts in eastern Iceland: facies architecture and structure of simple aphyric basalt groups. J. Volcanol. Geotherm. Res. 289:170–192. http://dx.doi.org/10.1016/j.jvolgeores.2014.11.009.

Passey, S.R., Bell, B.R., 2007. Morphologies and emplacement mechanisms of the lava flows of the Faroe Islands Basalt Group, Faroe Islands, NE Atlantic Ocean. Bull. Volcanol. 70:139–156. http://dx.doi.org/10.1007/s00445-007-0125-6.

Passey, S.R., Jolley, D.W., 2008. A revised lithostratigraphic nomenclature for the Palaeogene Faroe Islands Basalt Group, NE Atlantic Ocean. Earth Environ. Sci. Trans. R. Soc. Edinb. 99:127. http://dx.doi.org/10.1017/S1755691009008044.

Peate, D., 1997. The Paraná-Etendeka Province. Large Igneous Prov. Cont. Ocean. Planet. Flood Volcanism 100, 217–245.

Peate, D., Hawkesworth, C., Mantovani, M., Shukowsky, W., 1990. Mantle plumes and flood-basalt stratigraphy in the Paraná, South America. Geology 18, 1223–1226 (doi:10.1130/0091-7613(1990)018<1223:MPAFBS>2.3.CO;2).

Peate, D., Hawkesworth, C., Mantovani, M., 1992. Chemical stratigraphy of the Paraná lavas (South America): classification of magma types and their spatial distribution. Bull. Volcanol. 55, 119–139.

Peate, D., Hawkesworth, C., Mantovani, M., Rogers, N.W., Turner, S., 1999. Petrogenesis and stratigraphy of the high-Ti/Y Urubici magma type in the Paraná flood basalt province and implications for the nature of "Dupal"-type mantle in the. J. Petrol. 40, 451–473.

Petry, K., Jerram, D.a., de Almeida, D.D.P.M., Zerfass, H., 2007. Volcanic-sedimentary features in the Serra Geral Fm., Paraná Basin, southern Brazil: examples of dynamic lava-sediment interactions in an arid setting. J. Volcanol. Geotherm. Res. 159:313–325. http://dx.doi.org/10.1016/j.jvolgeores.2006.06.017.

Piccirillo, E.M., Melfi, A.J., 1988. The Mesozoic Flood Volcanism from the Paraná Basin (Brazil): Petrogenetic and Geophysical Aspects. Universidade de São Paulo, São Paulo.

Piccirillo, E.M., Raposo, M.I.B., Melfi, A.J., Comin-Chiaramonti, P., Bellieni, G., Cordani, U.G., Kawashita, K., 1987. Bimodal fissural volcanic suites from the Parana Basin (Brazil): K-Ar age, Sr-isotopes and geochemistry. Geochim. Bras. 1, 53–69.

Pinto, V.M., Hartmann, L.A., 2011. Flow-by-flow chemical stratigraphy and evolution of thirteen Serra Geral Group basalt flows from Vista Alegre, southernmost Brazil. An. Acad. Bras. Cienc. 83:425–440. http://dx.doi.org/10.1590/S0001-37652011000200006.

Pinto, V.M., Hartman, L.A., Santos, J.O.S., McNaughton, N.J., Wildner, V., 2011. Zircon U–Pb geochronology from the Paraná bimodal volcanic province support a brief eruptive cycle at ~135 Ma. Chem. Geol. 281, 93–102.

Polo, L.A., Janasi, V. de A., 2014. Volcanic stratigraphy of intermediate to acidic rocks in southern Paraná Magmatic Province, Brazil. Geol. USP. Série Científica 14:83–100. http://dx.doi.org/10.5327/Z1519-874X201400020005.

Raposo, M.I.B., Ernesto, M., Renne, P.R., 1998. Paleomagnetism and $^{40}Ar/^{39}Ar$ dating of the early Cretaceous Florianópolis dike swarm (Santa Catarina Island), Southern Brazil. Phys. Earth Planet. Inter. 108:275–290. http://dx.doi.org/10.1016/S0031-9201(98)00102-2.

Renne, P.R., Ernesto, M., Pacca, I.G., Coe, R.S., Glen, J.M.G., Prevot, M., Perrin, M., 1992. The age of Parana flood volcanism, rifting of Gondwanaland, and the Jurassic-Cretaceous boundary. Science 258:975–979 (80-). 10.1126/science.258.5084.975.

Riccomini, C., Sant'Anna, L.G., Fambrini, G.L., 2016. The Early Cretaceous Jacuí Group, a newly discovered volcaniclastic–epiclastic accumulation at the top of the Paraná Basin, southern Brazil. Cretac. Res. 59:111–128. http://dx.doi.org/10.1016/j.cretres.2015.10.020.

Rossetti, L.M.L.M., Lima, E.F.E.F., Waichel, B.L.B.L., Scherer, C.M.C.M., Barreto, C.J.C.J., 2014. Stratigraphical framework of basaltic lavas in Torres syncline main valley, southern Parana-Etendeka Volcanic Province. J. S. Am. Earth Sci. 56:409–421. http://dx.doi.org/10.1016/j.jsames.2014.09.025.

Salvador, A. (Ed.), 1994. International Stratigraphic Guide: A Guide to Stratigraphic Classification, Terminology, and Procedure (2nd edition). International Subcommission on Stratigraphic Classification. The International Union of Geological Sciences and The Geol. Soc. Am., Inc., Boulder, Colorado.

Scherer, C.M.S., 2002. Preservation of aeolian genetic units by lava flows in the lower Cretaceous of the Paran Basin, southern Brazil. Sedimentology 49:97–116. http://dx.doi.org/10.1046/j.1365-3091.2002.00434.x.

Self, S., Thordarson, T., Keszthelyi, L., Walker, G.P.L., Hon, K., Murphy, M.T., Long, P., Finnemore, S., 1996. A new model for the emplacement of Columbia River basalts as large, inflated Pahoehoe Lava Flow Fields. Geophys. Res. Lett. 23:2689–2692. http://dx.doi.org/10.1029/96GL02450.

Self, S., Thordarson, T., Keszthelyi, L., 1997. Emplacement of Continental Flood Basalt Lava Flows, Large Igneous Provinces: Continental, Oceanic, and Planetary Flood Volcanism. Geophysical Monograph SeriesAmerican Geophysical Union, Washington, D.C. http://dx.doi.org/10.1029/GM100.

Self, S., Keszthelyi, L., Thordarson, T., 1998. The importance of Pahoehoe. Annu. Rev. Earth Planet. Sci. 26:81–110. http://dx.doi.org/10.1146/annurev.earth.26.1.81.

Simões, M.S.M.S., De Rossetti, L.M.M., Lima, E.F.D.E.F. De, Ribeiro, B.P.B.P., Rossetti, L.D.M.M., Lima, E.F.D.E.F. De, Ribeiro, B.P.B.P., 2014. The role of viscosity in the emplacement of high-temperature acidic flows of Serra Geral formation in Torres Syncline (Rio Grande do Sul State, Brazil). J. Geol. 44:669–679. http://dx.doi.org/10.5327/Z2317488920140004001O.

Single, R., Jerram, D., 2004. The 3D facies architecture of flood basalt provinces and their internal heterogeneity: examples from the Palaeogene Skye Lava Field. J. Geol. Soc. Lond. 161, 911–926.

Stewart, K., Turner, S., Kelley, S., Hawkesworth, C., Kirstein, L., Mantovani, M., 1996. 3-D, 40Ar-39Ar geochronology in the Paraná continental flood basalt province. Earth Planet. Sci. Lett. 143:95–109. http://dx.doi.org/10.1016/0012-821X(96)00132-X.

Sun, S.-S., McDonough, W.F., 1989. Chemical and isotopic systematics of oceanic basalts: implications for mantle composition and processes. In: Saunders, A.D., Norry, M.I. (Eds.), Magmatism in the Ocean Basins, Spec. Publ. 42. The Geological Society, London, pp. 313–345.

Swanson, D.A., Wright, T.L., Helz, R.T., 1975. Linear vent systems and estimated rates of magma production and eruption for the Yakima Basalt on the Columbia Plateau. Am. J. Sci. 275, 877–905.

Thiede, D., Vasconcelos, P., 2010. Paraná flood basalts: rapid extrusion hypothesis confirmed by new $^{40}Ar/^{39}Ar$ results. Geology:747–750. http://dx.doi.org/10.1130/G30919.1.

Thordarson, T., Self, S., 1998. The Roza Member, Columbia River Basalt Group: a gigantic pahoehoe lava flow field formed by endogenous processes? J. Geophys. Res. Solid Earth 103:27411–27445. http://dx.doi.org/10.1029/98JB01355.

Uman, L.V., Lima, E.F., Sommer, C.A., De Liz, J.D., 2001. Vulcanismno acido de Cambara da Serra RS Litoquimica e discussão sobre a origem dos depositos.pdf. Rev. Bras. Geosci. 31, 357–364.

Waichel, B.L., de Lima, E.F., Lubachesky, R., Sommer, C.A., 2006. Pahoehoe flows from the central Paraná Continental Flood Basalts. Bull. Volcanol. 68:599–610. http://dx.doi.org/10.1007/s00445-005-0034-5.

Waichel, B., Scherer, C., Frank, H., 2008. Basaltic lava flows covering active aeolian dunes in the Paraná Basin in southern Brazil: features and emplacement aspects. J. Volcanol. Geotherm. Res. 171:59–72. http://dx.doi.org/10.1016/j.jvolgeores.2007.11.004.

Waichel, B.L., de Lima, E.F., Viana, A.R., Scherer, C.M., Bueno, G.V., Dutra, G., 2012. Stratigraphy and volcanic facies architecture of the Torres Syncline, Southern Brazil, and its role in understanding the Paraná–Etendeka Continental Flood Basalt Province. J. Volcanol. Geotherm. Res. 215–216:74–82. http://dx.doi.org/10.1016/j.jvolgeores.2011.12.004.

Walker, G.P.L., 1971. Compound and simple lava flows and flood basalts. Bull. Volcanol. 35:579–590. http://dx.doi.org/10.1007/BF02596829.

White, J., Bryan, S., Ross, P., 2009. Physical volcanology of continental large igneous provinces: update and review. In: Thordarson, T., Self, S., Larsen, G., Rowland, S.K., Hoskuldsson, A. (Eds.), Studies in Volcanology: The Legacy of George Walker. Special Publications of IAVCEI 2. Geological Society, London, pp. 291–321.

Wilmoth, R.A., Walker, G.P.L., 1993. P-type and S-type pahoehoe: a study of vesicle distribution patterns in Hawaiian lava flows. J. Volcanol. Geotherm. Res. 55:129–142. http://dx.doi.org/10.1016/0377-0273(93)90094-8.

Anexo II

Evaluating petrophysical properties of Volcano-sedimentary sequences: A case study in the Paraná-Etendeka Large Igneous Province

Submission Confirmation

Marine and Petroleum Geology <eesserver@eesmail.elsevier.com>

seg 30/04/2018 01:45

Para:lucasross@hotmail.com <lucasross@hotmail.com>; l.rossetti@abdn.ac.uk <l.rossetti@abdn.ac.uk>;

Article Type: Full Length Article.

Dear Lucas,

We have received your article "Evaluating petrophysical properties of Volcano-sedimentary sequences: A case study in the Paraná-Etendeka Large Igneous Province" for consideration for publication in Marine and Petroleum Geology.

Your manuscript will be given a reference number once an editor has been assigned.

To track the status of your paper, please do the following:

1. Go to this URL: https://ees.elsevier.com/jmpg/

2. Enter these login details:
Your username is: lucasross@hotmail.com
Your password is: *******

3. Click [Author Login]
This takes you to the Author Main Menu.

4. Click [Submissions Being Processed]

Thank you for submitting your work to this journal.

Kind regards,

Elsevier Editorial System
Marine and Petroleum Geology

****
Please note that the editorial process varies considerably from journal to journal. To view a sample editorial process, please click here: http://ees.elsevier.com/eeshelp/sample_editorial_process.pdf

For further assistance, please visit our customer support site at http://help.elsevier.com/app/answers/list/p/7923. Here you can search for solutions on a range of topics, find answers to frequently asked questions and learn more about EES via interactive tutorials. You will also find our 24/7 support contact details should you need any further assistance from one of our customer support representatives.

Evaluating petrophysical properties of Volcano-sedimentary sequences: A case study in the Paraná-Etendeka Large Igneous Province

Lucas M. Rossetti[1,2*], David Healy[2], Malcolm J. Hole[2], John M. Millett[2,3], Evandro F. de Lima[1], Dougal A. Jerram[4,5], Marcos M.M. Rossetti[1,6]

*Corresponding author. E-mail: l.rossetti@abdn.ac.uk, lucasross@hotmail.com

[1] Instituto de Geociências, Universidade Federal do Rio Grande do Sul - Av. Bento Gonçalves, 9500, Agronomia, CEP: 91501-970, Porto Alegre, RS, Brazil

[2] Department of Geology and Petroleum Geology, University of Aberdeen, Aberdeen - AB24 3UE, UK

[3] VBPR AS, Oslo Science Park, Gaustadalléen 21, N-0349 Oslo, Norway

[4] Centre for Earth Evolution and Dynamics (CEED), University of Oslo, Norway

[5] DougalEARTH Ltd., Solihull, UK

[6] Department of Geological Sciences, University of Canterbury, Private Bag 4800, Christchurch, New Zealand

Abstract

The Paraná-Etendeka represents a major magmatic province associated with the rifting of West Gondwana and the formation of the South Atlantic Ocean. The area represents a direct analogue for similar aged volcanic rocks buried within hydrocarbon rich basins offshore the South Atlantic margin. We present here a detailed integration of outcrop data with laboratory measurements of porosity, permeability, and ultrasonic acoustic velocities (P- and S-waves) for volcanic and interbedded sedimentary rocks of the Paraná-Etendeka Province in southern Brazil. The lava pile is formed of compound pahoehoe basaltic lavas at the base (Torres Formation) followed by thick tabular rubbly pahoehoe basaltic andesites (Vale do Sol Formation) and the upper stratigraphy is characterized by local fed and extensive tabular dacitic/rhyolitic units. Sedimentary interbeds occur along with the entire lava pile. For the volcanic rocks petrophysical properties have a cyclic variation controlled by the lava internal structure. Lava upper and lower crust have relatively high porosity (> 10%) and low acoustic velocities, whilst lava flow core is characterized by porosities of less than 5% and velocities typically 0.5-1.0 kms^{-1} higher. The highest porosities are found in the upper crust of both

rubbly pahoehoe (c. 28.3%) and pahoehoe lavas (c. 26.6%) where vesicles account for most of the pore space. Permeability is relatively low in the volcanic facies (< 1 mD), and this fact is associated with pore infilling during burial diagenesis/hydrothermal alteration. Sedimentary interbeds preserve relatively high porosity (>15%) and permeability (avg. 450 mD) and represent the best reservoir rocks in the Paraná-Etendeka Province. Nevertheless, where diagenesis is intense porosity and permeability are significantly diminished. The petrophysical properties of volcanic rocks are controlled primarily by lava emplacement mechanisms (e.g. inflation, degassing and flow fragmentation), and secondarily by bulk mineral composition. Petrophysical properties can be further modified by diagenetic and/or hydrothermal alteration processes. Understanding the interplay between primary and secondary processes on the final petrophysical characteristics of the rocks is key on defining reservoir properties in offshore areas, such as the North and South Atlantic margins, where volcanic rocks are intrinsically associated with prolific hydrocarbon bearing sedimentary basins.

Keywords: volcanic reservoirs; lava flow reservoir; basalt porosity; rock physics; acoustic velocity;

1. Introduction

The Paraná-Etendeka Large Igneous Province (Fig. 1) is the onshore portion of the South Atlantic continental rifted margins, formed during the fragmentation of Western Gondwana and the opening of the South Atlantic Ocean in the Early Cretaceous (e.g. Gladczenko et al., 1997). In the offshore areas thick wedges of seaward-dipping reflectors, are constrained between the Agulhas - Falkland and the Rio Grande - Walvis fracture zones, forming the magma rich austral segment of the margin. To the north of the Rio Grande-Walvis fracture zone, relatively minor volumes of volcanic rocks characterize the magma-poor sector of the margin. These lavas and volcanoclastic sediments are now deeply buried in offshore, hydrocarbon-rich, sedimentary basins in both the South American and African conjugate margins (Mizusaki et al., 1988, 1992, Mohriak et al., 1990, 2002; Stica et al., 2014; Torsvik et al., 2009; Jerram et al., submitted). These basins represent some of the most prolific oil-producing areas in Brazil (Coward et al., 1999; Stica et al., 2014), and prospective hydrocarbon basins in Africa (e.g. Kwanza/Namibe; Gindre-Chanu et al., 2016; Jerram et al., submitted), and include minor occurrences and production of hydrocarbons from volcano-sedimentary reservoirs such as in the Badejo, Pampo and Linguado Fields (e.g. Mizusaki et al., 1988).

Important occurrences of hydrocarbons with commercial significance have been reported in volcanic provinces globally (e.g. Schutter, 2003). A wide variety of igneous hosted reservoirs have been proven including in major facies units such as lava flows (Wilson et al., 2008; Farooqui et al., 2009), sill intrusions (Monreal et al., 2009; Senger et al., 2017), and pyroclastic rocks (Vernik, 1990; Sruoga et al., 2004; Feng et al., 2014) along with sedimentary reservoirs interbedded or buried by volcanic sequences (Stanistreet and Stollhofen, 1999; Jerram et al., 1999a; Schofield and Jolley, 2013). Understanding the interplay between volcanism and sedimentation is critical for defining facies distribution and geometries when evaluating potential targets within prolific basins (Jerram et al., 1999a; Ebinghaus et al., 2014; Schofield and Jolley, 2013; Vosgerau et al., 2015). Given their high degree of heterogeneity, and potential problems concerning clays, volcanic rocks have dominantly been considered secondary targets in hydrocarbon exploration (Schutter, 2003; Farooqui et al., 2009). A relative lack of detailed studies has lead to an often simplified vision of the

volcanic hosted pore systems, with reservoir properties commonly being attributed to the presence of tectonic fractures and weathering (e.g. the Serie Tobifera in the Austral basin; see discussion in Sruoga et al., 2004). In reality, the porosity of igneous rocks is a result of a complex interplay between primary and secondary processes (Sruoga and Rubinstein, 2007; Jiang et al., 2017), and the degree to which each factor contributes to the final petrophysical response of different volcanic rocks change in detail for each facies throughout any given province.

In this context, outcrop analogues are critical to understanding and correlating facies in offshore areas, and provide important information to support wireline log and seismic interpretation (Jerram et al., 2009; Nelson et al., 2009; Millett et al., 2014, 2015; Watton et al., 2014a), and can also have significant implications for drilling through volcanic sequences (Millett et al., 2016). Moreover, the measurement of petrophysical data from outcrop analogues is crucial to defining facies-porosity relationships and extrapolating facies specific property distribution to reservoir models (Single and Jerram, 2004; Sruoga et al., 2004; Sruoga and Rubinstein, 2007; Lenhardt and Götz, 2011; Grove et al., 2017).

In this study, we present a detailed integration of outcrop data with laboratory measurements of porosity, permeability, and ultrasonic acoustic velocities (P- and S-waves) for 160 core plug samples from the volcanic and interbedded sedimentary rocks of the Paraná-Etendeka Large Igneous Province, in southern Brazil. These samples constitute the first combined volcano-sedimentary dataset of its kind in this province and represent a direct analogue for similar-aged volcanic rocks present within the basins in the South Atlantic conjugate margin e.g. offshore Brazil, Angola and Namibia, where significant hydrocarbon prospectivity and discoveries exist.

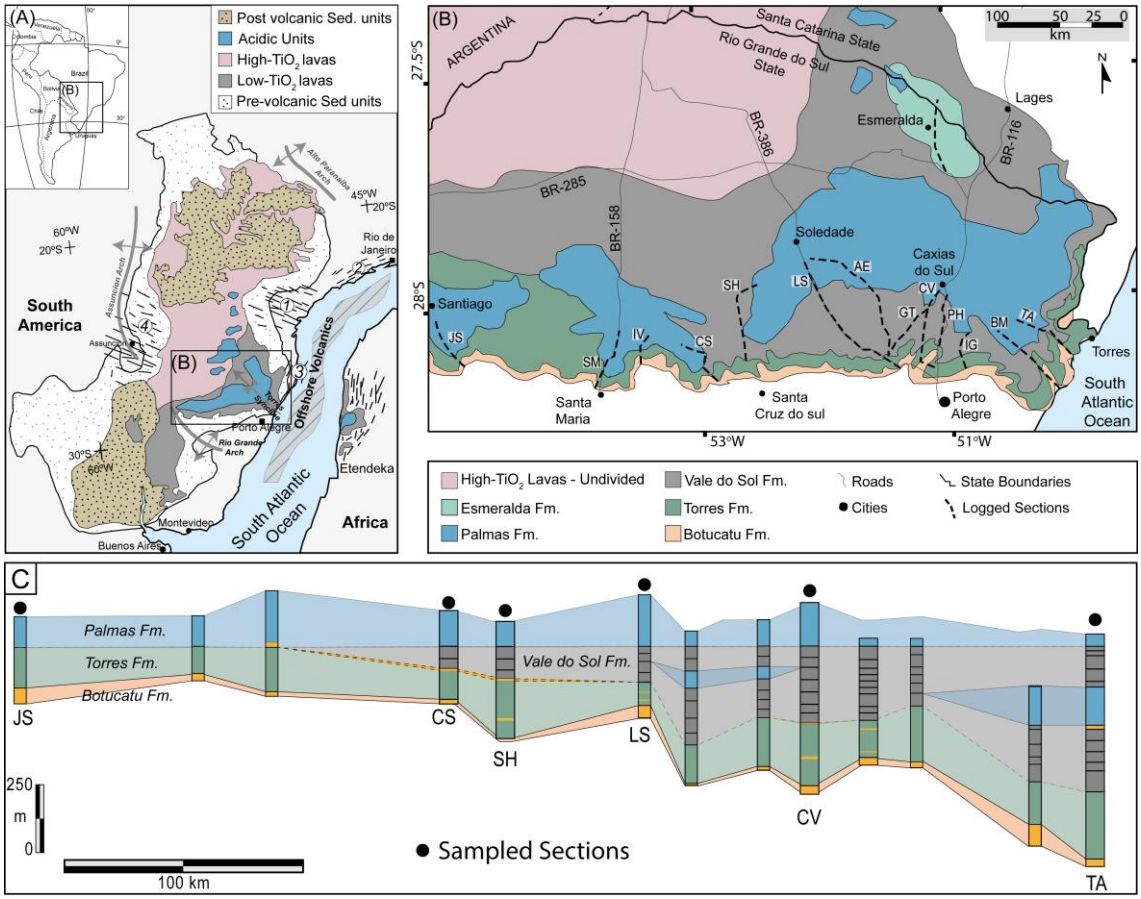

Fig. 1 – (A) Location of the Paraná-Etendeka Igneous Province, major dike swarms (1 - Ponta Grossa; 2 – Santos - Rio de Janeiro; 3 – Florianopolis; 4 – Paraguay) and tectonic structures in a pre-drift reconstruction of Western Gondwana (modified after Peate et al., 1992; Stewart et al., 1996). (B) Detailed geological map of the Paraná-Etendeka LIP in Southern Brazil, key localities and sampled sections (modified after Rossetti et al. 2017); (C) Volcano-stratigraphy and sampled localities. JS=Jaguari–Santiago; CS=Candelária–Sobradinho; SH - Santa Cruz do Sul-Herveiras; LS=Lajeado–Soledade; CV=São Sebastião do Caí–Caxias do Sul; TA=Terra de Areia – Aratinga (modified after Rossetti et al. 2017).

2. The Paraná-Etendeka Large Igneous Province

The Paraná-Etendeka LIP covers an onshore area of 1.6x 10^6 km^2 over the South American platform (Brazil, Argentina, Uruguay, and Paraguay), and minor portions of southwestern Africa, in Namibia and Angola (Piccirillo and Melfi, 1988; Peate, 1997). The province is composed mainly of subaerially emplaced basaltic lavas, and minor (<2.5%) silicic units. The lava pile has an onshore

preserved maximum thickness of 1.750 m in the central portion of the Paraná basin (Piccirillo and Melfi, 1988). In western Africa, the Etendeka Lava group occupies an area of $0.8x10^5$ km^2 (Erlank et al., 1984) and similar areas are also covered by the Paraná-Etendeka magmatism in Angola (Marzoli et al., 1999; Marsh and Swart, 2017; Jerram et al., submitted). Extensive dyke swarms occur along the coastal areas of Brazil, Angola, and Namibia, as well as volcanic centres (particularly well exposed along the African margin), which represent portions of the plumbing systems that fed the lavas (Raposo et al., 1998; Jerram et al., 1999a; Florisbal et al., 2014; Sarmento et al., 2017).

The rocks are Early Cretaceous in age, and the entire magmatic event is constrained to a c. 4 Ma interval, from 135 to 131 Ma (Janasi et al., 2011; Dodd et al., 2015) with the main peak of volcanism lasting c. 1 Ma (Renne et al., 1992; Jerram and Widdowson, 2005; Thiede and Vasconcelos, 2010; Baksi, 2017). In Brazil, the volcanic rocks fall within the Serra Geral Group, and the lavas cover an area of c. 917,000 km^2, overlying the sedimentary rocks of the Paraná basin (Frank et al., 2009). The chemical distribution of magma types provides a regional framework for the lava stratigraphy (Peate et al., 1992). In the south, low-TiO_2 (Ti/Y) Gramado and Esmeralda magma types prevail with minor occurrences of Urubici magma type (high-TiO_2); in contrast, the northern sector is characterized by Ribeira, Pitanga and Paranapanema high-TiO_2 magma type basalts, respectively (Peate, 1997). Acidic volcanic units are preserved in both sectors. Palmas dacites and rhyolites occur in the upper portions of the stratigraphy in the southern area (Peate, 1997; Nardy et al., 2008), while the Chapecó geochemical type occurs in the lower portion of the high-TiO_2 lava pile, covering low-TiO_2 lavas, in the central Paraná, and covering basement rocks in the northern limit of the basin (Piccirillo et al., 1987; Janasi et al., 2007). These chemical types can be correlated to their equivalents on the African side, allowing for further understanding of the connection and distribution of key facies within the Paraná-Etendeka (Peate et al., 1992; Milner et al., 1995; Jerram et al., 1999a).

In the southern sector of the province, the onset of magmatism is recorded by basalt lavas emplaced over a dry desert environment (Jerram et al., 2000; Scherer, 2002; Waichel et al., 2008). Sedimentation persisted throughout the magmatism and is preserved as peperites and sedimentary interbeds deposited during breaks in volcanic activity (Jerram et al., 1999a, 1999b; Jerram and

Stollhofen, 2002; Petry et al., 2007; Waichel et al., 2008). The initial lava eruptions preserved significant parts of the major erg structure which usually would have little preservation potential (e.g. Mountney et al., 1999). Pauses between the first eruptive phases lead to continuous sand bodies forming a minor erg that reached 60 m high and was buried and preserved by subsequent basalt lavas(Jerram et al., 1999b, 2000). Paleocurrents of these minor ergs show minor variations, from NW towards SE, when compared to those from the main erg, referred as Tweifelfontain-Botucatu Formation, which had a dominant flow towards NE (Mountney et al., 1998; Jerram et al., 1999b; Scherer, 2002). These sedimentary units are comparable to the composite interbedded lava-sedimentary reservoirs of the Kudu gas field offshore Namibia (Stanistreet and Stollhofen, 1999). Thick tabular basaltic andesitic lavas and more acidic units were emplaced during the climax of magmatism, and minor pahoehoe flow fields with restricted areal occurrence characterized the waning phase of volcanic activity (Jerram et al., 1999a; Waichel et al., 2012; Rossetti et al., 2017). Offshore Brazil, the lava flows from the Paraná-Etendeka province occur as a homonymous unit (Serra Geral) in the Pelotas Basin and are stratigraphically correlated with the Cabiúnas and Camburiú volcanic sequences, of Campos and Santos basins, respectively (Stica et al., 2014).

3. Key volcano-stratigraphic units and sampled stratigraphy

The lava pile was deposited over predominantly aeolian sandstones, known as the Botucatu Formation along the Brazilian margin, during the Early Cretaceous. The volcano-stratigraphy is composed of four volcanic units divided based on their lithological characteristics, facies architecture, flow morphologies, intra-facies, and geochemical compositions, namely: Torres, Vale do Sol, Palmas and Esmeralda Formations (Rossetti et al. 2017). Sedimentary interbeds are preserved throughout the lava pile and were formed during periods of volcanic quiescence. Before the petrophysical methods and data are introduced, the characteristics of the sampled lava units are described in terms of observations on the architecture of deposits, flow morphology and internal structures along with the key petrographic aspects of the units.

3.1. Torres Formation

The Torres Formation is the lowermost volcanic unit and represents the early stages of magmatic activity in the area (Rossetti et al. 2017). The unit has an average thickness of 200 m and is formed of basalt and basaltic andesite lavas emplaced as inflated sheet-like lobes (Fig. 2A), thick ponded lavas (Fig. 2B) and compound pahoehoe flow fields (Fig. 2C), distributed in a compound braided facies architecture (e.g. Jerram, 2002). The internal structure is typical of pahoehoe lavas with (1) a lower crust, composed of elongates pipe vesicles (Fig. 2D); (2) a poorly vesicular, crystalline lava core (Fig. 2E); and (3) a vesicle rich upper crust (Fig. 2F). Thick lava units (c. 60 m) occur where the lava is confined by topographic lows in the interdune paleo valleys and these ponded lavas are in general coarsely crystalline and characterized by irregular columnar joints (Fig. 2B). Torres Formation lavas are aphyric to poorly porphyritic (<5% phenocrysts), with plagioclase as the main phenocryst phase, and minor quantities of olivine (pseudomorphs). The groundmass is fine to medium grained and formed by plagioclase microphenocrysts (0.4 - 1.2 mm), with intergranular and subophitic augite (<1 mm), and minor volumes of iron oxides (Fig. 3A). Olivine occurs only as altered pseudomorphs in some lavas and is fully replaced by iddingsite and bowlingite aggregates (Fig. 3A). In general, lava flow cores are fresh, with only incipient alteration, mainly marked by olivine replacement. Where the alteration is more intense, augite is partial to completely replaced by smectite, and the calcic core of plagioclase crystals are transformed to albite. Spherical (0.5 -2.5 mm) vesicles represent the most abundant pore type and are concentrated in the lava upper crust, with many being filled by secondary zeolite to form amygdales (Fig. 3B-D). Subordinately, intercrystalline diktytaxitic voids (Fig.3C) contribute to the primary porosity. Secondary porosity is composed of micro-fractures and crystal dissolution (and sieve texture), particularly of the calcic cores of plagioclase phenocrysts (Fig. 3B-C).

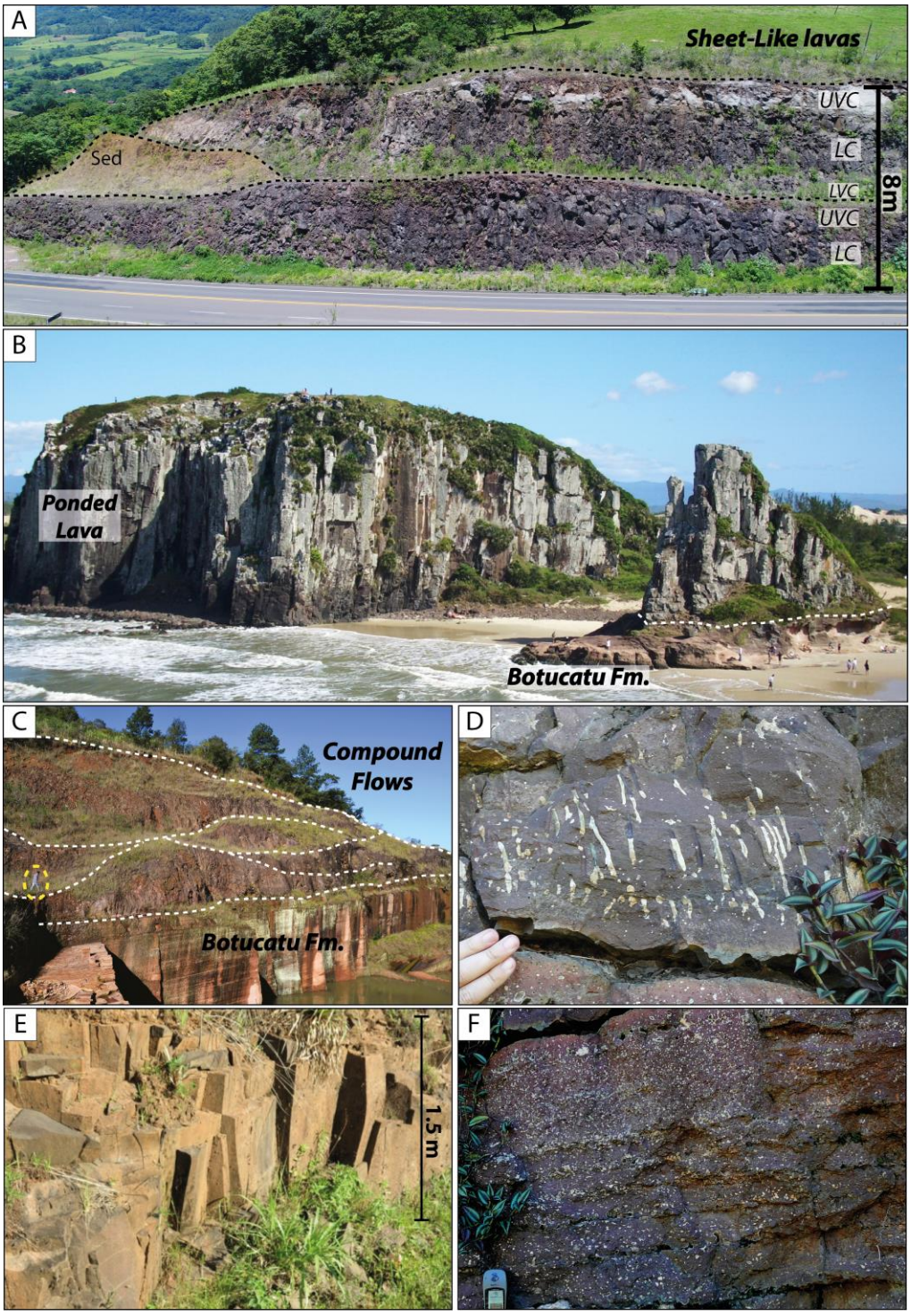

Fig. 2 – Architecture and internal structures of Torres Formation lavas. (A) Sheet-like pahoehoe lavas, with a tripartite structure of lower vesicular crust (LVC), lava core (LC), and upper vesicular crust (UVC). Two lavas are separated by a sedimentary interbed; (B) Thick ponded lava confined in the interdune valley of Botucatu sandstone; (C) Compound pahoehoe lava flow field composed of metric lava lobes; (D) lower vesicular crust, with elongated pipe vesicles/amygdales; (E) lava flow core with irregular columnar joints; (F) upper vesicular crust.

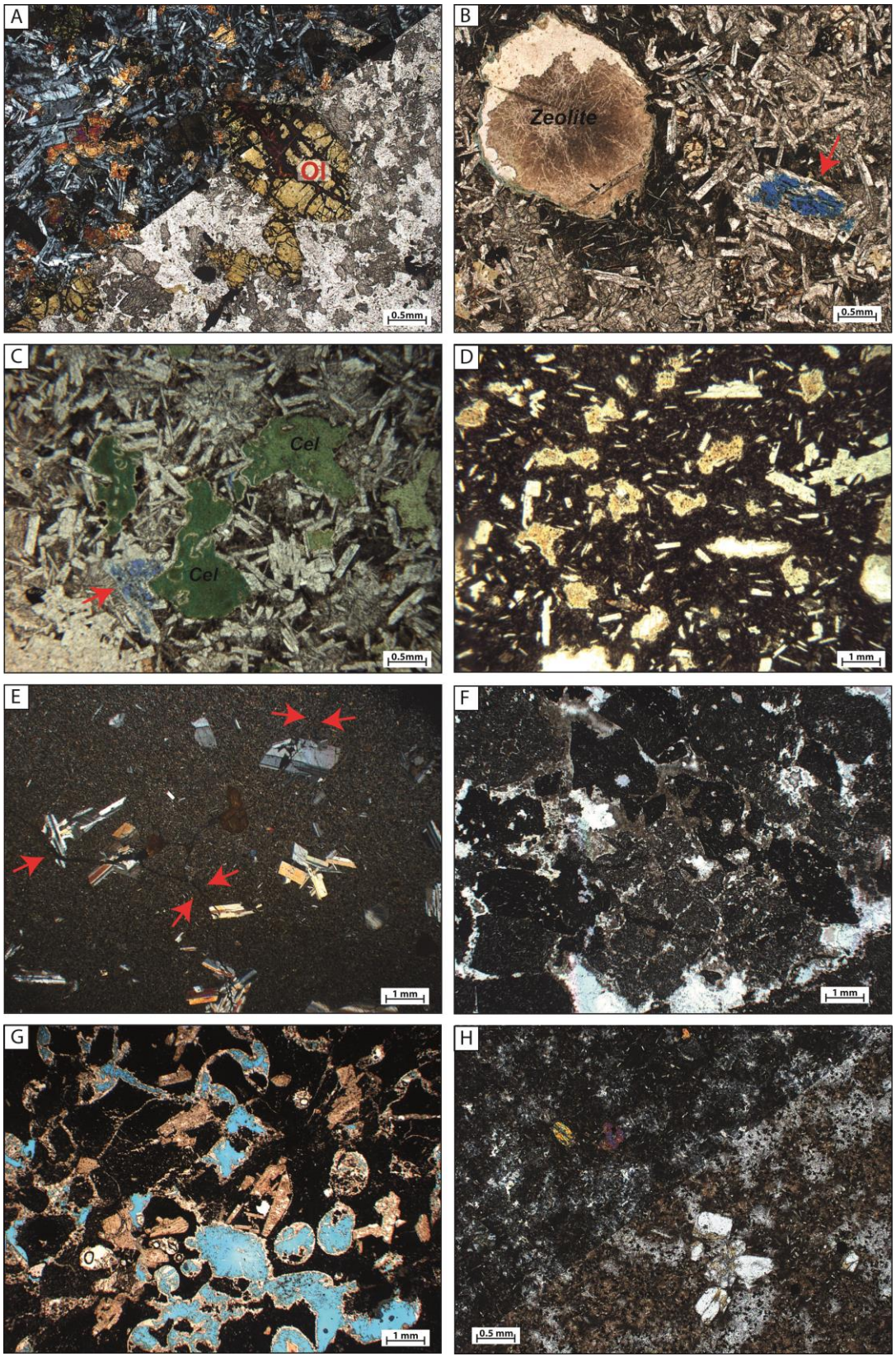

Fig. 3 – Representative photomicrography of volcanic rocks. (A) olivine-phyric basalt, lava core of pahoehoe lava, Torres Formation. (B) Vesicular basalt with primary pore filled by zeolite, and secondary porosity formed by dissolution of plagioclase phenocryst, Torres Formation. (C) Irregular intercrystalline pores

filled by celadonite (Cel) and secondary pore from crystal dissolution (red arrow) in lava flow core, Torres Formation. (D) Upper vesicular crust with irregular pores filled with clay minerals, Torres Formation. (E) plagioclase-phyric rubbly pahoehoe lava core, with microcrystalline groundmass, tectonic fracture cross-cutting groundmass and phenocrysts (red arrow), Vale do Sol Formation. (F) Irregular angular fragments in rubbly flow top, pore space filled with zeolite, Vale do Sol Formation. (G) Vesicular fragment of rubbly flow top of basaltic andesite lava, broken vesicle walls form minor angular fragments. Primary porosity (vesicles) partially filled by zeolite, Vale do Sol Formation. (H) Plagioclase and pyroxene microphenocrysts in a devitrified matrix of dacite lava core, Palmas Formation.

3.2. Vale do Sol Formation

The Vale do Sol Formation is dominantly composed of basaltic andesite lavas along with rare basalts. The lava package reaches 500 m in thickness in the central portion of the Torres Syncline and is formed of vertically stacked thick (c. 40m), sheet-like lavas displaying a classic tabular facies distribution (Jerram, 2002). The internal structure is typical of rubbly pahoehoe lavas (Keszthelyi et al., 2006; Duraiswami et al., 2008). (Keszthelyi et al., 2006; Duraiswami et al., 2008). These are typically found in equivalent sections along the Etendeka side of the sequence (e.g. Jerram et al., 1999a), and they can be internally divided into four sub-facies: (1) a smooth vesicular base (<1 m thick); (2) an aphanitic massive core with irregular joints; (3) a coherent upper vesicular crust and (4) a rubbly flow surface (Fig. 4A - E). The flow basal boundary of the flows is commonly glassy and oxidized and the basal crust is sparsely vesicular and aphanitic, ranging from 0.2 - 1 m in thickness, with spherical (2 - 5 mm, Fig. 4C) to sub-spherical stretched vesicles. The core of the lavas are aphanitic with irregular columnar joints (Fig. 4B) and represent most of the flow thickness (60 - 80%). The upper crust is composed of a coherent portion and a fragmented rubbly surface. The coherent upper crust is 1 - 3 m thick and coarsely vesicular/amygdaloidal (vesicles with 1 to 6 cm in diameter – Fig. 4D). The rubble layer is 3 - 10 m thick, with an irregular geometry, formed of vesicular basalt fragments of previously formed pahoehoe crust. The fragments vary from 5 to 25 cm diameter and are generally sub-angular to sub-rounded, in some cases,

cemented by zeolites (Fig. 4E). Petrographically, the lavas are plagioclase-phyric to aphyric, with a microcrystalline to fine-grained groundmass formed mainly of plagioclase, with augite as intergranular and subophitic crystals with subordinate iron oxides (Fig. 3E). Vesicles are typically irregular to elongated suggesting extensive coalescence and are set within a finely crystalline to glassy matrix. In the upper rubble, fragments are subangular and individual fragments displaying various degrees of crystallinity and vesicularity (Fig. 3F). The transition from coherent vesicular flow top to fragmented rubble is gradual and marked by the collapse of vesicles prior brecciation (Fig. 3G).

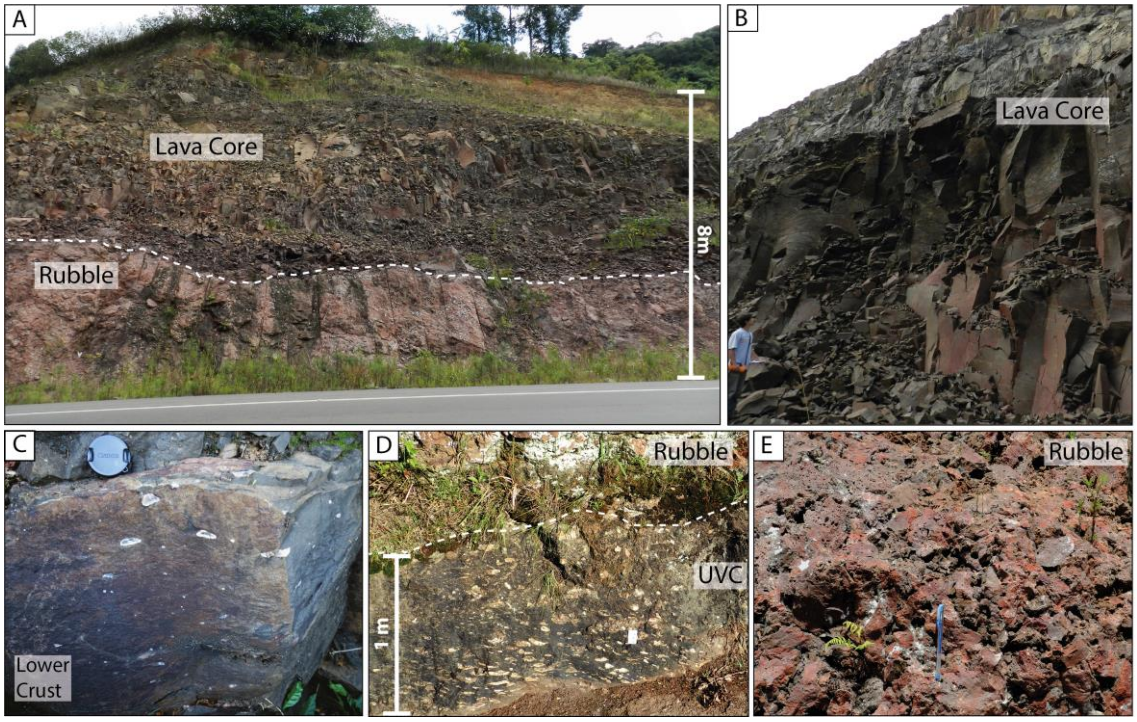

Fig. 4 – Morphology and lithofacies of rubbly pahoehoe lavas from Vale do Sol Formation. (A) Contact of rubbly flow top and coherent lava core; (B) Thick fractured lava core; (C) lower crust with sparse amygdales; (D) Upper coherent crust with large stretched vesicles filled with zeolite in contact with altered rubble; (E) Rubbly flow top.

3.3. Palmas Formation

The Palmas Formation occurs in the upper portions of the stratigraphy and is composed of dacite and rhyolite lava domes, coulees and extensive tabular flows, fed dominantly by fissure systems (Polo et al., 2017; Rossetti et al., 2017; Simões et al., 2017; Lima et al., 2018). The extensive tabular lavas of the Palmas

Formation are characterized by a basal flow-foliated and flow-folded portion with isolated elongated vesicles, that grades upwards to a fine-grained granophyric massive flow core. Locally the lava core is strongly fractured with regularly spaced horizontal joints. Autobreccias are found locally, usually forming pockets of angular vitric fragments in an altered fine-grained matrix in the extremities of the flows. Large unfilled gas cavities (10-20 cm in diameter) occur in the upper portions of flow core. The flow extremities are lobate, varying from 2 - 10 m in thickness and characterized by an altered external portion, a vesicular upper crust, and a massive core (see Fig. 10 – Rossetti et al. 2017). Minor, locally fed lavas display an external fragmented portion formed of vesicular lava blocks (Fig. 5A) that grades inwards to a coherent vesicular layer (Fig. 5B) and a massive fractured lava core (Fig. 5C). Petrographically, the rocks are aphanitic to vitrophyric, with sparse isolated or grouped plagioclase and augite phenocrysts, surrounded by a devitrified matrix composed of feldspar-quartz overgrowths (Fig. 3H).

3.4. Sedimentary interbeds

Sedimentary interbeds are preserved throughout within the entire lava pile. The accumulation of these deposits is controlled by the underlying lava field topography in some instances, but can also be captured and preserved by lava flow burial (e.g. Jerram et al., 2000; Waichel et al., 2008). The sedimentary beds are characterized by isolated sand bodies interlayered with lava flows, and these can occur as two different deposits: (1) thin lenses (<3 m thick) characterized by horizontal to low-angle wind ripple lamination formed by aeolian sand sheets; and (2) thick sand lenses (3–15 m) comprising cross-bedded co-sets generated by migration and climbing of simple to locally composite crescentic aeolian dunes (Scherer, 2002). The beds have an irregular and concave base and a flat top and occur as stratified and massive sandstones facies (Fig. 6A). The stratified facies are formed of fine to medium grained sand with wind ripple laminations, composed of quartz, subordinate K-feldspar, minor quantities of plagioclase, and volcanic fragments (Fig. 6B). Massive sandstones are altered, with K-feldspars, and plagioclase being partial to completely replaced by clay minerals and it is characterized by obliterated sedimentary structures relating to post-depositional alteration. In some cases, the sandstones are strongly silicified, due to

hydrothermal alteration and porosities are significantly diminished. Porosity is intergranular and higher in the stratified facies where diagenesis is mostly due to mechanic compaction. In the massive silicified facies, diagenesis is more intense and the precipitation of clay minerals and silica during alteration (diagenetic and hydrothermal) has led to a significant decrease in pore space.

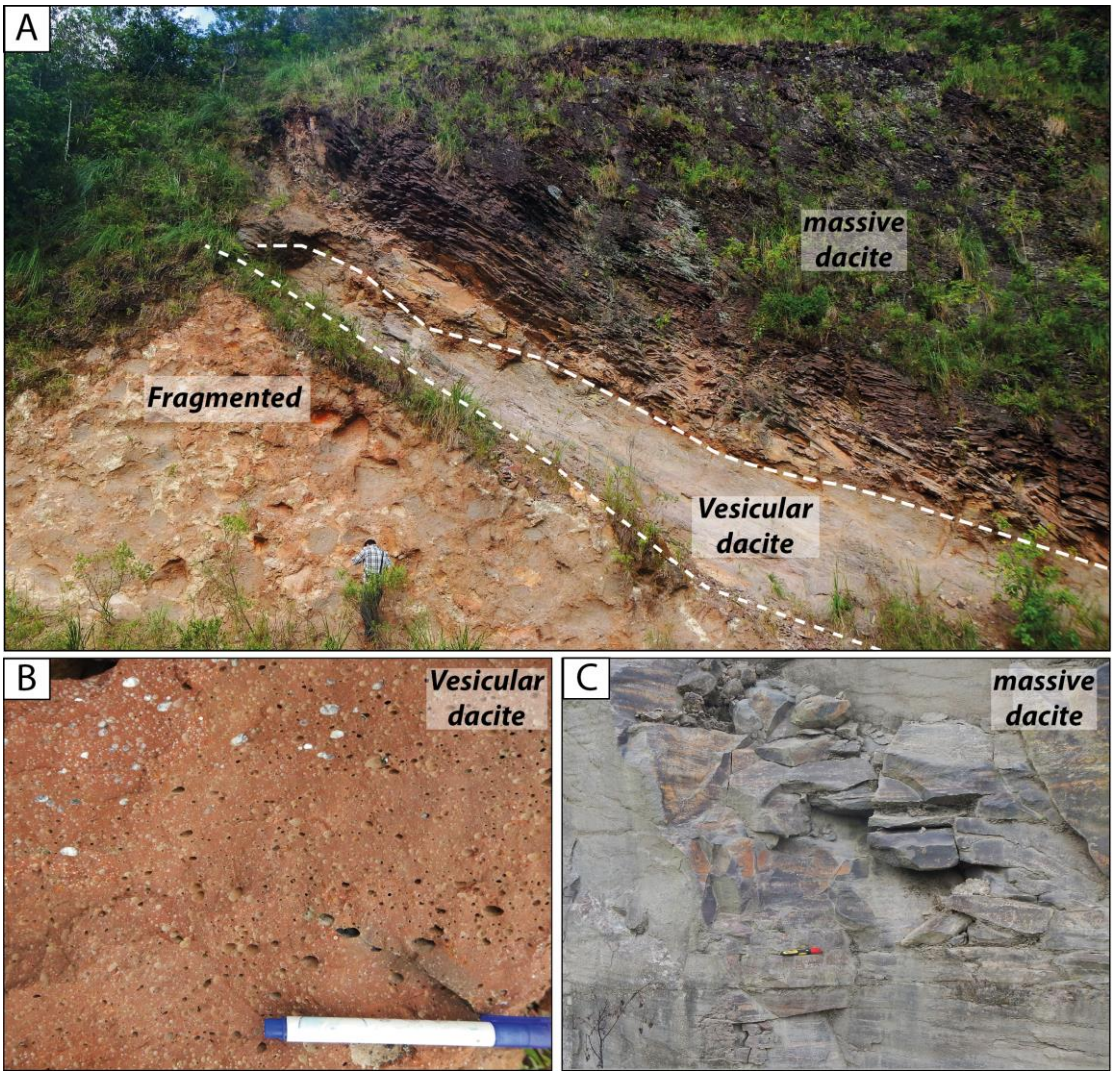

Fig. 5 – Lithofacies distribution of Palmas Formation lavas. (A) Dacitic lava flow with fragmented external portion, vesicular internal layer and massive-fractured flow core. (B) Coarsely vesicular dacite. (C) Massive dacite lava flow core.

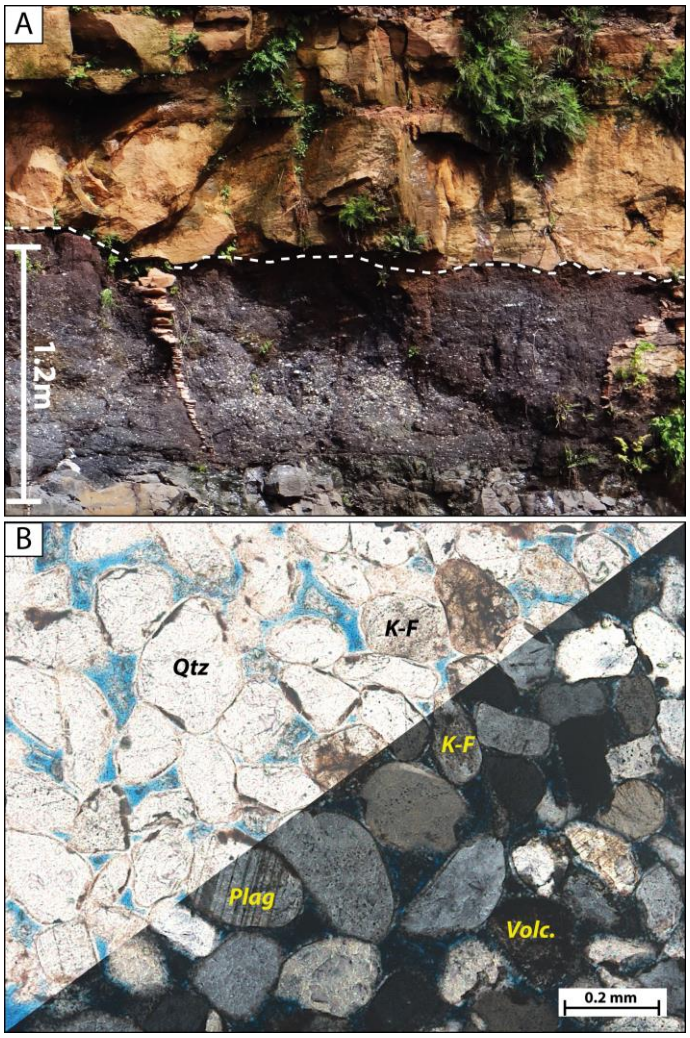

Fig. 6 – (A) Cross stratified sandstone covering vesicular lava surface and infilling flow fracture. (B) Thin section of well sorted and rounded, fine-grained aeolian sandstone from interbed, composed of quartz and minor contribution of k-feldspar plagioclase and volcanic fragments.

4. Methodology

The stratigraphic distribution and characteristics of volcanic and sedimentary lithotypes investigated in this study have been mapped and logged in detail along stratigraphic sections in Southern Brazil (Rossetti et al., 2017; Fig. 1B and 1C). Rock samples were collected along these sections, and a total of 160, one-inch (c. 25.4 mm) diameter core plugs were prepared and analysed for helium porosity, permeability and ultrasonic acoustic P- and S- wave velocities (V_p and V_s) at the *Rock Physics and Geomechanics Laboratory* at the University of Aberdeen. The analysis was carried out in oven-dried, unsaturated samples, under ambient (atmospheric) pressure and temperature conditions. Porosities

were measured in a helium porosimeter, and permeability was measured using a Hassler sleeve nitrogen permeameter, with gas slippage accounted for by Klinkenberg correction. Ultrasonic velocities (V_p and V_s) were measured using an ultrasonic pulser/receiver with a separate transducer on each side of the sample. The transducers were connected to a digital oscilloscope where the wave signal is recorded. Measurements were made with a voltage of 600V, and a gain of 40 dB. Thin sections (n=125) were prepared and impregnated with blue-resin to highlight pore space, and rock texture, mineral composition, and the types and geometry of pores were described. The dataset includes different volcanic lithofacies from basalt, basaltic andesite, and dacite lavas, along with a range of sedimentary rocks that occur interbedded with the lava sequence.

5. Defining the pore structure of volcanic and sedimentary rocks

Volcanic porosity can be classified either as (1) *primary*: formed during magma ascension and emplacement in the surface; or (2) *secondary*: formed by post-emplacement processes, such as alteration and tectonic fracturing (Petford, 2003; Sruoga et al., 2004; Sruoga and Rubinstein, 2007; Jiang et al., 2017). Primary porosity includes vesicles formed during magma degassing, intra-fragment pore space formed by autobrecciation of lava during emplacement, and cooling and quenching fractures (Sruoga and Rubinstein, 2007). Secondary porosity is mainly formed by alteration processes (diagenetic and/or hydrothermal) and includes crystal and matrix dissolution, and tectonic fracturing. Pore space in the sandstones is intergranular and controlled by grain size and packing, along with the degree of cementation. The nature and type of pores were defined using a combination of outcrop observation and microscopy analysis and is described in the following sections.

6. Petrophysical properties of the Paraná-Etendeka LIP

The Paraná-Etendeka rocks have highly heterogeneous petrophysical properties. The large variation in rock properties can be correlated with emplacement processes and to the different lithofacies, rather than rock composition e.g. massive basalt, and massive rhyolite have overlapping properties. Overall, porosity varies between 0.03 - 28.3% in the volcanic rocks

and from 2.5 - 34.2% in the sandstones. Acoustic velocities are inversely correlated to porosity with both V_p and V_s decreasing with increasing porosities for all lithologies (Fig. 7). Acoustic velocities range from 2.9 - 5.9 kms^{-1} for V_p and 1.8 - 3.8 kms^{-1} for V_s in the lavas and 2.0 - 5.4 km^{-1} (V_p) and 1.2 - 4.1 kms^{-1} (V_s) in the sandstones. The linear best-fit (least squares regression) porosity-velocity relationship for volcanic and sedimentary rocks is defined by the approximations:

$V_{pvulc} = -0.0934\phi + 5.3764$ ($R^2 = 0.6169$)
$V_{svulc} = -0.0579\phi + 3.1941$ ($R^2 = 0.694$)
$V_{psed} = -0.1063\phi + 5.3489$ ($R^2 = 0.6643$)
$V_{ssed} = -0.0817\phi + 3.707$ ($R^2 = 0.6614$)

The linear correlation between porosity and acoustic velocities for individual datasets of the volcanic and sedimentary rocks is presented in Figure 7. The data follow broadly linear trends of correlation but show variable scatter due to the grouping of different facies. Rock acoustic velocities reveal a clear negative correlation with porosity (Fig. 7A and B) whilst density is positively correlated with acoustic velocity (Fig. 7C and D). The results of the porosity, acoustic velocities and permeability analysis are described in the following sections and presented in Table 1 (see electronic appendix for all analysis) and in figures 7 to 10.

Table 1 – Main characteristics of units and lithofacies, porosity, permeability and acoustic velocity data for the Paraná-Etendeka Province.

Stratigraphic Unit	Intra-facies	Petrography - Mineralogy	N	Porosity (%)	Mean	Permeability (mD)	Mean	V_P and V_S (kms^{-1})	Mean
Palmas Formation									
Dacitic tabular lavas, domes and coullees. Massive to foliated core, vesicular crust, and	lava core	granophyric texture massive or closely spaced tabular joints	14	1.1 - 9.38	4.0	0.0 - 0.014	0.002	4.4 -5.6 2.6 - 3.3	4.8 3.0
isolated autobreccia pockets	vesicular crust	vesicle-rich layer with spherical to elyptical 0.5-2 cm vesicles	1	9.9	-	0.011	-	4.5 2.5	-
Vale do Sol Formation									
Tabular thick, vertically stacked, basaltic andesite rubbly pahoehoe lavas (~40m)	rubbly Flow top	Rubble layer formed of irregular fragments of vesicular-scoriaceous lava	13	11.0 -28.3	16.5	0.001 - 0.727	0.1	2.9 - 4.2 1.8 - 2.5	3.5 2.1
with four part structure.	upper crust	coherent coarsely vesicular or amygdaloidal upper crust	7	1.0 - 4.0	2.1	0.0 - 0.001	0.001	4.2 - 5.9 2.7 - 3.4	5.4 3.1
	core	Aphanitic to fine-grained lava core with irregular joints	19	0.03 - 8.7	2.1	0.001 - 0.003	0.001	4.9 - 5.9 3.0 - 3.4	5.4 3.2
	lower crust	aphanitic sparcely vesicular flow base	11	0.8 - 15.6	8.8	0.0 - 0.117	0.012	4.9 - 5.6 2.4 - 3.2	4.9 2.8
Torres Formation									
Compound pahoehoe flow fields formed by lava lobes, sheet-like	upper crust	spherical vesicles forming vesicle-rich flow top	15	3.4 - 26.6	12.3	0.0 - 415.7	27.8	3.2 - 5.0 1.9 - 3.8	4.3 2.5
lobes and thick interdune lavas.	core	vesicle poor massive to columnar flow core	37	0.4 - 7.4	2.7	0.001 - 0.185	0.007	4.1 - 5.9 2.6 - 3.5	5.2 3.1
	lower crust	elongated vesicles or pipes forming flow base	10	5.4 - 8.5	6.8	0.001 - 0.185	0.003	4.0 - 4.8 2.5 -3.4	4.3 3.1
Sedimentary units									
Sedimentary units deposit within the volcanic sequence. Irregular	peperite	irregular vesicular basalt fragments in sand matrix	2	14.6 - 15.5	15.0	0.003 - 0.045	0.024	4.1 - 4.3 2.6 - 2.7	4.2 2.7
concave base and flat sharp top.	massive sandstone	massive altered and silicified sandstone	15	3.5 - 28.4	16.3	0.03 - 77.71	17.2	2.4 - 5.4 1.5 - 4.1	3.4 2.3
	stratified sandstone	laminated well sorted aeolian sandstone	16	9.3 - 34.2	22.4	39.71 - 1115.3	449.0	2.0 - 4.9 1.2 - 3.2	3.1 1.9

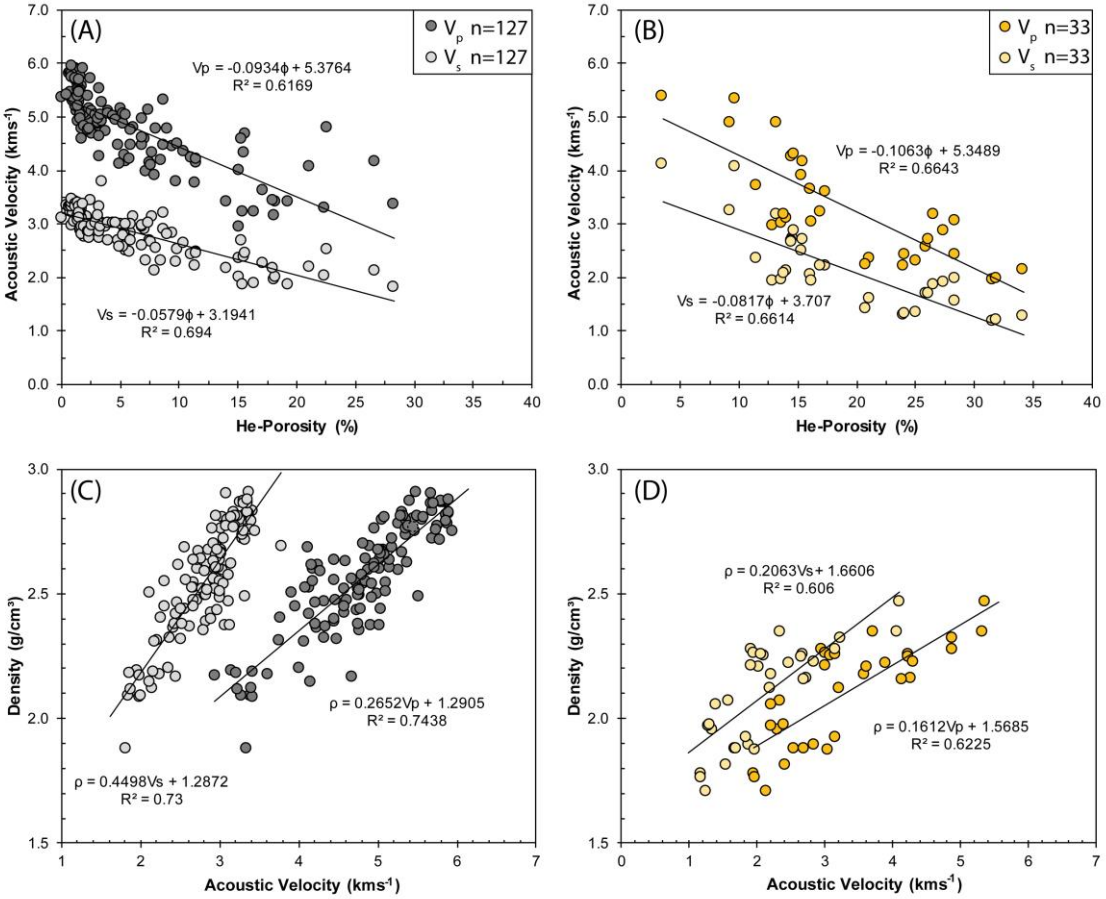

Fig. 7 – Petrophysical variations of the Paraná-Etendeka LIP samples and their relationship given by linear regression. (A) V_p and V_s plotted against He-porosity for volcanic rocks; (B) V_p and V_s plotted against He-porosity for sedimentary interbeds; (C) Density plotted against V_p and V_s for the volcanic rocks; (D) Density plotted against V_p and V_s for the sedimentary interbeds.

6.1. Porosity

For the Torres Formation lavas, a total of 62 samples were collected among the different lava lithofacies and within a single lava unit porosity varies systematically from crust to core. The vesicular lower crust has an average porosity of 6.8% (c. 5.4 - 8.5%) and pores occur as isolated elongated pipe vesicles, that are typically partial to completely filled with zeolite and celadonite. Lava flow cores have the lowest porosities, which are dominantly lower than 3%. Porosity is restricted to intercrystalline voids and partially dissolved phenocrysts and variations are constrained within c. 0.4 – 7.4%. The upper crust of the lava is highly vesicular and fractured and is characterized by high porosity values that range from 3.4 to 26.6% (mean 12.3%). In the upper vesicular crust lower

porosities typically occur where secondary minerals infill original pore space (e.g. amygdales).

For the basaltic andesite lavas of the Vale do Sol Formation, 50 samples were collected from representative lava lithofacies. Porosity varies from 0.03% in the massive flow core, up to 28.3% in the rubbly flow top. The vesicular lower crust has spherical (2 - 5 mm) and stretched vesicles with porosity ranges from 0.8 up to 15.6%. In the lava massive core, porosity is on average < 5% (0.4 – 7.4%), and pores occur as isolated intercrystallite vugs, typically filled with smectites. Even with the high density of primary vesicles, measured porosity is low in the upper vesicular crust, varying from 1 to 4%. However, this fact is partly due to the large size of vesicles (1 - 6 cm), which can be bigger than the core plug diameter and imparts an unavoidable sampling bias to this intra-facies. In most analysed samples vesicles were entirely filled with secondary minerals. The highest porosities among all the analysed volcanic facies are found in the rubbly flow tops (c. 28.3%). Primary porosity is formed by vesicles and fractures within the fragments and inter-fragment pore space, and porosity is typically higher than 10%, varying from 11 - 28.3%.

For the acidic rocks, 14 samples were analysed in the massive facies, and only one sample could be analysed from the vesicular crust. The massive lava core has low average porosity of c. 4.0%, with variations in the range of c. 1.1-9.4%. The vesicular dacite sample gave a porosity of 9.9%. In most cases, due to the advanced alteration of highly vesicular intervals, core plugs were not successfully recovered.

The sedimentary facies, in general, preserve relatively good porosity with sandstones revealing average porosity of 22.2% in the stratified facies and of 16.3% in the massive facies. The stratified sandstones preserve most of the primary sedimentary structures and interparticle pore space is high, with just minor diagenesis, which resuls in higher overall porosities (c. 9.3 – 34.2%). In the massive sandstones porosities vary between 3.5 and 28.4%, and the low porosities are controlled by diagenetic alteration, which reduces significantly pore space. Two additional samples of peperite were analysed, where porosity is 14.6 and 15.4%.

6.2. Acoustic Velocities

In general, acoustic velocities variations are tightly correlated with porosities and rock lithofacies. To all lava units, velocities present a systematic variation. Lower velocities occur in the lava crusts where porosities are higher (e.g. vesicular, fractured and rubble) and higher velocities occur in the massive lava core, where densities are higher and porosity is, in general, < 5% (Fig. 8). The scales of variations are controlled by the flow thickness and structure and vary in the different units.

For the Torres Formation lavas the vesicular lower crust has velocities values typically intermediate between lava flow core and upper crust with variations in the range of 4 to 4.8 kms^{-1} for V_p and 2.5 to 3.4 kms^{-1} for V_s. In the lava flow core velocities reach the highest values, with V_p c. 4.1 - 5.9 kms^{-1} and V_s c. 2.6 - 3.5 kms^{-1}, whilst in the upper crust acoustic velocities are relatively low c. 3.2 - 5 kms^{-1} for V_p and 1.9 – 3.8 kms^{-1} for V_s. For the basaltic andesite lavas of the Vale do Sol formation the vesicular lower crust has average velocities of 4.9 kms^{-1} for V_p and 2.8 kms^{-1} for V_s whilst lava flow core has velocities within the range of the basaltic lavas from Torres Formation, with V_p = 4.9 - 5.9 kms^{-1}, and V_s = 3.0 - 3.4 kms^{-1}. The coherent vesicular portion of the upper crust has average acoustic velocity values slightly lower than those of the massive flow core (V_p= 5.4 kms^{-1}; V_s= 3.1 kms^{-1}). The lower velocities within basaltic andesite lavas are found in the rubbly upper crust lithofacies, where porosity and alteration are generally higher. In this facies, velocities are in the range of 2.9 – 4.2 kms^{-1} (avg. 3.5 kms^{-1}) for V_p and c.1.8 – 2.5 kms^{-1} (avg. 2.1 kms^{-1}) for V_s. For the acidic rocks, velocities are relatively high, ranging from 4.4 - 5.6 kms^{-1} for V_p and 2.6 - 3.3 kms^{-1} for V_s, in the massive lithofacies and are within the range of basaltic rocks from the other formations. The vesicular lithofacies sample gave V_p and V_s of 4.5 kms^{-1} and 2.5 kms^{-1}, respectively.

The sedimentary facies have acoustic V_p and V_s varying from 2.0 to 4.9 kms^{-1}, and 1.2 to 3.2 kms^{-1}, respectively. In the massive sandstones, where feldspars are replaced by clay minerals, acoustic velocities are typically very low (c. V_p = 2.5 kms^{-1} and V_s=1.6 kms^{-1}), whilst where the rocks are strongly silicified, P and S-acoustic velocities are higher (c. 5.4 and 4.1 kms^{-1}). The peperite samples have acoustic velocities within the range of 4.1 and 4.3 kms^{-1} for V_p and 2.6 and 2.7 kms^{-1} for V_s.

In general, V_p and V_s are tightly correlated and show a broad variation within different units. Vp/Vs ratios vary from 1.3 to 2.0 in the volcanic rocks and from 1.3 to 1.9 in the sediments. Figure 9 presents the acoustic velocity relationships to the dataset. For the different lithologies (e.g. basalt and dacite), velocities show great overlap. When lithofacies are plotted separately for the individual lava formations, however, characteristically distinct V_p-V_s ranges of variation are identified in individual lithofacies (Fig.9 B-D).

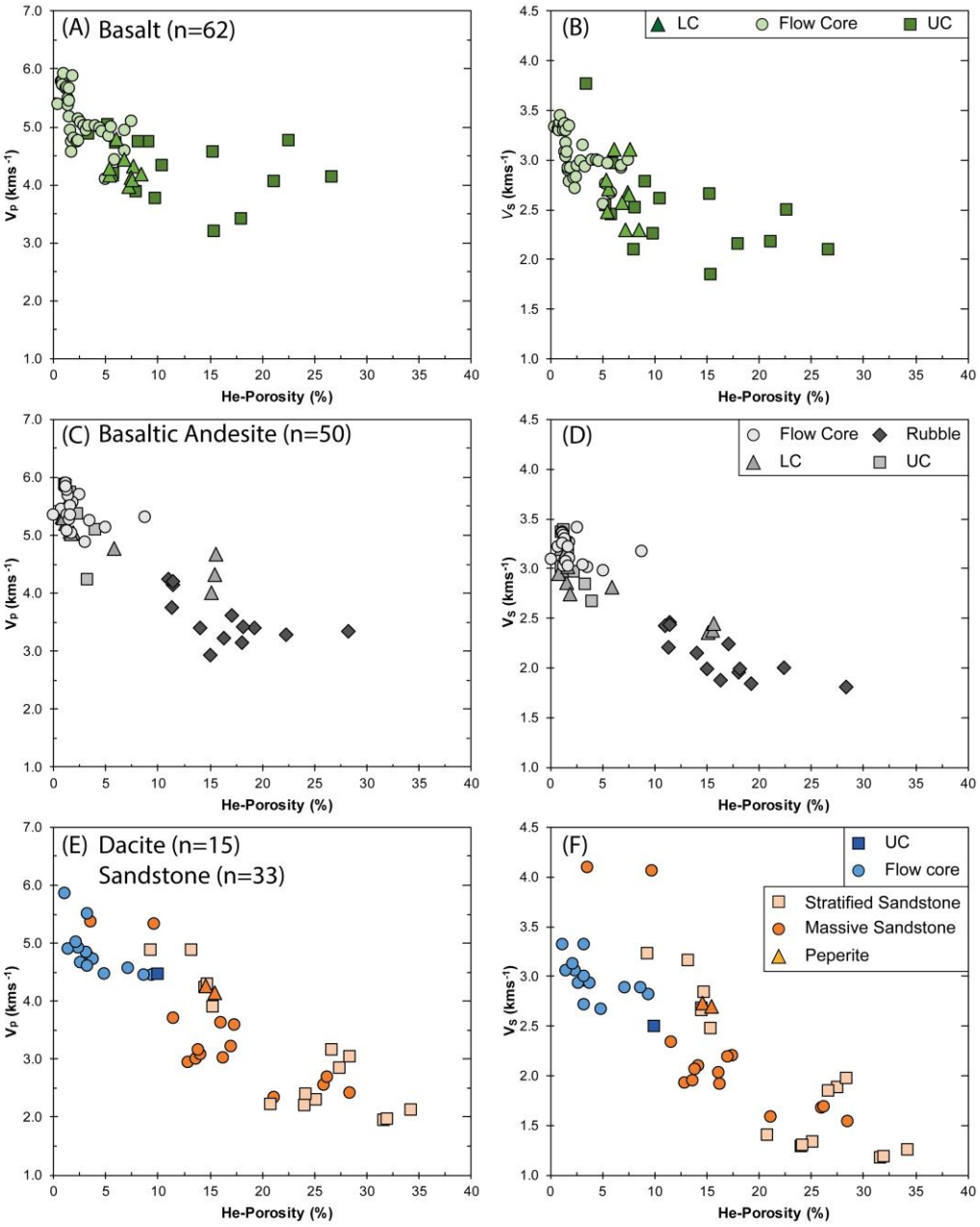

Fig. 8 –P and S acoustic velocity variations for different lithofacies plotted against He-porosity. (A) V_p v. He-Porosity and (B) V_s v. He-Porosity pahoehoe lavas of Torres Formation; (C) V_p v. He-Porosity and (D) V_s v. He-Porosity for rubbly

pahoehoe lavas of Vale do Sol Formation; (E) V_p v. He-Porosity and (F) V_s v. He-Porosity for Palmas Formation dacites and sedimentary interbeds.

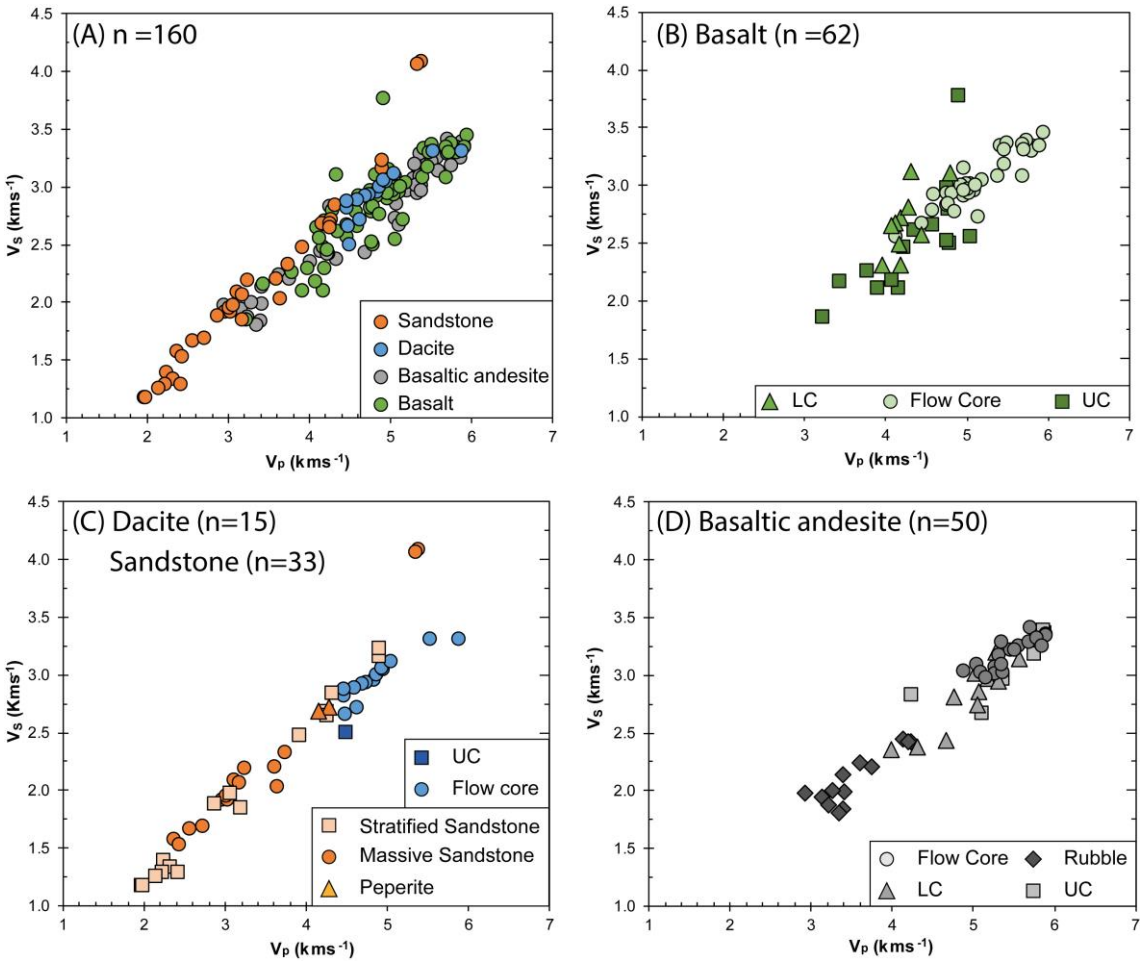

Fig. 9 – P and S acoustic wave velocity relationship for lithological and lithofacies variations. (A) Vs versus V_p by lithological variations to all samples; (B) V_s versus V_p by basalt lithofacies for Torres Formation lavas; (C) V_s versus V_p for dacite lithofacies of Palmas Formation and sedimentary interbeds; (D) V_s versus V_p for basaltic andesite lithofacies of Vale do Sol Formation lavas.

6.3. Permeability

Permeability is highly variable in the dataset and ranges between 0 (below detection of c. 0.001) and 1115 mD. Figure 10 presents the range of permeabilities for the analysed samples, plotted against porosity. The samples are clustered in two distinct trends: (1) a high permeability trend, that includes most of the sedimentary interbed samples, two vesicular upper crust basalt samples, and one lava core sample, from Torres Formation; and (2) a low

permeability trend that include all the other volcanic samples and silicified massive sandstone samples. The highest permeabilities are found in the cross-stratified sandstones (mean c. 450 mD), followed by the massive sandstones, mean c. 17 mD. Hydrothermally altered (silicified) massive sandstones have permeabilities < 1 mD and within the range of the volcanic rocks. Permeability is <1 mD in most lava samples, and it is directly correlated with porosity, increasing from lava core lithofacies, towards lower vesicular crust lithofacies and is higher in the upper vesicular crust of pahoehoe lavas and rubbly flow tops (up to 1 mD). Two samples from Torres Formation, SG-79D and SG-99-2, have high permeabilities, c. 2 and 416 mD, respectively. These samples are vesicular basalts with no apparent secondary mineral filling of pores and therefore appear to represent values closer to primary permeability.

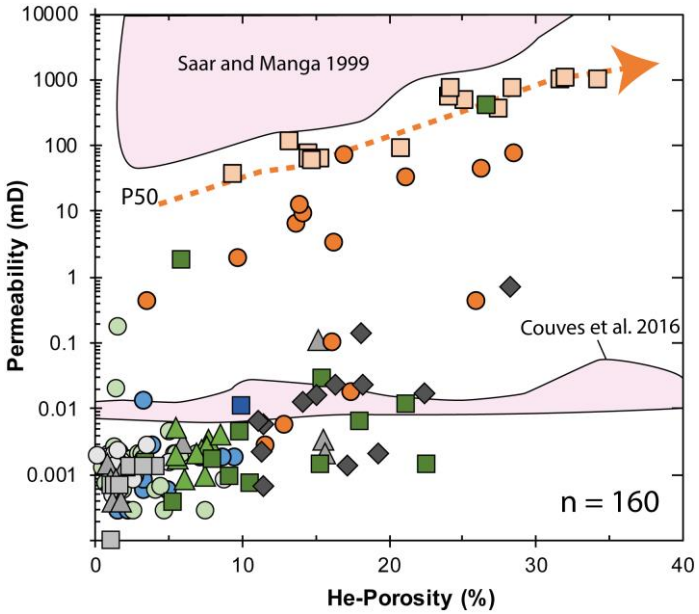

Fig. 10 – Graph of permeability plotted against He-porosity for the Paraná-Etendeka analysed samples. Porosity and permeability show positive correlation to all lithofacies with two distinct distribution trends (see text). Shaded areas represent literature data of volcanic rocks for comparison (Saar and Manga ,1999; Couves et al. 2016), and P50 represent 50% of international sandstone reservoirs (from Lenhardt and Götz, 2011).

7. Discussion

In the volcanic rock units, petrophysical properties are mainly controlled by the rock structure, bulk mineral composition, post-emplacement alteration

processes (e.g. deuteric and hydrothermal) and cooling/tectonic fracturing. Laboratory analysis of dry samples under ambient P-T provides a unique opportunity to isolate some of these factors and define their relative contributions to the final petrophysical signature. We focus here on the major control played by lava structure (lithofacies) and variations associated with primary mineralogy and diagenetic/hydrothermal alteration. Additionally, fluid saturation, pore structure, and confining pressure can significantly modify the elastic and petrophysical properties of the rocks and should be considered in any specific case, especially when correlating laboratory data with *in situ* petrophysical measurements. The effect of these particular factors on different volcanic rocks are discussed elsewhere (Adelinet et al., 2010; Adam and Otheim, 2013) and are not investigated in this contribution.

7.1. Effects of lava morphology and internal structures

In general flood basalt lava sequences are dominated by pahoehoe and rubbly pahoehoe lavas (e.g. White et al., 2009; Bryan et al., 2010), although different lava morphologies such as ´a´ā can occur locally (e.g. Brown et al., 2011; Duraiswami et al., 2014), as well as hydromagmatic rocks such as hyaloclastites when erupted into water (e.g. Jerram et al., 2009; Wright et al., 2012; Watton et al., 2014b). Pahoehoe lavas are emplaced as lobes or tabular sheets of lava, depending on eruptive volume and magma discharge rates. During emplacement of pahoehoe, the lower and upper surfaces of the lava chill by conductive and combined convective/radiative heat lost respectively to form the flow crust (Keszthelyi & Denlinger, 1996). With a continuous supply of material, pahoehoe lava grows endogenously by inflation (Hon et al., 1994; Cashman and Kauahikaua, 1997; Self et al., 1998). Vesicles commonly represent c. 30-40% of the original volume in the lava lower and upper crusts (Thordarson and Self, 1998) and vesicularity typically decreases downwards as a result of gas bubble nucleation and migration, cooling rate and pressure in the crust-melt interface (Hon et al., 1994; Cashman and Kauahikaua, 1997). When effusion rates are high, or during surges of magma supply, the internal pressure of volatiles in the core-crust interface, and tearing in the fast advancing flow front cause fragmentation of the vesicular upper crust (Duraiswami et al., 2008; Guilbaud et al., 2005; Keszthelyi et al., 2004, 2006), resulting in the formation of

rubbly pahoehoe lava, followed by ´a´ā lava at higher strain rates. These internal heterogeneities impart a clear internal structure which is also mirrored by primary rock properties such as velocity, density and porosity (e.g. Planke 1994; Nelson et al., 2009, 2015).

The study of Barreto et al. (2017), identified vesicle distribution patterns and types of pores for basaltic lavas within the Torres and Vale do Sol Formations. Porosity was estimated from thin section analysis to varies between 0.3 and 27%, with average porosities of 11.2% These results fall within the data range reported here for He-porosity analysis and provide important information on pore geometry and distribution. The authors considered that most of the porosity is secondary, e.g. crystal dissolution, and was formed during hydrothermal alteration.

For the Paraná lavas velocity varies cyclically within individual lava units. The lava upper and lower crusts are marked by low acoustic velocity values (V_p as low as 2.9 kms^{-1}) whilst lava flow core have typicall higher velocities (V_p up to 6 kms^{-1}). The frequency in which acoustic velocity profiles are arranged will be controlled by lava thickness, which varies systematically in the stratigraphy of the Paraná lavas. The volcanic pile is characterised at the base (Torres Fm.) by thin compound lobes whilst the main stratigraphy, Vale do Sol Formation, is composed of thick (up to 60 m) sheet-like flow units. In synthetic velocity profiles, the frequency in which velocities profile vary at the compound thin units is much higher than that of the thick tabular lavas and the different lava units would have very distinct velocity signatures (Fig. 11).

Our data shows that for the lavas of the Paraná-Etendeka LIP the most porous facies are found in the fragmented top of rubbly pahoehoe lavas of Vale do Sol Formation (c. 28%), and despite having measured permeability ≤ 1 mD, this lithofacies represent the best candidate for reservoir rocks. The breccias form a laterally continuous layer and reach 10 m in thickness, in some lavas. Another critical factor relating to these flow top facies is the inability of laboratory-based core testing to capture the permeability of the larger inter-rubble cavities which form a key aspect of their potential reservoir properties and almost certainly force our results towards an underestimate of bulk permeability (e.g. Millett et al., 2016). These flow tops are in stark contrast to the thick massive flow cores (Fig. 3A-B) which have very low porosity and are known to often form effective seals

(e.g. Burns et al., 2012). How these cooling joints and fracture networks within the core units affect their permeability during burial in different settings remains poorly constrained. In ideal cases, the columnar fractures of the thick massive cores (Fig. 3 A-B) may act as conduits for fluid percolations and connect porous layers, thereby increasing reservoir quality. Zakharova et al. (2012) identified a sequence of high and low porosity zones, corresponding to rubbly flow tops (minor vesicular flow tops) and lava flow cores, respectively from well data in the Grande Ronde Formation lavas (Columbia River Basalt Province). Porosity was estimated from wireline data and yielded high values for the brecciated rubbly tops (20 - 45% from well data) and permeabilities in the range of 75 – 150 mD. For the Grande Ronde lavas permeability decreases with depth, although high permeabilities are preserved in flow tops buried at depths of c.850 m, and these lava flow tops represent reservoir targets for carbon dioxide storage (Zakharova et al., 2012). In pahoehoe lavas of the Paraná, the upper crust has been demonstrated to have high porosity. When compared to the tabular and simple architecture of the rubbly pahoehoe lavas, the compound braided pahoehoe flow fields are much more heterogeneous. Pahoehoe lavas of the Torres Formation are compound in nature, and thick sheet-like lobes are less frequent than minor lava lobes. The compound flows are often highly altered with contacts marked by altered chilled margins, which introduces additional complexity to the lithofacies distribution and may represent permeability barriers for fluid percolation, decreasing their potential as porous reservoir targets.

The cyclic variations within flow units identified for the Paraná-Etendeka lavas, have been widely recognised in subaerial lava sequences elsewhere (Planke, 1994; Helm-Clark et al., 2004; Bartetzko et al., 2005; Nelson et al., 2009, 2011, 2015; Watton et al., 2014a; Millett et al., 2015; Couves et al., 2016). Despite the fact that particular characteristics change from province to province, these recurrent variations provide an important tool for predicting lava architecture and likely lateral facies distributions when direct data is not available (e.g. Jerram et al., 2009; Millett et al., 2015; Nelson et al., 2009, 2015).

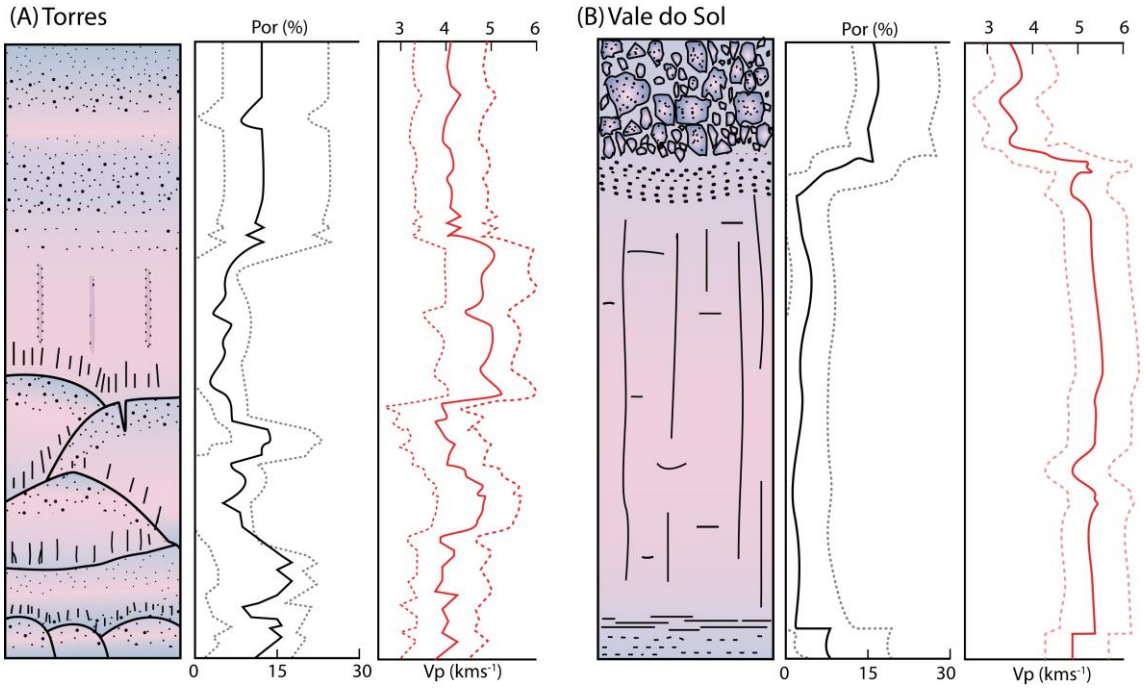

Fig. 11 – Simplified vertical section, and petrophysical variations through (A) typical compound pahoehoe flow field from Torres Formation; (B) tabular rubbly pahoehoe lava from Vale do Sol Formation. Solid lines represent average and dashed lines represent minimum and maximum values for porosity (in black) and V_p (in red). LVC – lower vesicular crust; LC – lava core; UVC – upper vesicular crust; RT – rubbly flow top.

7.2. Effects of rock composition and alteration

The chemical composition and bulk mineralogy of a rock determine its grain density, thus having a direct effect on elastic properties such as acoustic velocities. The presence and quantity of olivine crystals in basaltic lavas and hyaloclastites, for instance, can increase P-wave acoustic velocities by c.0.5-1.0 kms^{-1} (Watton et al., 2014b; Millett et al., 2015). In contrast, alteration of primary mineralogy decreases rock stiffness, consequently lowering acoustic velocities. Velocity data from the IODP Leg 990A shows that altered flow tops of basaltic lavas have significant lower P-wave acoustic velocities than massive unaltered lava core, with V_p being inversely correlated to the proportion of clay minerals in each facies (V_p = 2.5 kms^{-1} to smectite c. 50%, Planke et al., 1999). Rock-physics models can be used to test and estimate the relative effects of lithological variations for different circumstances (Avseth et al., 2010; Healy et al., 2014; Awdal et al., 2016). Elastic bounds were calculated from mineral proportion (fi)

and elastic moduli (Mi) of rock-forming minerals following the Voigt (1910) equations the for upper bound

$$M_V = \sum_{i=l}^{N} fi\, Mi$$

and Reuss (1929) for calculating the lower bound;

$$\frac{1}{M_R} = \sum_{i=l}^{N} \frac{fi}{Mi}$$

where M is the elastic modulus (bulk or shear) of the calculated mixture of different phases (e.g. minerals and pores). Porosity in these mixture models is included as a fluid component such as air or water. The calculated elastic bounds represent the stiffest and softest possible mixture of components at any one porosity and are defined by the phase proportions and moduli of the phases (including the pore filling fluid), without considering the distribution and coordination of components (Asveth et al., 2010). Here we use a simplified basalt composition of 50% plagioclase, and 50% pyroxene as a starting baseline, broadly equivalent to selected samples from the study. Primary mineralogical variation was tested by incrementally adding olivine to the starting composition. Furthermore, the effects of alteration were modelled by the incremental addition of smectite. Results are presented in Figure 12, and despite being a simplification, the physical bounds clearly demonstrate that effective alteration (40%) of primary mineralogy can decrease P-wave velocity by c. 1 kms^{-1} giving valuable insights into the relative variations between the analysed samples. The analysed data generally fall along the lower elastic bound with increased scatters towards low velocities (altered samples). This fact reflects compositional variations from altered, where clay forms continuous matrix joining, to fresh unaltered stiffer samples. The most porous samples fall above the lower bound indicating that for the given porosity the pore-rock framework is stiffer than expected for the given modelled minimum. This fact might be reflecting a less altered rock composition or alternatively, post-emplacement secondary filling of primary vesicles, which in turn decrease original porosity, and increase pore stiffness.

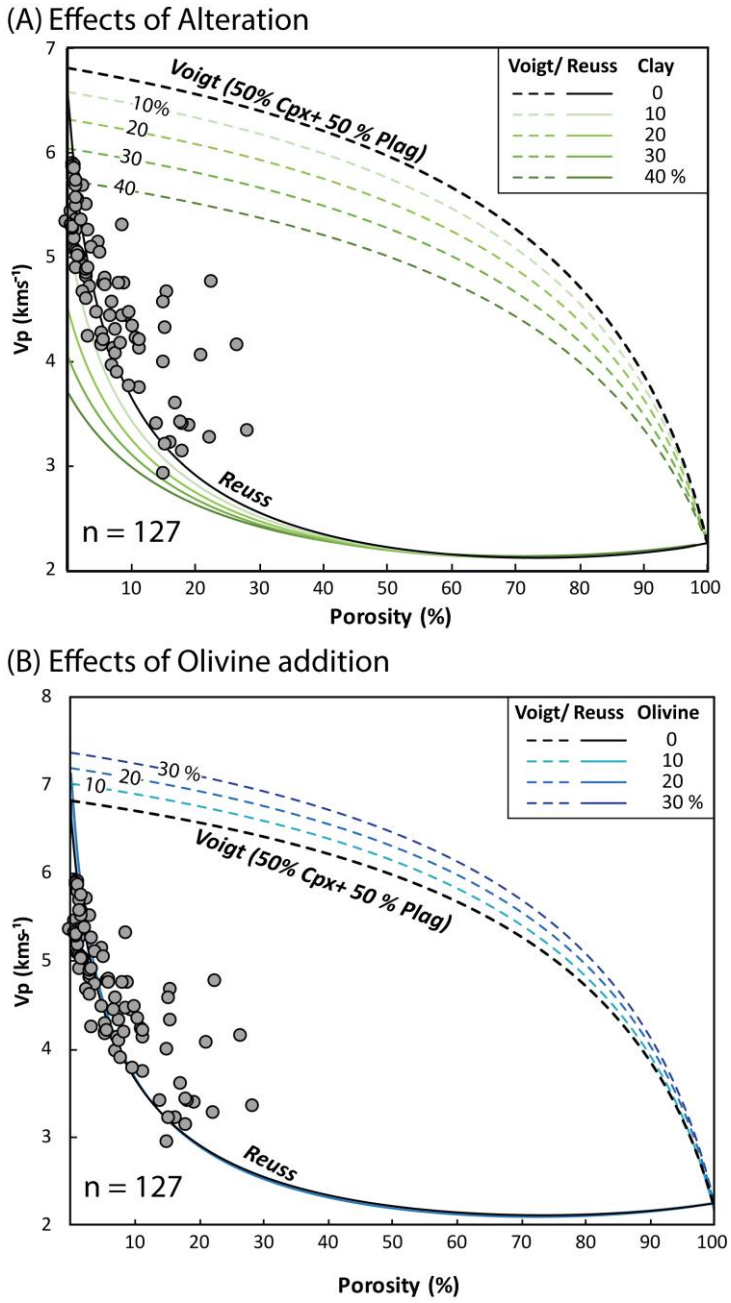

Fig. 12 – P-wave acoustic velocity versus porosity for all lava samples, plotted together with Voigt and Reus bounds for a starting basalt composition of 50% plagioclase + 50% pyroxene. (A) Effects of increasing alteration. (B) Effects of compositional variation or crystal accumulation.

In the Paraná-Etendeka lavas, alteration is variable and typically includes: (1) substitution of olivine by iddingsite and bowlingite in the basalt lavas; (2) substitution of augite and glass material by clay minerals, namely smectite and celadonite; (3) plagioclase albitization; (4) zeolite precipitation. The latter has a major effect in modifying rock properties especially by reducing porosity and

permeability by filling primary pore space and clogging pore connectivity, respectively. Based on the occurrence of different zeolite types along the lava pile Murata et al (1986) concluded that the lava sequence was subjected to hydrothermally zoned fluid circulation, with a fluid temperature of c. 100°C at the base of the lava pile, decreasing upwards. The alteration was selective and more intense in the permeable lava facies and precipitation followed the order: (1) celadonite, (2) chlorite+smectite, (3) zeolite (Schenato et al., 2003). Movement of hydrothermal fluids within the lava pile has also been identified by the diagenetic alteration of some of the sedimentary interbeds by later stage hydrothermal activity (e.g. Grove et al., 2017).

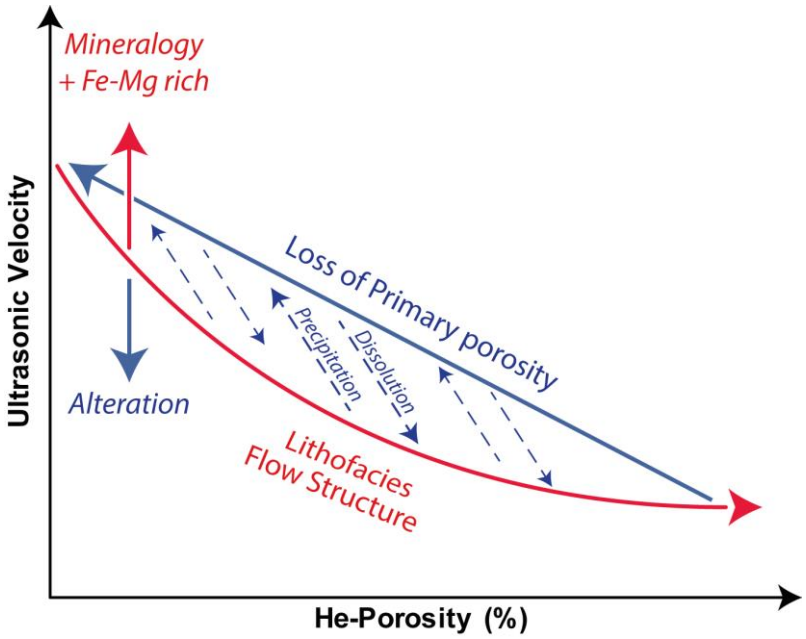

Fig. 13 – Velocity porosity schematic plot showing the controls in porosity-velocity relationships for the studied igneous rocks. Lithofacies have a first order control in porosity-velocity correlation and decrease progressively from massive facies, towards vesicular and finally fragmented-rubbly facies. Hydrothermal alteration can decrease porosity by precipitating secondary minerals, create secondary porosity by dissolving minerals, or both. Crystal accumulation and mineral alteration modify mainly acoustic velocities producing data scatter.

7.3. Controls in the petrophysical properties of sedimentary interbeds

Sedimentary interbeds have preserved in most cases high porosity and permeability. Sampled interbeds are dominated by well-sorted aeolian deposits, and the occurrence of clay minerals are mostly due to with diagenetic processes.

Locally, fluvial interbeds with more variable grain size and sorting occur within the lavas, however these deposits typically form thin layers or are preserved just as infilling material in the pore space among fragments in the top of rubbly lavas from Vale do Sol Formation (Rossetti et al., 2017), and no samples were successfully collected. In sandstones diagenesis and compaction generally, give strength to the sediments and porosity-permeability decrease with increasing burial depth (e.g. Avseth et al., 2010). Diagenesis and compaction play a major role in controlling porosity and permeability and consequently acoustic velocity of the sedimentary interbed facies. Grove et al. (2017), working on sandstone interbeds, and sediment lava contacts in the lower portion of the Etendeka side of the sequence identified three distinct diagenetic processes affecting the sandstones. *Type 1 diagenesis,* is represented by red sandstones characterized by mechanical compaction during burial processes; *Type 2 diagenesis,* occurs in bleached (white/yellow) sandstones and is characterized by a complex diagenetic story, with intense feldspar dissolution and authigenic cementation (calcite and kaolinite), which significantly lowers permeability and porosity. Type 2 diagenesis is related to intense hydrothermal fluid percolation driven by igneous intrusions; *Type 3 diagenesis* is composed of indurated sandstones near hot sediment-lava contacts formed by the emplacement of lava on top of unconsolidated sand dunes. The differences in type 1 and 2 diagenesis are attributed to the diagenetic compartmentalization associated with dike emplacements and the relative distribution of isolated sandbodies within the lower stratigraphy (Grove et al., 2017). The samples analysed here are dominated by characteristics comparable to Type 1 red dunes of Groove et al., where porosity and permeability are high and diagenesis is due to burial compaction. The exception is the silicified sandstones (trend of low permeability Fig. 9) which resemble dissolution and cementation processes comparable with type 2 diageneses of Grove et al. (2017). Interestingly, the cement composition varies from one province to the other and might be reflecting variations in hydrothermal fluid geochemistry, or superimposition of contrasting post-rift diagenetic processes. In this latter case, the sequences within the Etendeka side have not been significantly subject to latter diagenetic fluids. The work of Grove et al. (2017), together with the petrophysical evidence reported here, highlight the importance of differential diagenesis associated with intrusive magmatism in the deterioration of the pore-

network and generating reservoir heterogeneities. Similar processes have also affected older stratigraphic units of the Paraná basin (e.g. Furnas Formation, De Ros et al., 2009).

8. Summary and Conclusions

This work presents the first integrated outcrop and laboratory petrophysical study of the mixed volcanic and sedimentary sequence of rocks from the Paraná-Etendeka LIP. Emplacement mechanisms within the lavas are responsible for first-order controls on porosity and permeability and can be seen as a direct link between the general velocity trends that we see through the volcanic sequences (Fig.13). Correlating rock petrophysical properties with outcrop analogues improves our ability to use seismic and down borehole data (wireline/ image log etc.) in the interpretation and prediction of lithofacies distribution and reservoir heterogeneities (e.g. Nelson et al., 2009; Watton et al., 2014a). The mapping of lithostratigraphic units, as well as the direct measurements of the rock properties, can also form the basis of developing pseudo wireline logs, where the vertical stacking within the stratigraphy can be simulated to what might be expected in a well sequence (e.g. Angkasa et. al., 2017).

Primary pore space can be modified during burial diagenesis and hydrothermal fluid circulation, and to better understand porosity distribution in potential reservoirs, one needs to consider the interplay between pore destruction and secondary pore creation during diagenesis, which in volcanic provinces and wells have proven to be complex (De Ros et al., 2009; Watton et al., 2014b; Millett et al., 2015; Grove et al., 2017; Jiang et al., 2017). Future analyses should consider the effects of increasing confining pressure on rock properties to quantitatively define the conditions under which alteration takes place in the different lavas.

Our data reveal that better reservoir characteristics are found in the sedimentary interbeds trapped within the volcanic sequence than in the lavas themselves at the scale of core plug data. This scenario has demonstrated great potential for hosting oil and gas accumulations (e.g. Rosebank Field, Helland-Hansen 2009; Kudu gas field, Stanistreet and Stollhofen, 1999). In the lava flows, the highest porosities are found in the upper crust of both rubbly pahoehoe (c.

28.3%, rubbly flow top), and pahoehoe lavas (c. 26.6%, vesicular upper crust) whilst lava flow cores are characterized by low porosity values (< 5%) for all compositions. The generally low laboratory permeability values from the rubbly lava flow facies (core plug scale), do not capture the significant inter-clast porosity known from the field. This, along with evidence for very good reservoir properties in other global examples such as the CRBP suggests these units may also provide valuable reservoir intervals in the sub-surface. Similar lava sequences represent potential targets for CO_2 storage (McGrail et al., 2011; Sullivan et al., 2011; Zakharova et al., 2012) and hydrocarbon reservoirs (Mizusaki et al., 1988; Rogers et al., 2006; Gupta et al., 2012), and should be considered as potential targets in hydrocarbon basins.

Acknowledgements

The authors gratefully acknowledge support from Shell Brasil and CNPq through the *Sedimentary Systems* project hosted at the Federal University of Rio Grande do Sul and the strategic importance of the support given by ANP through the R&D levy regulation. Evandro Lima is thankful for CNPq research grants (402400/20 442812/2015-9). Dougal Jerram is partly funded through a Norwegian Research Council Centers of Excellence project (project number 223272, CEED). Collin Taylor is thanked for helpful assistance during sample preparation and analysis. F. Luz, and M. Simões are thanked for valuable assistance during fieldwork and sample collection.

References

Adam, L., Otheim, T., 2013. Elastic laboratory measurements and modeling of saturated basalts. J. Geophys. Res. Solid Earth 118, 840–851. doi:10.1002/jgrb.50090

Adelinet, M., Fortin, J., Guéguen, Y., Schubnel, A., Geoffroy, L., 2010. Frequency and fluid effects on elastic properties of basalt: Experimental investigations. Geophys. Res. Lett. 37. doi:10.1029/2009GL041660

Angkasa, S.S., Jerram, D.A, Millett, J.M., Svensen, H.H., Planke, S., Taylor, R.A., Schofield, N.,Howell, J. 2017. Mafic intrusions, hydrothermal venting, and the basalt-sediment transition: Linking onshore and offshore examples from the North Atlantic igneous province. Interpretation 5 (3), SK83-SK101.

Avseth, P., Mukerji, T., Mavko, G., Dvorkin, J., 2010. Rock-physics diagnostics of depositional texture, diagenetic alterations, and reservoir heterogeneity in high-porosity siliciclastic sediments and rocks — A review of selected models

and suggested work flows. Geophysics 75, 75A31. doi:10.1190/1.3483770

Awdal, A., Healy, D., Alsop, G.I., Fracture patterns and petrophysical properties of carbonates undergoing regional folding: A case study from Kurdistan, N Iraq, Marine and Petroleum Geology (2016), doi: 10.1016/j.marpetgeo.2015.12.017.

Baksi, A.K., 2017. Paraná flood basalt volcanism primarily limited to ~ 1 Myr beginning at 135 Ma: New 40 Ar/ 39 Ar ages for rocks from Rio Grande do Sul, and critical evaluation of published radiometric data. J. Volcanol. Geotherm. Res. 1–12. doi:10.1016/j.jvolgeores.2017.02.016

Barreto, C.J.S., de Lima, E.F., Goldberg, K., 2017. Primary vesicles, vesicle-rich segregation structures and recognition of primary and secondary porosities in lava flows from the Paran?? igneous province, southern Brazil. Bull. Volcanol. 79. doi:10.1007/s00445-017-1116-x

Brown, R.J., Blake, S., Bondre, N.R., Phadnis, V.M., Self, S., 2011. ´A´ā lava flows in the Deccan Volcanic Province, India, and their significance for the nature of continental flood basalt eruptions. Bull. Volcanol. 73, 737–752. doi:10.1007/s00445-011-0450-7

Bryan, S.E., Peate, I.U., Peate, D.W., Self, S., Jerram, D.A., Mawby, M.R., Marsh, J.S. (Goonie), Miller, J.A., 2010. The largest volcanic eruptions on Earth. Earth-Science Rev. 102, 207–229. doi:10.1016/j.earscirev.2010.07.001

Burns, E.R., Snyder, D.T., Haynes, J.V., Waibel, M.S., 2012. Groundwater Status and Trends for the Columbia Plateau Regional Aquifer System, Washington, Oregon, and Idaho. U.S. Geological Survey Scientific Investigations. Report 2012e5261.

Cashman, K. V, Kauahikaua, J.P., 1997. Reevaluation of vesicle distibutions in basaltic lava flows. Geology 25, 419–422. doi:10.1130/0091-7613(1997)025<0419

Couves, C., Roberts, S., Racey, A., Troth, I., Best, A., 2016. Use of X-ray computed tomography to quantify the petrophysical properties of volcanic rocks: a case study from Tenerife, Canary Islands. J. Pet. Geol. 39, 79–94. doi:10.1111/jpg.12629

Coward, M.P., Purdy, E.G., Ries, a. C., Smith, D.G., 1999. The distribution of petroleum reserves in basins of the South Atlantic margins. Geol. Soc. London, Spec. Publ. 153, 101–131. doi:10.1144/GSL.SP.1999.153.01.08

De Ros, L.F., Morad, S., Broman, C., De Césero, P., Gomez-Gras, D., 2009. Influence of Uplift and Magmatism on Distribution of Quartz and Illite Cementation: Evidence from Siluro-Devonian Sandstones of the Paraná Basin, Brazil. Quartz Cem. Sandstones 231–252. doi:10.1002/9781444304237.ch16

Dodd, S.C., Mac Niocaill, C., Muxworthy, A.R., 2015. Long duration (>4 Ma) and steady-state volcanic activity in the early Cretaceous Paraná–Etendeka Large Igneous Province: New palaeomagnetic data from Namibia. Earth Planet. Sci. Lett. 414, 16–29. doi:10.1016/j.epsl.2015.01.009

Duraiswami, R.A., Bondre, N.R., Managave, S., 2008. Morphology of rubbly pahoehoe (simple) flows from the Deccan Volcanic Province: Implications for style of emplacement. J. Volcanol. Geotherm. Res. 177, 822–836. doi:10.1016/j.jvolgeores.2008.01.048

Duraiswami, R.A., Gadpallu, P., Shaikh, T.N., Cardin, N., 2014. Pahoehoe-a'a transitions in the lava flow fields of the western Deccan Traps, India-implications for emplacement dynamics, flood basalt architecture and volcanic stratigraphy. J. Asian Earth Sci. 84, 146–166. doi:10.1016/j.jseaes.2013.08.025

Ebinghaus, A., Hartley, A.J., Jolley, D.W., Hole, M., Millett, J., 2014. Lava-Sediment Interaction and Drainage-System Development In A Large Igneous Province: Columbia River Flood Basalt Province, Washington State, U.S.A. J. Sediment. Res. 84, 1041–1063. doi:10.2110/jsr.2014.85

Erlank, A.J., Marsh, J.S., Duncan, A.R., Miller, R.McG., Hawkesworth, C.H., Betton, P.J., Rex, D.C., 1984. Geochemistry and petrogenesis of the Etendeka volcanic rocks from SWA/Namibia, 195–247. In: Erlank, A.J. (Ed.), Petrogenesis of Volcanic Rocks of the Karoo Province, vol. 13. Special Publication of the Geological Society of South Africa, p. 395.

Farooqui, M., Hou, H., Li, G., Machin, N., Neville, T., Pal, A., Schrivastva, C., Wang, Y., Fengping, Y., Changhai, Y., Zhao, J., Yang, X., 2009. Evaluating volcanic reservoirs. Oilf. Rev. 21, 36–47.

Feng, Z., Yin, C., Liu, J., Zhu, Y., Lu, J., Li, J., 2014. Formation mechanism of in-situ volcanic reservoirs in eastern China: A case study from Xushen gasfield in Songliao Basin. Sci. China Earth Sci. doi:10.1007/s11430-014-4969-2

Florisbal, L.M., Heaman, L.M., de Assis Janasi, V., de Fatima Bitencourt, M., 2014. Tectonic significance of the Florianópolis Dyke Swarm, Paraná–Etendeka Magmatic Province: A reappraisal based on precise U–Pb dating. J. Volcanol. Geotherm. Res. 289, 140–150. doi:10.1016/j.jvolgeores.2014.11.007

Frank, H.T., Elisa, M., Gomes, B., Luiz, M., Formoso, L., 2009. Review of the areal extent and the volume of the Serra Geral Formation , Paraná Basin , South America. Pesqui. em Geociencias 36, 49–57.

Gladczenko, T.P., Hinz, K., Eldholm, O., Meyer, H., Neben, S., Skogseid, J., 1997. South Atlantic volcanic margins. J. Geol. Soc. London. 154, 465–470. doi:10.1144/gsjgs.154.3.0465

Grove, C., Jerram, D.A., Gluyas, J.G., Brown, R.J., 2017. Sandstone diagenesis in sediment-lava sequences: Exceptional examples of volcanically driven diagenetic compartmentalization in dune valley, huab outliers, NW Namibia. J. Sediment. Res. 87, 1314–1335. doi:10.2110/jsr.2017.75

Gindre-Chanu, L., Perri, E., Sharp, R.I., Peacock, D.C.P., Swart, R., Poulsen, R., Ferreira, H., Machado, V. 2016. Origin and diagenetic evolution of gypsum and microbialitic carbonates in the Late Sag of the Namibe Basin (SW Angola), Sedimentary Geology, Volume 342, 2016, Pages 133-153, ISSN 0037-0738, https://doi.org/10.1016/j.sedgeo.2016.06.015.

Guilbaud, M., Self, S., Thordarson, T., Blake, S., 2005. Morphology, surface structures, and emplacement of lavas produced by Laki, AD 1783–1784. Geol. Soc. Am. Spec. Pap. 396, 81–102. doi:10.1130/2005.2396(07).

Gupta, S.D., Chatterjee, R., Farooqui, M.Y., 2012. Formation evaluation of fractured basement, Cambay Basin, India. J. Geophys. Eng. 9, 162–175. doi:10.1088/1742-2132/9/2/162

Healy, D., Neilson, J., Haines, T.J., Michie, E., Timms, N., Wilson, M., 2014. An investigation of porosity-velocity relationships in faulted carbonates using outcrop analogues. Geol. Soc. London, Spec. Publ. 261–280. doi:10.1144/SP406.13

Hon, K., Kauahikaua, J., Denlinger, R., Mackay, K., 1994. Emplacement and inflation of pahoehoe sheet flows: observations and measurements of active lava flows on Kilauea volcano, Hawaii. Geol. Soc. Am. Bull. 106, 351–370. doi:10.1130/0016-7606(1994)106<0351:EAIOPS>2.3.CO;2

Helland-Hansen, D., 2009, Rosebank: challenges to development from a subsurface perspective, 2nd Faroe Islands Exploration Conference, Proceedings: Annales Societatis Scientiarum Færoensis, Supplementum, v. 50, p. 241–245

Janasi, V. de A., Montanheiro, T.J., Azor de Freitas, V., Reis, P.M., de Assis Negri, F., Dantas, F.A., 2007. Geology, petrography and geochemistry of the acid volcanism of the Parana magmatic province in the Piraju-Ourinhos region, SE Brazil. Rev. Bras. Geociencias 37, 745–759.

Janasi, V.D.A., de Freitas, V.A., Heaman, L.H., 2011. The onset of flood basalt volcanism, Northern Paraná Basin, Brazil: A precise U–Pb baddeleyite/zircon age for a Chapecó-type dacite. Earth Planet. Sci. Lett. 302, 147–153. doi:10.1016/j.epsl.2010.12.005

Jerram, D.A., 2002. Volcanology and facies architecture of flood basalts, in: Special Paper 362: Volcanic Rifted Margins. Geological Society of America, pp. 119–132. doi:10.1130/0-8137-2362-0.119

Jerram, D.A., Moutney, N.P., Howell, J.A., Long, D., Stolhofen, H., 2000. Death of a sand sea: an active aeolian erg systematically buried by the Etendeka flood basalts of NW Namibia. J. Geol. Soc. London. 157, 513–516. doi:10.1144/jgs.157.3.513

Jerram, D. a., Single, R.T., Hobbs, R.W., Nelson, C.E., 2009. Understanding the offshore flood basalt sequence using onshore volcanic facies analogues: an example from the Faroe–Shetland basin. Geol. Mag. 146, 353. doi:10.1017/S0016756809005974

Jerram, D. a., Widdowson, M., 2005. The anatomy of Continental Flood Basalt Provinces: geological constraints on the processes and products of flood volcanism. Lithos 79, 385–405. doi:10.1016/j.lithos.2004.09.009

Jerram, D. a, Stollhofen, H., 2002. Lava–sediment interaction in desert settings; are all peperite-like textures the result of magma–water interaction? J. Volcanol. Geotherm. Res. 114, 231–249. doi:10.1016/S0377-0273(01)00279-7

Jerram, D., Mountney, N., Holzförster, F., Stollhofen, H., 1999a. Internal stratigraphic relationships in the Etendeka group in the Huab Basin, NW Namibia: understanding the onset of flood volcanism. J. Geodyn. 28, 393–418. doi:10.1016/S0264-3707(99)00018-6

Jerram, D., Mountney, N., Stollhofen, H., 1999b. Facies architecture of the Etjo Sandstone Formation and its interaction with the Basal Etendeka Flood Basalts of northwest Namibia: implications for offshore prospectivity. Geol. Soc. London, Spec. Publ. 153, 367–380. doi:10.1144/GSL.SP.1999.153.01.22

Jiang, F., Cheng, R., Ruan, B., Lin, B., Xu, Z., Li, Z., 2017. Formation mechanism of volcanic reservoirs within a volcanostratigraphic framework: The case of the Wangfu fault depression in the Songliao Basin, China. Mar. Pet. Geol. 84, 160–178. doi:10.1016/j.marpetgeo.2017.03.036

Keszthelyi, L. and Denlinger, R.. The Initial Cooling of Pahoehoe Flow Lobes. Bulletin of Volcanology. Vol. 58. pp. 5–18. 1996.

Keszthelyi, L., Self, S., Thordarson, T., 2006. Flood lavas on Earth, Io and Mars. J. Geol. Soc. London. 163, 253–264. doi:10.1144/0016-764904-503

Keszthelyi, L., Thordarson, T., McEwen, A., Haack, H., Guilbaud, M.-N., Self, S., Rossi, M.J., 2004. Icelandic analogs to Martian flood lavas. Geochemistry, Geophys. Geosystems 5, 1–32. doi:10.1029/2004GC000758

Lenhardt, N., Götz, A.E., 2011. Volcanic settings and their reservoir potential: An outcrop analog study on the Miocene Tepoztlán Formation, Central Mexico. J. Volcanol. Geotherm. Res. 204, 66–75. doi:10.1016/j.jvolgeores.2011.03.007

Lima, E.F., Waichel, B.L., Rossetti, L.D.M.M., Sommer, C.A., Simões, M.S., 2018. Feeder systems of acidic lava flows from the Paraná-Etendeka Igneous Province in southern Brazil and their implications for eruption style. J. South Am. Earth Sci. 81, 1–9. doi:10.1016/j.jsames.2017.11.004

Marsh, J.S., Swart, R., 2016. The Bero Volcanic Complex: Extension of the Paraná-Etendeka Igneous Province into SW Angola. J. Volcanol. Geotherm. Res. doi:10.1016/j.jvolgeores.2016.10.011

Marzoli, A., Melluso, L., Morra, V., Renne, P.R., Sgrosso, I., D'Antonio, M., Duarte Morais, L., Morais, E.A.A., Ricci, G., 1999. Geochronology and petrology of Cretaceous basaltic magmatism in the Kwanza basin (western Angola), and relationships with the Paranà-Etendeka continental flood basalt province. J. Geodyn. 28, 341–356. doi:10.1016/S0264-3707(99)00014-9

McGrail, B.P., Spane, F.A., Sullivan, E.C., Bacon, D.H., Hund, G., 2011. The Wallula basalt sequestration pilot project. Energy Procedia 4, 5653–5660. doi:10.1016/j.egypro.2011.02.557

Millett, J., Hole, M.J., Jolley, D.W., Schofield, N., Campbell, E., 2015. Frontier exploration and the North Atlantic Igneous Province : new insights from a 2 . 6 km offshore volcanic sequence in the NE Faroe-Shetland Basin. J. Geol. Soc. London. In press. doi:10.1144/0016-76492015-069

Millett, J.M., Hole, M.J., Jolley, D.W., 2014. A fresh approach to ditch cutting analysis as an aid to exploration in areas affected by large igneous province (LIP) volcanism. Geol. Soc. London, Spec. Publ. 397, 193–207. doi:10.1144/SP397.2

Millett, J.M., Wilkins, A.D., Campbell, E., Hole, M.J., Taylor, R.A., Healy, D., Jerram, D.A., Jolley, D.W., Planke, S., Archer, S.G., Blischke, A., 2016. The geology of offshore drilling through basalt sequences: Understanding operational complications to improve efficiency. Mar. Pet. Geol. 77, 1177–1192. doi:10.1016/j.marpetgeo.2016.08.010

Milner, S.C., Duncan, A.R., Whittingham, A.M., Ewart, A., 1995. Trans-Atlantic correlation of eruptive sequences and individual silicic volcanic units within the Paraná-Etendeka igneous province. J. Volcanol. Geotherm. Res. 69, 137–157. doi:10.1016/0377-0273(95)00040-2

Mizusaki, A.M.P., Petrini, R., Bellieni, P., Comin-Chiaramonti, P., Dias, J., De Min, A., Piccirillo, E.M., 1992. Basalt magmatism along the passive continental margin of SE Brazil (Campos basin). Contrib. to Mineral. Petrol. 111, 143–160. doi:10.1007/BF00348948

Mizusaki, A.M.P., Thomaz Filho, A., Valença, J., 1988. Volcano-sedimentary sequence of Neocomian age in Campos Basin (Brazil). Rev. Bras. Geociencias 18, 247–251.

Mohriak, W.U., Mello, M.R., Dewey, J.F., Maxwell, J.R., 1990. Petroleum geology of the Campos Basin, offshore Brazil. Class. Pet. Prov. 50, 119–141.

Mohriak, W.U., Rosendahl, B.R., Turner, J.P., Valente, S.C., 2002. Crustal architecture of South Atlantic volcanic margins. Geol. Soc. Am. Spec. Pap. 362, 159–202. doi:10.1130/0-8137-2362-0.159

Monreal, F.R., Villar, H.J., Baudino, R., Delpino, D. and Zencich, S., 2009. Modeling an atypical petroleum system: A case study of hydrocarbon generation, migration and accumulation related to igneous intrusions in the Neuquen Basin, Argentina. Marine and Petroleum Geology, 26(4), pp.590-605.

Mountney, N., Howell, J., Flint, S., and Jerram, D. A., 1998, Aeolian and alluvial deposition within the Mesozoic Etjo Sandstone Formation, northwest Namibia: Journal of African Earth Sciences, v. 27, p. 175-192.

Mountney, N., Howell, J., Flint, S., and Jerram, D. A., 1999, Relating eolian bounding-surface geometries to the bed forms that generated them: Etjo Formation, Cretaceous, Namibia: Geology, v. 27, p. 159.

Nardy, A., Machado, F., Oliveira, M., 2008. As rochas vulcânicas mesozóicas ácidas da Bacia do Paraná: litoestratigrafia e considerações geoquímico-estratigráficas. Rev. Bras. Geociencias 38, 178–195.

Nelson, C.E., Jerram, D.A., Clayburn, J.A.P., Halton, A.M., Roberge, J., 2015. Eocene volcanism in 1598 offshore southern Baffin Bay. Marine and Petroleum Geology 67, 678-691.

Nelson, C.E., Jerram, D.A., Hobbs, R.W.R., 2009. Flood basalt facies from

borehole data: implications for prospectivity and volcanology in volcanic rifted margins. Pet. Geosci. 15, 313–324. doi:10.1144/1354-079309-842

Nelson, C.E., Jerram, D. a., Hobbs, R.W., Terrington, R. & Kessler, H. 2011. Reconstructing flood basalt lava flows in three dimensions using terrestrial laser scanning. Geosphere, 7, 87–96, doi: 10.1130/GES00582.1.

Peate, D., 1997. The Paraná-Etendeka Province. Large igneous Prov. Cont. Ocean. Planet. flood Volcanism 100, 217–245.

Peate, D., Hawkesworth, C., Mantovani, M., 1992. Chemical stratigraphy of the Paraná lavas (South America): classification of magma types and their spatial distribution. Bull. Volcanol. 55, 119–139.

Peate, D., Hawkesworth, C., Mantovani, M., Shukowsky, W., 1990. Mantle plumes and flood-basalt stratigraphy in the Paraná, South America. Geology 18, 1223–1226. doi:10.1130/0091-7613(1990)018<1223:MPAFBS> 2.3.CO;2

Petford, N., 2003. Controls on primary porosity and permeability development in igneous rocks. Geol. Soc. London, Spec. Publ. 214, 93–107. doi:10.1144/GSL.SP.2003.214.01.06

Petry, K., Jerram, D. a., de Almeida, D.D.P.M., Zerfass, H., 2007. Volcanic-sedimentary features in the Serra Geral Fm., Paraná Basin, southern Brazil: Examples of dynamic lava-sediment interactions in an arid setting. J. Volcanol. Geotherm. Res. 159, 313–325. doi:10.1016/j.jvolgeores.2006.06.017

Piccirillo, E.M., Melfi, A.J., 1988. The Mesozoic flood volcanism from the Paraná Basin (Brazil): petrogenetic and geophysical aspects. Universidade de São Paulo, São Paulo.

Piccirillo, E.M., Raposo, M.I.B., Melfi, A.J., Comin-Chiaramonti, P., Bellieni, G., Cordani, U.G., Kawashita, K., 1987. Bimodal Fissural Volcanic Suites From the Parana Basin (Brazil): K-Ar Age, Sr-Isotopes and Geochemistry. Geoch. Bras 1, 53–69.

Planke, S., 1994. Geophysical response of flood basalts from analysis of wire line logs: Ocean Drilling Program Site 642,. J. Geophys. Res. 99, 9279–9296. doi:10.1029/9

Polo, L.A., Janasi, V.A., Giordano, D., Lima, E.F., Cañon-Tapia, E., Roverato, M., 2017. Effusive silicic volcanism in the Paraná Magmatic Province, South Brazil: Evidence for locally-fed lava flows and domes from detailed field work. J. Volcanol. Geotherm. Res. doi:10.1016/j.jvolgeores.2017.08.007

Raposo, M.I.B., Ernesto, M., Renne, P.R., 1998. Paleomagnetism and 40Ar/39Ar dating of the early Cretaceous Florianópolis dike swarm (Santa Catarina Island), Southern Brazil. Phys. Earth Planet. Inter. 108, 275–290. doi:http://dx.doi.org/10.1016/S0031-9201(98)00102-2

Renne, P.R., Ernesto, M., Pacca, I.G., Coe, R.S., Glen, J.M.G., Prevot, M., Perrin, M., 1992. The Age of Parana Flood Volcanism, Rifting of Gondwanaland, and the Jurassic-Cretaceous Boundary. Science (80-.).

258, 975–979. doi:10.1126/science.258.5084.975

Reuss, A., 1929. Berechnung der Fließgrenze von Mischkristallen auf Grund der Plastizitatsbedingung fur Einkristalle, Z. Angew. Math. Mech., 9(1),49–58.

Rogers, K.L., Neuhoff, P.S., Pedersen, A.K., Bird, D.K., 2006. CO2 metasomatism in a basalt-hosted petroleum reservoir, Nuussuaq, West Greenland. Lithos 92, 55–82. doi:10.1016/j.lithos.2006.04.002

Rossetti, L., Lima, E.F., Waichel, B.L., Hole, M.J., Simões, M.S., Scherer, C.M.S., 2017. Lithostratigraphy and volcanology of the Serra Geral Group, Paraná-Etendeka Igneous Province in Southern Brazil: Towards a formal stratigraphical framework. J. Volcanol. Geotherm. Res. 1–17. doi:10.1016/j.jvolgeores.2017.05.008

Saar, M., Manga, M., 1999. Permeability-porosity relationship in vesicular basalts. Geophys. Res. Lett. 26, 111–114.

Sarmento, C.C.T., Sommer, C.A., Lima, E.F., 2017. Mafic subvolcanic intrusions and their petrologic relation with the volcanism in the south hinge Torres Syncline, Paraná-Etendeka Igneous Province, southern Brazil. J. South Am. Earth Sci. 77, 70–91. doi:10.1016/j.jsames.2017.04.017

Schenato, F., Formoso, M.L.L., Dudoignon, P., Meunier, A., Proust, D., Mas, A., 2003. Alteration processes of a thick basaltic lava flow of the Paraná Basin (Brazil): Petrographic and mineralogical studies. J. South Am. Earth Sci. 16, 423–444. doi:10.1016/S0895-9811(03)00098-1

Scherer, C.M.S., 2002. Preservation of aeolian genetic units by lava flows in the Lower Cretaceous of the Paran Basin, southern Brazil. Sedimentology 49, 97–116. doi:10.1046/j.1365-3091.2002.00434.x

Schofield, N., Jolley, D.W., 2013. Development of intra-basaltic lava-field drainage systems within the Faroe-Shetland Basin. Pet. Geosci. 19, 273–288. doi:10.1144/petgeo2012-061

Schutter, S.R., 2003. Hydrocarbon occurrence and exploration in and around igneous rocks. Geol. Soc. London, Spec. Publ. 214, 7–33. doi:10.1144/GSL.SP.2003.214.01.02

Senger, K., Millett, J., Planke, S., Ogata, K., Eide, C.H., Festøy, M., Galland, O. and Jerram, D.A., 2017. Effects of igneous intrusions on the petroleum system: a review. First Break, 35(6), pp.47-56.

Self, S., Keszthelyi, L., Thordarson, T., 1998. The Importance of Pahoehoe. Annu. Rev. Earth Planet. Sci. 26, 81–110. doi:10.1146/annurev.earth.26.1.81

Simões, M.S.S., Lima, E.F.F., Sommer, C.A.A., Rossetti, L.M.M.M.M., 2017. Structures and lithofacies of inferred silicic conduits in the Paraná-Etendeka LIP, southernmost Brazil. J. Volcanol. Geotherm. Res. doi:10.1016/j.jvolgeores.2017.12.013

Single, R., Jerram, D., 2004. The 3D facies architecture of flood basalt provinces and their internal heterogeneity: examples from the Palaeogene Skye Lava Field. J. Geol. Soc. London. 161, 911–926.

Sruoga, P., Rubinstein, N., 2007. Processes controlling porosity and permeability in volcanic reservoirs from the Austral and Neuquén basins, Argentina. Am. Assoc. Pet. Geol. Bull. 91, 115–129. doi:10.1306/08290605173

Sruoga, P., Rubinstein, N., Hinterwimmer, G., 2004. Porosity and permeability in volcanic rocks: a case study on the Serie Tobífera, South Patagonia, Argentina. J. Volcanol. Geotherm. Res. 132, 31–43. doi:10.1016/S0377-0273(03)00419-0

Stanistreet, I.G., Stollhofen, H., 1999. Onshore equivalents of the main Kudu gas reservoir in Namibia. Geol. Soc. London, Spec. Publ. 153, 345–365. doi:10.1144/GSL.SP.1999.153.01.21

Stewart, K., Turner, S., Kelley, S., Hawkesworth, C., Kirstein, L., Mantovani, M., 1996. 3-D, 40Ar-39Ar geochronology in the Paraná continental flood basalt province. Earth Planet. Sci. Lett. 143, 95–109. doi:10.1016/0012-821X(96)00132-X

Stica, J.M., Zalán, P.V., Ferrari, A.L., 2014. The evolution of rifting on the volcanic margin of the Pelotas Basin and the contextualization of the Paraná–Etendeka LIP in the separation of Gondwana in the South Atlantic. Mar. Pet. Geol. 50, 1–21. doi:10.1016/j.marpetgeo.2013.10.015

Sullivan, E.C., Hardage, B.A., McGrail, B.P., Davis, K.N., 2011. Breakthroughs in seismic and borehole characterization of Basalt sequestration targets. Energy Procedia 4, 5615–5622. doi:10.1016/j.egypro.2011.02.551

Thiede, D., Vasconcelos, P., 2010. Paraná flood basalts: Rapid extrusion hypothesis confirmed by new 40Ar/39Ar results. Geology 747–750. doi:10.1130/G30919.1

Thordarson, T., Self, S., 1998. The Roza Member, Columbia River Basalt Group: A gigantic pahoehoe lava flow field formed by endogenous processes? J. Geophys. Res. Solid Earth 103, 27411–27445. doi:10.1029/98JB01355

Torsvik, T.H., Rousse, S., Labails, C., Smethurst, M.A., 2009. A new scheme for the opening of the South Atlantic Ocean and the dissection of an Aptian salt basin. Geophys. J. Int. 177, 1315–1333. doi:10.1111/j.1365-246X.2009.04137.x

Vosgerau, H., Passey, S.R., Svennevig, K., Strunck, M.N., Jolley, D.W., 2015. Reservoir architectures of interlava systems: a 3D photogrammetrical study of Eocene cliff sections, Faroe Islands. Geol. Soc. London, Spec. Publ. 44, 85201. doi:10.1144/SP436.7

Vernik, L., 1990. A new type of reservoir rock in volcaniclastic sequences. AAPG Bull. 74, 830e836.

Voigt, W., 1910. Lehrbuch der Kristallphysik, Leipzig.

Waichel, B., Scherer, C., Frank, H., 2008. Basaltic lava flows covering active aeolian dunes in the Paraná Basin in southern Brazil: Features and emplacement aspects. J. Volcanol. Geotherm. Res. 171, 59–72. doi:10.1016/j.jvolgeores.2007.11.004

Waichel, B.L., de Lima, E.F., Viana, A.R., Scherer, C.M., Bueno, G. V., Dutra, G.,

2012. Stratigraphy and volcanic facies architecture of the Torres Syncline, Southern Brazil, and its role in understanding the Paraná–Etendeka Continental Flood Basalt Province. J. Volcanol. Geotherm. Res. 215–216, 74–82. doi:10.1016/j.jvolgeores.2011.12.004

Watton, T.J., Cannon, S., Brown, R.J., Jerram, D. a., Waichel, B.L., 2014. Using formation micro-imaging, wireline logs and onshore analogues to distinguish volcanic lithofacies in boreholes: examples from Palaeogene successions in the Faroe-Shetland Basin, NE Atlantic. Geol. Soc. London, Spec. Publ. 397, 173–192. doi:10.1144/SP397.7

Watton, T.J., Wright, K.A., Jerram, D.A., Brown, R.J., 2014. The petrophysical and petrographical properties of hyaloclastite deposits: Implications for petroleum exploration. Am. Assoc. Pet. Geol. Bull. 98, 449–463. doi:10.1306/08141313029

Wilson, M.S., Dyman, T.S. and Condon, S.M., 2008. Evaluation of well-test results and the potential for basin-center gas in the Columbia Basin, central Washington. US Geol. Surv. Dig. Digital Data Series DDS-69-0.

White, J., Bryan, S., Ross, P., 2009. Physical volcanology of continental large igneous provinces: update and review, in: Thordarson, T., Self, S., Larsen, G., Rowland, S.K., Hoskuldsson, A. (Ed.), Studies in Volcanology: The Legacy of George Walker. Special Publications of IAVCEI, 2. Geological Society, London. pp. 291–321.

Wright, K.A., Davies, R.J., Jerram, D.A., Morris, J., Fletcher, R., 2012. Application of seismic and 1809 sequence stratigraphic concepts to a lava-fed delta system in the Faroe-Shetland Basin, UK and 1810 Faroes. Basin Research 24, 91-106.

Zakharova, N. V., Goldberg, D.S., Sullivan, E.C., Herron, M.M., Grau, J. a., 2012. Petrophysical and geochemical properties of Columbia River flood basalt: Implications for carbon sequestration. Geochemistry, Geophys. Geosystems 13, 1–22. doi:10.1029/2012GC004305

Anexo III

Geochemical stratigraphy and Magmatic evolution of the Paraná-Etendeka Large Igneous Province: Insights from shallow crystallization magmatic processes and magma genesis

Submission Confirmation

Gondwana Research <eesserver@eesmail.elsevier.com>

dom 08/07/2018 23:00

Para:lucasross@hotmail.com <lucasross@hotmail.com>; l.rossetti@abdn.ac.uk <l.rossetti@abdn.ac.uk>;

Article Type: Research Paper

Dear Lucas,

Your submission entitled "Geochemical stratigraphy and Magmatic evolution of the Paraná-Etendeka Large Igneous Province: Insights from shallow crystallization magmatic processes and magma genesis" has been received by Gondwana Research

You may check on the progress of your paper by logging on to the Elsevier Editorial System as an author. The URL is https://ees.elsevier.com/gr/.

Your username is: lucasross@hotmail.com
Your password is: *******

Your manuscript will be given a reference number once an Editor has been assigned.

Thank you for submitting your work to this journal.

Kind regards,

Elsevier Editorial System
Gondwana Research

Geochemical stratigraphy and Magmatic evolution of the Paraná-Etendeka Large Igneous Province: Insights from shallow crystallization magmatic processes and magma genesis

Lucas M. Rossetti[1,2*], Malcolm J. Hole[2], Evandro F. de Lima[1], Marcos M.M. Rossetti[1,3]

[1] Instituto de Geociências, Universidade Federal do Rio Grande do Sul - Av. Bento Gonçalves, 9500, Agronomia, CEP: 91501-970, Porto Alegre, RS, Brazil

[2] Department of Geology and Petroleum Geology, University of Aberdeen, Aberdeen - AB24 3UE, UK

[3]Department of Geological Sciences, University of Canterbury, Private Bag 4800, Christchurch, New Zealand

*Corresponding author. E-mail: l.rossetti@abdn.ac.uk, lucasross@hotmail.com

Abstract

The Paraná-Etendeka Large Igneous Province in southern Brazil that is associated with the fragmentation of the western Gondwana during the Early Cretaceous is formed of heterogenous packages of lava flows. The lava pile can be subdivided into four main lava formations, namely: Torres, Vale do Sol, Palmas and Esmeralda, and these units reflect the evolutive stages of the magmatism. Polybaric crystallization was key on the genesis of distinct magma groups and the progressive development of the magmatic plumbing system controlled lava composition at the surface. At mid-crustal depths (> 6 kbar), magma crystallization occurred along L+Cpx control lines and was responsible for a distinct geochemical signature for Torres Formation lavas (G1 and G2). Torres Formation lavas have been formed by melting in the asthenosphere (30 and 40 kbar) with contributions of SCLM melts and have fractionated polybaric and assimilated variable amounts of enriched materials in the crust prior to eruption. The evolution of these parental melts to more evolved compositions of Vale do Sol Formation is marked by the progressive shallowing of magma chambers during plumbing system development and the change from a L+Cpx±Ol to L+Ol+plag crystallization. At the main phase of magmatism silicic rocks of Palmas Formation were formed by extensive AFC of the parental basaltic melts.

Significant lithospheric thinning occur concomitant to magmatism and the final Esmeralda Formation lavas were formed by partial melting of asthenosphere at shallow depths in the spinel stability field of the upper mantle, with no significant contribution from enriched lithospheric melts. The surface expression and composition of lava fields are directly controlled by shallow crystallization processes, and these can account for broad geochemical variations within large igneous provinces.

Keywords: Paraná-Etendeka; Geochemical Correlation; Petrogenesis; Magma crystallization;

1. Introduction

The Paraná-Etendeka large igneous is formed by large volumes of lavas, mostly of tholeiitic compositions, emplaced over short time intervals and this massive volcanic event is closely linked to the continental break-up of western Gondwana in the Early Cretaceous (Peate, 1997; Renne et al., 1992). Along with the flood basalts, (1) primitive picrites and ferropicrites occur as dykes and thin lavas in the lower stratigraphic levels (e.g. Jerram et al., 1999; Gibson et al., 2000; Thompson et al., 2001, 2007); (2) evolved silicic magmatism is preserved in the upper portions of the stratigraphy (e.g. Bellieni et al., 1984; Milner et al., 1992; Peate, 1997); (3) intrusive magmatism occur as extensive dyke swarms and alkaline intrusive complexes bordering the lava fields (e.g. Gibson et al., 1995; Raposo et al., 1998; Ernesto et al., 1999; Gomes et al., 2011; Florisbal et al., 2014; Natali et al., 2018). This broad range of rock types and geochemical compositions require melting from both asthenosphere and lithosphere (Peate, 1997; Gibson et al., 2006; Natali et al., 2018).

The main flood basalt lavas are formed of heterogeneous geochemical magma types (Marsh et al., 2001; Peate et al., 1992) and most of the lava sequence is constituted of MgO-poor lavas (MgO < 7 wt.%) that have evolved significantly during fractional crystallization (± assimilation) at variable depths, in complex plumbing systems (Peate, 1997; Thompson et al., 2001; Jennings et al., 2017). These fractionated, and in most cases, contaminated magma are far removed from primitive primary magma compositions and have isotopic signatures that are distinct from MORB-like, and OIB-like basalts and the genesis of these enriched magmas have

been ascribed to: (1) whole scale hydrous melting of the heterogeneous subcontinental lithospheric mantle (SCLM - Gallagher and Hawkesworth, 1992; Hawkesworth et al., 1992, 2000; Peate et al., 1992, 1999; Turner and Hawkesworth, 1995; Peate, 1997); (2) plume-derived asthenospheric melts that have assimilated partial melts from the lithospheric mantle (e.g. Gibson et al., 1995; Thompson et al., 2001); (3) melting of asthenospheric mantle with contributions from recycled components, EM-I and EM-II (Ewart et al., 1998, 2004; Rocha-Júnior et al., 2012; Marques et al., 2018).

We present here a review on the geochemical stratigraphy of the Paraná-Etendeka large igneous province in southern Brazil and constraints on the pressure and temperature intervals of crystallization from thermobarometry data and forward crystallization modelling. The area has been recently mapped in detail (Rossetti et al., 2018) and the new lithostratigraphy provides a high-resolution framework to constrain the temporal evolution of the magmatism. The most important findings presented here concerns magma evolution within the shallower portions of the lithosphere and the direct control of the magma plumbing system in the genesis of distinct magma compositions from basalt to rhyolite. Finally, we used a combination of forward and reverse modelling to constrain possible scenarios for magma genesis.

2. The Paraná-Etendeka Large Igneous Province: Geological Context

The Paraná-Etendeka Large Igneous Province (PE-LIP) represent the onshore portion of the large South Atlantic Igneous Province (Gladczenko et al. 1997; Foulger, 2018), and covers 1.2 x10^6 km^2 mostly over the South America continent, and minor areas in its counterparts in Africa (Cordani and Vandoros, 1967; Peate, 1997). The lava pile has an onshore preserved maximum thickness of 1.750m in the central portion of the Paraná basin, in Brazil (Fig. 1 - Piccirillo and Melfi, 1988) and covers an area of 917,000 km^2 over Paraná basin sediments, reaching volumes, including intrusive bodies, of at least 600,000 km^3 (Frank et al., 2009). In western Africa, the Etendeka Lava group occupies an area of 0.8x10^5 km^2 (Erlank et al., 1984) and similar areas are also covered by the Paraná-Etendeka magmatism in Angola (Marzoli et al., 1999; Marsh and Swart, 2018; Jerram et al., submitted). Extensive dyke swarms occur along the coastal areas of Brazil, Angola, and Namibia, and together with volcanic centres represent portions of the plumbing systems that fed the lavas (Florisbal et al., 2014, 2018; Jerram et al., 1999; Raposo et al., 1998; Sarmento et al., 2017).

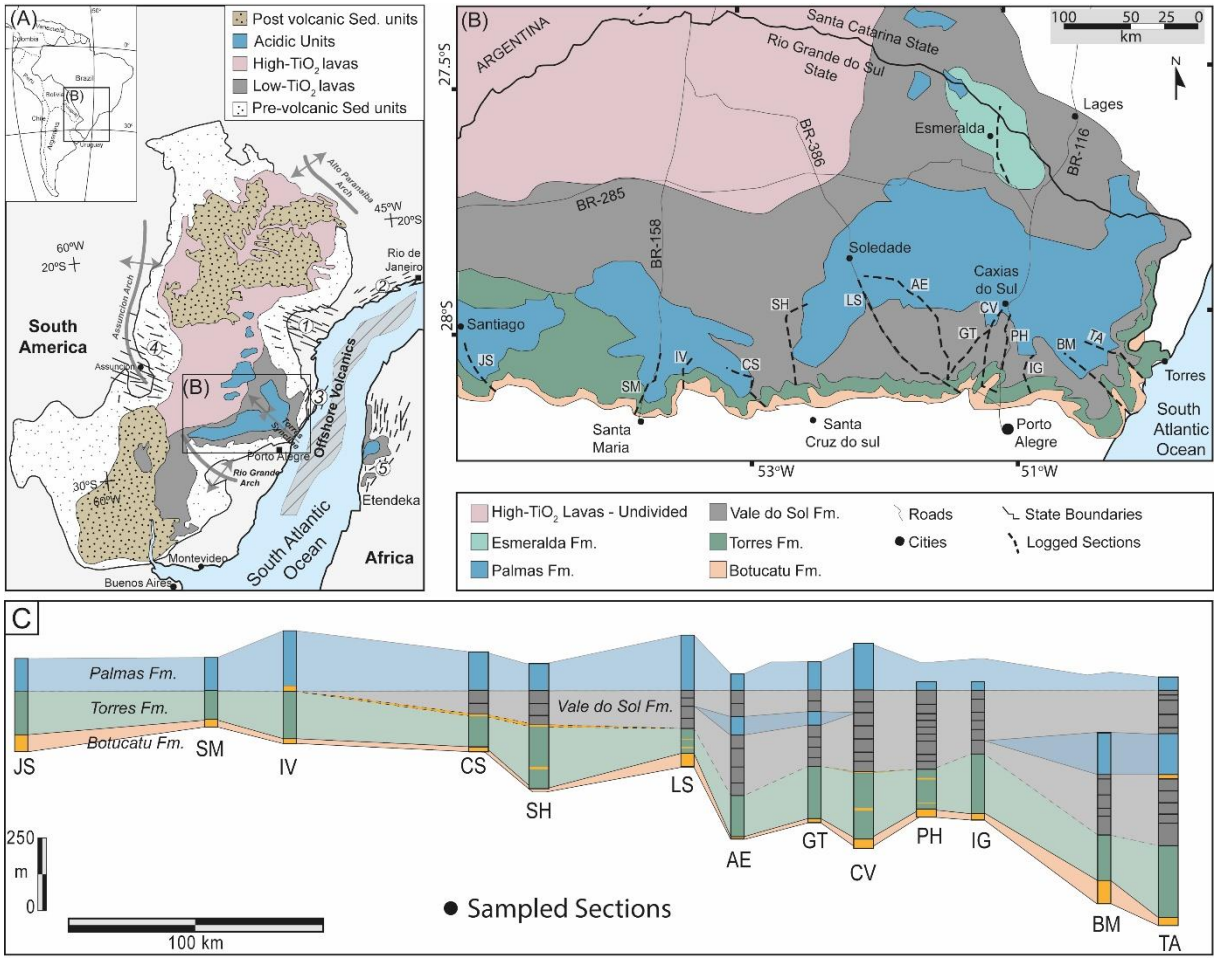

Figure. 1 – (A) Location of the Paraná-Etendeka Igneous Province, major dike swarms (1 - Ponta Grossa; 2 – Santos - Rio de Janeiro; 3 – Florianopolis; 4 – Paraguay; 5 Etendeka) and tectonic structures in a pre-drift reconstruction of Western Gondwana (modified after Peate et al., 1992; Stewart et al., 1996). (B) Detailed geological map of the Paraná-Etendeka LIP in Southern Brazil, key localities and sampled sections (modified after Rossetti et al. 2018); (C) Volcano-stratigraphy along key logged sections (modified after Rossetti et al. 2018).

The main phase of magmatism is constrained to a c. 4 Ma interval, beginning at c. 135 Ma and extending until 131 Ma (Janasi et al., 2011; Dodd et al., 2015) with the main peak of volcanism lasting c. 1 Ma (Renne et al., 1992; Jerram and Widdowson, 2005; Thiede and Vasconcelos, 2010; Baksi, 2018). The volcanic activity started in the southern portion of the province where the ages are clustered between 134.8–134.1 Ma ($^{40}Ar/^{39}Ar$ step-heating - Renne et al., 1992; Thiede and Vasconcelos, 2010) and migrated northwards where the lavas and associated intrusive bodies have slightly younger ages, ranging 133.6–131.5 Ma ($^{40}Ar/^{39}Ar$ step-heating - Ernesto et al., 1999).

The lavas present a geochemical provinciality and the subdivision of magma types provide a regional stratigraphic framework. The southern portion is dominated

by low-TiO_2 (LTi) lavas, is characterized by the Gramado magma type basalts overlaid by Palmas dacites and rhyolites and in the upper portion of the stratigraphy basalt lavas of the Esmeralda magma type (Peate et al., 1992; Peate, 1997). High-TiO_2 lavas (Urubici type) occur as a small strip (~100 km x 350 km) along the northeast limit of the lava escarpment in the south of Brazil and are contemporaneous and interbedded with Gramado lava flows (Peate et al., 1999; Bryan et al., 2010). The northern high-TiO_2 (Ti/Y >310) lavas are characterized by Ribeira, Pitanga and Paranapanema magma type basalts, respectively (Peate, 1997), covering the low-TiO_2 sequence towards north and west. The Chapecó acidic unitss occur in the lower portion of the high-TiO_2 lava pile covering the basement in the north or overlaying the top low-TiO_2 lavas in the central Paraná (Piccirillo et al., 1987; Peate et al., 1990; Janasi et al., 2007). Small volume of primitive picrite and ferropicrites compositions are found as dykes, sills and lava flows in the Etendeka region of NW Namibia (Gibson et al., 2000; Thompson et al., 2001), and similar compositions were recently recognized in dykes cross-cutting the base of the lava pile in the southernmost portion of the Paraná basin in Brazil (Sarmento et al., 2017).

3. Methods

A total of 190 samples of key stratigraphic positions and lava units were analysed for whole rock geochemical studies at Acme analytical laboratories Ltd., Vancouver, Canada. A total of 376 analyses were acquired in plagioclase and pyroxene phenocrysts and groundmass crystals of 15 thin sections of representative lava flow units within the sampled stratigraphy. From the entire geochemical dataset, a total of 16 representative samples were selected and analysed for Sr-, Nd- and Pb-isotope geochemical compositions at the Scottish Universities Environmental Research Centre – SUERC, East Kilbride, Scotland. Analytical methods applied in this study are presented and described in electronic appendix A. Representative geochemical compositions are presented in table 1, and 2 and the result of whole-rock, mineral and isotopic geochemical analyses for the entire dataset is presented as an electronic appendix B. Major and minor element compositions are expressed as weight % oxide and were recalculated to 100% on a dry basis, with iron concentrations expressed as FeO*, assuming Fe^{+2}/Fe^{+3} ratio of 0.89. Trace and rare-earth elements are presented as weight in ppm.

4. Geochemistry of the Paraná-Etendeka LIP in Southern Brazil

The lava pile was deposited over predominantly aeolian sandstones, known as the Botucatu Formation along the Brazilian margin, during the Early Cretaceous (Jerram et al., 2000; Scherer, 2002; Waichel et al., 2008). The volcano-stratigraphy is composed of four volcanic units divided based on their lithological characteristics, facies architecture, flow morphologies, intra-facies, and geochemical compositions, namely: Torres, Vale do Sol, Palmas and Esmeralda Formations (Rossetti et al. 2018). Torres Formation (TF) lavas are chemically more primitive compound pahoehoe flow fields. The Vale do Sol Formation (VSF) is characterized by the stacking of tabular sheet-like rubbly pahoehoe lavas dominantly basaltic andesitic in composition. These lavas covered the pahoehoe flow fields of Torres Fm. The upper part of the lava pile is characterized by tabular flows of dacitic to rhyolitic composition here defined as the Palmas Formation (PF). These lavas mainly overly VSF flows (Fig. 4C and D), although in the western limit of the lava pile they are deposited directly over the pahoehoe flow fields of TF. Esmeralda Formation (EF) is a pahoehoe flow field that covers the acidic flows of Palmas Fm., and locally the basaltic rocks of VSF in the north portion of the outcrop area.

Table 1 - Selected major trace and rare-earth element compositions for representative samples.

	Torres Fm.						Vale do Sol Fm.					
	Group 1 n=20		Group 2 n=15		Group 3 n=8		Group 1 n=8		Group 2 n=21		Group 3 n=18	
	SG-123Q	LBC-1	LR-48	LR-7A	SG-20	SG-27	LBC-16A	LR-23A	LBC-97	BR-10	SG-120	BR-19A
SiO2	51.12	57.48	50.31	50.65	52.87	53.12	51.74	53.07	51.64	59.21	50.53	55.56
TiO2	0.92	1.40	1.06	0.95	1.15	1.78	1.22	1.17	1.34	1.24	1.77	1.88
Al2O3	14.75	14.18	14.22	14.58	13.88	12.45	14.30	14.81	13.59	13.43	14.48	11.73
Fe2O3(t)	10.00	10.21	11.37	10.24	12.04	14.58	12.21	11.72	12.34	9.57	12.12	13.22
MnO	0.16	0.15	0.17	0.16	0.19	0.19	0.21	0.18	0.17	0.14	0.16	0.21
MgO	7.44	3.53	8.77	7.12	5.45	3.37	5.69	5.01	5.44	2.46	5.51	2.15
CaO	10.42	6.47	9.69	10.29	9.03	6.67	8.91	8.98	8.93	6.19	9.41	4.19
Na2O	1.96	2.76	1.88	2.04	2.67	2.58	2.33	2.43	2.30	2.46	2.44	2.53
K2O	0.95	2.54	0.96	0.67	1.30	2.44	1.21	1.73	0.69	2.16	1.17	4.64
P2O5	0.12	0.30	0.14	0.12	0.11	0.23	0.18	0.16	0.17	0.25	0.20	0.26
LOI	1.80	0.70	1.10	2.90	1.00	2.30	1.70	0.50	3.10	2.70	1.90	3.40
SUM	99.64	99.72	99.67	99.72	99.69	99.71	99.70	99.76	99.71	99.81	99.69	99.77
Hf	3.0	6.8	3.0	3.2	3.3	5.1	4.7	4.2	3.9	5.5	4.4	5.9
Ta	0.4	1.4	0.5	0.6	0.4	0.8	0.6	0.6	0.7	1.2	0.7	1.1
Th	2.9	8.8	3.7	3.2	3.8	6.3	5	5.4	4.8	9.5	3.8	9.9
U	0.3	1.9	0.7	0.6	1.1	1.8	0.8	0.9	1.2	2.5	0.7	3.3
Sc	36	29	36	34	36	32	36	35	35	26	25	31
V	233	264	254	256	348	445	342	253	369	228	309	461
Ni	38.1	22.0	61.7	89.0	19.6	9.3	43	48.0	47.0		46.5	
Rb	23.1	91.5	27.3	21.1	46.2	116.9	28.7	54.6	20.2	96.9	33.2	134.3
Sr	266.5	283.8	225.3	247.0	224.9	210.0	247.1	252.6	266.0	239.5	340.7	39.7
Y	22.6	32.9	20.2	19.6	24.7	37.0	30.6	26.4	32.5	32.0	26.6	41.6
Zr	117	245	105	110	118	190	160.3	135	143	197	166	211
Nb	7.3	22.3	7.2	6.8	7.4	13.7	11.9	10.1	10.7	14.5	11.5	16.2
Ba	321	627	240	236	253	393	411	394	287	540	330	526
Cr	252	0	345	219	70	0	1	34	42	0	161	0
Co	46	33	47	40	48	40	49.7	39	40	25	46	36
Pb	2.2	4.7	2.1	3.6	1.9	2.4	4.1	2.4	4.0	5.6	2.2	12.0
La	18.0	41.5	15.2	17.2	16.6	26.6	25.7	22.2	25.3	33.3	23.8	33.2
Ce	36.8	80.9	32.4	39.3	34.0	55.7	51.8	46.1	49.5	73.5	49.9	69.2
Pr	4.3	9.8	4.0	4.5	4.2	6.7	6.51	5.9	5.8	8.4	6.3	8.2
Nd	17.3	37.7	16.6	18.0	17.1	28.4	27.8	23.0	25.2	31.6	26.5	32.7
Sm	3.6	7.4	3.8	3.9	4.1	6.4	5.48	4.8	5.6	6.5	5.9	7.0
Eu	1.1	1.7	1.1	1.1	1.2	1.8	1.58	1.5	1.5	1.5	1.7	1.8
Gd	3.9	6.7	3.9	4.1	4.6	7.0	5.51	5.0	6.0	6.3	5.9	7.4
Tb	0.6	1.1	0.6	0.7	0.8	1.1	0.92	0.9	1.0	1.0	0.9	1.2
Dy	3.9	5.9	4.0	4.1	4.6	6.7	5.98	5.2	5.2	5.6	5.2	7.3
Ho	0.8	1.1	0.7	0.8	0.8	1.3	1.18	1.0	1.1	1.2	1.0	1.5
Er	2.3	3.4	2.3	2.1	2.4	3.8	3.3	3.2	3.2	3.0	2.8	4.0
Tm	0.3	0.5	0.3	0.3	0.4	0.5	0.49	0.5	0.5	0.5	0.4	0.6
Yb	2.0	3.1	2.0	2.1	2.1	3.4	3.04	2.8	3.1	2.8	2.5	3.8
Lu	0.3	0.5	0.3	0.3	0.3	0.5	0.47	0.4	0.4	0.5	0.3	0.6

Table 1 – continued

	Esmeralda Fm.		Palmas Fm.							
			Caxias do Sul		Santa Maria		Jacuí		Anita Garibaldi	
	n=4		n=60		n=12		n=10		n=3	
	LBC-39	LBC-38	LR-54D	SM-32	SM-40	SM-38	SM-27	LBC-17	LBC-40	LBC-50
SiO2	49.25	53.90	66.41	67.78	68.65	69.51	65.25	66.52	66.58	66.29
TiO2	1.26	1.72	0.89	0.89	0.68	0.70	1.04	1.06	1.04	1.05
Al2O3	14.32	13.02	12.87	12.22	12.38	12.45	12.83	12.80	12.55	13.43
Fe2O3(t)	13.49	15.00	6.05	7.06	6.01	5.71	7.32	7.59	6.73	6.60
MnO	0.20	0.18	0.11	0.08	0.09	0.05	0.12	0.07	0.09	0.08
MgO	6.56	2.32	1.52	0.75	0.92	0.33	1.47	0.86	1.30	0.99
CaO	11.00	5.34	2.95	2.04	1.80	1.47	3.50	2.16	3.27	2.16
Na2O	2.31	2.45	2.63	2.39	2.60	2.45	3.12	2.40	3.11	2.87
K2O	0.77	2.74	4.23	4.72	4.76	5.25	3.74	4.00	3.69	3.88
P2O5	0.14	0.27	0.28	0.23	0.20	0.18	0.27	0.28	0.32	0.32
LOI	0.60	2.80	1.90	1.70	1.80	1.80	1.20	2.10	1.20	2.20
SUM	99.90	99.75	99.84	99.86	99.89	99.90	99.86	99.84	99.88	99.87
Hf	2.4	5.6	5.8	7.7	8.4	9.2	6.6	7.8	6.3	6.9
Ta	0.4	1.1	1.3	1.6	1.8	2.2	1.4	1.7	1.6	1.5
Th	1.6	7.6	12.1	16.1	18.0	18.0	13.2	14.3	12.3	12.7
U	0.4	1.9	3.9	3.7	5.1	5.3	4.1	3.5	4.1	4.3
Sc	40	40	18	18	16	15	19	19	16	16
V	400	462	91	71	31	26	102	73	80	95
Ni	71.0		3.3	2.5	2.1	5.1	2.6			2.3
Rb	31.3	85.5	153.2	180.5	197.3	224.1	149.8	163.9	148.6	193.3
Sr	196.9	170.7	119.1	103.3	90.3	121.2	156.9	151.2	145.7	126.9
Y	25.9	79.6	31.4	42.7	48.2	44.4	35.8	57.5	40.2	151.5
Zr	94	200	206	279	286	344	228	300	254	260
Nb	5.8	15.8	15.8	20.3	20.4	27.3	16.9	22.4	20.0	19.1
Ba	157	480	506	639	646	678	588	787	571	637
Cr						14				
Co	47	38	11	7	5	4	13	14	11	11
Pb	0.9	3.6	5.7	6.3	6.4	3.7	3.0	4.3	2.2	3.5
La	10.2	42.3	36.2	45.3	46.7	47.4	37.9	57.8	39.9	74.2
Ce	21.9	59.9	75.7	82.5	94.0	89.9	77.6	106.3	84.4	137.2
Pr	2.9	9.6	8.6	10.7	11.0	10.9	9.4	14.9	9.9	22.0
Nd	14.2	37.6	33.5	42.3	42.6	41.1	35.9	57.2	36.5	99.8
Sm	3.6	8.3	6.5	8.5	9.0	8.5	7.4	11.6	8.1	22.5
Eu	1.2	2.4	1.3	1.8	1.6	1.7	1.5	2.4	1.7	5.3
Gd	4.2	9.7	6.2	8.6	8.9	8.3	7.3	10.6	7.6	25.7
Tb	0.8	1.7	1.1	1.4	1.4	1.4	1.2	1.7	1.3	4.2
Dy	5.0	10.9	5.9	8.3	8.5	8.1	6.8	9.9	7.9	25.4
Ho	1.0	2.1	1.1	1.7	1.7	1.6	1.3	1.9	1.4	5.2
Er	2.7	6.6	3.2	4.7	4.9	4.5	3.8	5.5	4.0	14.9
Tm	0.4	0.9	0.5	0.7	0.7	0.7	0.6	0.8	0.6	2.2
Yb	2.6	5.9	3.0	4.5	4.7	4.3	3.5	4.8	4.3	13.1
Lu	0.4	0.9	0.5	0.7	0.7	0.7	0.5	0.7	0.6	1.9

Table 2 – Sr, Nd and Pb isotopic data for the volcanic rocks of the southern Paraná-Etendeka LIP.

Sample ID.	Rb	Sr	$^{87}Sr/^{86}Sr_m$	Rb/Sr*	$^{87}Sr/^{86}Sr_{134Ma}$	Sm	Nd	$^{143}Nd/^{144}Nd_m$	$^{147}Sm/^{144}Nd$*	$^{143}Nd/^{144}Nd_{134Ma}$	εNd_{134Ma}	$^{208}Pb/^{204}Pb$	$^{207}Pb/^{204}Pb$	$^{206}Pb/^{204}Pb$
LBC.50	167.2	226.7	0.72181	4.41564	0.71365	8.1	41.6	0.51222	0.13596	0.51210	-7.17	38.94362	15.71638	19.12518
LBC.17	163.9	151.2	0.72560	3.14349	0.71979	11.6	57.2	0.51214	0.12288	0.51203	-8.51	38.89893	15.70337	18.96352
SG.4	244.6	77.4	0.73820	9.17560	0.72125	20.1	84.2	0.51216	0.14408	0.51204	-8.49	38.92401	15.70580	19.09352
SG.16	268.7	82.2	0.73899	9.49178	0.72145	8.3	40.9	0.51215	0.12269	0.51204	-8.37	38.91437	15.70957	19.07524
LR.48	27.3	225.3	0.70998	0.35067	0.70933	3.8	16.6	0.51226	0.13642	0.51214	-6.41	39.03660	15.69588	18.63880
BR.5A	17.7	204.8	0.71052	0.25012	0.71006	2.8	12.9	0.51233	0.13248	0.51221	-5.02	38.90470	15.66670	18.60810
SM.58	34.3	214.7	0.71016	0.46234	0.70930	3.7	15.8	0.51234	0.13951	0.51222	-4.90	38.86557	15.65834	18.68140
SG.26	75.4	217	0.71122	1.00556	0.70936	6.5	27.8	0.51238	0.14185	0.51226	-4.12	38.79878	15.69156	18.86359
SG.8B	69	238.8	0.70993	0.83621	0.70838	5.6	23.2	0.51229	0.14629	0.51216	-5.97	39.03008	15.70366	18.70877
BR.10	96.9	239.5	0.71882	1.17089	0.71665	6.5	31.6	0.51210	0.12402	0.51199	-9.37	39.00073	15.71680	18.90043
LR.18B	79.9	214.5	0.71448	1.07800	0.71249	6.5	29.6	0.51223	0.13302	0.51212	-6.87	39.00234	15.69370	18.75605
LR.16	79.4	133.2	0.71465	1.72510	0.71146	4.9	21.8	0.51230	0.13463	0.51218	-5.66	38.97710	15.70560	18.81355
BR.15	81.5	221.6	0.71179	1.06451	0.70983	4.5	19.4	0.51218	0.14039	0.51206	-8.02	38.90000	15.65600	18.44300
SM.29	70.1	161.8	0.71324	1.25383	0.71092	6.3	27.2	0.51234	0.14076	0.51222	-4.93	38.89130	15.67860	18.82556
LBC.51	20.8	187.1	0.70707	0.32180	0.70648	3.9	14.9	0.51239	0.15969	0.51225	-4.26	38.58596	15.56183	18.18771
LBC.39	31.3	196.9	0.70678	0.46013	0.70593	3.6	14.2	0.51250	0.15396	0.51237	-2.06	-	-	-

4.1. Torres Formation

A total of 43 samples of the Torres Formation lavas have been analysed for lithogeochemistry and the lavas can be separated into three geochemical groups with distinct major and trace element compositions. These represent spatial and stratigraphical domains that can be correlated with different evolutive stages of the onset of the magmatism in the area. Group 1 lavas make the bulk volume the Formation and extend from the east limit in the TA profile until the central-west area in the CS profile and occur dominantly as compound pahoehoe lava flow fields with variable thickness (from 1 – 15 m). Group 2 lavas are concentrated at the base of the lava stratigraphy in the central and eastern outcrop area and are generally restricted to the first 100 m lavas forming isolated interdune lava ponds, and minor compound flow fields. Group 3 lavas occur exclusively in the western portion of the studied area and in most cases, the lavas form thick interdune basaltic andesite units.

4.1.1. Petrography and Mineral Chemistry

Torres Formation lavas are aphyric, to poorly porphyritic basalt and basaltic andesites, formed by plagioclase, augite (±pigeonite), and iron oxides (Ti-magnetite and magnetite) ± altered olivine phenocrysts. Plagioclase and olivine are the most common phenocryst phases and typically account for less than 5% of rock volume. The groundmass is fine to medium-grained composed of plagioclase microphenocrysts (0.4 - 1.2 mm), with intergranular and subophitic augite (< 1 mm), and minor quantities of Ti-Fe oxides. Olivine-phyric lavas are restricted to the lowermost portions of the lava stratigraphy and typically occur in samples with MgO > 6 wt.%. Olivine pseudomorphs are equant, euhedral to subhedral (c. 0.5 mm) and are fully replaced by iddingsite and bowlingite aggregates.

***Plagioclase*.** Plagioclase phenocrysts occur as euhedral laths 1 - 3 mm in size and commonly present multiple twinning are normally zoned with crystal cores characteristically having higher anorthite content (An47-82), near equilibrium conditions with liquid compositions (based on K_D (An-Ab) for T< 1050^{o}C = 0.1±0.05 and for T> 1050^{o}C = 0.28±0.11 - Putirka, 2008), whilst crystal rims are compositionally more evolved (An_{38-67}) and commonly present sieved texture with reabsorbed margins and are not in equilibrium with whole-rock composition (Fig.2A). The compositional

variation in plagioclase crystals is explained by a progressive crystallization of crystals from a fractionating magma batch.

Pyroxene. Pyroxene phenocrysts are typically subhedral plates and range from 0.1 to 0.5 mm and occur associated with plagioclase forming glomerocrysts; ophitic and sub-ophitic textures are also common, with plagioclase partially or completely enclosed by late-stage pyroxene crystals. Micro-phenocrysts and microlites in the groundmass are typically intergranular to plagioclase. Crystals with KD(Fe-Mg)cpx-liq within 0.28±0.08 were considered to represent cpx-liquid equilibrium conditions (Putirka, 2008). The most primitive augite compositions are in equilibrium with melt, and the progressive decreasing in Mg#cpx from cores towards rims and groundmass crystals is concordant with a continuous differentiation during magma fractionation. Clinopyroxene is pressure-sensitive and disequilibrium conditions can be associated with abrupt pressure changes due to magma transport to the shallower crustal levels prior eruption, without significant time to homogenize crystal compositions. Cpx composition range from Wo25-42 En34-52 Fs12-37 for group 1 lavas; Wo25-40 En40-52 Fs14-32 for group 2; group 3 is characterized by both augite (Wo34-38 En24-40 Fs23-41) and pigeonite (Wo10-14 En29-44 Fs44-58) (Fig.3.A). Augite crystals are zoned with more restrict compositional array in crystal cores for any one group with higher concentrations of MgO, CaO, SiO_2, and Al_2O_3. Crystal rims and groundmass crystals are scattered from core compositions towards the ferrosilite apex. Crystals with Mg#cpx (molar MgO/MgO+FeO*100) >75 have enriched Cr_2O_3 and Al_2O_3 compositions, > 0.25 wt.% and > 2 wt.%, respectively. Group 3 lavas are characterized by simultaneous crystallization of augite and pigeonite, which results in CaO-rich augite compositions. Pigeonite is characterized by iron-rich compositions that are depleted in TiO_2 (<0.8) and Al_2O_3 (<1.5) and have crystallized in equilibrium conditions with evolved magmas (MgO c. 4 wt.%).

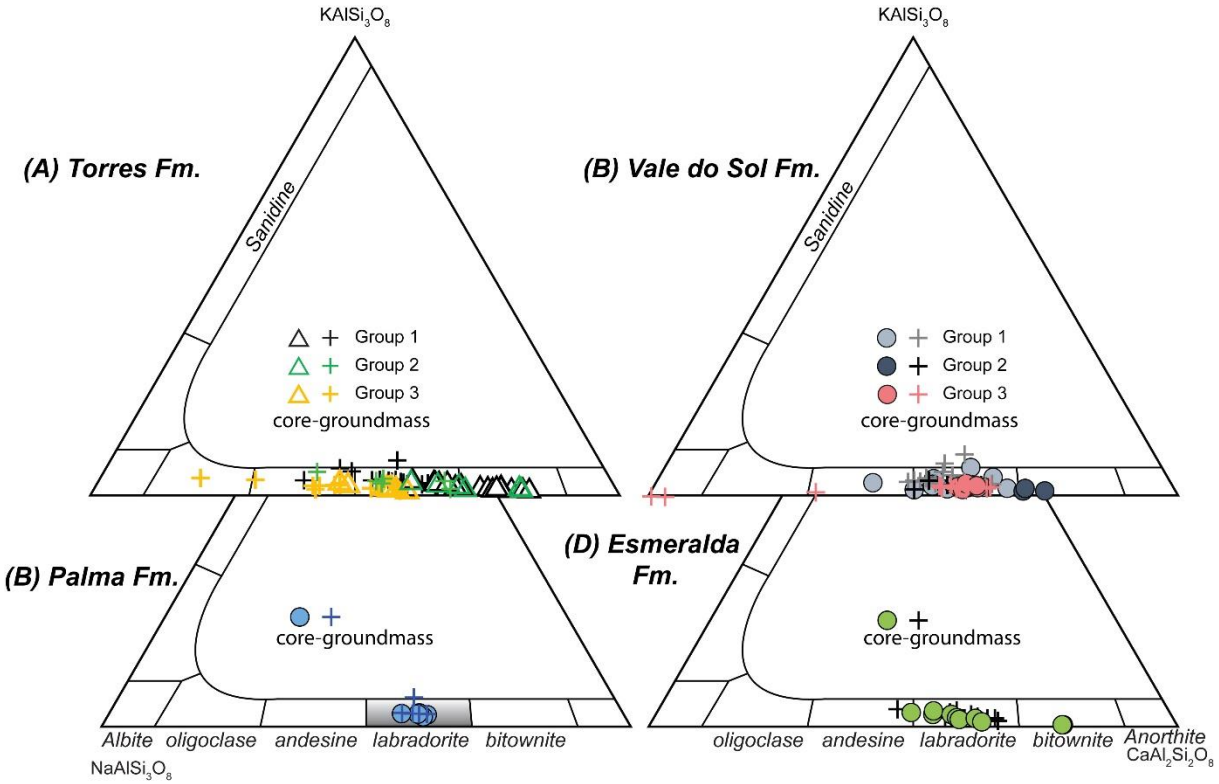

Figure 2 - Plagioclase compositions represented in the An-Ab-Or ternary diagram for (A) Torres Formation; (B) Vale do Sol Formation; (C) Palmas Formation; (D) Esmeralda Formation. Grey field for Palmas plagioclase composition is from Bellieni et al. (1986).

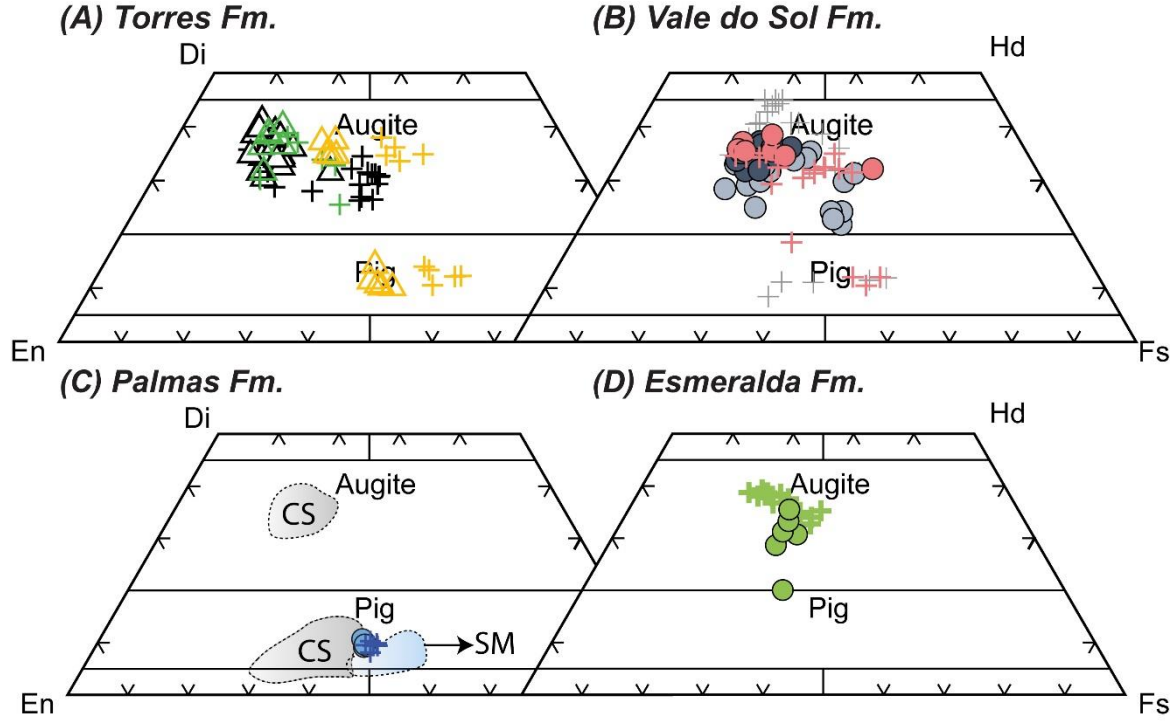

Figure 3 – Pyroxene compositions plotted in end member enstatite-wollastonite-ferrosilite ternary diagram (after Morimoto, 1988). (A) Torres Formation; (B) Vale do Sol Formation; (C) Palmas Formation; (D) Esmeralda Formation. Fields for Santa Maria (SM) and Caxias do Sul (CS) are from Bellieni et al. (1986), and Polo et al. (2018b). Symbols as in Figure 2.

4.1.2. Geochemistry Torres Formation

Figure 4 presents selected major and trace element compositions for the different lava units. Torres Formation lavas have a broad whole-rock geochemistry, with Mg# varying between 30 and 62.1 (MgO c. 3.5 -8.9 wt.%) for equivalent SiO_2 variations of c. 49.8 - 58.1 wt.%. TiO_2 is typically lower than 1.5 wt.% for group 1 and 2 samples and it is c. 1.5 - 2 wt.% for group 3 lavas. Groups 2 lavas have the most primitive compositions within all units sampled here, with Mg# > 54, reaching 62.1, MgO (wt.%) c. 6.5 - 8.9, Cr >200 ppm and SiO_2 < 52 wt.%. These high-MgO compositions are uncommon in the low-TiO_2 (LTi) basalts of the Paraná-Etendeka LIP that is dominated by evolved tholeiitic compositions (MgO < 7 wt.% - Peate, 1997). Despite minor overlap with group 1, group 2 primitive magmas extend to higher concentrations of both TiO_2 (c. 0.15 wt.%) and FeO* (c. 0.5 wt.%) and are characterized by lower concentrations of HSF and LIL, with Ti/Y > 300, Zr < 100 ppm, Y < 20ppm, Nb < 8ppm and Ba < 300 ppm. Group 2 has the shallow distribution for REE with $[La/Yb]_{CN}$ of 4.6 - 7.6, $[Tb/Yb]_{CN}$ 1.3 - 1.5, these slopes are within the range of group 1 samples, although, at a given MgO (wt.%), absolute concentrations of REE are lower.

Group 1 lavas are characterized by a steep rise in silica abundances along with a strong depletion of FeO* concentrations, and mild fractionation of TiO_2 in the most evolved samples (Mg# < 50). Al_2O_3 and CaO composition overlap those of group 2 lavas and extent to lower values in the evolved compositions. Trace element compositions overlap group 2 and extend towards higher values, Zr c. 110 – 240 ppm, Y c. 20 – 33, Nb c. 6 – 20. Group 3 is formed of basaltic andesites and represent the most differentiated lavas of Torres Formation. These lavas have Mg# < 50 (MgO c. 3.5 – 5.5 wt.%) and SiO_2 concentrations higher than 53 wt.% (c. 53.4 – 54.7 wt.%) and geochemical compositions that overlap those of Vale do Sol Formation group 2 and 3. The lavas are characterized by higher FeO* and TiO_2 concentrations, and typically lower K_2O and P_2O_5 and incompatible trace elements (Zr, Nb, Y, Ba) when compared to group 1 lavas.

In chondrite normalized diagrams, Torres formation lavas are LREE-enriched and have a marked inflexion from steep LREE to flatter middle to heavy REE distribution (Fig.5). $[La/Yb]_N$ is in the range of 4.0 to 9.5, whilst $[Tb/Yb]_N$ ranges from 1.3 to 1.6. In primitive mantle normalized multi-element diagrams, all lavas are

enriched in LILE and present strong negative anomalies of Nb and Ta (not shown) relative to U, Th, K and La, with $[La/Nb]_N$ 1.8 - 3.0 and $[Th/Nb]_N$ 1.6 - 5.7 (Th/Ta 3 - 10), and this has been previously linked to an inherited subduction-related signature that has been recognized in most southern Gondwana large igneous provinces (Rocha-Júnior et al., 2012; Hole et al., 2016; Marques et al., 2018). All lava groups also display marked trough for P and Ti, that is typical of the low-TiO_2 magma types of the Paraná-Etendeka province (Peate, 1997), with the steeper slopes for group 1 lavas. Torres Formation lavas have radiogenic $^{87}Sr/^{86}Sr_{134Ma}$, c. 0.709 to 0.710 and unradiogenic $^{143}Nd/^{144}Nd$ compositions varying from 0.5121 – 0.5123 (εNd_{134Ma} c. -6.8 to -4.1). Concentrations of $^{208}Pb/^{204}Pb$ and $^{207}Pb/^{204}Pb$ are within the range for the low-TiO_2 magma types of the Southern Paraná (Esmeralda and Gramado, Peate et. al 1992) and range from c. 38.8 – 39.1 and 15.65 to 15.7, respectively for variations of $^{206}Pb/^{204}Pb$ c. 18.5 to 19.

4.2. Vale do Sol Formation

The lavas of Vale do Sol Formation can be subdivided into three geochemical groups with distinct stratigraphical positions, and minor petrographic differences. Group 2 is the most abundant magma composition and forms the base and uppermost portion of the stratigraphy of the formation, group 1 lavas occur in the mid portions of the stratigraphy and represents a more primitive magmatic pulse with MgO > 5wt.% and low TiO_2 (< 1.25 wt.%) and P_2O_5 (< 0.2 wt.%). Group 3 lavas occur at the top of the first rubbly pahoehoe lavas package in the TA and LS profiles just before the first acidic lavas. In the other profiles, group 3 follows group 1 lavas in the mid portions of the stratigraphy. Vale do Sol lavas have been sampled in several road profiles, and the complete lava section have been sampled in the in the TA and CV profiles; the SH profile has been entirely sampled by Barreto et al., (2016).

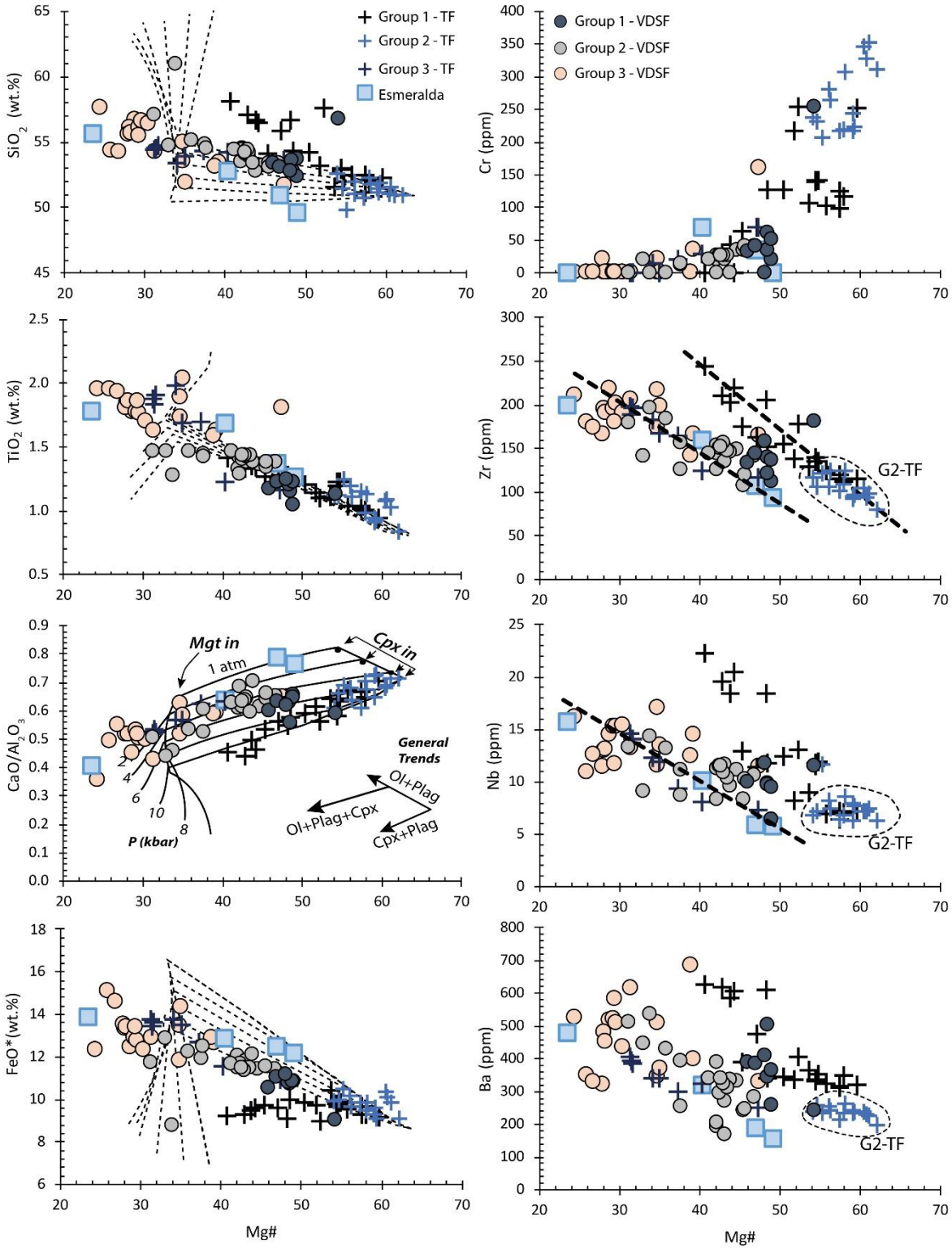

Figure 4 – Selected major and trace element compositions for the basaltic and intermediate rock composition of the southern Paraná-Etendeka large igneous province. LLD calculated from 0.01 % crystallization increments using Petrolog 3.1 (Danyushevsky and Plechov, 2011) from sample BR-05A over a range of pressures from 1 atm to 10 kbar.

4.2.1. Petrography and Mineral Chemistry

Vale do Sol Formation lavas are aphyric to plagioclase-phyric basaltic-andesites. The lavas are composed of plagioclase (An_{58}), augite (En_{45} Wo_{32} Fs_{25}), pigeonite (En_{42} Wo_{11} Fs_{47}), and Ti-magnetite. Plagioclase and augite phenocrysts occur isolated or as sparse clusters forming glomeroporphyritic texture, that reaches together 2.5 mm. Phenocrysts are involved by an aphanitic-microcrystalline to fine-grained groundmass (<0.1 mm) formed of laths of plagioclase and small anhedral augite and pigeonite. In group 1 lavas, MgO > 5 wt.%, oxidized olivine pseudomorphs occur as equant euhedral to subhedral micro-phenocrysts. Pigeonite occurs exclusively in group 2 and 3 lavas (MgO < 5 wt.%), mostly as microlites in the groundmass.

Plagioclase. Plagioclase phenocrysts are tabular, euhedral to subhedral, ranging between 0.7 and 2 mm and are characterized by multiple twinning. Matrix microlites are dominantly < 0.1 mm long with columnar to acicular shapes. The compositional variation in plagioclase crystals of Vale do Sol lavas is within the range of the most evolved Torres Formation lavas (Fig.2B). Plagioclase is mostly labradorite (An_{31-74}) and compositions are near equilibrium with liquid compositions. Phenocrysts present normal zoning although variations from core to rim, typically range only c. 5% for An, and, moreover, are minor when compared to those of Torres Formation lavas. Group 1 plagioclase shows the wider compositional variations within Vale do Sol lavas and, the only bytownite compositions (An_{49-74}). Acicular albite crystals replace the calcic core of plagioclase phenocrysts in some of group 3 lavas.

Pyroxene. Augite and pigeonite represent typically the late crystalizing phases occupying the intergranular spaces among plagioclase crystals, or, in some cases, partially involving plagioclase, in a subophitic texture. Micro phenocrysts are 0.3 mm in average and groundmass microlites are typically <0.1 mm. In general, high Mg#, early crystals are in equilibrium conditions and most crystal analysis present a linear distribution from equilibrium compositions towards lower Mg# concentrations, which are representative of a continuous fractional crystallization. For group 1 pyroxenes are augite (Wo_{32-37} En_{37-47} Fs_{19-27}) and display minor compositional variations that largely overlap the most primitive compositions from the other chemical groups (Fig.3B). For group 2 phenocryst, zonation is characterized by crystal cores clustered in the augite field, with low-CaO (Wo_{21-27}), whilst phenocryst rims microlites are scattered towards

the ferrosilite apex and have higher CaO (Wo_{32-45}). These occur together with pigeonite composition that is dominantly found as groundmass crystals. For group 3 phenocryst cores are CaO-rich augite whilst crystal rims and groundmass crystals have lower CaO concentrations and are scatter towards the Fs apex. Pigeonite forms groundmass crystals and is compositionally within the range of group 2 crystals. The clinopyroxene geochemical variations within Vale do Sol Formation lavas are similar to those of Torres Formation, with more evolved compositions marked by the crystallization of augite + pigeonite, (e.g. groups 2 and 3 VDS Fm.; group 3 Torres Fm.). The transition from augite (±olivine) stability conditions to augite+pigeonite in the evolved magmas is typical of advanced fractional crystallization of tholeiitic magmas (Thy et al., 2006; Villiger et al., 2004, 2007).

4.2.2. Geochemistry of the Vale do Sol Formation

Vale do Sol Formation lavas are composed of quartz-normative tholeiites that have SiO_2 typically higher than 52 wt.%, ranging from 51.66 to 60.97 wt.%, for MgO variations of 2 to 6 wt.% Vale do Sol and have Ni and Cr concentrations that are lower than 60 ppm and 100ppm, respectively. Most trace elements show a good linear correlation and increase with decreasing Mg#, with variations of Zr c. 100-220 ppm; Y c. 20-50ppm; Nb c. 8-16 ppm.

Group 1 lavas are MgO-rich basaltic andesites (MgO > 5wt.%) and have TiO_2 < 1.3 wt.% and P_2O_5 < 0.2 wt.%, and group 1 samples are characterized by increasing CaO/Al_2O_3 for Mg# > 43 (MgO > 5 wt.%) that is typical of L+Ol+Plag fractionation, and petrographically these lavas are characterized by oxidized olivine micro-phenocrysts. Group 2 samples have compositions intermediate between group 1 and 3 that are clustered mainly between Mg# 40 - 50 (MgO 4.6 – 5.6 wt.%). SiO_2 varies from 52.8 to 61.0 wt.%, and TiO_2 and P_2O_5 variations are constrained between 1.28 and 1.47 wt.% and between 0.15 - 0.26 wt.% respectively. For CaO group 2 samples present one main cluster between 8.5 - 9.4 wt.% and subordinate samples scatter between 6.0 and 8.1. Al_2O_3 displays minor variations, ranging from 13.2 to 14.3 wt.%. Group 3 lavas present the most evolved compositions with higher TiO_2 and P_2O_5 concentrations among all Vale do Sol lavas, c. 1.6 – 2.0 wt.% and 0.20 - 0.29 wt.%, respectively. For most samples SiO_2 > 52 wt.% and MgO < 5 wt.%. Al_2O_3 and CaO are positively correlated with Mg# and display a linear distribution, with minor scatter.

For the Vale do Sol Formation lavas, REE have a negative slope with marked enrichment in LREE, with normalized abundances of c. 100 times that of the chondrite and with $[La/Yb]_N$ ratios, in the range of c. 3.7-8.6. Middle to heavy REE show a relatively flat distribution, c. 20 higher than chondrite values, and $[Tb/Yb]_N$ display minor variation, c. 1.3 - 1.7. Most of the lava samples have at least a minor Eu negative anomaly and Eu/Eu* values vary between 0.71 and 0.89. Intergroup REE variations are marked by a progressive increase in $[La/Yb]_N$ towards the most evolved composition of each group, with $[La/Yb]_N$ c. 5.3 for group 1, c. 4.7 for group 2 and c. 3.7 for group 3. Primitive mantle normalized multi-element diagrams display a negative slope highlighting the gradual enrichment towards the most incompatible elements, with marked troughs for Ba, Nb, Sr, P, and Ti. Vale do Sol Formation lavas are characterized by isotopic compositions intermediate between Torres and Palmas lavas with radiogenic $^{87}Sr/^{86}Sr$ compositions, c. 0.7083 - 0.7166, and low $^{143}Nd/^{144}Nd$ 0.5120 to 0.5122 (εNd_{134Ma} c. -9.4 to -4.9) that is in the range of Torres Formation lavas. Pb-isotopic compositions are constrained between $^{208}Pb/^{204}Pb$ c. 38.9 – 39.0, $^{207}Pb/^{204}Pb$ c. 15.65 – 15.7, and $^{206}Pb/^{204}Pb$ c.18.4- 18.9.

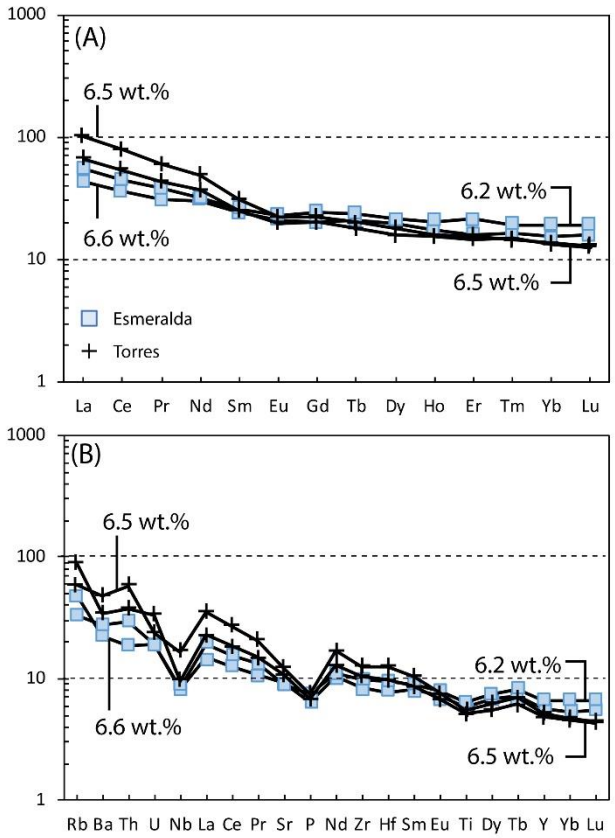

Figure 5 – Chondrite normalized rare-earth element diagram (A) and primitive mantle normalized spider diagram (B) for Torres and Esmeralda Formation lavas. Chondrite and primitive mantle compositions are from Sun and McDonough (1989).

4.3. Palmas Formation

The Palmas Formation occurs in the upper portions of the stratigraphy and is composed of dacite and rhyolite as tabular lavas that have been fed dominantly trough fissure systems (Lima et al., 2018; Simões et al., 2018), locally fed lava domes and coulees (Polo et al., 2018a) and high-grade lava-like rheoignimbrites (Luchetti et al., 2018). Palmas acidic rocks have been divided into several groups (or magma types), based on their major and trace element geochemistry and their spatial-stratigraphical distribution, and these are correlated with silicic units from the Etendeka namely: (1) Caxias do Sul – Springbok/Grootberg; (2) Jacuí-Goboboseb II; (3) Anita Garibaldi - Beacon; (4) Santa Maria - Fria; (5) Clevelândia; and (6) Barros Cassal (Peate et al., 1992; Garland et al., 1995; Marsh et al., 2001; Nardy et al., 2008; Bryan et al., 2010; Polo et al., 2018a,2018b). Caxias do Sul, Santa Maria, Jacuí and Anita Garibaldi groups were sampled here. Caxias do Sul group is composed of dacites and is the most abundant unit within Palmas Formation in Brazil, overlying an area of c.16.000 km² (Peate et al., 1992). These rocks overlap the Jacuí lavas and, in most cases, rest on top of the Vale do Sol Formation lavas. The Anita Garibaldi group overlies an area of c. 4.486 km^2, near the border of Rio Grande do Sul and Santa Catarina in southern Brazil and occurs as isolated plateaus (Garland et al., 1995; Nardy et al., 2008). The Santa Maria rhyolites cover an almost continuous area of c. 12.300 km^2 in the western outcrop area (Nardy et al., 2008; Peate et al., 1992).

4.3.1. Petrography and Mineral Chemistry

Palmas Formation lavas are, in general, aphyric to vitrophyric with phenocrysts and microphenocrysts frequently involved by glass or a microcrystalline groundmass. Phenocrysts are typically euhedral to subhedral and occur isolated or clustered forming glomeroporphyritic textures. The most common phases are plagioclase (An_{55-65}) and pigeonite ($En_{45}\ Wo_{10}\ Fs_{45}$) and individual phenocrysts typically display reabsorbed, sub-rounded edges and are commonly dissolved or replaced by clay material. The groundmass is formed of plagioclase, Ti-Fe-oxides, and less commonly pigeonite. Plagioclase microlites have typically columnar to acicular shapes and display swallow-tail terminations, and subordinately empty prismatic shapes and hooper habits. Rock matrix forms a patchy pattern with brownish areas composed of isotropic glassy

material and light areas characterized by devitrified microcrystalline quartz+K-feldspar overgrowths.

Plagioclase. Only one sample of Palmas Formation has been analysed for mineral chemistry (sample LBC-80). Plagioclase is labradorite and shows just minor chemical variations from core to rims, with anorthite ranging from 55 to 60 (Fig.2C). All phenocrysts are within equilibrium conditions with whole rock compositions.

Pyroxene. Pyroxene is pigeonite and it is characterized by similar proportions of En and Fs and low-CaO concentrations (Wo > 20) (Fig.3C). Crystal compositions are in equilibrium with liquid and phenocryst have neglectable compositional variations from core to rims. Samples plot in the limit of the Santa Maria and Caxias do Sul pyroxene compositional fields (Bellieni et al., 1986 and Polo et al., 2018b).

4.3.2. Geochemistry Palmas Formation

Lava composition is characterized by high-SiO_2, scattered between 63.8 to 71.8 wt.% for MgO variations in the range of c. 0.3 – 1.7 wt.%. All lavas are high-K_2O, with abundances typically > 3 wt.%, and have moderate Na_2O (c. 2-3.5 wt.%). Total alkalis (Na_2O+K_2O) are in the range of c. 5 – 9 wt.% and most compositions, including Caxias do Sul, Jacuí and Anita Garibaldi are metaluminous, with Al/(Na+K) > 1 and Al/(Ca+Na+K) < 1 (following the Shand index). For Santa Maria (SM) lavas, samples are dispersed from metaluminous towards peraluminous compositions.

The difference among geochemical types is clearly identified by natural compositional gaps in the P_2O_5 (wt.%) versus TiO_2 (wt.%) variation (Fig.6). The Caxias do Sul (CS group), Jacuí (J group) and Anita Garibaldi (AG group) are dacitic in composition with minor scatter towards trachyte, and are relatively enriched in TiO_2 (> 0.85 wt.%) and P_2O_5 (> 0.23 wt.%). The Jacuí and Anita Garibaldi lavas are characterized by higher TiO_2 concentrations when compared to Caxias do Sul lavas, with TiO_2 (wt.%) typically > 1. The distinction between Jacuí and Anita Garibaldi is highlighted by the higher P_2O_5 abundances of the latter (> 0.3 wt.%). SM group lavas are characterized by the most evolved compositions with SiO_2 variations between 69.6 and 71.8 wt. % to MgO on the range of 0.35 to 0.95 wt.%. Together with the higher SiO_2 Santa Maria rhyolites have are HFSE-enriched and have the highest Zr (>285 ppm) and Th (>16.5 ppm) concentrations among all the silicic lavas. SM group lava compositions are also distinguished from the CS group lavas by its lower TiO_2 (< 0.8

wt.%) and lower P_2O_5 (< 0.2 wt.%) along with low V and Sr compositions. Palmas Formation lavas have enriched isotopic compositions and represent the highest $^{87}Sr/^{86}Sr$ values among all volcanic units, with $^{87}Sr/^{86}Sr$ c. 0.7134 – 0.720 for $^{143}Nd/^{144}Nd$ variations of c. 0.5120 – 0.5121 (εNd_{134Ma} c.-7 to -8.5). $^{207}Pb/^{204}Pb$ and $^{208}Pb/^{204}Pb$ are within the range of the other lava formations at typically higher $^{206}Pb/^{204}Pb$ (>18.9)

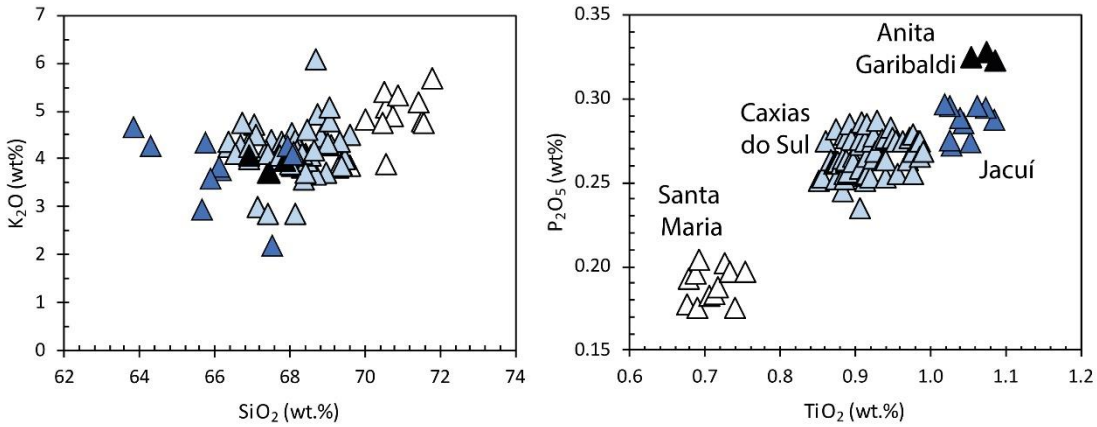

Figure 6 - (A) K_2O (wt.%) versus SiO_2 (wt.%) and (B) P_2O_5 (wt.%) versus TiO_2 (wt.%) diagrams showing the geochemical composition and distinction among groups within Palmas Formation.

4.4. Esmeralda Formation

The Esmeralda Formation (EF) is the uppermost unit of the low-TiO_2 volcanic succession. It comprises the Esmeralda magma-type basalts (Peate et al., 1992). The flow field is mainly exposed in the northeast border of Rio Grande do Sul and Santa Catarina states and has a smaller areal extent than other volcanic units. The lavas are not commonly preserved in road sections and their occurrence is restricted to inland shallow outcrops, where the lavas partially overlie Palmas dacites. Samples were collected along the main inland outcrop area, near the city of Esmeralda.

4.4.1. Petrography and Mineral Chemistry

Esmeralda Formation lavas are aphyric to poorly porphyritic basalts and basaltic andesites. The rocks commonly have aphanitic-microcrystalline and vitrophyric textures. In the microcrystalline facies, plagioclase occurs as euhedral to subhedral laths, as isolated phenocrysts or grouped forming glomerocrysts. The rock

groundmass is fine-grained (0.1 – 0.3 mm) and it is formed of columnar subhedral plagioclase, and subhedral to anhedral augite and Ti-Fe-oxides with typical intergranular and subophitic textures. The vitrophyric lavas are formed by acicular to skeletal microphenocrysts of plagioclase that commonly have swallow-tail terminations, augite also occurs as microcrystals (0.2 – 0.5 mm) and these are typically involved by a glass-rich or aphanitic matrix, forming vitrophyric texture.

Plagioclase. Most plagioclase is labradorite, with minor andesine and bytownite compositions. Crystals have a general homogeneous composition from core to the rim and An ranges from 45 to 78 % (Fig.2D). Only 2 out of 24 analyses represent crystal-liquid equilibrium conditions for plagioclase crystals.

Pyroxene. Esmeralda Formation pyroxene is augite in composition and forms a relatively continuous trend from Fe-rich augite ($En_{40}\,Wo_{38}\,Fs_{22}$) towards the Fs apex in the ternary En-Fs-Wo diagram (Fig.3D). The few phenocryst core analysis (sample LBC-38) have compositions that are enriched in CaO (a.f.u.) and are in disequilibrium with whole-rock compositions. These have Mg# higher than expected for the given rock composition and might represent crystals formed in a primitive magma with higher Mg#. In phenocryst rims and groundmass crystals the most MgO-rich augite compositions were obtained in a fine-grained holocrystalline basalt (sample LBC-39) and crystals are in disequilibrium with whole rock compositions (rock Mg# = 50). The most evolved compositions ($En_{35}\ Wo_{30}\ Fs_{35}$) represent augite microlites from a vitrophyric basalt sample LBC-38 and are in crystal-liquid equilibrium conditions, with $K_D(Fe\text{-}Mg)^{cpx\text{-}liq}$ within 0.28±0.08.

4.4.2 Geochemistry Esmeralda Formation

Esmeralda Formation is compositions are roughly constrained between 50 and 54 wt.% for equivalent MgO variations of c. 2.7 - 7.3 wt.%. TiO_2 and FeO* have slightly higher concentrations for correspondent MgO, (c. 0.2 wt.% and 1.5 wt.%, respectively) when compared to the other sampled compositions of Vale do Sol and Torres Formation, whilst SiO_2 is typically lower (c. 1 – 2 wt.%). When compared to group 1 and 2 lavas from Torres Formation, however, Esmeralda Formation lavas have lower concentrations of Ba (c. 100 ppm) and Sr (c. 50 ppm), and higher Sc (c. 10 – 15 ppm) and V (c. 50 ppm) and partially overlap Vale do Sol Fm. and group 3 of Torres formation compositions. Esmeralda lavas have a relatively flat REE distribution with $[La/Yb]_{CN}$

between 2.1 and 4.5 and $[La/Sm]_{CN}$ 2.1 and 3.9. Absolute abundances are typically 40 to 100 times the chondrite values for LREE and 20 to 40 for HREE. Eu anomaly gradually increases from primitive to evolved compositions and Eu/Eu* is in the range of c. 0.80 – 0.95, and for the most primitive analysed samples (MgO > 6.0 wt.%) Eu anomalies are neglectable. Esmeralda Formation lavas have the most depleted composition for $^{87}Sr/^{86}Sr_{134Ma}$, in comparison to the other lava units, with just minor variations constrained between 0.7059 and 0.7065, and the higher εNd_{134Ma} values, ranging from – 4.2 to – 2.0 ($^{143}Nd/^{144}Nd$ c. 0.5122 – 0.5124). Only one sample was analysed for Pb-isotopes and it has $^{208}Pb/^{204}Pb$ = 38.6, $^{207}Pb/^{204}Pb$ = 15.56, $^{206}Pb/^{204}Pb$ = 18.15, and fall within the compositional range of the Gough component of the Tristan-Gough system.

5. Geochemical Correlation and Stratigraphy

The general geochemical variations within large igneous provinces lava sequences is well documented worldwide and represent the basis for defining the regional stratigraphy of these major volcanic events (Cox and Hawkeshworth, 1985; Hooper, 1982; Peate et al., 1992; Hooper, 2000). Furthermore, a better understanding and a detailed stratigraphic framework can be obtained by combining geochemistry with field-based studies, and within a tight stratigraphic control, high-resolution geochemistry can aid on the identification of individual eruptive units, or eruptive cycles (e.g. Kerr, 1995; Thordarson and Self, 1998; Jay and Widdowson, 2008; Millett et al., 2015, 2017).

A general overview of the geochemical stratigraphy was obtained here by correlating the chemical groups within individual formations laterally along the stratigraphic lava profiles (Fig. 7). The onset of magmatism, Torres Formation lavas, is characterized by pahoehoe flow fields and interdune ponded lavas. The most primitive eruptions (group 2) formed isolated volcanic units at the base of the lava pile. These lavas were overlaid by more widespread and voluminous flow fields with group 1 geochemical composition. In the western outcrop area, group 3 lavas make the base of the lava pile and cover group 1 lavas towards east. Torres Formation lava flows are covered by thick vertically stacked basaltic andesite lavas from the Vale do Sol Formation. Group 2 of VDS represents the most common magma composition and forms the lower and upper lava flows in the stratigraphy. The compositional shift from

relatively evolved basaltic andesites (VDS-G2) to MgO-rich basaltic andesites (VDS-G1) and these might represent recharge of basic magmas in the shallow magma chambers. Group 3 magmas form an interval of lavas in the central portion of the stratigraphy of the Vale do Sol Formation and occur also as isolated lava flows in the central areas (PH profile), based on its stratigraphical position it is possible to correlate VDS-G3 lavas laterally over long distances (c. 200 km). The silicic magmatism is characterized by flow units that occur intercalated with the upper Vale do Sol lavas, and these correspond to the Caxias do Sul type. The Jacuí type lavas cover the last basaltic andesite eruptions in the area and are overlaid by more voluminous acidic eruptions with Caxias do Sul composition. Santa Maria type lavas occur in the western outcrop area laying directly on top of the group 3 lavas of Torres Formation, and in the central areas covering Caxias do Sul dacites. Esmeralda and Anita Garibaldi chemical types were not sampled in the southern profiles and occur isolated to inland areas, and represent the upper stratigraphy intervals.

6. Discussion

The geochemical composition of a cooled lava in a flood basalt provinces, in general, represent a complex interplay of several petrological processes such as the composition of the source rock; the dynamic of partial melting; re-equilibration with host rock; fractional crystallization during magma transport; mixing; assimilation of wall-rock and magma contamination (e.g. Cox et al. 1979; Thompson et al., 2007; Jennings et al., 2017; Hole, 2018). For the southern section of the Paraná-Etendeka, major elements compositional variation can be produced by means of fractional crystallization of different proportions of Ol ± Cpx ± Plag ± Fe-Ti oxides. However, trace element and isotopic compositions require variable inputs from enriched materials (e.g. continental crust) implying that crystallization occurred in open-systems with the assimilation of wall-rock (e.g. AFC), and/or addition of enriched lithospheric materials (e.g. Gibson et al., 1995; Thompson et al., 2001, 2007; Marques et al., 2018). The degree to which these factors contributed to the final magma compositions within the studied section of Paraná-Etendeka LIP and the possible scenarios for magma genesis will be explored and discussed in the following sections.

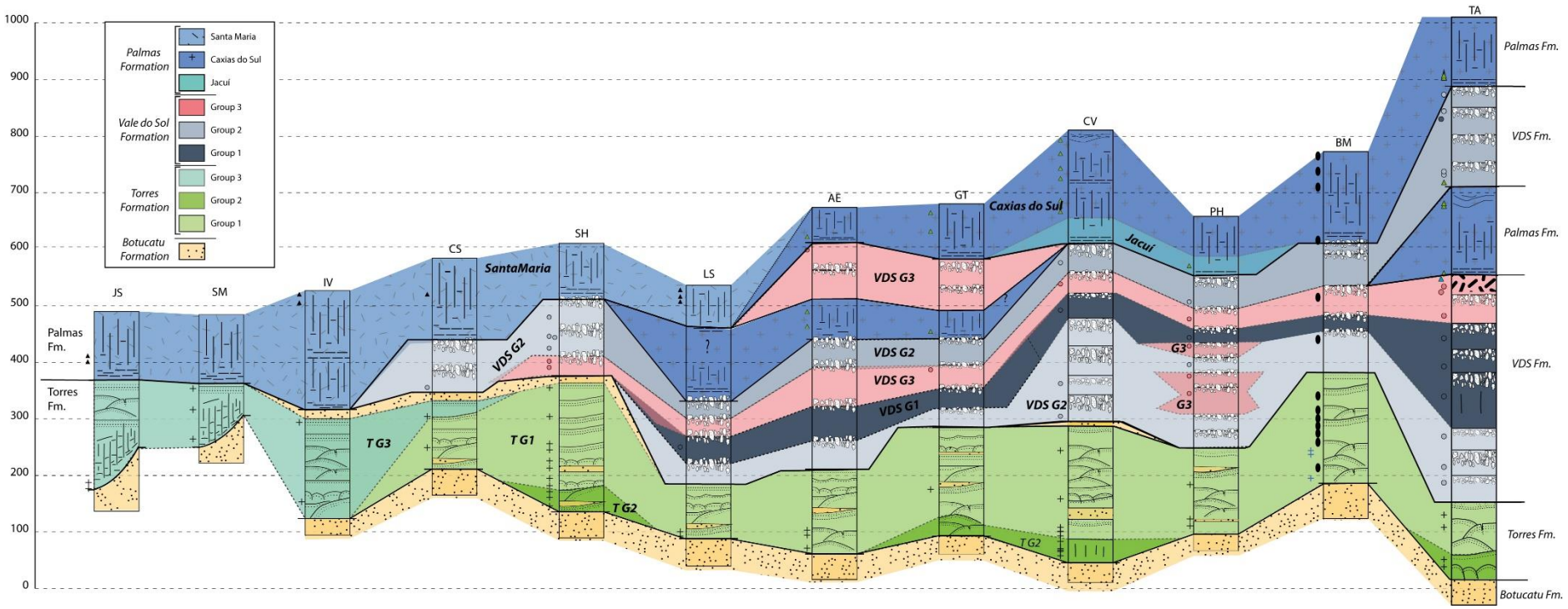

Figure 7 - Combined lithostratigraphy (from Rossetti et al. 2018) and geochemical stratigraphy and the lateral correlation of the different geochemical groups for the Southern Paraná-Etendeka LIP.

6.1 Shallow magmatic evolution: constrains from thermobarometry data

A combination of whole-rock and crystal-liquid thermometers and barometers along with modelled liquid lines of descent (LLD) are used here to constrain the range of pressure and temperature for the crystallization of the southern Paraná-Etendeka lavas. The results of thermobarometry studies are presented in Table 3 and Figure 8.

Overall clinopyroxene and plagioclase thermobarometers show a good correlation, registering pressures, in general, < 9 kbar, and temperatures within the range of 1000 - 1225ºC. Whole rock temperature derived intervals are within the range of clinopyroxene and plagioclase data (Table 3). From the thermobarometry data it is suggested that crystallization was polybaric with magmas stopping at different crustal levels and the pressure variations derived from mineral-liquid barometers, show great consistency with mechanical discontinuities within the crust with most of the data concentrating between pressures of 4 - 5 kbar that coincides with the brittle-ductile transition zone of the upper crust (BDT, c. 12 - 15 km). The basalts from group 2, of Torres Formation, that represent the most primitive magma compositions (MgO > 6.5 wt.%) yield the higher crystallization temperatures (c.1180 – 1250ºC), and clinopyroxene and plagioclase appeared to have crystalized simultaneously at deep crustal levels (c. 7 kbar), most likely in the limit between the lower and upper crust (c. 20 km, as suggested by gravity models - Mariani et al., 2013) prior eruption. Group 1 of Torres Formation has equilibrium pressures that range from lower crust to shallower pressures in the upper crust (c. 2.5 – 6.7 kbar), and thermobarometry indicate an early crystallization for clinopyroxene. In the most evolved lavas of Torres Formation, Group 3, magmas underwent fractional crystallization mostly at shallower depths (< 5 kbar) with clinopyroxene crystallization at depths of c. 12km (4.6 kbar) slightly higher than plagioclase. For Vale do Sol and Palmas Formation lavas, crystallization occurred dominantly at low-pressure (< 4 – 5 kbar), with early plagioclase fractionation, although some disequilibrium clinopyroxene record deeper pressures. Esmeralda lavas have a broad crystal-liquid equilibrium pressures that range from 2 – 8 kbar, with most samples constrained between 4-6 kbar. These magmas were transported within a well-established plumbing system that permitted magma to ascend efficiently and with just minor interaction with crustal rocks.

Table 3 - Thermobarometry data for the analysed Paraná-Etendeka LIP rocks, (A) whole rock, Equation 14 (Putirka, 2008); (B) CPX-liquid, equation 33 (Putirka, 2008); (C) CPX-liquid barometer, Neave and Putirka (2017); (D) pyroxene only barometer, equation 32b (Putirka, 2008); (E) Plagioclase-liquid thermometer and barometer, equations 24a and 25a, respectively (Putirka, 2008).

	Whole rock	**CPX-Liquid**		**CPX only**	**Plagioclase-Liquid**	
	Putirka 2008	**Putirka 2008**	**N&P 2017**	**Putirka 2008**	**Putirka 2005**	
	T (°C)	**T(°C)**	**P (kbar)**	**P (kbar)**	**T(°C)**	**P (kbar)**
Torres Fm.						
G1	1100 - 1203	1075 - 1223	0.9 - 6.6	0.3 - 6.7	1129 - 1202	2.4 - 5.5
G2	1180 - 1249	1114 - 1205	6.2 - 7.8	5.6 - 6.9	1202	6.5
G3	1120 - 1262	1064 - 1126	3.7 - 4.6	0.2 - 6.0	1134 - 1139	0.8 - 1.7
Vale do Sol Fm						
G1	1145 - 1180	1133 -1155	0.5 - 3.1	0.1 - 6.9	1170 - 1180	2.8 - 4.5
G2	1048 - 1160	1022 - 1190	0.1 - 8.7	2.2 - 4.6	1127 - 1180	1.1 - 3.6
G3	1091 - 1162	1025 - 1125	0.2 - 6.4	0.2 - 4.4	1105 - 1128	0.9 - 4.2
Palmas Fm						
CS	983 - 1035	1003 - 1031	0.9	1.1 - 4.4	1007 - 1015	2.0 - 3.1
SM	955 - 993					
Jacuí	978 - 1036					
AG	991 - 1010					
Esmeralda Fm.						
	1088 - 1192	1033 - 1109	2.4 - 8.6	4.1 - 8.0	1085	3.5

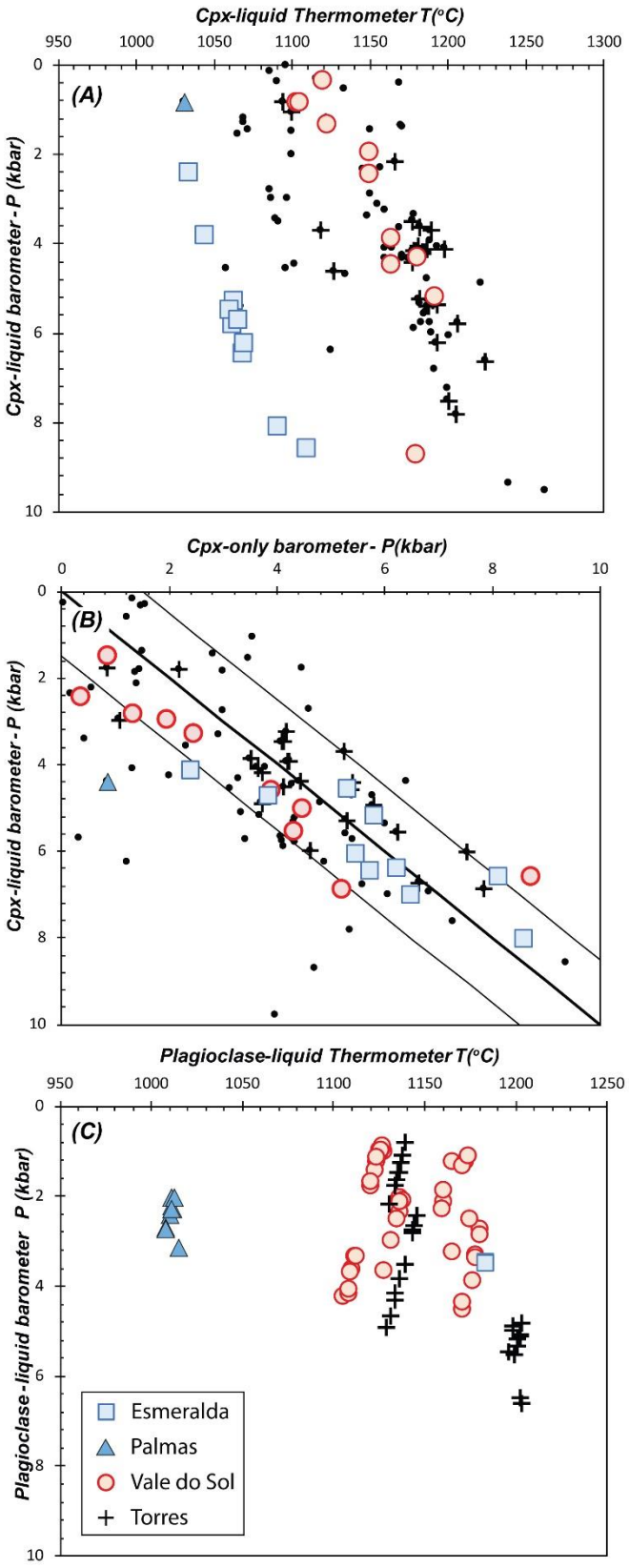

Figure 8 – Results of thermobarometry data for the southern Paraná-Etendeka lava formations in southern Brazil. (A) Cpx-liquid equilibrium P (kbar) versus T (ºC); (B) Cpx-liquid P (kbar) versus Cpx-only P (kbar). (C) Plagioclase-liquid equilibrium P (kbar) versus T (ºC).

6.2. *Shallow magmatic evolution: constrains from modelled LLD*

The paths formed in variation diagrams by continuous fractional crystallization from the most primitive high-temperature magmas towards evolved, low-temperature compositions represent an approximate trajectory of crystallization that is known as the liquid line of descent (LLD, Cox et al., 1979). Different LLD were modelled here using Petrolog 3.1 (Danyushevsky and Plechov, 2011). The pressure was kept constant during each simulation, and different models were built for 1 atm, 2, 4, 6, 8 and 10 kbar for a parental rock composition (BR-05A). The modelled LLD are presented together with major element data in Figure 4. The CaO/Al_2O_3 vs. Mg# plot is particularly useful to constrain the onset of the different mineral phases fractionating. The crystallization at pressures > 6 kbar is characterized by (1) L+Cpx; (2) L+Cpx+Plag; (3) L+Cpx+Plag+Ol; (4) L+Cpx+Plag+Mgt and the onset of clinopyroxene fractionation is marked by an decrease in CaO/Al_2O_3 ratios with decreasing Mg#. At pressures < 6 kbar, olivine and plagioclase form the high-temperature paragenesis and this variation is marked by an increase in the CaO/Al_2O_3 ratio with decreasing Mg#, the sequence of crystallization is (1) L+Ol+Plag; (2) L+Ol+Cpx+Plag; (3) L+Cpx+Plag+Mgt. The early pyroxene crystallization can modify substantially erupted magma compositions and account for the CaO-depletion in many flood basalt lavas (e.g. the British Palaeogene Igneous Province, Hole, 2018). Most of the geochemical data presented here fall within the modelled LLD (between 1 atm and 10 kbar) indicating that all magmas fractionate, at least partially within the continental crust (< 30 - 40 km).

Group 1 and 2 of Torres have distinct fractionation trajectories than those of TF-G3 and Vale do Sol Formation lavas, with a steep slope in CaO/Al_2O_3 vs. Mg# and overlap the 6, 8, and 10 kbar LLD. These variations are also identified in most major and trace elements compositions and reflect a Cpx-controlled fractionation in magma compositions. For G1-TF compositions with Mg# < 50 samples form a distinct trajectory that has a relatively flat FeO* distribution and is enriched in SiO_2 and these might represent the late onset of olivine fractionation. For Vale do Sol Fm. magmas olivine appears to be stable until MgO concentrations of c. 5 wt.% (Mg# c. 40 – G1-VDS) and these are marked by an increase in CaO/Al_2O_3 ratios with decreasing Mg#. More evolved basaltic magmas (MgO < 5 wt.%, Mg# <40) have characteristically steep slopes for CaO/Al_2O_3 marking the onset of augite fractionation, and in some of the

magmas the start of pigeonite crystallization (Groups 2 and 3 of Vale do Sol Fm. and group 3 of Torres Fm.). Esmeralda samples fall near low-pressure fractionation trends for most elements. The general relationship between major element compositions and the modelled LLD correlate well with the thermobarometry data presented above.

Figure 9 presents a schematic model for magma storage in the different magma groups and lava formations, based on the thermobarometry and LLD models described above. The plumbing system that fed the lavas in surface developed gradually from the onset of magmatism towards the main phase and crystallization was polybaric with magmas showing a progressive decrease in the mean pressures of fractionation and becoming gradually more evolved from the early lavas towards the upper stratigraphic units. The magma distribution within the plumbing system results in a chemically stratified plumbing system and this have been proposed to represent a key feature in flood basalt genesis (Thompson et al. 2007). The thermobarometry and crystallization characteristics presented here are in good agreement with the range of pressure (depths) and compositions (c. MgO and isotopes) recorded within the Spitzkoppe dyke swarm in the Etendeka (Thompson et al., 2007) and we suggest that these dyke swarms might represent the feeders of the southern Paraná-Etendeka lavas.

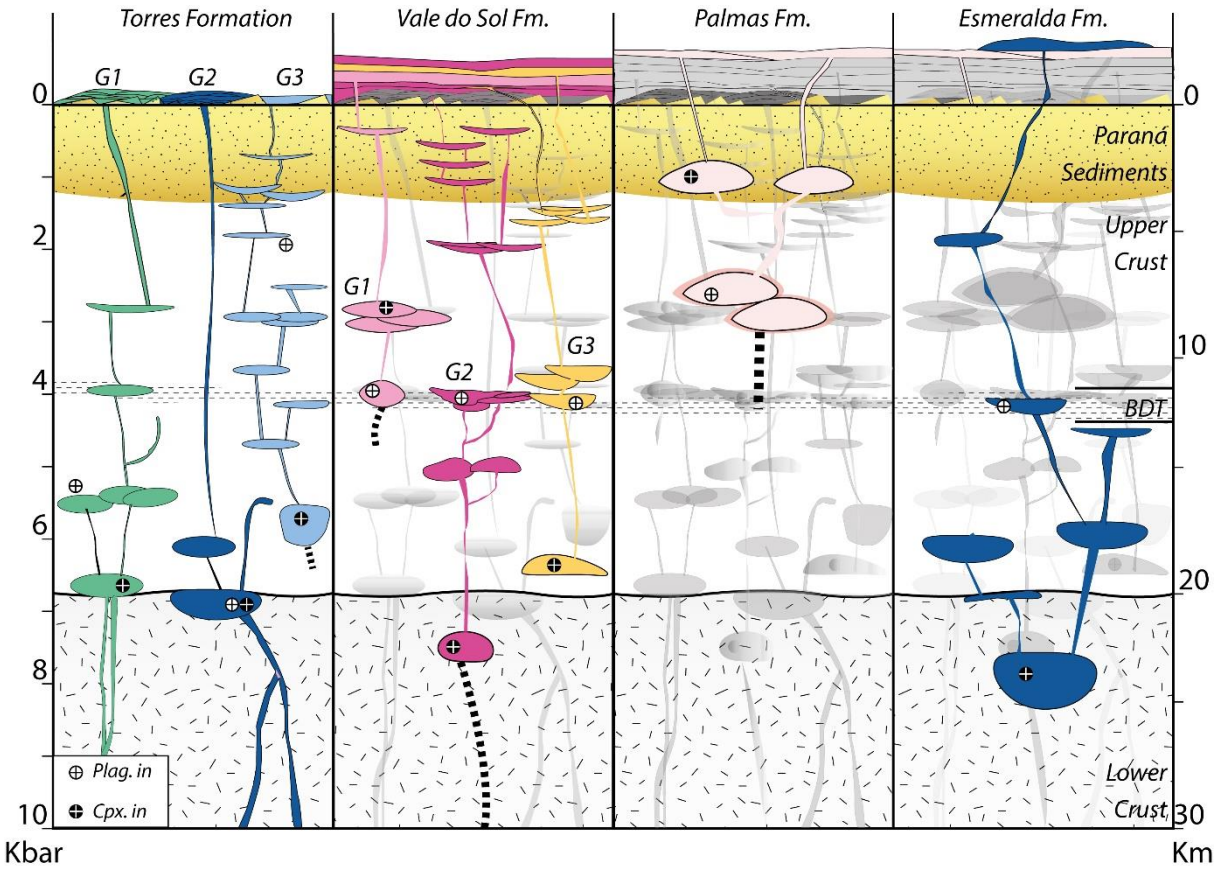

Figure 9 - Conceptual model for crystallization of the southern Parana magmas based on thermobarometry data. White circles represent the onset of plagioclase crystallization, and black circle represents the onset of clinopyroxene crystallization. BDT – Brittle-ductile transition zone.

6.3. Source Composition and Crustal assimilation: Constrains from Sr-Nd-Pb isotopes

The dataset presented here shows a vast range of compositions (MgO c. 0.34 to 8.9 wt.%; $^{87}Sr/^{86}Sr$ c.0.706 – 0.724) that have evolved through polybaric fractional crystallization in variable crustal depths, as discussed above. Even the most primitive magmas (MgO c. 8.9 wt.%) show clear evidence for fractionation along the L+Ol+Cpx cotectic line, and thus, any assumptions on magma source and genesis should consider carefully these evolved compositions. It is generally accepted that post genesis magma contamination and assimilation processes played a critical role in the final geochemical composition of the LTi rocks that make the southern Paraná-Etendeka (e.g. Peate, 1997; Gibson et al., 2000; Thompson et al., 2001; 2007; Ewart et al., 2004; Barreto et al., 2016, Marques et al. 2018, and many others). In the Spitzkoppe picrite-rhyolite dyke suite of the Etendeka, that represent intrusive equivalents of the main lava sequence, isotopic signatures recorded signals of magma

interaction with lower-, mid- and upper-crustal rocks during polybaric crystallization (Thompson et al., 2007).

The presence of primitive picrite and ferropicrite magma compositions in NW Namibia, and the close association of these with more evolved basaltic-rhyolitic magmas along dyke swarms provide more realistic constrains in the magma genesis and sources for the southern Paraná-Etendeka lavas. The primitive rocks occur as thin lava flows at the base of the volcanic succession (viz. the Tafelkop interdune member - Jerram et al., 1999, or ferropicrites - Gibson et al. 2000) and as dyke swarms (viz. Horingbaii, and Spitzkoppe - Thompson et al., 2001, 2007). These magmas are believed to represent asthenospheric melts formed at the Tristan-Gough plume-head (or proto-Tristan), and have escaped major lithospheric contamination and therefore represent a good proxies for the composition of asthenospheric melts during the Paraná-Etendeka magmatism (Gibson et al., 2000; Thompson et al., 2001).

The ferropicrite (Tafelkop) magmas have high-MgO (>10 wt.%) and high-FeO (between 12 and 16 wt.%) allied to isotopic compositions within the range of ocean island basalts (OIB) with unradiogenic $^{87}Sr/^{86}Sr$ (c. 0.704) and positive εNd_{134Ma} (c. +4), and are ascribed to melting of fertile garnet-pyroxenite streaks in the upwelling plume-head (Gibson et al., 2000). In these lavas, O-isotopes have a mantle-like signature with just minor indications of crustal contamination (Harris, 2015), that corroborate to their sublithospheric genesis. High-MgO (MgO c. 10 wt.%) compositions, that are similar to the Tafelkop ferropicrites have been recently identified in intrusions that cross-cut the lowermost lavas of Torres Formation in the southern part of the Paraná lava pile (Sarmento et al., 2017), and might represent the continuation of such dykes towards west in the Paraná area. Picritic magmas from the Horingbaii dyke swarm represent more depleted mantle compositions (MORB-like) and are characterized by $\varepsilon Nd_{134Ma} > 8$ and initial $^{87}Sr/^{86}Sr$ of c. 0.703, and were formed by melting of depleted peridotite under attenuated lithosphere in the plume-head (Thompson et al., 2001). Finally, the Spitzkoppe dyke suite is characterized by isotopically more evolved compositions that are within the range of the southern Paraná-Etendeka lavas (Fig. 10 and 11). These are assumed to have been formed by melting of depleted asthenosphere source with variable contributions of the SCLM (or a deep recycled enriched component) that underwent variable degrees of contamination within the continental crust (Thompson et al., 2007).

Figure 10 presents mixing lines propagated from sample PB17 that is a picrite dyke (MgO c.14.3 wt.%) from the Horingbaii-Nil Desperandum dyke swarm in the Etendeka, towards lithospheric components from the Dom Feliciano belt and from the Rio de La Plata Craton. The parameters used in the mixing models are presented in table 4. The compositional range of the Etendeka dykes and ferropicrite lavas cited above are plotted together with the Low-Ti Paraná magma types, Gramado and Esmeralda from Peate et al. (1992), and with the samples analysed here. Our samples fall within the range of the three mixing lines, indicating that at least, for what concerns the Nd and Sr isotopic compositions, most magma composition can be explained by mixing of a primitive composition, similar to the Etendeka picrites, with enriched lithospheric reservoirs (viz. Rio de La Plata Craton; Dom Feliciano belt). From the starting composition of the PB17 picrite (Thompson et al., 2001), it is required only 14% mixing with a lithospheric melt to reproduce the most primitive Torres Formation composition, and c. 4 - 10% to reach the compositions of Esmeralda Formation (Fig. 10). Thompson et al. (2007) obtained similar results for AFC models derived from a picrite from the Spitzkoppe dyke swarm and using contaminant compositions from the Damara Belt which represents the continuation of the Ribeira-Dom Feliciano belt in the African continent. The main argument here is that with minor assimilation of lithospheric melts (< 20%) the primitive picritic compositions are shifted towards isotopically enriched compositions similar to that of the main lava pile. Based on Os-isotopic signatures Rocha-Júnior et al. (2012) also suggested that the Paraná lavas were formed by an asthenospheric-dominated mantle source, however the authors attributed the enriched composition of these magmas to the addition of metasomatic fluids related to Neoproterozoic subduction events that were latter frozen and coupled to the base of the Paranapanema craton.

Table 4 - Parameters used to calculate mixing lines in figure 10. PB17 is a picrite form the Horingbaii-Nil Desperandum dyke swarm in the Etendeka (Thompson et al. 2001); A38 and A40 are Middle Proterozoic (1.6 Ga) rocks with basaltic composition from the Rio de La Plata Craton (Iacumin et al., 2001); GS-07E is a Neoproterozoic (630 – 620 Ma) granite from the Paulo Lopes suite (Florisbal et al., 2009).

	PB17	A38	A41	GS-07E
Sr	260	237.91	577.84	191
Rb/Sr	0.05	0.761	0.21	5.808
$^{87}Sr/^{86}Sr_{134Ma}$	0.7041	0.7205	0.7095	0.7556
Nd	13.2	48.003	25.056	54
Sm/Nd	0.1574	0.13124	0.11246	0.08677
$^{144}Nd/^{143}Nd_{134Ma}$	0.51266	0.51178	0.51128	0.51182
εNd_{134Ma}	4	-13	-23	-13
TDM	1.40E+08	5.85E+08	9.06E+08	4.79E+08

Figure 11 presents the range $^{206}Pb/^{204}Pb$, $^{207}Pb/^{204}Pb$ and $^{208}Pb/^{204}Pb$ compositions for the Etendeka picrite and ferropicrites and for the OIB from Tristan, Gough and Walvis ridge plotted alongside the sampled intervals of the southern Paraná-Etendeka lavas. In general, Pb-isotopic compositions of the Spitzkoppe rocks overlap those of the Paraná, and overlap the Gough-Walvis for $^{208}Pb/^{204}Pb$, and fall at high values for $^{207}Pb/^{204}Pb$, whilst samples from Tristan display typically lower $^{207}Pb/^{204}Pb$ (c.15.5 – 15.6) for equivalent $^{206}Pb/^{204}Pb$ compositions and the Horingbaii dykes extend towards lower $^{208}Pb/^{204}Pb$ (Fig.11). Many authors argument against the plume source for the Paraná-Etendeka magmatism based on the difference of isotopic composition from the lava pile and the present-day Tristan (e.g. Marques et al., 2018; Rocha-Júnior et al., 2012), however it was recently demonstrated that the Tristan-Gough plume system is zoned and have changed compositionally since the onset of magmatism (c. 135 Ma), to the present-day Tristan composition (e.g. Gibson et al., 2005; Hoernle et al., 2015). The single Esmeralda sample analysis presente here overlap the Gough-Walvis compositions and these magma type have been typically ascribed to melting of asthenosphere mantle with little interaction with lithospheric melts (Peate and Hawkesworth, 1996).

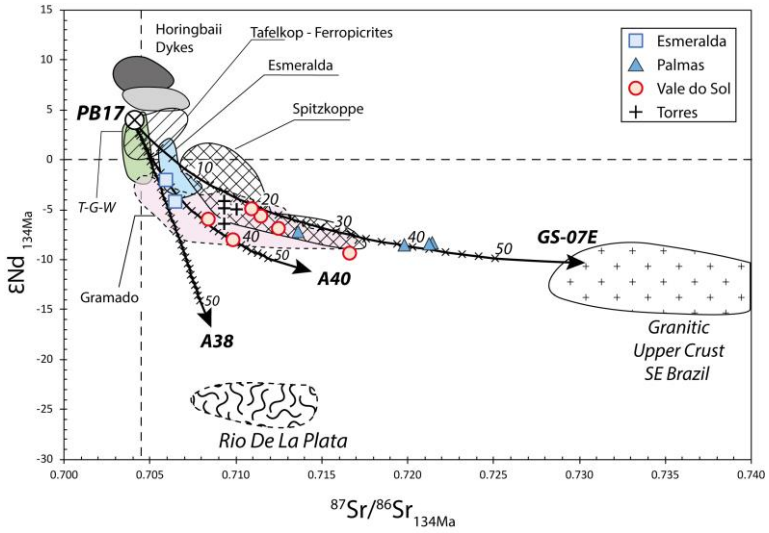

Figure 10 - Mixing lines from sample PB-17 (14.3 wt.% MgO) towards lower and upper crustal compositions in εNd_{134Ma} vs. $^{87}Sr/^{86}Sr_{134Ma}$ space; isotopic compositions of the southern Paraná-Etendeka lavas: Gramado and Esmeralda (Mantovani et al., 1985; Garland et al., 1996; Peate and Hawkesworth, 1996) plotted alongside the primitive compositions from Horingbaii dykes (Thompson et al., 2001); Etendeka ferropicrites (Gibson et al., 2000); Spitzkoppe picrite-intermediate dyke swarm (Thompson et al., 2007). Crosses indicate 2% mixing increments with samples: GS-07E, a Neoproterozoic (630 – 620 Ma) granite from the Paulo Lopes suite (Florisbal et al., 2009); and samples A-38 and A-40, that are represent Middle Proterozoic (1.6 Ga) rocks with basaltic composition from the Rio de La Plata Craton (Iacumin et al., 2001).

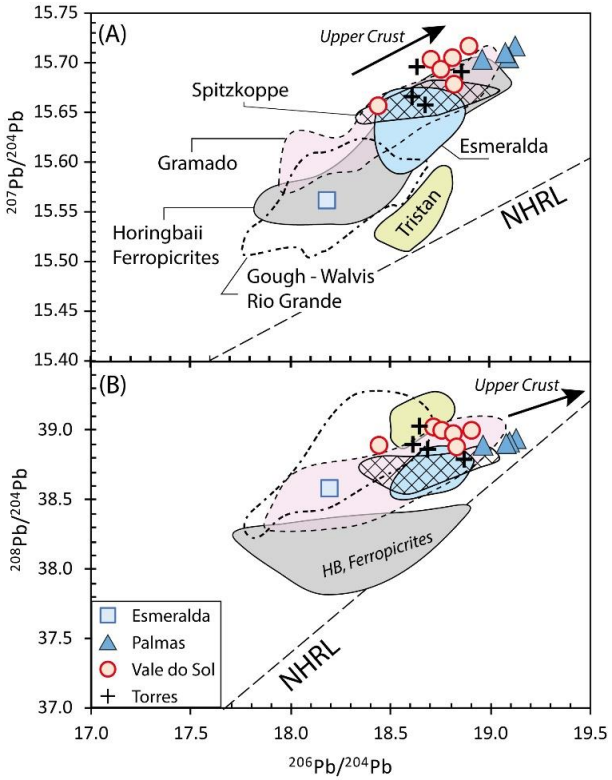

Figure 11 – (A) 207Pb/204Pb vs. 206Pb/204Pb; (B) 208Pb/204Pb vs. 206Pb/204Pb isotopic compositions of the southern Paraná-Etendeka lavas. Data is plotted alongside compositional fields for Gramado and Esmeralda (Mantovani et al., 1985; Garland et al., 1996; Peate and Hawkesworth, 1996), Horingbaii dykes (Thompson et al., 2001), Etendeka ferropicrites (Gibson et al., 2000), Spitzkoppe picrite-intermediate dyke swarm (Thompson et al., 2007) and Tristan, Walvis and Gough (Class and le Roex, 2008; Hoernle et al., 2015; Rohde et al., 2013; Salters et al., 2011).

6.4. Petrogenesis I: constrains on primary magma compositions from forward models

For the Southern Paraná-Etendeka lavas, even the most primitive magma composition (8.9 wt.% MgO) fall away from an olivine-controlled LLD and magmas present clear evidence for fractionation along LLD saturated in L+Ol+Cpx (group 2 and part of group 1 of Torres Formation) and L+Ol+Plag±Cpx, as discussed above. For this reason, the application of reverse crystallization models, that are based in L+Ol compositions, to reconstruct primary magmas are not suitable and typically produce inaccurate primary magma solutions (Herzberg and Asimow, 2015). As an alternative, primary magma and T-P conditions can be estimated by forward modelling experimentally obtained mantle melts compositions (e.g. Hirose and Kushiro, 1993; Kushiro, 1995; Walter, 1998). The composition of primary mantle melts typically vary with pressure, and for increasing pressure of melt, primary magmas became gradually deficient in SiO_2, Al_2O_3 and CaO, whilst concentrations of MgO, FeO, MnO increase (O'Hara, 1965; Mckenzie and Bickle, 1988; Hirose and Kushiro, 1993; Kushiro, 1996; Walter, 1998). In the experimental dataset of Walter (1998), low-degree partial melts are enriched in incompatible elements such as TiO_2 and alkalis, and the concentration of these elements gradually decrease with increasing partial melts. A set of experimental compositions produced by partial melting of a dry peridotite sample, KR-4003 (Walter, 1998), under a range of pressures from 3 to 7 GPa was used here and from selected compositions, LLD's were constructed using Petrolog 3.1 (Danyushevsky and Plechov, 2011). One important limitation of this methodology is that it does not reproduce AFC processes and thus does not take into account compositional gain associated with wall-rock assimilation. The results of forward modelling are presented in Figures 12 to 14.

For the dataset presented here, the best fit for LLD is obtained by forward modelling KR-4003 compositions produced by 24 % partial melting at 3 GPa (sample 30.14 from Walter, 1998). Most samples, fall within the LLD's of 2 and 6 Kbar, whilst the primitive samples from Torres Formation fall over high-pressure LLD (between 6 and 10 kbar), and this fact agrees with thermobarometry data. At higher pressures (40 kbar), melts of KR-4003 result in higher TiO_2, FeO*, CaO, and lower SiO_2 and Al_2O_3 when compared to the 30 kbar melts (Fig. 12). The Etendeka ferropicrite lavas, Horingbaii- Nils Desperandum dyke swarm, and the Spitzkoppe dyke swarm are

plotted alongside the southern Brazil Paraná-Etendeka lavas in the CaO (wt.%) vs. MgO (wt.%) diagram of figure 12. The relatively evolved Etendeka compositions (MgO < 10 wt.%) show strong correlation with the Paraná analyses presented here and overlap Torres Formation compositions. The primitive compositions (MgO > 10 wt.%) fall near and below the 40 kbar LLD, with the pyroxenite samples occupying areas below the division of peridotite-pyroxenite derived melts (from Herzberg and Asimow, 2008).

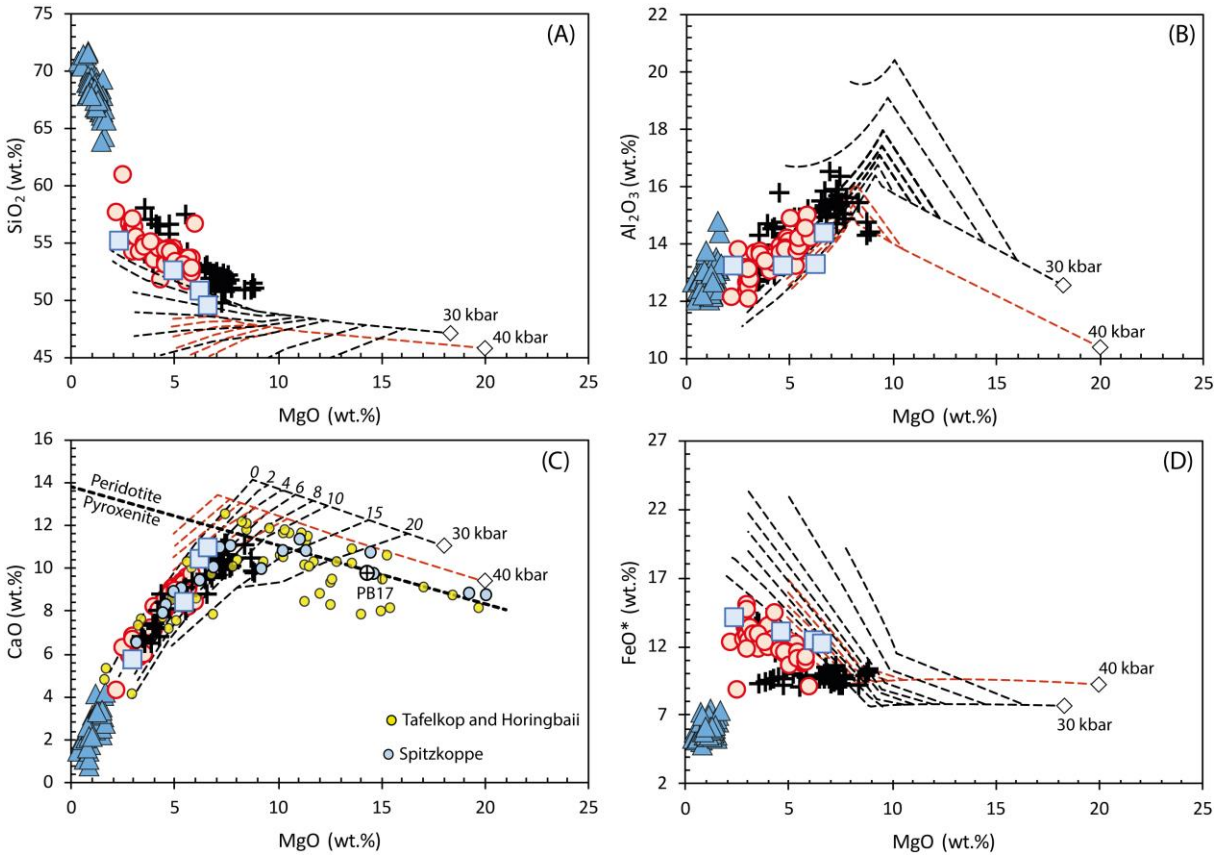

Figure 12 - Modelled LLD from KR-4003 peridotite, melt compositions at 30kbar and 40 kbar from Walter (1998). (A) SiO_2 (wt.%)vs. MgO (wt.%) (B) Al_2O_3 (wt.%) vs. MgO (wt.%) (C) CaO (wt.%) vs. MgO (wt.%) FeO* (wt.%) vs. MgO (wt.%). Peridotite-pyroxenite divide derived from CaO = 13.81 – 0.274MgO (Herzberg and Asimow, 2008). Etendeka picrite, ferropicrite and associated evolved compositions are from Gibson et al. (2000), Thompson et al. (2001, 2007). Symbols as in Figure 4.

In normative CIPW and plagioclase-projected CMAS diagrams, samples fall between the 2 and 8 kbar LLD, with Torres Formation lavas occupying the high-pressure areas whilst all other samples plot in pressures that are < 6 kbar (Fig. 13). Esmeralda compositions fall over the 2 kbar LLD. In both diagrams, the general trend of samples is not coincident with a single LLD, in the Ol-Di-Hy-Qz-Ne diagram samples are projected from c. 6 kbar perpendicularly towards lower pressure LLD, and this fact might be reflecting the polybaric nature of the magmatic system. For the CMAS

diagram samples have a similar distribution and the general trend in the most evolved lavas is parallel to the pigeonite trajectory of the 1 atm cotectic from Grove et al. (1982), and the inflection towards the quartz apex might be representing the onset of pigeonite fractionation, that for group 3 Torres Formation and groups 2 and 3 of Vale do Sol lavas occur at MgO < 5 wt.%. The range of compositions of the Spitzkoppe and Horingbaii dyke swarms are plotted as fields in Figure 13B. The primitive compositions fall slightly below the field of partial melts of the KR-4003 between 30 and 40 kbar, and according to Thompson et al. (2007) these high-MgO compositions reflect olivine accumulation, and this will shift samples towards the Ol-apex in the CIPW normative diagram. The range of compositions for the most evolved Spitzkoppe dykes coincides with the majority of Torres and Vale do Sol lavas. Horingbaii dykes form a separated trend that evolve along olivine control lines towards low pressure.

From the forward models presented above, the genesis of Torres Formation primitive magmas can be attributed to partial melting of anhydrous peridotite at pressures near 30 kbar. The compositions show a misfit for a few elements, in especial SiO_2, and from graphical analysis, it appears that this Si-enrichment is c. 2 wt.% and can be attributed to the assimilation of crustal materials by basic magmas during ascent. The Esmeralda magma composition fit fractionation trends from low-pressure LLD (c. 2 kbar), projected from KR-4003 melts at 30 kbar, and in general, do not require the addition of crustal materials.

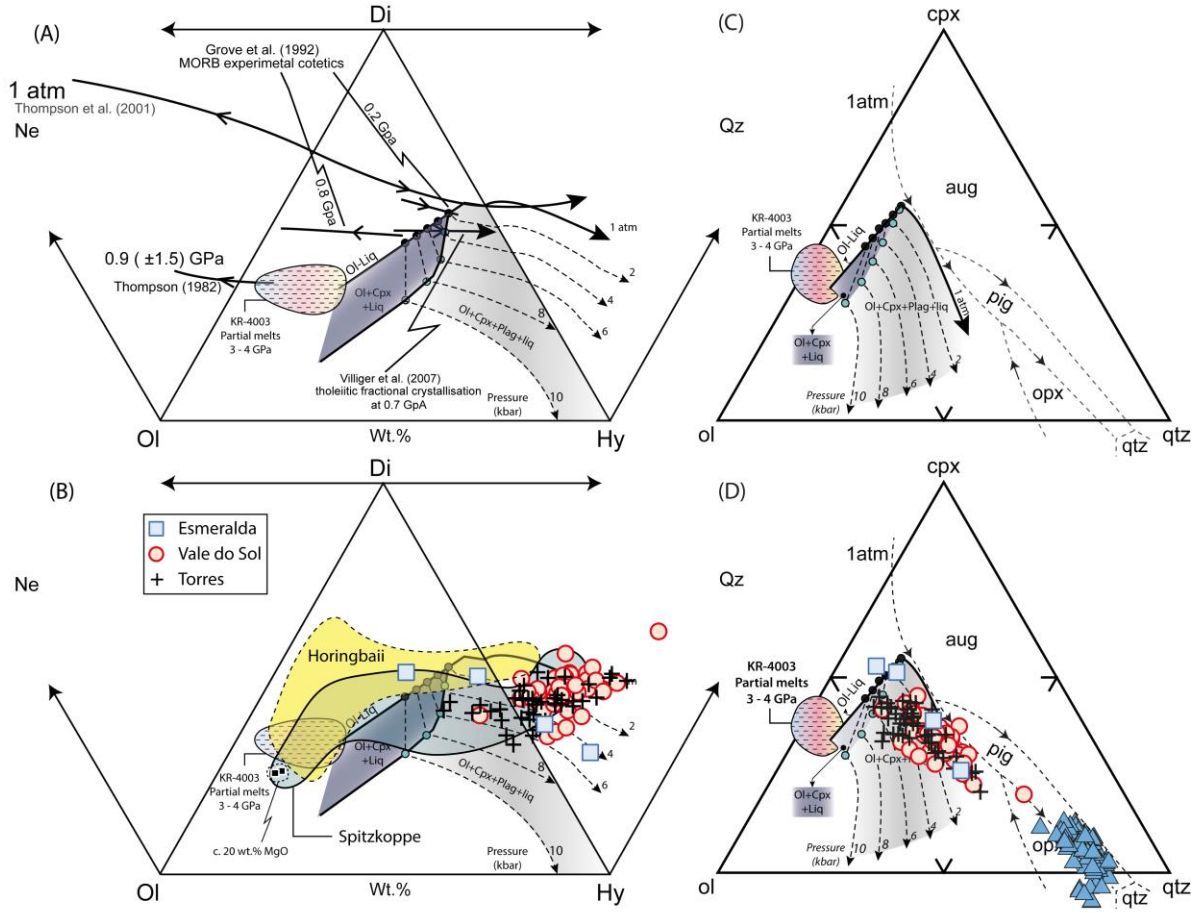

Figure 13 - Modelled LLD for KR-4003 dry peridotite melt produced at 30 GPa (sample 30.11 from Walter, 1998) projected in the ternary Ol-Di-Hy-Qz-Ne diagram (A); (B) Compositional range of basalt and basaltic andesite rocks from Torres, Esmeralda and Vale do Sol Formations. Field for Spitzkoppe, and black squares that represent c. 20wt.% MgO samples are from Thompson et al. (2007), and field for the Horingbaii dykes from Thompson et al. (2001). Experimental cotectic lines at pressures of 1 atm, 0.2, 0.7, 0.8 and 0.9 GPa are from Thompson (1982), Grove et al. (1992) Villiger et al. (2007); (C) Plagioclase-projected CMAS diagram (Grove 1993); (D) Compositional range of the southern Paraná-Etendeka lavas. Mineral components were calculated from molecular compositions using the expressions from Grove (1993), and 1 atm cotectic line from (Grove et al., 1982). Black dots represent onset of clinopyroxene fractioantion, and blue dots represent onset of plagioclase fractionation. Fields of Ol+Cpx+Liq and Ol+Cpx+Plag+Liq drawn based on the LLD inflections. Field of KR-Partial melts between 30 and 40 kbar, represent melt compositions for values of F c. 9 - 25% (Walter, 1998).

6.5 Petrogenesis II: Primary magma compositions from reverse modeling

The reverse models presented here represent a good test for the forward modelled compositions presented above, and an opportunity to test the applicability of more complex (multiple-phase saturated) reverse models in evolved continental flood basalts. For the construction of reverse models, only samples with Mg > 6.5 wt.%, and Mg# > 55, from Torres Formation groups 1 and 2 were selected. These samples represent the parental magma compositions within the sampled lava sections.

Esmeralda Formation samples are too fractionated (c. MgO < 7wt.%; Mg# < 55) and no sample provided a suitable starting composition for reverse modelling. The models were constructed here using Petrolog 3.1 to extrapolate composition from evolved magmas towards L+Ol control-lines, and from L+Ol towards primary magma compositions we obtained using PRIMELT 3 (Herzberg and Asimow, 2015) and TPCalc (Putirka, 2016). The interval of crystallization of each mineral phase were set based on the thermobarometry data and modelled LLD presented above. A total of 5 samples from group 1 and 12 from group 2 of Torres Formation provided primary magma solutions for reverse modelling, and additionally the melt compositions of Walter (1998) for KR-4003 at 30 and 40 kbar, and two picrite dyke samples from Thompson et al. (2001) were also modelled for comparison.

From primary magma compositions it is possible to calculate mantle potential temperature (T_P), initial pressure of melting ($P_{solidus}$) and melt fraction from batch melting (F) and aggregated fractional melt ($F\text{-}AFM$), and these were also calculated using PRIMELT and TPCalc (Herzberg and Asimow, 2015; Putirka, 2016). Final melting pressures (P_f) represent the limit to which mantle can melt adiabatically and this coincides with the asthenosphere lithosphere boundary – LAB (Gazel et al., 2011). Estimating the final pressure of melt is important to constrain the thickness of the melting column and estimate lithospheric thickness (Hole and Millett, 2016). Several methods have been used to estimate P_f and these rely mostly in the relation of melt fraction and initial pressure of melting, or primary magma compositions (e.g. Putirka, 2008; Herzberg and Gazel, 2009; Herzberg and Asimow, 2015; Hole and Millett, 2016). Table 5 summarizes the results obtained from primary magma modelling and compares final melting pressures obtained from Putirka (2008) and Herzberg and Gazel (2009). As an alternative, final pressure was calculated based on the average melt fraction (F) and using magma production rates of 1.5 % $kbar^{-1}$ (Langmuir et al., 1992).

Table 5 - Summary of results obtained from primary magma models. Psolidus and TP were calculated from Herzberg and Asimow (2015); P_{f1} from Putirka (2008); P_{f2} from (Herzberg and Gazel, 2009); P_{f3} was calculated assuming melt production rates of 1.5 % $Kbar^{-1}$.

	MgO (wt.%)	$P_{solidus}$ (kbar)	T_P (°C)	F	P_{f1}	P_{f2} (kbar)	P_{f3}
Group 1	15.9 -16.5	29 -32	1458 -1474	0.17 -0.19	17 -19	13 -18	18 -20
Group 2	16.1 -18.6	30 -41	1465 -1525	0.18 -0.22	18 -22	16 -31	18 -26
KR-4003 30 - 40 kbar	18.2 -19.9	30 -40	1518 -1566	0.19 -0.23	24 -31	-	23 -35
HB – Picrites	20.2 -21.5	50 -58	1570 -1600	0.06 -0.13	33 -35	-	46 -50

The average composition obtained for primary magmas using TpCalc and PRIMELT3 are listed in Table 6. Primary magmas produced by PRIMELT3 models yield typically higher values for SiO_2 (c. 0.5%), Al_2O_3 (c. 0.7%) and CaO (c. 0.5%) and lower MgO (c. 2%) when compared to T_PCalc solutions. T_P derived from P RIMELT3 solutions (Herzberg and Asimow, 2015) are typically c. 50 ºC and $P_{solidus}$ 5 kbar lower than those of primary magmas produced by T_PCalc (Putirka, 2016), these variations are virtually within the method error that is ± 46 ºC for T_P and 3 kbar for $P_{solidus}$, respectively. In general, the produced primary magmas compositions are enriched in SiO_2 (c. 49 – 50 wt.%) and depleted in MgO (c. 14 – 17 wt.%) in comparison to primary melts produced by dry peridotite experiments of Walter (c. 45 – 48 wt.%). Again, this enrichment might be a consequence of compositional gains associated to AFC processes that are not considered in the reverse crystallization models. In general, compositions obtained by T_PCalc are near those of KR-4003 partial melts and thus the following discussions are based on the higher-MgO primary magma compositions obtained using T_PCalc (Putirka, 2018).

Table 6 - Calculated primary magma compositions for Torres Formation group 1 and 2, composition KR-4003 produced by 24% melt at 30 kbar (Walter, 1998), and composition of Horingbaii picrite dykes from the Etendeka Province (Thompson et al., 2001).

	Group 1		**Group 2**		**KR-4003**	**Etendeka Picrites**	
	TPCalc	Primelt	TPCalc	Primelt	30.14	97SB34	97SB37
SiO_2	49.58	50.04	49.11	49.47	46.91	46.15	46.65
TiO_2	0.63	0.66	0.66	0.70	0.64	1.02	1.09
Al_2O_3	12.37	13.08	11.74	12.33	12.46	10.97	13.19
FeO_t	9.01	9.04	9.42	9.49	8.86	12.11	11.52
MnO	0.13	0.15	0.13	0.15	0.17	0.16	0.16
MgO	16.23	14.30	17.01	15.36	18.22	18.45	15.29
CaO	9.68	10.21	9.74	10.20	10.86	8.75	10.63
Na_2O	1.53	1.62	1.38	1.45	0.82	1.42	1.7
K_2O	0.61	0.65	0.55	0.57	0.34	0.27	0.23
Cr_2O_3	0.14	0.16	0.17	0.18	0.43	0.19	0.15

Group 1 primary magmas have MgO c. 15.8 – 16.5 wt.% which required T_P of c. 1467 ºC with the adiabat intercepting the dry peridotite solidus at pressures of c. 31 kbar. For group 2 calculated primary magmas have a broad MgO variations overlapping those of group 1 and extending towards higher concentrations of MgO, from 16.1 to 18.3 wt.%. These compositions require slightly higher mean T- P intervals with T_P c. 1481 ± 20ºC with melt starting between 30 and 40 kbar. For Torres Formation primary magmas, calculated final pressure of melting obtained from the different methods varies from 13 to 20 kbar with a mean of 17±1.5 kbar for group 1, and 16 to 31 kbar, with a mean of 21±3.5 kbar for group 2. Given the relatively enriched SiO_2 (wt.%) content of Torres Formation primary magmas, it is most likely that the equation provided by Putirka (2008), that is based on the Si-activity, underestimate the final pressures for the primary magmas calculated here. In general, despite being a simplification, the compositional independent method provides more constant results with mean 18± 0.6 kbar for group 1 samples and 21±2.5 kbar for group 2. This pressure range imply a lithospheric thickness of c. 60 – 85 km at time of magmatism and this estimations fall within the suggestion of Gibson et al. (2006), according to the authors lithosphere would have been thinned to < 70 km prior tholeiitic magmatism. Average melt fractions (F_{avg}) for both geochemical groups varies from 17 and 22% and these values are within estimations suggested by Thompson et al. (2001) for the Horingbaii - Nil Desperandum basalt-picrite dyke swarm in the Etendeka. (F c. 12 - 22%).

For the two Horingbaii samples presented in table 5 (97SB34 and 97SB37), primary melt compositions calculated here have MgO of 21.5 and 20.3 wt.%,

respectively, and derived T_P of 1560 and 1600 ºC with melting starting at 58 and 50 kbar of pressure, and average melt fractions of 20-22%. This modelled T_P are within the T_P interval (c. 1560 to 1680ºC) suggested by Thompson et. al. (2001), that was calculated based on forsterite content of olivine macrocrysts found in some of the Horingbaii dykes (Fo_{93}). For the general Horingbaii dyke compositions, that show a broad range of MgO compositions, the authors suggested that T_P was within the range of 1470 and 1560 ºC, and these temperatures would require melt to commence at pressures between 30 and 40 kbar. Hole (2015) obtained similar T_P values, of c. 1490 – 1563ºC, for corresponding primary magma compositions of the Etendeka picrites, with melts starting between 32 and 39 kbar.

Calculated primary magma compositions are plotted together with the southern Paraná-Etendeka lava compositions and forward models of LLD from KR-4003 at 30 kbar in Figure 14. The primary magma compositions fall in the limit of KR-4003 melts produced by experiments at 30 and 40 kbar (Walter, 1998). In general, calculated compositions show a good correlation with modelled LLD. Torres Formation samples are clustered parallel to the L+Ol+Cpx control-line and overlap part of the Etendeka primitive compositions, and form a continuum trend from calculated primary magma compositions. If this continuum represents a natural compositional trend and the lower Torres Formation is genetically correlated with the Etendeka dyke swarms, Cpx is in the liquidus for MgO compositions of c. 10.5 wt.% (Mg# c. 65) and this would require that magmas have fractionated at pressures of at least 10 kbar, that coincide approximately with the Moho discontinuity in the area, prior ascending to upper crustal levels. Vale do Sol Fm. compositions form a separated cluster of distribution with samples falling within L+Ol+Plag+Cpx control lines at relatively shallower pressures. The most primitive Vale do Sol samples have a marked increase in CaO/Al_2O_3 ratios from Mg# c. 45 – 50 and this might represent the transition along a L+Ol+Plag control line from deep (10 kbar) to shallower crustal levels (6 kbar) during polybaric crystallization and in fact Vale do Sol lavas with Mg# > 45 (group 1) are petrographically characterized by altered olivine microphenocryst, whilst in the more evolved lavas no olivine is preserved (see chapter 4, section 4.5.1). Esmeralda composition occupy shallow pressure LLD and fall along L+Ol+Plag+Cpx control lines, the samples are aligned to a cluster of samples from the Horingbaii and Tafelkop ferropicrites.

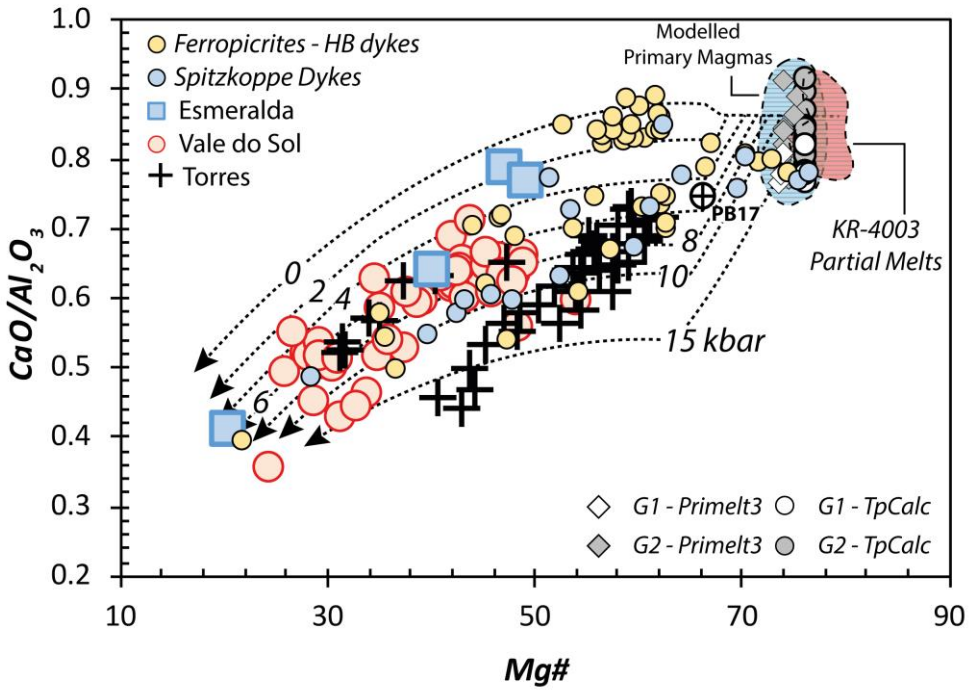

Figure 14 - CaO/Al2O3 vs. Mg# diagram for the calculated primary magma composition from reverse crystallization models plotted together with KR-4003 partial melt compositions for 30 to 40 kbar experiments. Southern Paraná-Etendeka lavas from Torres, Esmeralda and Vale do Sol Formation, and Basalt-Picrite Horingbaii, Tafelkop (ferropicrite lavas) and Spitzkoppe dykes are plotted together for comparison (data from Gibson et al., 2000; Thompson et al., 2001, 2007). LLD are from forward crystallization of KR-4003 sample 30.14 from Walter (1998).

6.6. Constrains on pressure and degree of melting from the rare-earth elements

From the geochemical behaviour of rare-earth elements during partial melting it is possible to estimate depth, pressure of melting and melt fraction and these models have been widely used in the study of LIP's and other volcanic areas (e.g. Hole et al., 2015; Hunt et al., 2012; McKenzie and O'Nions, 1991; White and McKenzie, 1995). $[La/Yb]_N$ have high values for low-degree partial melts that gradually decrease with increasing melt fraction (Hunt et al., 2012; Hole et al., 2015; Millett et al., 2017). The $[Dy/Yb]_N$ ratio is sensitive to the volume of garnet in the source and provide can be used as a proxy for depth and pressure of melting. Figure 5.17 presents incremental batch melt modelled curves of a primitive mantle composition (Sun and McDonough, 1989) with decompression trajectories, illustrated by mixing lines from the garnet to the spinel stability field, plotted in the $[Dy/Yb]_N$ versus $[La/Yb]_N$ space and these are plotted along with the basaltic compositions of Torres, Vale do Sol and Esmeralda formations (MgO > 5%). Torres and Vale do Sol compositions fall between the garnet and spinel

modelled melting trajectories, constrained between the mixing lines with 5 – 8% garnet, whilst Esmeralda Formation samples fall near the spinel lherzolite melting trajectory, indicative of shallower melting.

Torres Formation lavas are strongly enriched in LREE and incompatible elements and in general $[La/Yb]_N > 4.5$ and display a gradual decreasing slope from middle to heavy REE, with $[Sm/Lu]_N$ in the range of c. 1.7 – 2.7, $[Dy/Yb]_N$ c. 1.7 – 2.2. These variations require melts to have been produced from both garnet and spinel stability field (or within the garnet-spinel transition). The fractionation corrected compositions of Torres Formation lavas can be modelled by incremental batch melting with *F* of c. 20%, with 8% of the melting being formed in the garnet stability field and 12% in the spinel stability field (Fig. 15). To reproduce the light-REE slope, a source different from the primitive mantle is required, and this was assumed to have a depleted composition (avg. DMM of Workman and Hart, 2005) with addition of 2 % melts from the SCLM (modelled from mafic potassic intrusions from Gibson et al., 1995). These source assumptions correlate well with the range of isotopic compositions of Torres Formation. Differently, Esmeralda Formation lavas have a flat REE distribution, with just minor enrichment in the LREE, with $[La/Yb]_N$ c. 2.85 and horizontal distribution for medium and heavy REE, $[Sm/Lu]_N < 2$ with variations of c. 1.35 – 1.82, and $[Dy/Yb]_N$ <1.5, and require melting to have occur in the spinel stability field of the upper mantle (< 80 km). The fractionation corrected composition of Esmeralda magmas can be reproduced by incremental batch melting of c. 10 - 15% of spinel peridotite with REE composition of the primitive mantle (Sun and McDonough, 1989).

Despite being dependent on input parameters (e.g. K_D and source composition), REE models provide useful information on melting conditions, and for the Paraná-Etendeka lavas they show a good correlation with data derived from both forward and reverse major element models indicating that for Torres Formation melts were formed during decompressional melt near the garnet-spinel transition of the upper mantle. For Esmeralda Formation REE models indicate that melts were formed at lower pressures mostly in the spinel stability field of the upper mantle (< 80 km) and from the range of geochemical compositions including isotopic data it has been suggest dominance of an asthenospheric source for the Esmeralda magmas (e.g. Peate and Hawkesworth, 1996). This would imply lower mantle potential temperatures (c. 1400ºC) and significantly lithospheric thinning for the genesis of Esmeralda magmas when compared to Torres parental melts.

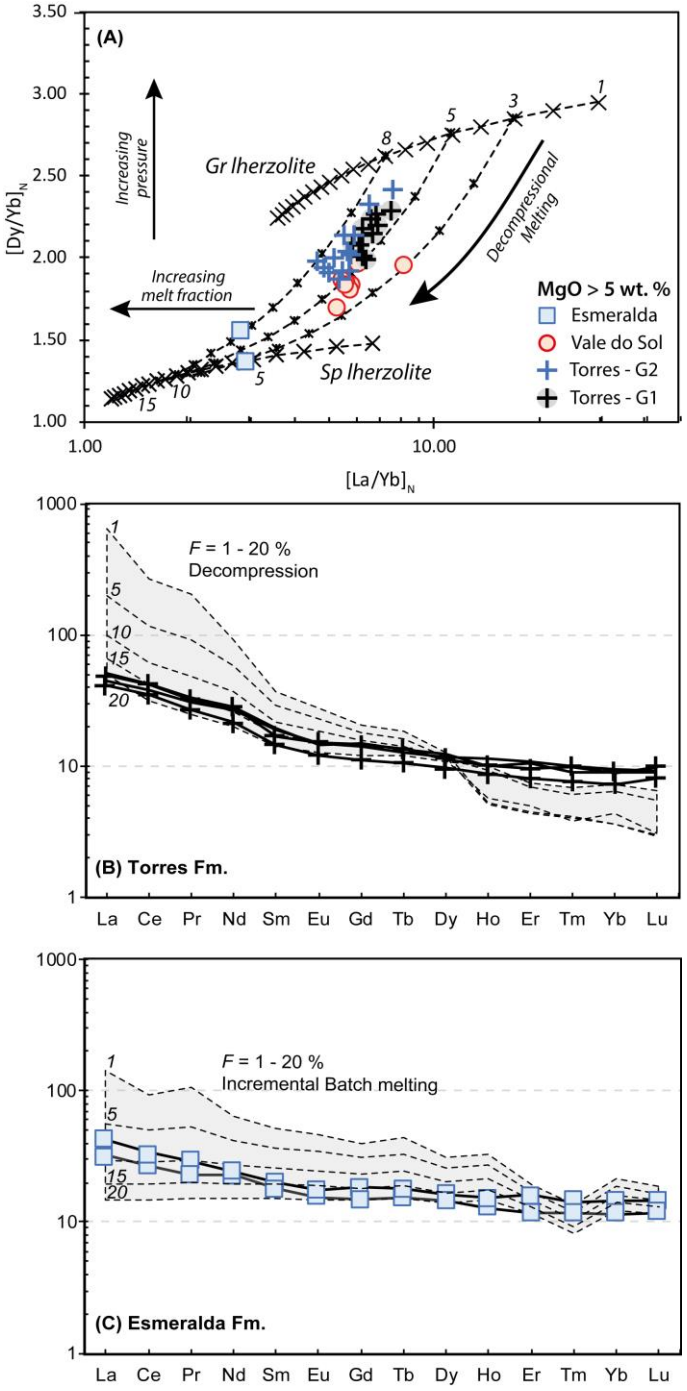

Figure 15 - Composition of the basaltic rocks from Torres (G1 and 2), Esmeralda and Group 1 of Vale do Sol Formation plotted in a chondrite normalized $[Dy/Yb]_N$ versus $[La/Yb]_N$ diagram. Modelled incremental batch melting curves for garnet lherzolite and spinel lherzolite with REE compositions of the primitive mantle of Sun and McDonough (1989), using partition coefficients from Rollinson (1993), and McKenzie and O'Nions (1991). X represent 1 % increments and mixing curves represent decompressional melting from the garnet into the spinel stability field of the upper mantle.

6.7. Geodynamic implications and Petrogenesis

The magmatic products of the Paraná-Etendeka province were emplaced over a subsidising sedimentary basin (Peate, 1997; Foulger, 2018), indicating that tectonic extension was ongoing prior the main magmatic event. It is assumed that along the western Gondwana, extension have started at the late Jurassic to the Early Cretaceous through the Brazilian-Pan African structures with break-up being latter propagated northward (Buiter and Torsvik, 2014; Will and Frimmel, 2018) and that the Paraná-Etendeka magmatism is closely linked to the rift of the western Gondwana (Courtillot et al., 1999; Foulger, 2018; White and McKenzie, 1989). Palaeo-reconstruction maps of the western Gondwana at the time of the magmatic activity places the Paraná-Etendeka over the margin of the Tuzo Large Low Shear-wave Velocity Province (LLSVP) that is suggested by Burke and Torsvik (2004) to be the area from which most mantle plumes, including the Tristan mantle plume, have propagated. Buiter and Torsvik (2014) proposed that for areas where rifting have been initiated by tectonic forces, plume material can be directed and migrate towards thinned lithospheric spots. Alternatively, it has been suggested that the Paraná-Etendeka magmatism was formed as a response to complex tectonic extension along tectonic blocks with no thermic of chemical contributions from a mantle plume, and the geochemical heterogeneity within the province is assumed to be related to mixing between asthenospheric and lithospheric melts (Foulger, 2018).

Based on forward modelling from dry peridotite melts, reverse modelling, and REE modelling it is suggested here that the primary magma that give rise to the parental Torres Formation magmas had MgO of c. 16 – 18 wt.% and were formed by adiabatic melting of asthenospheric mantle peridotite at pressures between 30 – 45 kbar, corresponding to depths of c. 110 to 150 km, with mantle potential temperature > 1450ºC (c. 1450 – 1500 °C). Therefore, for the genesis of the parental Torres Formation melts it is required excess temperatures of c. +150ºC in comparison to ambient mantle *TP* (1350ºC) and these could be achieved by internal heating under insulating lithosphere, as suggested for the Central Atlantic and Ferrar magmatic provinces (Hole, 2015). However, for the genesis of picrites and ferropicrite rocks from the Etendeka, that are temporally linked to the Torres magmas, it is required *TP* > 1550ºC and these have been associated to the early impact of the Tristan mantle plume (Gibson et al., 2000; Thompson et al., 2001). It is assumed here that the Paraná-

Etendeka magmatism occur as a response to melting of an heated mantle, most likely associated to the arrival of the Tristan plume as suggested by many authors (White and McKenzie, 1995; Gibson et al., 2000, 2006; Thompson et al., 2001; Torsvik et al., 2006; Buiter and Torsvik, 2014; Svensen et al., 2017; Natali et al. 2018). The differences in potential temperature and compositions from the lower portions of the Paraná-Etendeka stratigraphy appears to be reflecting the proximity to the plume location, with the Etendeka ferropicrites and picrites being formed over the plume head whilst Torres Formation magmas formed in the plume periphery, and these is compatible with the hotspot locations suggested by White and McKenzie (1989). A similar scenario occurred in the Paleoce-Eocene North Atlantic Igneous Provinces. The West Greenland picrite magmas are suggested to have formed at high T_P (>1550 ºC) and these high temperatures occur near the postulated plume locality (Herzberg and O'Hara, 2002; Hole and Millett, 2016; Larsen and Pedersen, 2009) with variations in T_P being controlled by proximity with the postulated thermal anomaly (e.g. Hole and Millett, 2016).

Esmeralda Formation lavas mark the waning phase of magmatism formed by partial melting of asthenosphere at the spinel stability field in the upper mantle with no significant contribution from enriched lithospheric melts (e.g. Peate and Hawkesworth 1999), and this require mantle potential temperatures relatively lower (c. 1400ºC, estimated from REE) in comparison to the onset of magmatism. The overall evolution of the southern portion of the Paraná-Etendeka magmatism requires significant lithospheric extension prior and during the main flood basalt magmatism.

7. Summary and Conclusions

As suggested by Jerram and Widdowson (2005) and Bryan and Ernst (2008) LIP's are characterized by a magmatic onset, a main phase, and a waning phase that represent the different evolutive stages of magmatism. For the Paraná-Etendeka these different phases of volcanic evolution preserved at the surface as large piles of lava are directly correlated with evolutive stages of the magmatic plumbing system, with the volume and composition of magmas reaching the surface being controlled by the dynamic and depth of magma crystallization. Thompson et al. (2007) studying the Spitzkoppe dyke swarm, that was believed to have fed at least part of these lavas suggested that a compositionally stratified plumbing system was developed during LIP

magmatism and one of the highlights of the research presented here is that from the study of the thermobarometry and geochemistry of the main lava pile we obtained very similar results of those of Thompson et al for the dykes. Consequently, we suggested here that the range on compositions and geochemical evolution of continental flood basalt lavas is directly controlled by their shallow magmatic evolution in complex plumbing systems and in the case of the Paraná, this magmatic evolution was marked by the contribution of variable amounts of enriched materials from both lithospheric mantle and crust.

Acknowledgements

The authors gratefully acknowledge support from Shell Brasil and CNPq through the Sedimentary Systems project hosted at the Federal University of Rio Grande do Sul and the strategic importance of the support given by ANP through the R&D levy regulation. Evandro Lima is thankful for CNPq research grants (402400/20 442812/2015-9). Dougal Jerram is partly funded through a Norwegian Research Council Centers of Excellence project (project number 223272, CEED). Collin Taylor is thanked for helpful assistance during sample preparation and analysis. F. Luz, and M. Simões are thanked for valuable assistance during fieldwork and sample collection.

References

Baksi, A.K., 2018. Paraná flood basalt volcanism primarily limited to ~ 1 Myr beginning at 135 Ma: New40Ar/39Ar ages for rocks from Rio Grande do Sul, and critical evaluation of published radiometric data. J. Volcanol. Geotherm. Res. 355, 66–77. doi:10.1016/j.jvolgeores.2017.02.016

Barreto, C.J.S., Lafon, J.M., De Lima, E.F., Sommer, C.A., 2016. Geochemical and Sr-Nd-Pb isotopic insight into the low-Ti basalts from southern Paraná Igneous Province, Brazil: The role of crustal contamination. Int. Geol. Rev. 58, 1324–1349. doi:10.1080/00206814.2016.1147988

Bellieni, G., Brotzu, P., Comin-Chiaramonti, P., Ernesto, M., Melfi, A., Pacca, I.G., Piccirillo, E.M., 1984. Flood Basalt to Rhyolite Suites in the Southern Paraná, Plateau (Brazil): Palaeomagnetism, Petrogenesis and Geodynamic Implications. J. Petrol. 25, 579–618. doi:10.1093/petrology/25.3.579

Bellieni, G., Comin-chiaramonti, P., Marques, L.S., Melfi, A.J., Nardy, A.J.R., Papatrechas, C., Piccirillo, E.M., Roisenberg, A., Stolfa, D., 1986. Petrogenetic aspects of acid and basaltic lavas from the paraná plateau (Brazil): Geological, mineralogical and petrochemical relationships. J. Petrol. 27, 915–944. doi:10.1093/petrology/27.4.915

Bryan, S.E., Peate, I.U., Peate, D.W., Self, S., Jerram, D.A., Mawby, M.R., Marsh, J.S. (Goonie), Miller, J.A., 2010. The largest volcanic eruptions on Earth. Earth-Science Rev. 102, 207–229. doi:10.1016/j.earscirev.2010.07.001

Buiter, S.J.H., Torsvik, T.H., 2014. A review of Wilson Cycle plate margins: A role for mantle plumes in continental break-up along sutures? Gondwana Res. 26, 627–653. doi:10.1016/j.gr.2014.02.007

Burke, K., Torsvik, T.H., 2004. Derivation of Large Igneous Provinces of the past 200 million years from long-term heterogeneities in the deep mantle. Earth Planet. Sci. Lett. 227, 531–538. doi:10.1016/j.epsl.2004.09.015

Class, C., le Roex, A.P., 2008. Ce anomalies in Gough Island lavas - Trace element characteristics of a recycled sediment component. Earth Planet. Sci. Lett. 265, 475–486. doi:10.1016/j.epsl.2007.10.030

Cordani, U.G., Vandoros, P., 1967. Basaltic rocks of the Parani basin. In: Bigarella, J.J., Becker, R.D., Pinto, J.D. (Eds.), Problems in Brazilian Gondwana Geology, pp. 207–231.

Courtillot, V., Jaupart, C., Manighetti, I., Tapponnier, P., Besse, J., 1999. On casual links between flood basalts and continental breakup. Earth Planet. Sci. Lett. 166, 177–195.

Cox, K.G., Hawkeshworth, C.. J., 1985. Geochemical Stratigraphyof the Deccan Traps at Mahabaleshwar, Western Ghats, India, with implications for Open system magmatic Processes. J. Petrol. 26, 355–377.

Cox, K.G., Bell, J.D. and Pankhurst, R.J. (1979) The Interpretation of Igneous Rock. Allen & Unwin, London, 450 p.

Danyushevsky, L. V., Plechov, P., 2011. Petrolog3: Integrated software for modeling crystallization processes. Geochemistry, Geophys. Geosystems 12, n/a-n/a. doi:10.1029/2011GC003516

Dodd, S.C., Mac Niocaill, C., Muxworthy, A.R., 2015. Long duration (>4 Ma) and steady-state volcanic activity in the early Cretaceous Paraná–Etendeka Large Igneous Province: New palaeomagnetic data from Namibia. Earth Planet. Sci. Lett. 414, 16–29. doi:10.1016/j.epsl.2015.01.009

Erlank, A.J., Marsh, J.S., Duncan, A.R., Miller, R.McG., Hawkesworth, C.H., Betton, P.J., Rex, D.C., 1984. Geochemistry and petrogenesis of the Etendeka volcanic rocks from SWA/Namibia, 195–247. In: Erlank, A.J. (Ed.), Petrogenesis of Volcanic Rocks of the Karoo Province, vol. 13. Special Publication of the Geological Society of South Africa, p. 395.

Ernesto, M., Raposo, M.I.B., Marques, L.S., Renne, P.R., Diogo, L. a., De Min, a., 1999. Paleomagnetism, geochemistry and 40Ar/39Ar dating of the North-eastern Parana Magmatic Province: Tectonic implications. J. Geodyn. 28, 321–340. doi:10.1016/S0264-3707(99)00013-7

Ewart, A., Marsh, J.S., Milner, S.C., Duncan, A.R., Kamber, B.S., Armstrong, R.A., 2004. Petrology and Geochemistry of Early Cretaceous Bimodal Continental Flood Volcanism of the NW Etendeka, Namibia. Part 1: Introduction, Mafic Lavas and Re-evaluation of Mantle Source Components. J. Petrol. 45, 59–105. doi:10.1093/petrology/egg083

Ewart, A., Milner, S.C.S., Armstrong, R. a. A., Duncan, A.R.R., 1998. Etendeka volcanism of the Goboboseb Mountains and Messum Igneous Complex, Namibia. Part I: Geochemical evidence of early cretaceous Tristan plume melts and the role of crustal contamination in the Paraná-Etendeka CFB. J. Petrol. 39, 191–225. doi:10.1093/petroj/39.2.191

Florisbal, L.M., Bitencourt, M. de F., Nardi, L.V.S., Conceição, R.V., 2009. Early post-collisional granitic and coeval mafic magmatism of medium- to high-K tholeiitic affinity within the Neoproterozoic Southern Brazilian Shear Belt. Precambrian Res. 175, 135–148. doi:10.1016/j.precamres.2009.09.003

Florisbal, L.M., Heaman, L.M., de Assis Janasi, V., de Fatima Bitencourt, M., 2014. Tectonic significance of the Florianópolis Dyke Swarm, Paraná–Etendeka Magmatic Province: A reappraisal based on precise U–Pb dating. J. Volcanol. Geotherm. Res. 289, 140–150. doi:10.1016/j.jvolgeores.2014.11.007

Florisbal, L.M., Janasi, V.A., Bitencourt, M.F., Nardi, L.V.S., Marteleto, N.S., 2018. Geological, geochemical and isotope diversity of ~ 134 Ma dykes from the Florianópolis Dyke Swarm, Paraná Magmatic Province: Geodynamic controls on petrogenesis. J. Volcanol. Geotherm. Res. 355, 181–203. doi:10.1016/j.jvolgeores.2017.08.002

Foulger, G.R., 2018. Origin of the South Atlantic igneous province. J. Volcanol. Geotherm. Res. 355, 2–20. doi:10.1016/j.jvolgeores.2017.09.004

Frank, H.T., Elisa, M., Gomes, B., Luiz, M., Formoso, L., 2009. Review of the areal extent and the volume of the Serra Geral Formation , Paraná Basin , South America. Pesqui. em Geociencias 36, 49–57.

Gallagher, K., Hawkesworth, C., 1992. Dehydration melting and the generation of continental flood basalts. Nature. doi:10.1038/358057a0

Garland, F., Hawkesworth, C.J., Manto, 1995. Description and Petrogenesys of the Parana Rzhyolites Southern Brazil. J. Petrol. 36, 1193–1227.

Gazel, E., Hoernle, K., Carr, M.J., Herzberg, C., Saginor, I., den Bogaard, P. van, Hauff, F., Feigenson, M., Swisher, C., 2011. Plume-subduction interaction in southern Central America: Mantle upwelling and slab melting. Lithos 121, 117–134. doi:10.1016/j.lithos.2010.10.008

Gladczenko, T.P., Hinz, K., Eldholm, O., Meyer, H., Neben, S., Skogseid, J., 1997. South Atlantic volcanic margins. J. Geol. Soc. London. 154, 465–470. doi:10.1144/gsjgs.154.3.0465

Gibson, S.A., Thompson, R.N., Day, J.A., 2006. Timescales and mechanisms of plume-lithosphere interactions:40Ar/39Ar geochronology and geochemistry of alkaline igneous rocks from the Paraná-Etendeka large igneous province. Earth Planet. Sci. Lett. 251, 1–17. doi:10.1016/j.epsl.2006.08.004

Gibson, S.A., Thompson, R.N., Day, J.A., Humphris, S.E., Dickin, A.P., 2005. Melt-generation processes associated with the Tristan mantle plume: Constraints on the origin of EM-1. Earth Planet. Sci. Lett. 237, 744–767. doi:10.1016/j.epsl.2005.06.015

Gibson, S.A., Thompson, R.N., Dickin, A.P., 2000. Ferropicrites: Geochemical evidence for Fe-rich streaks in upwelling mantle plumes. Earth Planet. Sci. Lett. 174, 355–374. doi:10.1016/S0012-821X(99)00274-5

Gibson, S.A., Thompson, R.N., Dickin, A.P., Leonardos, O.H., 1995. High-Ti and low-Ti mafic potassic magmas: Key to plume-lithosphere interactions and continental flood-basalt genesis. Earth Planet. Sci. Lett. 136, 149–165. doi:10.1016/0012-821X(95)00179-G

Grove, T.L., Gerlach, D.C., Sando, T.W., 1982. Origin of calc-alkaline series lavas at Medicine Lake Volcano by fractionation, assimilation and mixing. Contrib. to Mineral. Petrol. 80, 160–182. doi:10.1007/BF00374893

Grove, T.L.T.L., Kinzler, R.J.R.J., Bryan, W.B.W., 1992. Fractionation of mid-ocean ridge basalt (MORB). Gephysical Monogr. Geophys. Union 71, 281–310. doi:10.1029/GM071p0281

Grove, T.L., 1993. Corrections to expressions for calculating mineral components in “Origin of calc-alkaline series lavas at medicine lake volcano by fractionation, assimilation and mixing” and "Experimental petrology of normal MORB near the kane fracture zone: 22º-22ºN,. Contrib. to Mineral. Petrol. 114, 422–424. doi:10.1007/BF01046543

Hawkesworth, C.J., Gallagher, K., Kelley, S., Mantovani, M., Peate, D.W., Regelous, M., Rogers, N.W., 1992. Paraná magmatism and the opening of the South Atlantic. Geol. Soc. London, Spec. Publ. 68, 221–240. doi:10.1144/GSL.SP.1992.068.01.14

Hawkesworth, C.J., Gallagher, K., Kirstein, L., Mantovani, M.S.M., Peate, D.W., Turner, S.P., 2000. Tectonic controls on magmatism associated with continental break-up: an example from the Paraná–Etendeka Province. Earth Planet. Sci. Lett. 179, 335–349. doi:10.1016/S0012-821X(00)00114-X

Herzberg, C., Gazel, E., 2009. Petrological evidence for secular cooling in mantle plumes. Nature 458, 619–622. doi:10.1038/nature07857

Herzberg, C.T., Asimow, P.D., 2015. PRIMELT3 MEGA.XLSM software for primarymagma calculation: Peridotite primarymagma MgO contents fromthe liquidus to the solidus. Geochemistry, Geophys. Geosystems 16, 563–578. doi:10.1002/2014GC005631.Received

Herzberg, C.T., O’Hara, M.J., 2002. Plume-Associated Ultramafic Magmas of Phanerozoic Age. J. Petrol. 43, 1857–1883. doi:10.1093/petrology/43.10.1857

Hirose, K., Kushiro, I., 1993. Partial melting of dry peridotites at high pressures: Determination of compositions of melts segregated from peridotite using aggregates of diamond. Earth Planet. Sci. Lett. 114, 477–489. doi:10.1016/0012-821X(93)90077-M

Hoernle, K., Rohde, J., Hauff, F., Garbe-Schönberg, D., Homrighausen, S., Werner, R., Morgan, J.P., 2015. How and when plume zonation appeared during the 132 Myr evolution of the Tristan Hotspot. Nat. Commun. 6, 7799. doi:10.1038/ncomms8799

Hole, M.J., 2018. Mineralogical and geochemical evidence for polybaric fractional crystallization of continental flood basalts and implications for identification of peridotite and pyroxenite source lithologies. Earth-Science Rev. 176, 51–67. doi:10.1016/j.earscirev.2017.09.014

Hole, M.J., Ellam, R.M., Macdonald, D.I.M., Kelley, S.P., 2016. Gondwana break-up related magmatism in the Falkland Islands. J. Geol. Soc. London. 173, 108–126. doi:10.1144/jgs2015-027

Hole, M.J., Millett, J.M., 2016. Controls of Mantle Potential Temperature and Lithospheric Thickness on Magmatism in the North Atlantic Igneous Province. J. Petrol. 57, 417–436. doi:10.1093/petrology/egw014

Hole, M.J., Millett, J.M., Rogers, N.W., Jolley, D.W., 2015. Rifting and mafic magmatism in the Hebridean basins. J. Geol. Soc. London. 172, 218–236. doi:10.1144/jgs2014-100

Hole, M.J., 2015. The generation of continental flood basalts by decompression melting of internally heated mantle. Geology 43, 1–4. doi:10.1130/G36442.1

Hooper, P.R., 1982. The Columbia River Basalts. Science (80-.). 215, 1463–1468. doi:10.1126/science.215.4539.1463

Hooper, P.R., 2000. Chemical discrimination of Columbia River basalt flows. Geochemistry, Geophys. Geosystems 1, 1–14. doi:10.1029/2000GC000040

Hunt, A.C., Parkinson, I.J., Harris, N.B.W., Barry, T.L., Rogers, N.W., Yondon, M., 2012. Cenozoic Volcanism on the Hangai Dome , Central Mongolia :

Geochemical Evidence for Changing Melt Sources and Implications for Mechanisms of Melting 53, 1913–1942. doi:10.1093/petrology/egs038

Iacumin, M., Piccirillo, E.M., Girardi, V.A.V., Teixeira, W., Bellieni, G., Echeveste, H., Fernandez, R., Pinese, J.P.P., Ribot, A., 2001. Early Proterozoic calc-alkaline and Middle Proterozoic tholeiitic dyke swarms from Central-Eastern Argentina: Petrology, geochemistry, Sr-Nd isotopes and tectonic implications. J. Petrol. 42, 2109–2143. doi:10.1093/petrology/42.11.2109

Janasi, V. de A., Montanheiro, T.J., Azor de Freitas, V., Reis, P.M., de Assis Negri, F., Dantas, F.A., 2007. Geology, petrography and geochemistry of the acid volcanism of the Parana magmatic province in the Piraju-Ourinhos region, SE Brazil. Rev. Bras. Geociencias 37, 745–759.

Janasi, V.D.A., de Freitas, V.A., Heaman, L.H., 2011. The onset of flood basalt volcanism, Northern Paraná Basin, Brazil: A precise U–Pb baddeleyite/zircon age for a Chapecó-type dacite. Earth Planet. Sci. Lett. 302, 147–153. doi:10.1016/j.epsl.2010.12.005

Jay, A.E., Widdowson, M., 2008. Stratigraphy, structure and volcanology of the SE Deccan continental flood basalt province: implications for eruptive extent and volumes. J. Geol. Soc. London. 165, 177–188. doi:10.1144/0016-76492006-062

Jennings, E.S., Gibson, S.A., Maclennan, J., Heinonen, J.S., 2017. Deep mixing of mantle melts beneath continental flood basalt provinces: Constraints from olivine-hosted melt inclusions in primitive magmas. Geochim. Cosmochim. Acta 196, 36–57. doi:10.1016/j.gca.2016.09.015

Jerram, D.A., Moutney, N.P., Howell, J.A., Long, D., Stolhofen, H., 2000. Death of a sand sea: an active aeolian erg systematically buried by the Etendeka flood basalts of NW Namibia. J. Geol. Soc. London. 157, 513–516. doi:10.1144/jgs.157.3.513

Jerram, D., Mountney, N., Holzförster, F., Stollhofen, H., 1999. Internal stratigraphic relationships in the Etendeka Group in the Huab Basin, NW Namibia: Understanding the onset of flood volcanism. J. Geodyn. 28, 393–418. doi:10.1016/S0264-3707(99)00018-6

Jerram, D.A., Sharp, I. R., Torsvik, T. H., Poulsen, R., Watton, T., Freitag, U., Halton, A.,
Sherlock, S. C., Malley, J. A. S., Finley, A., Roberge, J., Swart, R., Fabregas, P., Ferreira, C., H., Machado, V. Volcanic constraints on the unzipping of Africa from South America; insights from new geochronological controls along the Angola margin. Submitted to Tectonphysics Dec 2017

Jerram, D. a., Widdowson, M., 2005. The anatomy of Continental Flood Basalt Provinces: geological constraints on the processes and products of flood volcanism. Lithos 79, 385–405. doi:10.1016/j.lithos.2004.09.009

Kerr, A.C., 1995. The Geochemical Stratigraphy, Field Relations and Temporal Variation of the Mull-Morvern Tertiary Lava Succession, Nw Scotland. Trans. R. Soc. Edinburgh-Earth Sci. 86, 35–47. doi:doi:10.1017/S0263593300002145

Kushiro, I., 1996. Partial Melting of a Fertile Mantle Peridotite at High Pressures: An Experimental Study Using Aggregates of Diamond, in: Geophysical Monograph Series. pp. 109–122. doi:10.1029/GM095p0109

Langmuir, C.H., Klein, Emily, M., Plank, T., 1992. Petrological systematics of MORBs Constraints on melt generation beneath oceanic ridges, in: Mantle Flow and Melt Generation at Mid-Ocean Ridges. pp. 183–279.

Larsen, L.M., Pedersen, A.K., 2009. Petrology of the paleocene picrites and flood basalts on disko and nuussuaq, West Greenland. J. Petrol. 50, 1667–1711. doi:10.1093/petrology/egp048

Lima, E.F., Waichel, B.L., Rossetti, L.D.M.M., Sommer, C.A., Simões, M.S., 2018. Feeder systems of acidic lava flows from the Paraná-Etendeka Igneous Province in southern Brazil and their implications for eruption style. J. South Am. Earth Sci. 81, 1–9. doi:10.1016/j.jsames.2017.11.004

Luchetti, A.C.F., Gravley, D.M., Gualda, G.A.R., Nardy, A.J.R., 2018a. Textural evidence for high-grade ignimbrites formed by low-explosivity eruptions, Paraná Magmatic Province, southern Brazil. J. Volcanol. Geotherm. Res. 355, 87–97. doi:10.1016/j.jvolgeores.2017.04.012

Mariani, P., Braitenberg, C., Ussami, N., 2013. Explaining the thick crust in Paraná basin, Brazil, with satellite GOCE gravity observations. J. South Am. Earth Sci. 45, 209–223. doi:10.1016/j.jsames.2013.03.008

Marques, L.S., De Min, A., Rocha-Júnior, E.R.V., Babinski, M., Bellieni, G., Figueiredo, A.M.G., 2018. Elemental and Sr-Nd-Pb isotope geochemistry of the Florianópolis Dyke Swarm (Paraná Magmatic Province): crustal contamination and mantle source constraints. J. Volcanol. Geotherm. Res. 355, 149–164. doi:10.1016/j.jvolgeores.2017.07.005

Marsh, J.S., Ewart, A., Milner, S.C., Duncan, A.R., Miller, R.M.G., 2001. The Etendeka Igneous Province: Magma types and their stratigraphic distribution with implications for the evolution of the Paraná-Etendeka flood basalt province. Bull. Volcanol. 62, 464–486. doi:10.1007/s004450000115

Marsh, J.S., Swart, R., 2018. The Bero Volcanic Complex: Extension of the Paraná-Etendeka Igneous Province into SW Angola. J. Volcanol. Geotherm. Res. 355, 21–31. doi:10.1016/j.jvolgeores.2016.10.011

Marzoli, A., Melluso, L., Morra, V., Renne, P.R., Sgrosso, I., D'Antonio, M., Duarte Morais, L., Morais, E.A.A., Ricci, G., 1999. Geochronology and petrology of Cretaceous basaltic magmatism in the Kwanza basin (western Angola), and relationships with the Parana-Etendeka continental flood basalt province. J. Geodyn. 28, 341–356. doi:10.1016/S0264-3707(99)00014-9

Mckenzie, D., Bickle, M.J.J., 1988. The volume and composition of melt generated by extension of the lithosphere. J. Petrol. 29, 1–55. doi:10.1093/petrology/29.3.625

McKenzie, D., O'Nions, R.K., 1991. Partial melt distribution from inversion of rare earth element concentrations. J. Petrol. 32, 1021–1091. doi:10.1093/petrology/32.5.1021

Millett, J., Hole, M.J., Jolley, D.W., Schofield, N., Campbell, E., 2015. Frontier exploration and the North Atlantic Igneous Province : new insights from a 2 . 6 km offshore volcanic sequence in the NE Faroe-Shetland Basin. J. Geol. Soc. London. In press. doi:10.1144/0016-76492015-069

Millett, J.M., Hole, M.J., Jolley, D.W., Passey, S.R., 2017. Geochemical stratigraphy and correlation within large igneous provinces: The final preserved stages of the Faroe Islands Basalt Group. Lithos 286–287, 1–15. doi:10.1016/j.lithos.2017.05.011

Milner, S.C., Duncan, A.R., Ewart, A., 1992. Quartz latite rheoignimbrite flows of the Etendeka Formation, north-western Namibia. Bull. Volcanol. 54, 200–219. doi:10.1007/BF00278389

Nardy, A., Machado, F., Oliveira, M., 2008. As rochas vulcânicas mesozóicas ácidas da Bacia do Paraná: litoestratigrafia e considerações geoquímico-estratigráficas. Rev. Bras. Geociencias 38, 178–195.

Natali, C., Beccaluva, L., Bianchini, G., Siena, F., 2018. Coexistence of alkaline-carbonatite complexes and high-MgO CFB in the Paranà-Etendeka province: Insights on plume-lithosphere interactions in the Gondwana realm. Lithos 296–299, 54–66. doi:10.1016/j.lithos.2017.11.001

Neave, D.A., Putirka, K.D., 2017. A new clinopyroxene-liquid barometer, and implications for magma storage pressures under Icelandic rift zones. Am. Mineral. 102, 777–794. doi:10.2138/am-2017-5968

O'Hara, M.J., 1965. Primary magmas and the origin of basalts. Scottish J. Geol. 1, 19–40. doi:10.1144/sjg01010019

Peate, D.W, Hawkesworth, C.J, Mantovani, M., 1992. Chemical stratigraphy of the Paraná lavas (South America): classification of magma types and their spatial distribution. Bull. Volcanol. 55, 119–139.

Peate, D.W., Hawkesworth, C.J., Mantovani, M., Rogers, N.W., Turner, S.P., 1999. Petrogenesis and Stratigraphy of the High- Ti / Y Urubici Magma Type in the Parana Flood Basalt Province and Implications for the Nature of ' Dupal ' -Type Mantle in the South Atlantic Region. J. Petrol. 40, 451–473.

Peate, D.W, Hawkesworth, C.J, Mantovani, M., Shukowsky, W., 1990. Mantle plumes and flood-basalt stratigraphy in the Paraná, South America. Geology 18, 1223–1226. doi:10.1130/0091-7613(1990)018<1223:MPAFBS>2.3.CO;2

Peate, D.W., Hawkesworth, C.J., 1996. Lithospheric to asthenospheric transition in low-Ti flood basalts from southern Parana, Brazil. Chem. Geol. 127, 1–24.

Peate, D., 1997. The Paraná-Etendeka Province. Large igneous Prov. Cont. Ocean. Planet. flood Volcanism 100, 217–245.

Piccirillo, E.M., Melfi, A.J., 1988. The Mesozoic flood volcanism from the Paraná Basin (Brazil): petrogenetic and geophysical aspects 600.

Piccirillo, E.M., Raposo, M.I.B., Melfi, A.J., Comin-Chiaramonti, P., Bellieni, G., Cordani, U.G., Kawashita, K., 1987. Bimodal Fissural Volcanic Suites From the Parana Basin (Brazil): K-Ar Age, Sr-Isotopes and Geochemistry. Geoch. Bras 1, 53–69.

Polo, L.A., Janasi, V.A., Giordano, D., Lima, E.F., Cañon-Tapia, E., Roverato, M., 2018a. Effusive silicic volcanism in the Paraná Magmatic Province, South Brazil: Evidence for locally-fed lava flows and domes from detailed field work. J. Volcanol. Geotherm. Res. 355, 204–218. doi:10.1016/j.jvolgeores.2017.08.007

Polo, L.A., Giordano, D., Janasi, V.A., Guimarães, L.F., 2018b. Effusive silicic volcanism in the Paraná Magmatic Province, South Brazil: Physico-chemical conditions of storage and eruption and considerations on the rheological behavior during emplacement. J. Volcanol. Geotherm. Res. 355, 115–135. doi:10.1016/j.jvolgeores.2017.05.027

Putirka, K., 2016. Rates and styles of planetary cooling on Earth, Moon, Mars, and Vesta, using new models for oxygen fugacity, ferric-ferrous ratios, olivine-liquid Fe-Mg exchange, and mantle potential temperature. Am. Mineral. 101, 819–840. doi:10.2138/am-2016-5402

Putirka, K.D., 2008. Thermometers and Barometers for Volcanic Systems. Rev. Mineral. Geochemistry 69, 61–120. doi:10.2138/rmg.2008.69.3

Raposo, M.I.B., Ernesto, M., Renne, P.R., 1998. Paleomagnetism and 40Ar/39Ar dating of the early Cretaceous Florianópolis dike swarm (Santa Catarina Island), Southern Brazil. Phys. Earth Planet. Inter. 108, 275–290. doi:http://dx.doi.org/10.1016/S0031-9201(98)00102-2

Renne, P.R., Ernesto, M., Pacca, I.G., Coe, R.S., Glen, J.M.G., Prevot, M., Perrin, M., 1992. The Age of Parana Flood Volcanism, Rifting of Gondwanaland, and the

Jurassic-Cretaceous Boundary. Science (80-.). 258, 975–979. doi:10.1126/science.258.5084.975

Rocha-Júnior, E.R.V., Puchtel, I.S., Marques, L.S., Walker, R.J., Machado, F.B., Nardy, A.J.R., Babinski, M., Figueiredo, A.M.G., 2012. Re-Os isotope and highly siderophile element systematics of the Paraná continental flood basalts (Brazil). Earth Planet. Sci. Lett. 337–338, 164–173. doi:10.1016/j.epsl.2012.04.050

Rohde, J., Hoernle, K., Hauff, F., Werner, R., O'Connor, J., Class, C., Garbe-Schönberg, D., Jokat, W., 2013. 70 Ma chemical zonation of the Tristan-Gough hotspot track. Geology 41, 335–338. doi:10.1130/G33790.1

Rollinson, H., 1993. Using Geochemical Data: Evaluation, presentation, interpretation, Using Geochemical Data: Evaluation, presentation, interpretation. doi:10.1097/00010694-199411000-00010

Rossetti, L., Lima, E.F., Waichel, B.L., Hole, M.J., Simões, M.S., Scherer, C.M.S., 2018. Lithostratigraphy and volcanology of the Serra Geral Group, Paraná-Etendeka Igneous Province in Southern Brazil: Towards a formal stratigraphical framework. J. Volcanol. Geotherm. Res. 355, 98–114. doi:10.1016/j.jvolgeores.2017.05.008

Salters, V.J.M., Mallick, S., Hart, S.R., Langmuir, C.E., Stracke, A., 2011. Domains of depleted mantle: New evidence from hafnium and neodymium isotopes. Geochemistry, Geophys. Geosystems 12. doi:10.1029/2011GC003617

Sarmento, C.C.T., Sommer, C.A., Lima, E.F., 2017. Mafic subvolcanic intrusions and their petrologic relation with the volcanism in the south hinge Torres Syncline, Paraná-Etendeka Igneous Province, southern Brazil. J. South Am. Earth Sci. 77, 70–91. doi:10.1016/j.jsames.2017.04.017

Scherer, C.M.S., 2002. Preservation of aeolian genetic units by lava flows in the Lower Cretaceous of the Paran Basin, southern Brazil. Sedimentology 49, 97–116. doi:10.1046/j.1365-3091.2002.00434.x

Simões, M.S., Lima, E.F., Sommer, C.A., Rossetti, L.M.M., 2018. Structures and lithofacies of inferred silicic conduits in the Paraná-Etendeka LIP, southernmost Brazil. J. Volcanol. Geotherm. Res. doi:10.1016/j.jvolgeores.2017.12.013

Stewart, K., Turner, S., Kelley, S., Hawkesworth, C., Kirstein, L., Mantovani, M., 1996. 3-D, 40Ar-39Ar geochronology in the Paraná continental flood basalt province. Earth Planet. Sci. Lett. 143, 95–109. doi:10.1016/0012-821X(96)00132-X

Sun, S. -s., McDonough, W.F., 1989. Chemical and isotopic systematics of oceanic basalts: implications for mantle composition and processes. Geol. Soc. London, Spec. Publ. 42, 313–345. doi:10.1144/GSL.SP.1989.042.01.19

Svensen, H.H., Torsvik, T.H., Callegaro, S., Augland, L., Heimdal, T.H., Jerram, D.A., Planke, S., Pereira, E., 2017. Gondwana Large Igneous Provinces: plate reconstructions, volcanic basins and sill volumes. Geol. Soc. London, Spec. Publ. SP463.7. doi:10.1144/SP463.7

Thiede, D.S., Vasconcelos, P.M., 2010. Paraná flood basalts: Rapid extrusion hypothesis confirmed by new40Ar/39Ar results. Geology 38, 747–750. doi:10.1130/G30919.1

Thompson, R.N., 1982. Magmatism of the British Tertiary Volcanic Province. Scottish J. Geol. 18, 49–107. doi:10.1144/sjg18010049

Thompson, R.N., Riches, A.J.V., Antoshechkina, P.M., Pearson, D.G., Nowell, G.M., Ottley, C.J., Dickin, A.P., Hards, V.L., Nguno, A.K., Niku-Paavola, V., 2007. Origin of CFB magmatism: Multi-tiered intracrustal picrite-rhyolite magmatic plumbing at Spitzkoppe, Western Namibia, during early cretaceous Etendeka magmatism. J. Petrol. 48, 1119–1154. doi:10.1093/petrology/egm012

Thompson, R.N.N., Gibson, S.A.A., Dickin, A.P.P., Smith, P.M.M., 2001. Early cretaceous basalt and picrite dykes of the Southern Etendeka Region, NW Namibia: Windows into the role of the Tristan mantle plume in Paraná-Etendeka magmatism. J. Petrol. 42, 2049–2081. doi:10.1093/petrology/42.11.2049

Thordarson, T., Self, S., 1998. The Roza Member, Columbia River Basalt Group: A gigantic pahoehoe lava flow field formed by endogenous processes? J. Geophys. Res. Solid Earth 103, 27411–27445. doi:10.1029/98JB01355

Thy, P., Lesher, C.E., Nielsen, T.F.D., Brooks, C.K., 2006. Experimental constraints on the Skaergaard liquid line of descent. Lithos 92, 154–180. doi:10.1016/j.lithos.2006.03.031

Torsvik, T.H., Smethurst, M.A., Burke, K., Steinberger, B., 2006. Large igneous provinces generated from the margins of the large low-velocity provinces in the deep mantle. Geophys. J. Int. 167, 1447–1460. doi:10.1111/j.1365-246X.2006.03158.x

Turner, S., Hawkesworth, C., 1995. The nature of the sub-continental mantle: constraints from the major-element composition of continental flood basalts. Chem. Geol. 120, 295–314. doi:10.1016/0009-2541(94)00143-V

Villiger, S., Ulmer, P., Müntener, O., 2007. Equilibrium and fractional crystallization experiments at 0.7 GPa; the effect of pressure on phase relations and liquid compositions of tholeiitic magmas. J. Petrol. 48, 159–184. doi:10.1093/petrology/egl058

Waichel, B.L., Scherer, C.M.S., Frank, H.T., 2008. Basaltic lava flows covering active aeolian dunes in the Paraná Basin in southern Brazil: Features and emplacement aspects. J. Volcanol. Geotherm. Res. 171, 59–72. doi:10.1016/j.jvolgeores.2007.11.004

Walter, M.J., 1998. Melting of garnet peridotite and the origin of komatiite and depleted lithosphere. J. Petrol. 39, 29–60. doi:10.1093/petroj/39.1.29

White, R., McKenzie, D., 1989. Magmatism at rift zones: The generation of volcanic continental margins and flood basalts. J. Geophys. Res. 94, 7685. doi:10.1029/JB094iB06p07685

White, R.S., McKenzie, D., 1995. Mantle plumes and flood basalts. J. Geophys. Res. 100, 17543–17585. doi:10.1029/95JB01585

Will, T.M., Frimmel, H.E., 2018. Where does a continent prefer to break up? Some lessons from the South Atlantic margins. Gondwana Res. 53, 9–19. doi:10.1016/j.gr.2017.04.014

Workman, R.K., Hart, S.R., 2005. Major and trace element composition of the depleted MORB mantle (DMM). Earth Planet. Sci. Lett. 231, 53–72. doi:10.1016/j.epsl.2004.12.005

Anexo IV

Apresentação de Trabalhos e
Resumos Publicados em Anais de Eventos

47 º Congresso Brasileiro de Geologia

ARCABOUÇO ESTRATIGRÁFICO DA FORMAÇÃO SERRA GERAL NO VALE PRINCIPAL DA SINCLINAL DE TORRES

Rossetti, L.M.[1]; Lima, E.F.[1]; Waichel, B.L.[2]; Scherer, C.M.S.[1]; Barreto, C.J.[1]
[1]Universidade Federal do Rio Grande do Sul; [2]Universidade Federal de Santa Catarina

RESUMO: A Sinclinal de Torres é uma estrutura tectônica localizada na porção sul do Brasil onde ocorrem preservadas as seqüência vulcânicas do magmatismo Paraná-Etendeka, denominados Formação Serra Geral. A Província Basáltica Continental do Paraná-Etendeka registra o intenso vulcanismo do Cretáceo inferior que precedeu a fragmentação do supercontinente Gondwana. Tradicionalmente investigações sobre estas rochas priorizaram a aquisição de dados geoquímicos e isotópicos, considerando a pilha vulcânica como uma monótona sucessão de derrames tabulares e espessos. O presente trabalho propõe a análise das características físicas deste vulcanismo aplicando conceitos de arquitetura de fácies vulcânicas, integrados a estudos petrográficos e geoquímicos. A área de estudo localiza-se na região nordeste do estado do Rio Grande do Sul, no vale principal da Sinclinal de Torres. Neste estudo foram analisadas as seqüência vulcânicas basálticas da Formação Serra Geral que recobrem os arenitos eólicos da Formação Botucatu e estão abaixo das unidades vulcânicas ácidas, para tal foram desenvolvidos dois perfis ao longo das rodovias BR-116 entre as cidades de Dois Irmãos e Caxias do Sul, e RS-122, entre as cidades de Feliz e Farroupilha. Neste contexto as rochas vulcânicas básicas podem ser divididas em duas unidades: derrames e campos de derrames *pahoehoe* (Unidade I), que ocorre entre cotas de 35 to 290 m, e derrames simples do tipo *rubbly* (Unidade II), que afloram entre 290 e 530 metros de cota. Geoquimicamente as duas unidades pertencem a serie de baixo- TiO_2 e ao magma tipo Gramado. As primeiras lavas *pahoehoe* são olivina basaltos, mais primitivos e apresentam os maiores teores de MgO. A unidade I é composta por inúmeros derrames *pahoehoe* que ocorrem sobre os arenitos eólicos da Formação Botucatu. Essas lavas ocorrem como *shee*t *pahoehoe*, *compound* lavas, e lavas do tipo *ponded* nos vales interduna. O *emplacement* dessas lavas esta relacionado a baixas taxas de erupção sustentadas por longos intervalos de tempo em relevo com paleotopografia relativamente plana. A unidade II é formada por espessas lavas simples, com até 50 metros, do tipo *rubbly*, estas são caracterizadas por topo fragmentado (*rubbly tops*), porção superior de topo coerente vesiculada, núcleo maciço, e base vesiculada. Essas lavas são formadas por altas taxas de erupção e durante a fase principal do vulcanismo na área, onde as maiores quantidades de magma atingem a superfície em um curto intervalo de tempo. O vale principal da Sinclinal de Torres tem uma evolução formada por derrames compostos na porção basal e derrames simples nas porções superiores, similar a de outras Províncias Basálticas Continentais como o Deccan e o Columbia River.

PALAVRAS-CHAVE: PROVÍNCIA BASÁLTICA CONTINENTAL; EMPLACEMENTE DE LAVAS; ESTRATIGRAFIA DE VULCÂNICAS

Volcanic Stratigraphy inside the Low TiO_2 Sequence of Parana-Etendeka Province in Brazil

***Rossetti, L.[1], Lima, E.F.[2], Hole, M.[1] and Waichel, B.L[3].**

***l.rossetti@abdn.ac.uk, [1]University of Aberdeen, School of Geosciences, Meston Building, AB24 2UE;**

[2] Department of Mineralogy and Petrology, Federal University of Rio Grande do Sul, Av. Bento Gonçalves 9500, Porto Alegre, Brazil;

[3] Federal University of Santa Catarina, Campus Universitário Trindade, Florianópolis, Brazil;

The south limit of Parana-Etendeka Basaltic Province (PEBP) in southern Brazil exposes several stratigraphic sections along road cuts. Those sections were intensely studied in the 90s using geochemistry, geochronology and, magnetic stratigraphy, but their physical volcanology has not been studied in detail up until now. Chemically the PEBP has been divided into High-TiO_2 sequence, north portion of the province, and Low-TiO_2 sequence in the south portion. The volcanic pile once considered as one single Formation known in Brazil as Serra Geral Formation, is in fact characterized by highly heterogeneous packages of lavas with distinct morphologies, architecture and chemistry and internal unconformities. We present a detailed study of the stratigraphy inside Torres Syncline (TS), a NW structure that control the deposition and distribution of the Low TiO_2 lava sequence where we identified four distinct lava units. The first lavas (Unit I) were deposited over a large dune field (paleo erg) known as Botucatu Fm. These lavas are olivine-phyric basalts arranged in a compound braided architecture formed by a complex stacking of *pahoehoe* lobes and flow fields that spread regionally in the TS. Chemically the lavas from this unit are more primitive basalts with higher contents of Mg. The first lavas are covered by thick (~50m), chemically more evolved basaltic-andesite, simple lavas with *rubbly* tops in a classic tabular architecture (Unit II). The deposition of these lavas is controlled by TS structure, reaching maximum thickness in (500m) in the main valley of TS and thinning towards the structure limit to WSW. These two basaltic Units are overlain by silicic lavas, which are wide spread vitrophyres with tabular and lobular geometries, locally interbedded with the tabular flows of Unit II. In the Western end of TS the Silicic lavas (Unit III) are deposited directly over the compound *pahoehoe* lavas form Unit I. The upper portion of low-TiO2 sequence is characterized by primitive aphanitic-basalts in *pahoehoe* morphologies with restrict areal occurrence. The distinct lava morphologies, architecture and chemical compositions reflects different evolutional stages inside the volcanic pile.

Preferred Presentation Format: Poster
Session: Emplacement Processes

Rubbly-pahoehoe lavas from southern Paraná-Etendeka Continental Basaltic Province

L. Rossetti[1], E.F. Lima[2], B. Waichel[3], M. Hole[4]

[1]University of Aberdeen / UFRGS, Geology & Petroleum Geology, Aberdeen, United Kingdom

[2]UFRGS, Mineralogy and Petrology, Porto Alegre, Brazil

[3]UFSC, Geosciences, Florianopolis, Brazil

[4]University of Aberdeen, Geology & Petroleum Geology, Aberdeen, United Kingdom

Recently *rubbly-pahoehoe* lavas were identified in the southern portion of Paraná-Etendeka LIP. These lavas represent an important component of the volcanic stratigraphy in the southern portion of Brazil. They occur as thick (40-45 m) tabular lavas that spread for several kilometers and cover *pahoehoe* flow fields. The *rubbly* lavas are characterized by a tabular classic architecture marked by the vertical stacking of several lava flows, which together can reach a maximum thickness of 500 m in the main valley of Torres Syncline. The internal structure of single *rubbly-pahoehoe* lava can be divided in four parts. The basal portion is characterized by aphanitic and vesicular basalt, and the basal surface is commonly glassy and oxidized. The core is mainly aphanitic and aphyric basalt and in some cases with irregular columnar joints, and the upper portion of the core is coarsely vesicular or amygdaloidal basalt. The cavities range from 1 to 6 cm in diameter in a sub spherical shape and a random distribution and are filled mainly by zeolite. The flow surface is brecciated, and forms a rubble layer with an irregular geometry and have an average thickness of 5-7 m. It is formed of vesicular basalt fragments with random distribution. The diameter of the fragments varies from 5 cm to 25 cm with an average of 10 cm. The occurrence of *rubbly-pahoehoe* lavas imply in a change of the dynamic of the volcanism and may represent an increase in volcanic activity. The absence of multiple lobes or associated *pahoehoe* lobes indicates that *rubbly-pahoehoe* lavas emplaced as simple flow, probably formed during sustain eruptions. The disruption of flow surfaces may indicate oscillations in effusion rates during the emplacement.

BG GROUP RESEARCH FORUM 2015– READING, UNITED KINGDOM

Stratigraphy and Petrophysics of Volcanic Rocks: Examples from the Parana-Etendeka Igneous Province

Lucas Rossetti[1, 2] [l.rossetti@abdn.ac.uk]

David Healy[1]; Evandro Lima[2]; Malcolm Hole[1]

[1]University of Aberdeen / [2]Federal University of Rio Grande do Sul (UFRGS)

Volcanic rocks are present in many petroliferous basins and often present real challenges in hydrocarbon exploration, development and production (North Sea, South Atlantic Margins). Our study provides an integration of outcrop and laboratory analyses to understand the petrophysical behaviour of different volcanic facies, using outcrop analogues from the Parana-Etendeka Igneous Province in Brazil. This area exposes a 1 km thick lava pile with four lava groups: 1) basaltic *pahoehoe* flow fields with a compound braided architecture; 2) basaltic andesite lavas with tabular geometry, massive aphanitic cores and *rubbly* flow tops in a classic tabular architecture; 3) tabular dacitic and rhyolitic units; 4) basaltic *pahoehoe* flow fields with a compound braided architecture, chemically distinct from unit 1. Several sedimentary units of aeolian and fluvial facies occur within the lava sequence. Measurements of porosity, permeability, density, and acoustic velocities (P- and S-waves) were carried out in 68 samples of different lithofacies from the lavas and the interbeds. The preliminary results point to a clear distinction between lava flow cores and flow crusts. The proportion of these two and members is related to the lava morphology and architecture. The core of the lava flows is composed of massive, columnar or poorly vesicular facies. Porosities are less than 8% and P- and S-wave velocities are on average ~5.1 km/s and 3.1 km/s, respectively. The lava crusts vary from highly vesicular to brecciated facies and have variable porosities depending on the content of their filled pores, varying from 5- 20%, and V_p and V_s are 4.0 km/s and 2.5 km/s respectively. The sedimentary interbeds are porous and permeable (>20% and 10-750 mD), and velocities are lower than the lavas, ~2.8km/s for V_p and 1.8 km/s V_s. Factors controlling petrophysical responses in volcanic rocks are: rock composition (mineralogy and alteration); structure and texture; proportion of glass and matrix vs crystals; and, presence of cracks and fractures. In the intervolcanic sedimentary units the petrophysical behaviour is controlled by the grain size, sorting, thickness of the interbed, grade of compaction and diageneses. Further work aims to quantify the relationship among these factors and the petrophysical responses using rock physics approach.

Anexo V

Análises petrofísicas das rochas vulcânicas e sedimentares da Província do Paraná-Etendeka

Amostra	*Formação*	*Litologia*	*Litofacies*	*ϕ (%)*	*KL (mD)*	*Grain Den. (g/cm^3)*	*Rock Den. (g/cm^3)*	*V_P (kms^{-1})*	*V_S (kms^{-1})*	*V_P/V_S*
SG-79E-3	Torres	Basalt	Lower Crust	6.08	0.0009	2.74	2.57	4.80	3.11	1.54
SG-79E-1	Torres	Basalt	Lower Crust	7.67	0.0034	2.66	2.47	4.32	3.11	1.39
SG-79E-2	Torres	Basalt	Lower Crust	7.22	0.0025	2.61	2.45	3.96	2.30	1.72
SG-80a-1	Torres	Basalt	Lower Crust	5.57	0.0018	2.74	2.60	4.18	2.71	1.54
SG-80A-2	Torres	Basalt	Lower Crust	7.45	0.001	2.74	2.53	4.13	2.67	1.54
SG-80a-3	Torres	Basalt	Lower Crust	5.42	0.002	2.75	2.62	4.16	2.49	1.67
SG-80A-4*	Torres	Basalt	Lower Crust	7.58	0.0028	2.73	2.53	4.08	2.65	1.54
Sg-80d-1a	Torres	Basalt	Lower Crust	5.41	0.0054	2.72	2.59	4.28	2.81	1.52
SG-80D-1b	Torres	Basalt	Lower Crust	8.47	0.0041	2.77	2.55	4.18	2.31	1.81
SG-80-D3	Torres	Basalt	Lower Crust	6.85	0.0021	2.74	2.56	4.45	2.58	1.73
LR-55-1	Torres	Basalt	Core	1.41	0.0206	2.95	2.91	5.49	3.37	1.63
LR-55-2	Torres	Basalt	Core	1.54	0.0023	2.95	2.90	5.68	3.09	1.84
SG94-Z1	Torres	Basalt	Core	7.43	0.0003	2.71	2.51	5.11	3.00	1.70
SG-94-X	Torres	Basalt	Core	4.40	0.0007	2.61	2.50	5.00	3.01	1.66
SG-94-Z2	Torres	Basalt	Core	4.62	0.0003	2.61	2.49	4.93	3.00	1.64
LR-1B	Torres	Basalt	Core	1.89	0.0006	2.75	2.70	4.81	2.93	1.64
LR-1C	Torres	Basalt	Core	1.45	0.1846	2.76	2.72	5.18	3.05	1.70
SG-70A	Torres	Basalt	Core	4.99	0.0046	2.83	2.69	4.12	2.56	1.61
SG-79-B	Torres	Basalt	Core	5.85	0.0022	2.85	2.63	4.45	2.68	1.66
SG-80B-1	Torres	Basalt	Core	2.35	0.0017	2.70	2.63	5.14	2.73	1.89
SG80B-2	Torres	Basalt	Core	2.85	0.0022	2.70	2.63	5.02	3.00	1.67
SG-80b-A1	Torres	Basalt	Core	3.11	0.0021	2.68	2.62	4.96	3.16	1.57
SG-80B-A2	Torres	Basalt	Core	3.29	0.0018	2.69	2.60	5.03	2.94	1.71
SG-81A	Torres	Basalt	Core	2.56	0.0003	2.73	2.66	5.09	2.96	1.72
SG-103-1	Torres	Basalt	Core	1.37	0.0015	2.81	2.77	5.38	3.09	1.74
SG-96A-X1	Torres	Basalt	Core	4.00	0.0006	2.77	2.66	5.04	3.01	1.67
SG-96A-Y	Torres	Basalt	Core	5.29	0.0021	2.79	2.64	4.85	2.77	1.75
SG-96A-X2	Torres	Basalt	Core	6.81	0.0022	2.79	2.60	4.95	2.96	1.67
SG-107-B1	Torres	Basalt	Core	1.46	0.0021	2.79	2.75	5.46	3.31	1.65
SG-113B-X	Torres	Basalt	Core	1.64	0.0009	2.81	2.76	4.96	2.91	1.70

Amostra	*Formação*	*Litologia*	*Litofacies*	*ϕ (%)*	*KL (mD)*	*Grain Den. (g/cm^3)*	*Rock Den. (g/cm^3)*	*V_P (kms^{-1})*	*V_S (kms^{-1})*	*V_P/V_S*
SG-107B-Z1	Torres	Basalt	Core	0.91	0.0021	2.78	2.75	5.94	3.46	1.72
SG-119A-X4	Torres	Basalt	Core	0.81	0.0018	2.89	2.87	5.81	3.32	1.75
SG-119A-X3	Torres	Basalt	Core	0.84	0.0018	2.90	2.87	5.80	3.30	1.76
SG-98-Z2	Torres	Basalt	Core	2.26	0.0018	2.55	2.49	4.75	2.83	1.68
SG-103-Z	Torres	Basalt	Core	1.51	0.0015	2.81	2.77	5.45	3.18	1.71
SG-106-X	Torres	Basalt	Core	1.24	0.0027	2.90	2.86	5.70	3.31	1.72
SG96A-Y2	Torres	Basalt	Core	6.81	0.0021	2.82	2.63	4.60	2.92	1.57
SG-96A-X3	Torres	Basalt	Core	5.46	0.0022	2.83	2.68	5.01	2.97	1.69
SG-119A-X2	Torres	Basalt	Core	1.83	0.0018	2.93	2.88	5.89	3.35	1.76
SG-90-A-Y	Torres	Basalt	Core	1.22	0.0013	2.90	2.86	5.68	3.36	1.69
SG-93-Z1	Torres	Basalt	Core	1.71	0.0018	2.57	2.52	4.76	2.93	1.62
SG-119A-X1	Torres	Basalt	Core	0.83	0.0018	2.89	2.87	5.80	3.35	1.73
SG-90A-X	Torres	Basalt	Core	0.41	0.0013	2.88	2.87	5.41	3.34	1.62
SG-107B-Z2	Torres	Basalt	Core	0.87	0.0021	2.78	2.76	5.74	3.39	1.69
SG-98Q-2	Torres	Basalt	Core	2.41	0.0018	2.58	2.51	4.77	2.84	1.68
SG-98Q-Z	Torres	Basalt	Core	1.73	0	2.56	2.52	4.57	2.79	1.64
SG-90A-Z	Torres	Basalt	Core	0.69	0.0008	2.89	2.87	5.80	3.32	1.75
SG-70D	Torres	Basalt	Upper Crust	7.92	0.0018	2.72	2.50	3.90	2.11	1.85
SG-74-B	Torres	Basalt	Upper Crust	3.39	0.0016	2.78	2.69	4.90	3.78	1.30
SG-74C	Torres	Basalt	Upper Crust	15.38	0.031	2.58	2.18	3.21	1.86	1.73
SG-76-A	Torres	Basalt	Upper Crust	9.78	0.0046	2.68	2.40	3.77	2.26	1.66
SG-76B	Torres	Basalt	Upper Crust	17.93	0.0066	2.67	2.19	3.42	2.17	1.58
SG-79-a	Torres	Basalt	Upper Crust	9.04	0.001	2.57	2.35	4.76	2.80	1.70
SG-79-D	Torres	Basalt	Upper Crust	5.74	1.8927	2.66	2.46	4.21	2.47	1.71
SG-80C-1	Torres	Basalt	Upper Crust	5.95	0	2.59	2.43	4.74	2.98	1.59
SG-81B	Torres	Basalt	Upper Crust	5.23	0.0004	2.57	2.44	5.05	2.56	1.97
SG-99-2	Torres	Basalt	Upper Crust	26.60	415.68	2.93	2.15	4.16	2.11	1.97
SG-90-B	Torres	Basalt	Upper Crust	10.43	0.0008	2.64	2.37	4.34	2.62	1.66
SG-99-1	Torres	Basalt	Upper Crust	21.12	0.0127	2.93	2.31	4.07	2.18	1.86
SG-96B-3	Torres	Basalt	Upper Crust	15.25	0.0015	2.89	2.45	4.58	2.66	1.72

Amostra	*Formação*	*Litologia*	*Litofacies*	*ϕ (%)*	*KL (mD)*	*Grain Den. (g/cm^3)*	*Rock Den. (g/cm^3)*	*V_P (kms^{-1})*	*V_S (kms^{-1})*	*V_P/V_S*
SG-96B-4	Torres	Basalt	Upper Crust	22.55	0.0015	3.15	2.44	4.78	2.51	1.91
SG-81D	Torres	Basalt	Upper Crust	8.08	0	2.59	2.38	4.76	2.53	1.88
SG-110X	Vale do Sol	Bas. Andesite	Lower Crust	1.59	0.0004	2.72	2.68	5.07	2.86	1.77
SG-110Z	Vale do Sol	Bas. Andesite	Lower Crust	1.90	0.0014	2.72	2.67	5.05	2.74	1.84
SG-110X-2	Vale do Sol	Bas. Andesite	Lower Crust	1.16	0.0004	2.72	2.68	5.19	2.98	1.74
SG-75F-Y	Vale do Sol	Bas. Andesite	Lower Crust	0.83	0.0015	2.84	2.81	5.32	2.95	1.80
SG-114-Z	Vale do Sol	Bas. Andesite	Lower Crust	5.88	0.0031	2.65	2.49	4.76	2.81	1.69
SG-75F-Z	Vale do Sol	Bas. Andesite	Lower Crust	0.98	0.0009	2.84	2.81	5.28	3.20	1.65
SG-110-X3	Vale do Sol	Bas. Andesite	Lower Crust	1.67	0.0004	2.72	2.67	5.03	3.02	1.67
SG-75F-X	Vale do Sol	Bas. Andesite	Lower Crust	1.40	0.0009	2.85	2.81	5.58	3.14	1.78
SG-76-F1	Vale do Sol	Bas. Andesite	Lower Crust	15.11	0.1166	2.61	2.20	4.00	2.36	1.70
SG-8F-1	Vale do Sol	Bas. Andesite	Lower Crust	15.52	0.0034	2.75	2.32	4.32	2.38	1.82
SG-8F-2	Vale do Sol	Bas. Andesite	Lower Crust	15.64	0.0021	2.57	2.17	4.68	2.44	1.92
LR-16-1	Vale do Sol	Bas. Andesite	Core	2.50	0.0009	2.90	2.83	5.70	3.42	1.67
LR-16-2	Vale do Sol	Bas. Andesite	Core	1.09	0.0015	2.85	2.82	5.90	3.37	1.75
SG-16-3(lr)	Vale do Sol	Bas. Andesite	Core	1.14	0.0007	2.86	2.83	5.90	3.36	1.76
SG-77-B	Vale do Sol	Bas. Andesite	Core	8.73	0.0009	3.08	2.82	5.31	3.18	1.67
SG-77F-1	Vale do Sol	Bas. Andesite	Core	1.75	0.0017	2.86	2.80	5.05	3.11	1.63
SG-77F-2	Vale do Sol	Bas. Andesite	Core	0.75	0.0019	2.84	2.80	5.45	3.23	1.69
SG-77F-3	Vale do Sol	Bas. Andesite	Core	1.27	0.0022	2.83	2.81	5.09	3.03	1.68
SG-78	Vale do Sol	Bas. Andesite	Core	1.77	0.0014	2.85	2.80	5.56	3.26	1.70
SG-82-1	Vale do Sol	Bas. Andesite	Core	1.43	0.0015	2.76	2.72	5.69	3.29	1.73
SG-82-2	Vale do Sol	Bas. Andesite	Core	1.25	0.0014	2.75	2.72	5.78	3.33	1.74
SG-82-3	Vale do Sol	Bas. Andesite	Core	1.33	0.0009	2.77	2.73	5.35	3.30	1.62
SG-117B	Vale do Sol	Bas. Andesite	Core	1.15	0.0005	2.90	2.87	5.85	3.26	1.80
SG-113A-Z1	Vale do Sol	Bas. Andesite	Core	1.51	0.0025	2.82	2.78	5.27	3.08	1.71
SG-8E-Z1	Vale do Sol	Bas. Andesite	Core	3.47	0.003	2.69	2.60	5.26	3.01	1.75
SM-48	Vale do Sol	Bas. Andesite	Core	1.65	0.0006	2.86	2.81	5.50	3.22	1.71
SG-8E-X	Vale do Sol	Bas. Andesite	Core	3.07	0.0016	2.68	2.60	4.88	3.04	1.60
SG-113B-Z	Vale do Sol	Bas. Andesite	Core	1.65	0.0009	2.81	2.76	5.36	3.03	1.77

Amostra	*Formação*	*Litologia*	*Litofacies*	*ϕ (%)*	*KL (mD)*	*Grain Den. (g/cm^3)*	*Rock Den. (g/cm^3)*	*V_P (kms^{-1})*	*V_S (kms^{-1})*	*V_P/V_S*
SG-113B-Y	Vale do Sol	Bas. Andesite	Core	0.03	0.002	2.80	2.80	5.35	3.10	1.73
SG-8E-X2	Vale do Sol	Bas. Andesite	Core	4.99	0.0016	2.74	2.61	5.15	2.98	1.73
SG-114-Y	Vale do Sol	Bas. Andesite	Upper Crust	3.99	0.0013	2.65	2.54	5.10	2.68	1.90
SG-111Z	Vale do Sol	Bas. Andesite	Upper Crust	1.06	0.0001	2.69	2.67	5.30	3.01	1.76
SG-111X	Vale do Sol	Bas. Andesite	Upper Crust	2.25	0.0013	2.69	2.63	5.36	2.97	1.80
SG-113C-Z	Vale do Sol	Bas. Andesite	Upper Crust	1.02	0.0007	2.81	2.78	5.88	3.37	1.74
SG-113C-Y	Vale do Sol	Bas. Andesite	Upper Crust	1.22	0.0007	2.83	2.79	5.86	3.39	1.73
SG-108B	Vale do Sol	Bas. Andesite	Upper Crust	3.27	0.0013	2.70	2.62	4.24	2.84	1.49
SG-113C-X	Vale do Sol	Bas. Andesite	Upper Crust	1.65	0.0007	2.82	2.77	5.75	3.19	1.80
SG-75C-3A	Vale do Sol	Bas. Andesite	Rubble	19.26	0.0022	2.59	2.09	3.39	1.84	1.84
SG-75-B*	Vale do Sol	Bas. Andesite	Rubble	18.06	0.1435	2.68	2.19	3.15	1.95	1.61
SG-75C2	Vale do Sol	Bas. Andesite	Rubble	17.09	0.0014	2.62	2.18	3.61	2.24	1.61
SG-75C3B	Vale do Sol	Bas. Andesite	Rubble	18.19	0.0243	2.55	2.09	3.41	1.99	1.71
SG-75C-4	Vale do Sol	Bas. Andesite	Rubble	15.05	0.0164	2.56	2.17	2.93	1.99	1.48
SG-75G-1	Vale do Sol	Bas. Andesite	Rubble	11.42	0.0059	2.73	2.42	4.14	2.45	1.69
SG-113D-2	Vale do Sol	Bas. Andesite	Rubble	28.28	0.7268	2.62	1.88	3.34	1.81	1.85
SG-108C-1	Vale do Sol	Bas. Andesite	Rubble	14.07	0.0132	2.47	2.12	3.40	2.15	1.59
SG-108C-2	Vale do Sol	Bas. Andesite	Rubble	22.34	0.0173	2.69	2.09	3.28	2.01	1.63
SG-75-G4	Vale do Sol	Bas. Andesite	Rubble	11.00	0.0067	2.66	2.36	4.23	2.42	1.75
SG-75G-3	Vale do Sol	Bas. Andesite	Rubble	11.41	0.0007	2.69	2.38	4.21	2.43	1.73
SG-75-G2	Vale do Sol	Bas. Andesite	Rubble	11.33	0.0023	2.61	2.32	3.75	2.21	1.70
SG-108-C3	Vale do Sol	Bas. Andesite	Rubble	16.35	0.0233	2.53	2.12	3.22	1.87	1.72
Sg-66A-1	Palmas	Dacite	Core	3.22	0.0006	2.62	2.54	4.81	2.96	1.63
MS-51	Palmas	Obsidian	Core	3.23	0.0009	2.57	2.49	5.51	3.32	1.66
SG-66A-2B	Palmas	Dacite	Core	3.78	0.0030	2.65	2.55	4.73	2.93	1.61
SG-66A-2C	Palmas	Dacite	Core	2.62	0.0010	2.63	2.56	4.67	2.93	1.59
SG-68-1	Palmas	Dacite	Core	3.15	0.0015	2.63	2.55	4.85	3.01	1.61
SG-68-2	Palmas	Dacite	Core	2.38	0.0016	2.60	2.54	4.93	3.06	1.61
SG-83B-1A	Palmas	Dacite	Core	3.21	0.0141	2.56	2.47	4.61	2.72	1.69
SG-83B-1B	Palmas	Dacite	Core	4.86	0.0006	2.60	2.47	4.47	2.67	1.67

Amostra	*Formação*	*Litologia*	*Litofacies*	*ϕ (%)*	*KL (mD)*	*Grain Den. (g/cm^3)*	*Rock Den. (g/cm^3)*	*V_P (kms^{-1})*	*V_S (kms^{-1})*	*V_P/V_S*
SG-109-A	Palmas	Dacite	Core	1.10	0.0012	2.85	2.82	5.87	3.32	1.77
SG-91B-1	Palmas	Rhyolite	Core	1.43	0.0003	2.41	2.37	4.91	3.07	1.60
SG-101-X2	Palmas	Rhyolite	Core	9.38	0.0019	2.64	2.39	4.45	2.82	1.58
SG-101-Z	Palmas	Dacite	Core	7.11	0.0019	2.61	2.42	4.57	2.89	1.58
SG-101-X1	Palmas	Dacite	Core	8.66	0.0019	2.63	2.40	4.45	2.89	1.54
SG-91B-2	Palmas	Dacite	Core	2.13	0.0003	2.42	2.37	5.02	3.13	1.61
SG-83A	Palmas	Dacite	Upper Crust	9.90	0.0113	2.58	2.32	4.48	2.51	1.79
SG-13e	Sed. Interbed	Sandstone	Sm	11.52	0.0029	2.66	2.35	3.72	2.34	1.59
SG-13E-Z	Sed. Interbed	Sandstone	Sm	17.34	0.0185	2.64	2.18	3.59	2.21	1.62
SG-13E-X	Sed. Interbed	Sandstone	Sm	16.07	0.1092	2.63	2.21	3.63	2.04	1.78
SG-72-1	Sed. Interbed	Sandstone	Sm	25.92	0.444	2.54	1.88	2.56	1.68	1.52
SG-76-I	Sed. Interbed	Sandstone	Sm	3.52	0.4511	2.56	2.47	5.37	4.10	1.31
SG-76-H	Sed. Interbed	Sandstone	Sm	9.65	1.985	2.60	2.35	5.33	4.07	1.31
SG-118A-X	Sed. Interbed	Sandstone	Sm	16.20	3.5437	2.64	2.21	3.02	1.93	1.57
SG-118C-Z	Sed. Interbed	Sandstone	Sm	13.64	6.8349	2.62	2.26	3.01	1.95	1.54
SG-118C-X	Sed. Interbed	Sandstone	Sm	14.10	9.9467	2.62	2.25	3.09	2.10	1.47
SG-118C-Y	Sed. Interbed	Sandstone	Sm	13.80	12.928	2.62	2.26	3.16	2.07	1.52
SG-118A-Z	Sed. Interbed	Sandstone	Sm	21.12	33.33	2.63	2.07	2.35	1.58	1.48
sg-72-2	Sed. Interbed	Sandstone	Sm	26.19	47.531	2.55	1.88	2.70	1.69	1.60
SG-67D	Sed. Interbed	Sandstone	Sm	12.86	0.0061	2.62	2.28	2.95	1.93	1.53
SG-91A-Y	Sed. Interbed	Sandstone	Sm	16.95	74.368	2.55	2.12	3.22	2.19	1.47
SG-72-3	Sed. Interbed	Sandstone	Sm	28.42	77.708	2.54	1.82	2.42	1.54	1.57
SG-69-A2	Sed. Interbed	Sandstone	Ss	9.29	39.714	2.56	2.32	4.88	3.23	1.51
SG-107-A2	Sed. Interbed	Sandstone	Ss	14.46	79.873	2.64	2.26	4.24	2.68	1.58
SG-8G	Sed. Interbed	Sandstone	Ss	14.68	63.176	2.61	2.23	4.30	2.85	1.51
SG-70A-z	Sed. Interbed	Sandstone	Ss	20.79	97.889	2.60	2.06	2.22	1.40	1.59
SG-69A-1	Sed. Interbed	Sandstone	Ss	13.22	122.41	2.62	2.28	4.89	3.17	1.54
SG-67B-1	Sed. Interbed	Sandstone	Ss	27.43	372.77	2.61	1.90	2.85	1.89	1.51
SG-67B-3	Sed. Interbed	Sandstone	Ss	26.60	423.2	2.62	1.92	3.17	1.85	1.71
SG-70F-Y2	Sed. Interbed	Sandstone	Ss	25.06	522.27	2.61	1.95	2.30	1.34	1.72

Amostra	*Formação*	*Litologia*	*Litofacies*	*ϕ (%)*	*KL (mD)*	*Grain Den. (g/cm^3)*	*Rock Den. (g/cm^3)*	*V_P (kms^{-1})*	*V_S (kms^{-1})*	*V_P/V_S*
SG-107A-3	Sed. Interbed	Sandstone	Ss	15.29	65.857	2.63	2.22	3.90	2.48	1.57
SG-107A-1	Sed. Interbed	Sandstone	Ss	14.48	68.148	2.63	2.25	4.24	2.66	1.60
SG-70A-Y	Sed. Interbed	Sandstone	Ss	24.04	578.22	2.59	1.97	2.21	1.29	1.71
SG-70A-X	Sed. Interbed	Sandstone	Ss	24.15	760.37	2.61	1.98	2.41	1.30	1.85
SG-67B-2	Sed. Interbed	Sandstone	Ss	28.37	766.27	2.61	1.87	3.05	1.98	1.54
SG-70F-Y	Sed. Interbed	Sandstone	Ss	31.58	1036.2	2.60	1.78	1.96	1.18	1.66
SG-70F-X	Sed. Interbed	Sandstone	Ss	34.18	1062.4	2.60	1.71	2.14	1.26	1.70
SG-70F-Z	Sed. Interbed	Sandstone	Ss	31.92	1115.3	2.59	1.77	1.97	1.19	1.66
SG-8D-1	Sed. Interbed	Peperite	Peperite	14.60	0.0029	2.53	2.16	4.27	2.73	1.56
SG-8D-2	Sed. Interbed	Peperite	Peperite	15.46	0.045	2.55	2.16	4.15	2.69	1.54

Anexo VI

Litogeoquímica e Isótopos de Sr-Nd-Pb

Amostra	Elev.	UTM E	UTM N	Fm.	Grupo	SiO2	TiO2	Al2O3	Cr2O3	Fe2O3(t)	MnO	MgO	CaO	Na2O	K2O	P2O5	LOI	SUM
						0.01	*0.01*	*0.01*	*0.002*	*0.04*	*0.01*	*0.01*	*0.01*	*0.01*	*0.01*	*0.01*		
LBC-1	100	486142	6722205	Torres	1	57.48	1.40	14.18	0.00	10.21	0.15	3.53	6.47	2.76	2.54	0.30	0.70	99.72
LR-02-A	53	465391	6725755	Torres	1	55.94	1.30	14.45	0.00	10.17	0.13	3.85	6.38	2.82	2.65	0.28	1.80	99.77
LR-04-A	53	465957	6738398	Torres	1	55.65	1.33	14.29	0.01	10.39	0.15	4.08	7.11	2.63	2.34	0.29	1.50	99.77
LBC-12	99	485761	6740538	Torres	1	55.42	1.31	14.33	0.00	10.50	0.14	4.20	6.69	2.91	2.37	0.28	1.60	99.75
SG-124Q	225	566506	6735037	Torres	1	53.08	1.24	15.49	0.01	10.65	0.15	4.45	8.26	2.53	1.99	0.20	1.70	99.75
LBC-56	172	485425	6722218	Torres	1	54.64	1.23	14.28	0.01	9.81	0.14	4.61	7.88	2.05	1.63	0.26	3.20	99.74
SG-125Q	232	566662	6735194	Torres	1	54.85	1.23	14.14	0.01	10.52	0.14	4.72	7.97	2.51	2.02	0.20	1.40	99.71
BR-08	117	580519	6745276	Torres	1	53.52	1.18	14.73	0.02	10.94	0.17	5.20	8.50	2.42	1.72	0.20	1.20	99.80
LBC-46	24	558442	6694631	Torres	1	55.85	1.07	13.90	0.04	9.73	0.15	5.39	7.81	1.93	1.05	0.15	2.70	99.77
BR-07	95	581642	6744356	Torres	1	53.35	1.18	14.65	0.02	10.81	0.17	5.55	8.65	2.24	1.57	0.20	1.40	99.79
SG-6	228	322854	6726872	Torres	1	51.86	1.11	14.89	0.03	10.58	0.15	5.74	9.20	2.19	1.70	0.14	2.10	99.69
SG-106Q	27	537300	6711178	Torres	1	52.08	1.17	14.95	0.02	10.58	0.16	6.38	9.62	2.04	1.32	0.16	1.20	99.68
SG-103Q	198	514217	6709776	Torres	1	51.71	1.19	14.75	0.02	10.64	0.17	6.41	8.59	2.37	1.54	0.17	2.20	99.76
CT-3	79	396874	6750864	Torres	1	50.56	1.00	14.77	0.01	10.27	0.18	6.53	9.92	1.97	1.06	0.14	3.30	99.71
SG-102Q	216	512193	6708245	Torres	1	50.68	1.19	14.98	0.02	10.73	0.17	6.57	9.52	2.18	1.42	0.17	2.10	99.73
LBC-78C	167	446604	6789975	Torres	1	50.65	1.09	14.68	0.02	11.43	0.23	6.67	9.45	2.53	1.36	0.15	1.50	99.76
CT-1-B	79	396874	6750864	Torres	1	50.14	0.97	14.86	0.01	9.89	0.15	6.74	9.93	2.01	0.79	0.13	4.10	99.72
LR14-B	144	464115	6751292	Torres	1	50.38	0.97	14.94	0.02	10.03	0.14	6.99	9.68	2.28	1.23	0.13	2.90	99.69
LR-14A	144	464115	6751292	Torres	1	49.40	1.00	15.17	0.02	10.40	0.17	7.08	10.11	2.08	1.02	0.13	3.10	99.68
SG-123Q	185	566305	6734415	Torres	1	51.12	0.92	14.75	0.04	10.00	0.16	7.44	10.42	1.96	0.95	0.12	1.80	99.68
SM-57	69	413484	6760789	Torres	2	50.00	1.06	14.76	0.03	10.47	0.13	6.21	9.02	2.04	1.22	0.14	4.70	99.78
LR-15-A	230	464324	6752965	Torres	2	48.69	1.06	15.02	0.03	10.51	0.18	6.38	9.94	1.66	1.14	0.14	5.00	99.75
SM-55	78	410568	6770828	Torres	2	48.84	1.06	15.85	0.04	10.30	0.14	6.68	10.12	1.94	0.65	0.14	4.00	99.76
SG-80B	41	408877	6734554	Torres	2	46.39	1.16	14.82	0.03	10.90	0.16	6.79	10.23	1.97	0.54	0.20	6.50	99.69
SM-58*	52	407441	6746948	Torres	2	48.14	1.09	15.53	0.03	10.40	0.16	7.07	9.46	2.02	0.85	0.13	4.90	99.78
LR-7A	86	466053	6745005	Torres	2	50.65	0.95	14.58	0.03	10.24	0.16	7.12	10.29	2.04	0.67	0.12	2.90	99.75
LR-11-A	55	465785	6743253	Torres	2	50.91	1.17	14.42	0.04	11.08	0.17	7.14	9.81	2.03	1.06	0.16	1.70	99.69
BR-05B	25	589139	6731070	Torres	2	50.24	0.89	15.10	0.03	10.10	0.15	7.35	10.96	1.75	0.98	0.13	2.10	99.78
SG-119Q	40	589140	6731055	Torres	2	51.09	0.92	15.10	0.03	9.98	0.16	7.35	11.04	1.78	0.92	0.12	1.20	99.69
LR-7B	86	466053	6745005	Torres	2	48.85	0.90	14.94	0.03	10.20	0.15	7.44	9.71	2.31	0.98	0.11	4.10	99.72
LR-55A	50	466186	6742685	Torres	2	51.36	1.12	14.76	0.04	10.92	0.16	7.65	10.00	1.98	1.03	0.15	0.60	99.77
BR-05A*	25	589139	6731070	Torres	2	49.56	0.81	15.07	0.04	9.84	0.16	8.14	10.78	1.85	0.89	0.11	2.50	99.75

Amostra	Elev.	UTM E	UTM N	Fm.	Grupo	SiO2	TiO2	Al2O3	Cr2O3	Fe2O3(t)	MnO	MgO	CaO	Na2O	K2O	P2O5	LOI	SUM
						0.01	*0.01*	*0.01*	*0.002*	*0.04*	*0.01*	*0.01*	*0.01*	*0.01*	*0.01*	*0.01*		
LR-55B	50	466186	6742685	Torres	2	50.23	1.01	14.58	0.05	10.83	0.17	8.59	10.39	1.82	0.86	0.12	1.10	99.75
LR-12-A	43	469516	6741931	Torres	2	50.56	1.07	14.09	0.05	11.06	0.16	8.62	9.71	1.82	0.92	0.14	1.50	99.70
LR-48*	94	476590	6748279	Torres	2	50.31	1.06	14.22	0.05	11.37	0.17	8.77	9.69	1.88	0.96	0.14	1.10	99.72
SG-27	386	233075	6716743	Torres	3	53.12	1.78	12.45	0.00	14.58	0.19	3.37	6.67	2.58	2.44	0.23	2.30	99.71
SG-23	279	253576	6722998	Torres	3	53.05	1.83	12.67	0.00	14.92	0.18	3.42	6.63	2.62	1.98	0.24	2.20	99.74
SG-26*	350	232596	6716551	Torres	3	53.74	1.87	12.51	0.00	14.92	0.20	3.48	6.58	2.69	1.99	0.24	1.50	99.72
SG-95Q	183	700841	6803597	Torres	3	52.64	1.95	12.79	0.00	15.08	0.21	3.93	7.29	2.53	1.92	0.23	1.10	99.67
SG-25	295	231606	6716245	Torres	3	53.38	1.67	13.00	0.00	14.88	0.21	4.05	7.40	2.68	1.55	0.20	0.70	99.72
SG-96Q	190	698163	6876309	Torres	3	53.72	1.68	12.81	0.00	13.95	0.22	4.19	8.00	2.76	1.43	0.20	0.80	99.76
SG-7	274	322979	6727423	Torres	3	53.54	1.21	13.79	0.00	12.71	0.20	4.33	8.72	2.41	1.81	0.12	0.90	99.74
SG-20	138	251840	6732548	Torres	3	52.87	1.15	13.88	0.01	12.04	0.19	5.45	9.03	2.67	1.30	0.11	1.00	99.70
BR-16B	430	579172	6750312	VDS	1	49.91	1.04	13.99	0.01	10.43	0.13	3.67	8.99	2.13	0.87	0.16	**8.40**	99.73
GA-30	417	484805	6797738	VDS	1	52.24	1.21	14.00	0.01	12.11	0.19	5.38	8.90	2.54	1.53	0.17	1.50	99.78
BR-16C	430	579172	6750312	VDS	1	48.53	1.14	13.91	0.01	11.21	0.18	5.40	9.06	2.20	0.77	0.17	**7.20**	99.78
BR-15*	380	578766	6750296	VDS	1	51.26	1.12	14.31	0.01	11.65	0.20	5.52	8.01	2.66	2.16	0.17	2.70	99.77
BR-14	327	578567	6749559	VDS	1	52.70	1.19	14.03	0.01	11.82	0.18	5.57	8.90	2.41	1.26	0.17	1.50	99.74
LBC-16A	432	487089	6747089	VDS	1	51.74	1.22	14.30	0.00	12.21	0.21	5.69	8.91	2.33	1.21	0.18	1.70	99.70
SG-108Q	820	580333	6752548	VDS	1	54.81	1.09	13.77	0.04	9.77	0.15	5.82	8.21	1.69	1.05	0.15	**3.20**	99.75
BR-10*	184	578960	6748867	VDS	2	59.21	1.24	13.43	<0.002	9.57	0.14	2.46	6.19	2.46	2.16	0.25	2.70	99.81
LR-18-B*	349	465352	6754868	VDS	2	56.84	1.46	13.10	<0.002	13.03	0.18	2.97	6.69	2.52	2.55	0.22	0.20	99.76
LR-16*	290	464947	6754332	VDS	2	52.90	1.42	13.21	0.00	13.89	0.18	3.44	5.86	2.98	2.61	0.18	**3.10**	99.77
LBC-19	494	487072	6750458	VDS	2	54.41	1.45	13.25	0.00	13.48	0.19	3.79	7.13	2.51	2.16	0.20	1.20	99.77
BR-11	202	578784	6749058	VDS	2	54.17	1.43	13.38	0.00	13.16	0.18	3.98	7.07	2.71	2.37	0.21	1.10	99.76
BR-13A	256	577936	6749602	VDS	2	51.72	1.35	12.67	0.00	13.22	0.14	4.02	7.72	1.99	1.89	0.16	**4.90**	99.78
GA-22	543	486323	6796834	VDS	2	53.19	1.44	13.42	0.00	12.73	0.18	4.48	8.47	2.45	1.22	0.19	2.00	99.77
BR-27B	862	580158	6752932	VDS	2	52.59	1.37	13.30	0.00	12.39	0.18	4.53	8.22	2.39	1.21	0.20	**3.40**	99.78
CT-5-A	530	470168	6787792	VDS	2	52.33	1.36	13.76	0.00	12.62	0.19	4.68	8.50	2.32	0.69	0.19	**3.10**	99.74
GA-14B	625	488882	6795558	VDS	2	52.09	1.37	13.36	0.00	12.34	0.18	4.69	8.72	2.44	0.60	0.19	**3.80**	99.78
BR-25	833	580445	6752802	VDS	2	53.16	1.41	13.58	0.00	12.57	0.18	4.69	8.68	2.53	1.06	0.19	1.70	99.75
LR-38-A	524	483052	6796353	VDS	2	53.39	1.41	13.65	0.00	12.44	0.19	4.70	8.78	2.53	0.78	0.18	1.70	99.75
GA-24	470	485995	6797200	VDS	2	52.20	1.30	13.91	0.00	12.95	0.19	4.73	8.56	2.14	1.38	0.18	2.20	99.74
LBC-71	273	458473	6755667	VDS	2	53.20	1.26	13.07	<0.002	13.14	0.20	4.81	8.98	2.20	0.61	0.15	2.10	99.72

Amostra	Elev.	UTM E	UTM N	Fm.	Grupo	SiO2	TiO2	Al2O3	Cr2O3	Fe2O3(t)	MnO	MgO	CaO	Na2O	K2O	P2O5	LOI	SUM
						0.01	*0.01*	*0.01*	*0.002*	*0.04*	*0.01*	*0.01*	*0.01*	*0.01*	*0.01*	*0.01*		
SM-23	466	451212	6814400	VDS	2	52.34	1.34	13.51	0.00	12.79	0.19	4.87	8.76	2.33	0.76	0.17	2.80	99.86
IT-05A				VDS	2	52.81	1.42	13.97	0.00	12.72	0.19	4.93	8.40	2.75	1.56	0.17	0.80	99.72
LR-23-A	465	466941	6757812	VDS	2	53.07	1.17	14.81	0.01	11.72	0.18	5.01	8.98	2.43	1.73	0.16	0.50	99.77
SG-8b*	312	322915	6727699	VDS	2	52.15	1.34	13.81	0.01	12.54	0.17	5.08	8.51	2.48	1.77	0.16	1.80	99.82
LBC-25	385	487593	6752204	VDS	2	52.22	1.37	13.13	0.00	13.40	0.20	5.26	9.32	2.46	1.25	0.19	0.90	99.70
BR-24	711	579511	6751658	VDS	2	52.39	1.32	13.52	0.01	12.64	0.18	5.30	8.72	2.36	1.47	0.17	1.70	99.78
BR-21A	735	579780	6751935	VDS	2	51.94	1.36	13.67	0.01	12.62	0.19	5.31	9.09	2.45	1.02	0.18	1.90	99.74
LBC-97	437	340003	6733201	VDS	2	51.64	1.34	13.59	0.01	12.34	0.17	5.44	8.93	2.30	0.69	0.17	**3.10**	99.72
CT-4-B	231	386610	676350	VDS	2	52.61	1.03	14.09	0.00	11.88	0.19	5.73	9.32	2.24	0.79	0.12	1.70	99.70
BR-19A	535	579390	6750567	VDS	3	55.56	1.88	11.73	<0.002	13.22	0.21	2.15	4.19	2.53	4.64	0.26	**3.40**	99.77
IT-08				VDS	3	55.74	1.74	13.00	<0.002	13.64	0.20	2.77	5.86	2.73	2.42	0.21	1.40	99.71
SM-29*	595	406232	6838756	VDS	3	53.05	1.90	12.09	<0.002	16.37	0.21	2.88	5.97	2.62	2.16	0.28	2.20	99.73
LBC-10	368	486100	6737230	VDS	3	55.53	1.83	12.54	0.00	14.69	0.18	2.89	6.51	2.46	2.16	0.21	0.70	99.70
LBC-8	422	491750	6731364	VDS	3	54.80	1.83	12.86	0.00	14.72	0.19	2.92	6.65	2.33	1.97	0.22	1.30	99.79
SM-48	575	399859	6787433	VDS	3	55.15	1.79	12.29	0.00	14.97	0.19	2.92	6.39	2.63	2.55	0.29	0.60	99.77
LBC-9	464	491756	6731836	VDS	3	55.39	1.75	12.63	0.00	14.15	0.18	2.95	6.75	2.53	2.17	0.22	1.00	99.72
BR-17A	470	579542	6749982	VDS	3	55.49	1.73	11.90	<0.002	13.98	0.20	2.96	5.99	2.85	2.72	0.25	1.70	99.77
SM-49	597	399596	6787769	VDS	3	53.57	1.91	12.35	<0.002	16.08	0.21	2.97	6.80	2.93	1.75	0.27	0.90	99.74
BR-17B	470	579542	6749982	VDS	3	55.95	1.69	12.97	<0.002	13.65	0.18	3.01	6.47	2.67	2.45	0.24	0.50	99.78
LBC-6	335	491136	6730593	VDS	3	54.63	1.83	12.61	0.00	14.68	0.19	3.07	6.52	2.44	2.24	0.20	1.30	99.71
LBC-82A	153	448681	6789935	VDS	3	52.97	1.59	13.42	<0.002	14.04	0.18	3.23	5.76	2.59	3.64	0.22	2.10	99.74
LBC-81	377	443332	6796021	VDS	3	54.35	1.71	13.62	0.00	13.05	0.19	3.51	7.05	2.82	2.29	0.28	0.90	99.77
LBC-43	727	481297	6926014	VDS	3	52.54	1.85	12.85	0.00	14.74	0.20	3.96	8.07	2.56	1.15	0.25	1.60	99.77
IT-2				VDS	3	49.55	1.94	13.15	<0.002	15.28	0.22	4.16	7.69	2.50	0.73	0.25	**4.20**	99.67
LR-27-B	596	467971	6759967	VDS	3	51.11	1.52	13.44	<0.002	13.80	0.21	4.42	7.95	2.12	1.40	0.19	**3.50**	99.66
SM-19	372	455676	6805376	VDS	3	52.40	1.60	13.39	0.01	13.83	0.21	4.50	7.97	2.51	1.51	0.25	1.50	99.68
SG-120	520	579471	6750289	VDS	3	50.53	1.77	14.48	0.02	12.12	0.16	5.51	9.41	2.44	1.17	0.20	1.90	99.71
SM-38	430	342961	6834955	Palmas	SM	69.51	0.70	12.45	0.00	5.71	0.05	0.33	1.47	2.45	5.25	0.18	1.80	99.90
SG-10v	488	321356	6729035	Palmas	SM	70.06	0.70	11.95	0.00	6.35	0.07	0.47	1.91	2.47	4.86	0.18	0.80	99.83
SG-94Q	429	711449	6762328	Palmas	Sm	69.78	0.72	12.58	<0.002	5.60	0.07	0.54	1.99	2.80	4.73	0.20	0.80	99.81
SM-39	448	342369	6829773	Palmas	SM	69.70	0.67	12.28	0.00	5.97	0.08	0.55	1.67	2.66	5.04	0.19	1.10	99.91
SG-4*	436	332614	6729157	Palmas	SM	69.43	0.72	12.40	<0.002	5.66	0.06	0.61	1.06	2.09	5.04	0.17	2.60	99.84

Amostra	Elev.	UTM E	UTM N	Fm.	Grupo	SiO2	TiO2	Al2O3	Cr2O3	Fe2O3(t)	MnO	MgO	CaO	Na2O	K2O	P2O5	LOI	SUM
						0.01	*0.01*	*0.01*	*0.002*	*0.04*	*0.01*	*0.01*	*0.01*	*0.01*	*0.01*	*0.01*		
SG-15	503	242590	6731533	Palmas	SM	69.34	0.67	12.13	<0.002	5.43	0.05	0.78	1.44	2.33	4.65	0.17	2.90	99.89
SG-18	333	248952	6729976	Palmas	SM	67.88	0.69	12.09	<0.002	5.70	0.09	0.78	2.33	2.73	3.75	0.18	3.60	99.82
SG-16*	495	243333	6729632	Palmas	SM	69.04	0.65	12.13	<0.002	5.06	0.05	0.82	0.79	1.99	5.48	0.17	3.70	99.88
SG-93Q	400	712960	6760595	Palmas	SM	69.34	0.73	12.11	<0.002	5.21	0.06	0.84	1.43	2.36	4.62	0.19	2.90	99.79
SM-42	496	347399	6821987	Palmas	SM	68.64	0.67	12.38	0.00	5.63	0.08	0.85	1.44	2.23	5.26	0.19	2.50	99.87
SM-40	555	343104	6826858	Palmas	SM	68.65	0.68	12.38	0.00	6.01	0.09	0.92	1.80	2.60	4.76	0.20	1.80	99.89
SG-10p	488	321356	6729035	Palmas	SM	67.29	0.71	12.28	0.00	6.26	0.09	0.82	2.42	2.84	3.76	0.19	3.20	99.87
BR-23	707	579500	6751613	Palmas	CX	65.63	0.84	12.68	0.00	6.07	0.10	1.02	3.02	2.77	3.67	0.27	3.80	99.87
BR-41B	667	579507	6751188	Palmas	CX	67.72	0.85	12.61	<0.002	6.27	0.09	0.87	1.10	2.82	6.01	0.27	1.30	99.91
GA-07	647	488839	6795526	Palmas	CX	68.96	0.85	11.95	0.00	6.06	0.10	1.13	2.76	2.59	4.46	0.25	0.80	99.91
LBC-33A	655	489066	6795500	Palmas	CX	69.24	0.85	12.15	0.00	6.48	0.11	1.16	2.96	2.69	3.90	0.25	0.10	99.89
BR-41C	667	579507	6751188	Palmas	CX	66.71	0.86	12.82	0.00	5.89	0.11	1.01	2.95	2.91	3.58	0.27	2.80	99.91
LR-35-A	530	470168	6787792	Palmas	CX	68.41	0.86	12.47	0.00	6.08	0.11	0.99	2.63	2.94	4.25	0.26	0.90	99.90
LBC-68A	402	340415	6761251	Palmas	CX	67.08	0.87	12.66	0.00	6.33	0.08	0.95	2.14	2.42	4.82	0.25	2.30	99.90
LBC-68B	402	340415	6761251	Palmas	CX	67.28	0.87	12.86	0.00	5.84	0.11	1.46	2.86	2.76	4.07	0.26	1.50	99.87
CPM-2-P	655	489066	6795500	Palmas	CX	67.56	0.87	12.09	0.01	7.45	0.10	1.30	3.06	2.73	3.95	0.25	0.50	99.87
LBC-31	617	490438	6785509	Palmas	CX	67.62	0.87	12.17	0.00	6.37	0.10	1.27	2.74	2.45	4.29	0.25	1.70	99.83
Jade 1-P	666	489062	6801738	Palmas	CX	67.78	0.87	12.17	0.01	7.50	0.11	1.20	3.09	2.80	3.88	0.26	0.20	99.87
SG-33	657	468143	6780217	Palmas	CX	68.20	0.87	12.09	<0.002	6.52	0.09	0.97	2.88	2.63	3.80	0.24	1.60	99.89
LBC-33B	655	489066	6795500	Palmas	CX	68.85	0.87	12.23	0.00	6.11	0.10	1.24	3.04	2.84	3.82	0.26	0.50	99.86
GA-03P	652	489079	6795474	Palmas	CX	68.88	0.87	12.13	0.00	6.05	0.10	1.21	2.96	2.72	3.99	0.26	0.70	99.87
BR-29B	897	579851	6752918	Palmas	CX	67.79	0.87	12.43	0.00	5.69	0.10	1.52	2.25	2.61	4.28	0.27	2.10	99.91
LBC-54A	708	492355	6796437	Palmas	CX	66.83	0.88	12.79	0.00	6.05	0.11	1.29	2.78	2.71	4.48	0.27	1.70	99.89
SG-121Q	543	579389	6750499	Palmas	CX	66.95	0.88	12.98	<0.002	6.14	0.09	0.81	1.62	2.35	4.92	0.25	2.80	99.79
BR-20A	546	579390	6750696	Palmas	CX	67.18	0.88	12.91	0.00	6.29	0.09	1.20	2.47	2.91	4.25	0.28	1.40	99.86
LBC-87B	487	420504	6810792	Palmas	CX	67.53	0.88	12.46	0.00	6.10	0.09	1.14	2.76	2.50	4.41	0.26	1.70	99.83
CPM-1-P	655	489066	6795500	Palmas	CX	67.74	0.88	12.13	0.00	6.85	0.11	1.19	3.02	2.82	3.95	0.26	0.90	99.85
CPM-4-P	655	489066	6795500	Palmas	CX	67.78	0.88	12.19	0.00	6.82	0.11	1.24	3.05	2.77	4.01	0.26	0.80	99.91
Jade 10	666	489062	6801738	Palmas	CX	68.01	0.88	12.25	0.00	6.93	0.11	1.15	2.99	2.85	3.97	0.25	0.50	99.89
LBC-3-A	666	489062	6801738	Palmas	CX	68.56	0.88	12.15	0.00	6.61	0.11	1.24	3.20	2.71	3.69	0.25	0.50	99.90
Jade 11	666	489062	6801738	Palmas	CX	67.87	0.88	12.21	0.00	7.28	0.11	1.34	3.03	2.90	3.88	0.26	0.10	99.87
LBC-54B	708	492355	6796437	Palmas	CX	66.41	0.89	12.87	0.00	6.05	0.11	1.52	2.95	2.63	4.23	0.28	1.90	99.84

Amostra	Elev.	UTM E	UTM N	Fm.	Grupo	SiO2	TiO2	Al2O3	Cr2O3	Fe2O3(t)	MnO	MgO	CaO	Na2O	K2O	P2O5	LOI	SUM
						0.01	*0.01*	*0.01*	*0.002*	*0.04*	*0.01*	*0.01*	*0.01*	*0.01*	*0.01*	*0.01*		
GA-10	747	491862	6795360	Palmas	CX	66.51	0.89	12.87	0.00	5.99	0.11	1.22	3.10	2.86	4.30	0.27	1.80	99.92
LBC-87A	487	420504	6810792	Palmas	CX	67.61	0.89	12.71	0.00	6.22	0.11	1.18	3.06	2.81	4.39	0.26	0.60	99.84
SM-32	530	389376	6846306	Palmas	CX	67.78	0.89	12.22	0.00	7.06	0.08	0.75	2.04	2.39	4.72	0.23	1.70	99.86
CPM-3-B	655	489066	6795500	Palmas	CX	65.72	0.90	12.60	0.01	8.06	0.10	1.24	2.74	2.80	4.14	0.27	1.30	99.87
LBC-60	621	441937	6758846	Palmas	CX	66.18	0.90	13.06	0.00	6.23	0.10	1.44	3.14	2.79	4.12	0.26	1.70	99.92
BR029A	897	579851	6752918	Palmas	CX	66.38	0.90	12.84	0.00	6.10	0.11	1.23	3.33	3.46	2.78	0.27	2.50	99.90
GA-04	702	487754	6795526	Palmas	CX	66.91	0.90	13.10	0.00	5.93	0.07	0.92	2.14	2.54	4.19	0.26	2.90	99.86
GA-13	767	492287	6794956	Palmas	CX	67.01	0.90	12.76	0.00	5.90	0.09	1.31	3.03	2.87	4.14	0.28	1.60	99.89
LR-54B	676	488057	6802763	Palmas	CX	67.03	0.90	12.13	0.00	7.11	0.11	1.21	2.97	2.83	4.03	0.25	1.30	99.87
CPM-4-B	655	489066	6795500	Palmas	CX	67.05	0.90	12.47	0.01	7.53	0.11	1.18	2.79	2.65	4.37	0.27	0.60	99.93
IT-04				Palmas	CX	67.39	0.90	13.01	<0.002	5.86	0.08	1.04	2.71	3.03	4.03	0.25	1.50	99.80
SG-34	613	468092	6779894	Palmas	CX	66.34	0.91	13.06	<0.002	6.21	0.10	1.42	3.26	2.78	4.07	0.26	1.50	99.91
LBC-59	657	448591	6761318	Palmas	CX	66.70	0.91	13.06	0.00	6.23	0.12	1.31	3.14	2.89	3.97	0.27	1.30	99.90
Jade 1-V	666	489062	6801738	Palmas	CX	66.81	0.91	12.60	0.00	6.74	0.11	1.28	3.08	3.02	3.98	0.25	1.10	99.88
GA-11	750	492004	6795333	Palmas	CX	66.88	0.91	12.74	0.00	5.90	0.09	1.31	2.94	2.84	4.02	0.28	2.00	99.91
LR-54A	676	488057	6802763	Palmas	CX	67.21	0.91	12.17	0.01	7.95	0.11	1.33	3.20	2.87	3.72	0.25	0.20	99.92
GA-12	752	492231	6795245	Palmas	CX	67.07	0.92	13.05	0.00	5.96	0.11	0.95	2.50	2.80	4.09	0.27	2.20	99.92
GA-16	635	488643	6795622	Palmas	CX	67.24	0.92	12.74	0.00	6.30	0.11	1.00	2.50	2.63	4.54	0.27	1.70	99.95
CPM-4-V	655	489066	6795500	Palmas	CX	66.24	0.93	12.88	0.00	7.54	0.13	1.17	2.87	2.99	3.96	0.26	0.90	99.88
LR-28-A	715	467051	6763368	Palmas	CX	66.24	0.93	12.78	0.00	6.51	0.10	1.33	2.82	2.83	4.00	0.27	2.10	99.91
LR-54D	676	488057	6802763	Palmas	CX	66.26	0.93	12.66	<0.002	7.04	0.11	1.39	3.07	2.71	4.46	0.26	1.00	99.89
IT-01A				Palmas	CX	67.63	0.93	12.60	<0.002	6.25	0.10	1.34	3.14	3.15	3.54	0.25	0.80	99.73
Jade 12	666	489062	6801738	Palmas	CX	65.58	0.94	12.91	0.00	6.88	0.11	1.28	3.34	2.83	4.24	0.27	1.50	99.88
SM-54	438	406478	6775318	Palmas	CX	65.86	0.94	12.75	0.00	6.68	0.08	1.29	2.99	2.76	4.64	0.25	1.60	99.84
CPM-2-V	655	489066	6795500	Palmas	CX	65.86	0.94	13.25	0.00	6.92	0.14	1.36	3.14	3.12	4.22	0.28	0.60	99.83
GA-37	771	494494	6795204	Palmas	CX	65.25	0.95	12.87	0.00	6.38	0.11	1.36	3.48	3.55	2.94	0.27	2.70	99.86
LR-54C	676	488057	6802763	Palmas	CX	65.37	0.95	12.87	0.00	7.20	0.11	1.57	3.09	2.72	4.32	0.27	1.40	99.87
LR-33-B	788	480998	6788340	Palmas	CX	65.49	0.95	12.78	0.00	6.41	0.11	1.38	3.49	3.47	2.80	0.26	2.70	99.84
LR-53B	520	482846	6762862	Palmas	CX	65.57	0.95	12.84	0.00	6.97	0.09	1.48	2.48	2.66	4.40	0.27	2.20	99.91
SG35-A	649	469474	6778918	Palmas	CX	65.44	0.96	13.15	<0.002	6.47	0.11	1.43	3.37	3.07	4.06	0.25	1.60	99.91
LR-29-A	733	467842	6766734	Palmas	CX	66.05	0.96	13.23	0.00	6.13	0.08	0.93	2.45	2.86	4.02	0.26	2.90	99.87
GA-35B	850	494631	6796310	Palmas	CX	67.66	0.96	12.92	0.00	6.09	0.09	1.15	3.02	3.05	3.68	0.26	1.00	99.88

Amostra	Elev.	UTM E	UTM N	Fm.	Grupo	SiO2	TiO2	Al2O3	Cr2O3	Fe2O3(t)	MnO	MgO	CaO	Na2O	K2O	P2O5	LOI	SUM
						0.01	*0.01*	*0.01*	*0.002*	*0.04*	*0.01*	*0.01*	*0.01*	*0.01*	*0.01*	*0.01*		
SM-16A	690	470398	6807558	Palmas	CX	65.57	0.97	12.19	0.00	7.63	0.18	1.64	2.72	2.43	4.68	0.26	1.60	99.87
LR-32-A	751	480974	6788912	Palmas	CX	65.83	0.97	13.05	0.00	6.48	0.10	1.39	3.14	2.96	4.19	0.27	1.50	99.88
LBC-53	720	489511	6801745	Palmas	CX	66.97	0.97	13.00	0.00	6.47	0.09	1.19	2.78	2.91	3.84	0.27	1.40	99.89
LBC-61	444	432831	6751387	Palmas	CX	64.02	0.99	12.33	0.00	7.26	0.11	1.13	3.94	2.70	2.08	0.27	5.00	99.83
SM-16B	690	470398	6807558	Palmas	JC	62.36	1.01	12.63	0.00	7.66	0.16	1.62	4.02	2.40	2.82	0.28	4.90	99.86
LBC-32C	666	489062	6801738	Palmas	JC	62.50	1.01	14.01	0.00	7.04	0.11	1.57	3.97	2.54	4.17	0.28	2.60	99.80
GA-03V	652	489079	6795474	Palmas	JC	62.60	1.00	14.53	0.00	6.78	0.13	1.48	3.31	3.34	4.58	0.29	1.80	99.84
LBC-32B	666	489062	6801738	Palmas	JC	64.71	1.01	13.23	0.00	7.05	0.12	1.49	3.20	3.00	4.30	0.29	1.50	99.90
GA-34	890	494773	6796310	Palmas	JC	64.99	1.06	13.14	0.00	7.31	0.15	1.52	3.48	3.15	3.57	0.29	1.20	99.86
SM-50	510	403239	6782073	Palmas	JC	65.03	1.01	13.30	<0.002	6.80	0.10	1.43	3.57	3.06	3.78	0.27	1.50	99.85
SM-27	512	422567	6830984	Palmas	JC	65.25	1.04	12.83	0.00	7.32	0.12	1.47	3.50	3.12	3.74	0.27	1.20	99.86
LBC-17*	548	487999	6748244	Palmas	JC	66.52	1.06	12.80	0.00	7.59	0.07	0.86	2.16	2.40	4.00	0.28	2.10	99.84
SM-51	465	404116	6780824	Palmas	JC	67.40	1.02	12.13	0.00	7.92	0.13	0.79	2.65	2.67	4.24	0.27	0.70	99.92
LBC-50*	782	481976	6928332	Palmas	AG	66.29	1.05	13.43	0.00	6.60	0.08	0.99	2.16	2.87	3.88	0.32	2.20	99.87
LBC-49	835	483059	6929942	Palmas	AG	66.49	1.08	12.89	0.00	6.71	0.12	1.24	3.28	3.18	4.05	0.32	0.50	99.86
LBC-40	918	483167	6918854	Palmas	AG	66.58	1.04	12.55	0.00	6.73	0.09	1.30	3.27	3.11	3.69	0.32	1.20	99.88
LBC-51	915	490969	6874828	Esmeralda	-	50.40	1.36	13.20	0.00	13.79	0.26	6.15	10.43	2.44	0.74	0.16	0.9	99.83
LBC-39	896	490648	6873983	Esmeralda	-	49.25	1.26	14.32	0.00	13.49	0.20	6.56	11.00	2.31	0.77	0.14	0.6	99.90
LBC-38	891	491059	6863473	Esmeralda	-	53.9	1.72	13.02	0	15	0.18	2.32	5.34	2.45	2.74	0.27	2.8	99.75
LBC-52	923	504391	6843863	Esmeralda	-	52.41	1.68	13.31	0.005	14.26	0.22	4.87	8.49	2.71	1.24	0.21	0.3	99.73
SG-97Q	132	688034	6896040	High-Ti	-	49.89	3.46	12.50	<0.002	15.68	0.22	4.29	8.24	2.71	0.97	0.37	1.30	99.63
SG-98Q	247	767576	6862142	High-Ti	-	50.42	2.33	12.62	0.01	15.28	0.21	4.73	8.72	2.57	1.56	0.25	1.00	99.70
SM-37	508	333073	6859775	High-Ti	-	49.58	2.22	12.91	0.00	14.63	0.22	5.23	9.45	2.40	1.23	0.25	1.50	99.62
LBC-55	137	484886	6754550	Dike	-	51.69	1.41	13.26	0.00	13.86	0.17	5.37	9.45	2.66	0.97	0.16	0.70	99.70
IT-2-DQ				Dike	-	51.75	1.65	13.13	0.01	14.78	0.22	4.76	8.93	2.89	0.61	0.20	0.80	99.73
LR-38-B	524	483052	6796353	Dike	-	52.32	1.36	13.84	0.00	12.52	0.19	5.18	9.37	2.46	0.84	0.18	1.50	99.76
LR-50	75	479441	6752617	Dike	-	50.33	1.43	13.57	0.00	14.42	0.22	5.43	9.07	2.66	1.01	0.16	1.40	99.70
Bas-106	0	589206	6731133	Dike	-	50.39	0.90	15.15	0.00	10.81	0.17	7.32	11.00	1.80	0.95	0.12	1.10	99.71
SG-13a	106	306649	6707653	Sill	-	52.17	1.29	13.32	0.01	12.73	0.18	5.25	8.79	2.55	1.31	0.13	2.00	99.73
Bas-105	14	600945	6739279	Sill	-	53.27	1.82	12.74	0.00	15.73	0.21	3.21	5.08	3.11	2.61	0.27	1.60	99.65

Amostra	Fm.	Grupo	Hf	Ta	Th	U	Sc	V	Ni	Rb	Sr	Y	Zr	Nb	Ba	Be	Co
			0.1	0.1	0.2	0.1	1	8	20	0.1	0.5	0.1	0.1	0.1	1	1	0.2
LBC-1	Torres	1	6.80	1.40	8.80	1.90	29.00	264.00	22.00	91.50	283.80	32.90	244.80	22.30	627.00	3.00	32.70
LR-02-A	Torres	1	5.90	1.30	8.90	1.60	30.00	253.00	27.00	87.80	272.90	28.10	211.00	19.60	619.00	1.00	33.00
LR-04-A	Torres	1	5.50	1.30	8.50	1.40	31.00	257.00	28.00	81.50	275.10	27.10	203.40	18.50	585.00	1.00	33.90
LBC-12	Torres	1	6.00	1.40	8.00	1.40	29.00	279.00	21.00	86.20	299.40	30.40	220.60	20.50	608.00	2.00	36.00
SG-124Q	Torres	1	4.60	0.90	6.10	0.70	31.00	232.00	25.90	50.50	277.90	28.40	175.00	13.00	391.00	1.00	41.70
LBC-56	Torres	1	5.40	1.30	8.00	1.70	29.00	265.00	9.00	32.00	320.60	29.10	205.90	18.50	611.00	<1	34.00
SG-125Q	Torres	1	4.20	0.70	5.30	1.50	32.00	263.00	17.10	68.00	275.10	27.40	164.10	11.40	475.00	2.00	41.50
BR-08	Torres	1	3.60	0.90	5.80	0.90	33.00	241.00	73.00	48.80	234.20	25.90	153.20	11.90	341.00	1.00	38.00
LBC-46	Torres	1	5.60	0.90	8.90	1.10	30.00	232.00	17.60	23.20	288.20	27.20	178.90	13.10	406.00	2.00	36.30
BR-07	Torres	1	4.20	0.90	6.20	1.00	33.00	247.00	77.00	47.00	246.20	26.30	155.10	12.50	345.00	<1	40.90
SG-6	Torres	1	3.80	0.60	4.30	0.70	34.00	267.00	55.90	59.60	229.40	24.70	138.90	8.30	337.00	2.00	39.20
SG-106Q	Torres	1	3.90	0.60	4.90	0.50	33.00	245.00	22.50	37.90	257.80	23.40	140.30	11.80	332.00	1.00	44.00
SG-103Q	Torres	1	3.70	0.60	4.60	0.60	33.00	245.00	23.40	38.40	262.00	25.10	136.00	11.60	338.00	1.00	44.60
CT-3	Torres	1	3.00	0.40	3.90	0.80	36.00	290.00	98.00	33.10	282.70	23.90	124.60	7.00	325.00	2.00	43.80
SG-102Q	Torres	1	3.60	0.70	5.00	0.60	34.00	250.00	27.30	43.50	271.90	24.40	136.30	12.00	353.00	<1	44.00
LBC-78C	Torres	1	3.30	0.40	4.00	0.60	38.00	285.00	74.00	39.50	240.80	24.50	129.90	9.00	364.00	2.00	45.50
CT-1-B	Torres	1	2.90	0.50	3.90	0.70	35.00	279.00	96.00	28.00	256.80	20.80	120.30	7.30	311.00	2.00	43.80
LR14-B	Torres	1	3.40	0.60	3.70	0.80	35.00	253.00	94.00	24.60	253.50	20.90	113.30	7.10	348.00	<1	39.80
LR-14A	Torres	1	3.30	1.20	4.00	0.70	35.00	266.00	97.00	21.30	246.30	21.80	116.60	6.50	315.00	<1	38.40
SG-123Q	Torres	1	3.00	0.40	2.90	0.30	36.00	233.00	38.10	23.10	266.50	22.60	116.60	7.30	321.00	<1	46.00
SM-57	Torres	2	3.00	0.40	3.20	0.70	33.00	231.00	59.20	57.30	225.50	22.00	117.30	6.80	241.00	2.00	39.90
LR-15-A	Torres	2	3.30	0.40	4.10	0.70	35.00	231.00	114.00	42.10	138.90	21.00	106.80	7.20	260.00	<1	38.80
SM-55	Torres	2	3.30	0.50	4.10	0.80	32.00	244.00	72.80	16.30	225.90	21.70	124.40	7.50	242.00	<1	40.00
SG-80B	Torres	2	3.00	0.80	2.60	0.40	36.00	251.00	56.10	8.40	270.10	20.00	121.80	11.70	235.00	<1	43.90
SM-58*	Torres	2	2.90	0.40	2.90	0.70	35.00	294.00	70.40	34.30	214.70	20.80	101.80	6.50	216.00	2.00	44.20
LR-7A	Torres	2	3.20	0.60	3.20	0.60	34.00	256.00	89.00	21.10	247.00	19.60	109.80	6.80	236.00	<1	39.90
LR-11-A	Torres	2	3.40	0.60	3.70	0.90	37.00	276.00	99.00	32.20	230.10	22.00	106.70	8.30	256.00	<1	40.70
BR-05B	Torres	2	2.50	0.50	2.80	0.70	38.00	241.00	106.00	25.60	224.40	18.90	92.10	8.00	234.00	<1	41.40
SG-119Q	Torres	2	2.60	0.40	2.90	0.50	37.00	238.00	39.30	22.60	234.20	19.70	97.70	7.70	238.00	1.00	45.10
LR-7B	Torres	2	2.70	0.50	2.80	0.50	35.00	262.00	88.00	24.80	221.40	19.80	96.30	6.40	244.00	<1	39.80
LR-55A	Torres	2	3.30	0.90	3.80	0.90	38.00	278.00	119.00	32.30	234.70	21.20	124.80	8.70	265.00	<1	45.40
BR-05A*	Torres	2	2.00	0.40	3.00	0.50	38.00	236.00	119.00	17.70	204.80	17.20	80.20	6.30	198.00	<1	43.30

Amostra	Fm.	Grupo	Hf	Ta	Th	U	Sc	V	Ni	Rb	Sr	Y	Zr	Nb	Ba	Be	Co
			0.1	0.1	0.2	0.1	1	8	20	0.1	0.5	0.1	0.1	0.1	1	1	0.2
LR-55B	Torres	2	3.00	0.80	2.90	0.80	35.00	270.00	156.00	25.10	224.40	19.80	98.40	7.50	226.00	<1	46.40
LR-12-A	Torres	2	2.80	0.50	3.10	0.80	36.00	255.00	161.00	27.60	214.50	19.40	95.10	7.30	233.00	<1	46.40
LR-48*	Torres	2	3.00	0.50	3.70	0.70	36.00	254.00	61.70	27.30	225.30	20.20	104.80	7.20	240.00	1.00	47.40
SG-27	Torres	3	5.10	0.80	6.30	1.80	32.00	445.00	9.30	116.90	210.00	37.00	189.70	13.70	393.00	2.00	40.40
SG-23	Torres	3	5.30	1.00	6.80	1.60	34.00	465.00	10.40	75.50	235.60	38.90	198.80	14.60	408.00	1.00	43.70
SG-26*	Torres	3	5.30	1.00	6.50	2.00	33.00	471.00	10.40	75.40	217.00	38.90	197.00	14.20	385.00	<1	41.60
SG-95Q	Torres	3	4.90	0.70	6.00	1.40	37.00	459.00	9.90	76.50	187.70	39.80	184.00	12.40	342.00	2.00	44.60
SG-25	Torres	3	4.50	0.90	5.40	1.50	34.00	449.00	12.80	57.60	236.60	34.10	168.20	12.00	342.00	2.00	44.50
SG-96Q	Torres	3	4.50	0.60	4.30	1.80	36.00	390.00	7.80	53.00	189.90	39.50	164.70	9.40	299.00	<1	41.20
SG-7	Torres	3	3.50	0.50	4.10	1.10	39.00	381.00	19.40	54.90	219.00	24.70	125.80	8.10	324.00	1.00	45.40
SG-20	Torres	3	3.30	0.40	3.80	1.10	36.00	348.00	19.60	46.20	224.90	24.70	118.10	7.40	253.00	2.00	47.50
BR-16B	VDS	1	3.30	0.50	4.40	0.60	33.00	240.00	49.00	51.40	######	23.70	122.30	9.30	525.00		30.20
GA-30	VDS	1	4.10	0.60	4.90	0.70	-	300.00	52.00	45.70	239.60	27.00	145.40	-	390.00	-	43.60
BR-16C	VDS	1	3.60	0.40	5.10	1.10	37.00	300.00	56.00	12.30	256.10	29.70	137.80	9.60	368.00		46.40
BR-15*	VDS	1	3.50	0.50	4.50	0.70	34.00	265.00	43.00	81.50	221.60	24.40	123.30	10.00	507.00	<1	39.00
BR-14	VDS	1	4.40	0.60	5.20	1.00	37.00	287.00	43.00	36.60	227.00	27.60	141.00	9.80	348.00	1.00	43.60
LBC-1-A	VDS	1	4.70	0.60	5.00	0.80	36.00	342.00	43.00	28.70	247.10	30.60	160.30	11.90	411.00	1.00	49.70
SG-108Q	VDS	1	4.70	0.70	9.00	0.80	31.00	221.00	16.70	27.40	239.00	30.00	182.30	11.60	244.00	2.00	38.70
BR-10*	VDS	2	5.50	1.20	9.50	2.50	26.00	228.00	<20	96.90	239.50	32.00	197.40	14.50	540.00	2.00	24.60
LR-18-B*	VDS	2	5.60	0.90	8.80	1.80	35.00	325.00	27.00	79.90	214.50	32.90	181.10	13.40	516.00	2.00	37.30
LR-16*	VDS	2	4.10	0.60	5.60	1.80	41.00	301.00	16.60	79.40	133.20	26.50	143.10	9.20	449.00	<1	40.70
LBC-19	VDS	2	4.60	0.80	7.30	1.30	36.00	378.00	<20	82.70	208.50	33.70	185.00	13.30	432.00	2.00	45.20
BR-11	VDS	2	4.20	0.80	6.30	1.50	37.00	343.00	31.00	75.70	173.20	29.20	157.60	11.30	398.00	1.00	42.30
BR-13A	VDS	2	3.50	0.70	5.30	1.20	39.00	355.00	43.00	68.30	96.80	25.60	127.40	8.90	259.00	1.00	45.90
GA-22	VDS	2	4.40	0.70	5.80	1.40	-	389.00	35.00	36.50	237.30	29.80	145.80	-	343.00	-	40.80
BR-27B	VDS	2	3.90	0.70	5.00	1.40	34.00	392.00	30.00	34.70	231.50	29.60	145.20	11.40	198.00	2.00	41.20
CT-5-A	VDS	2	4.10	0.70	5.70	1.50	35.00	409.00	49.00	32.70	264.30	32.20	152.20	11.70	299.00	3.00	41.40
GA-14B	VDS	2	3.80	0.70	5.20	1.50	-	366.00	30.00	13.10	229.00	27.60	136.10	-	170.00	-	39.00
BR-25	VDS	2	4.00	0.70	5.40	1.50	35.00	411.00	40.00	30.00	225.50	30.90	154.00	11.70	344.00	1.00	40.40
LR-38-A	VDS	2	4.20	0.80	5.90	1.50	35.00	383.00	39.00	44.70	223.90	27.90	158.40	11.00	327.00	2.00	40.10
GA-24	VDS	2	4.20	0.70	5.60	1.00	-	333.00	46.00	43.90	251.30	29.90	155.70	-	391.00	-	48.40
LBC-71	VDS	2	3.10	0.50	4.70	1.20	41.00	366.00	46.00	35.70	226.10	26.40	126.60	8.50	210.00	<1	48.10

Amostra	Fm.	Grupo	Hf	Ta	Th	U	Sc	V	Ni	Rb	Sr	Y	Zr	Nb	Ba	Be	Co
			0.1	0.1	0.2	0.1	1	8	20	0.1	0.5	0.1	0.1	0.1	1	1	0.2
SM-23	VDS	2	4.00	0.80	5.20	1.50	33.00	362.00	7.30	32.00	250.60	29.70	153.20	11.80	273.00	2.00	40.00
IT-05A	VDS	2	4.10	0.70	5.40	1.40	35.00	352.00	13.70	54.50	210.50	29.90	149.00	10.50	313.00	<1	42.70
LR-23-A	VDS	2	4.20	0.60	5.40	0.90	35.00	253.00	48.00	54.60	252.60	26.40	135.20	10.10	394.00	<1	39.20
SG-8b*	VDS	2	3.80	0.70	4.80	1.30	35.00	358.00	16.30	69.00	238.80	31.90	150.00	11.30	334.00	<1	43.50
LBC-25	VDS	2	3.80	0.70	4.20	1.00	38.00	381.00	39.00	46.50	210.70	32.10	147.90	9.70	340.00	1.00	46.20
BR-24	VDS	2	2.60	0.60	4.60	1.00	35.00	283.00	49.00	43.50	171.10	22.10	109.40	8.40	246.00	1.00	32.30
BR-21A	VDS	2	3.60	0.60	4.90	1.10	36.00	327.00	43.00	35.40	207.20	24.30	121.90	10.40	250.00	1.00	37.90
LBC-97	VDS	2	3.90	0.70	4.80	1.20	35.00	369.00	47.00	20.20	266.00	32.50	143.30	10.70	287.00	<1	40.40
CT-4-B	VDS	2	2.70	0.50	4.00	0.70	39.00	322.00	44.00	32.10	255.40	23.50	112.90	6.60	263.00	<1	49.30
BR-19A	VDS	3	5.90	1.10	9.90	3.30	31.00	461.00	<20	134.30	39.70	41.60	211.30	16.20	526.00	2.00	35.70
IT-08	VDS	3	5.90	1.00	9.60	1.70	33.00	375.00	6.30	84.60	214.30	39.40	219.40	14.60	521.00	2.00	39.40
SM-29*	VDS	3	5.40	0.80	6.50	1.80	38.00	372.00	6.90	70.10	161.80	43.20	181.70	11.00	350.00	1.00	38.00
LBC-10	VDS	3	5.00	1.00	7.90	1.70	37.00	514.00	<20	78.00	230.80	48.30	196.10	13.10	482.00	2.00	56.20
LBC-8	VDS	3	4.90	0.80	7.50	1.80	37.00	505.00	<20	74.70	229.00	35.30	191.90	13.20	452.00	<1	48.10
SM-48	VDS	3	4.90	0.80	7.10	2.00	37.00	381.00	10.90	109.60	152.20	35.40	167.00	11.50	324.00	<1	37.60
LBC-9	VDS	3	5.10	1.00	7.60	2.00	35.00	476.00	<20	83.40	226.70	34.00	196.20	15.40	522.00	1.00	44.70
BR-17A	VDS	3	5.60	0.90	8.20	1.70	36.00	291.00	<20	83.20	119.20	35.10	202.60	15.40	512.00	2.00	36.70
SM-49	VDS	3	4.80	0.90	6.30	1.90	39.00	495.00	9.70	62.90	181.90	40.80	175.20	12.70	330.00	2.00	39.60
BR-17B	VDS	3	4.90	0.90	9.30	1.70	35.00	323.00	20.00	76.30	180.10	33.60	192.20	15.50	438.00	2.00	37.40
LBC-6	VDS	3	5.20	0.80	7.50	1.80	37.00	424.00	7.10	85.70	200.30	70.90	181.30	11.80	584.00	2.00	42.30
LBC-82A	VDS	3	5.00	0.70	7.80	1.70	36.00	425.00	27.00	103.10	152.90	36.90	206.70	13.30	618.00	<1	46.80
LBC-81	VDS	3	5.40	1.10	9.20	2.00	33.00	304.00	39.00	85.40	221.20	39.60	218.10	17.20	512.00	<1	36.80
LBC-43	VDS	3	4.60	0.90	6.10	1.50	37.00	454.00	30.00	62.10	197.80	36.50	175.60	11.60	348.00	4.00	42.60
IT-2	VDS	3	5.10	1.00	7.20	1.70	35.00	466.00	6.80	30.90	292.60	54.10	199.60	13.60	374.00	1.00	45.70
LR-27-B	VDS	3	4.30	0.70	6.30	1.30	37.00	369.00	35.00	91.90	259.80	32.00	142.70	12.60	685.00	1.00	38.50
SM-19	VDS	3	4.70	0.90	5.60	1.20	36.00	394.00	15.40	38.20	256.20	31.40	167.80	14.60	400.00	2.00	39.50
SG-120	VDS	3	4.40	0.70	3.80	0.70	25.00	309.00	46.50	33.20	340.70	26.60	166.30	11.50	330.00	1.00	45.60
SM-38	Palmas	SM	9.20	2.20	18.00	5.30	15.00	26.00	5.10	224.10	121.20	44.40	344.00	27.30	678.00	5.00	4.40
SG-10v	Palmas	SM	8.50	1.80	16.70	5.70	15.00	36.00	6.10	209.60	107.80	47.50	309.20	23.60	714.00	4.00	6.40
SG-94Q	Palmas	Sm	7.50	1.70	16.50	4.20	16.00	25.00	1.70	187.80	101.40	47.10	288.30	21.80	619.00	1.00	6.60
SM-39	Palmas	SM	8.40	1.80	18.00	5.10	16.00	31.00	2.10	197.30	90.30	48.20	285.90	20.40	646.00	4.00	5.20
SG-4*	Palmas	SM	8.80	1.80	17.10	5.00	16.00	46.00	3.70	244.60	77.40	137.40	333.70	25.40	790.00	6.00	5.70

Amostra	Fm.	Grupo	Hf 0.1	Ta 0.1	Th 0.2	U 0.1	Sc 1	V 8	Ni 20	Rb 0.1	Sr 0.5	Y 0.1	Zr 0.1	Nb 0.1	Ba 1	Be 1	Co 0.2
SG-15	Palmas	SM	8.20	1.90	17.40	5.60	15.00	27.00	2.90	214.90	94.60	61.20	319.40	24.20	702.00	4.00	5.90
SG-18	Palmas	SM	8.20	2.00	17.10	5.60	15.00	28.00	3.40	219.60	117.80	51.80	320.00	23.60	646.00	3.00	6.40
SG-16*	Palmas	SM	8.70	2.00	17.00	5.40	15.00	22.00	2.60	268.70	82.20	43.50	324.70	25.00	842.00	4.00	4.90
SG-93Q	Palmas	SM	8.00	1.80	16.60	3.60	15.00	32.00	1.80	187.60	88.70	39.60	289.10	21.90	594.00	5.00	5.80
SM-42	Palmas	SM	8.50	1.80	18.30	5.90	16.00	38.00	2.00	199.80	104.60	49.60	294.80	21.20	660.00	4.00	5.00
SM-40	Palmas	SM	8.50	2.00	18.00	5.10	16.00	29.00	7.30	186.10	94.10	49.70	298.50	22.40	664.00	5.00	5.40
SG-10p	Palmas	SM	9.10	1.80	16.70	5.20	15.00	35.00	7.60	218.30	113.40	48.20	303.90	22.90	671.00	2.00	6.70
BR-23	Palmas	CX	6.00	1.50	14.40	4.60	15.00	35.00	<20	143.50	127.70	31.30	211.60	16.40	493.00	3.00	7.70
BR-41B	Palmas	CX	7.10	1.60	15.10	4.80	16.00	53.00	<20	211.80	66.20	40.70	251.00	20.60	648.00	3.00	9.50
GA-07	Palmas	CX	5.90	1.50	12.80	4.60	-	86.00	20.00	181.90	130.90	34.60	218.60	-	565.00	-	11.50
LBC-33A	Palmas	CX	6.30	1.40	13.40	4.50	16.00	84.00	<20	167.20	149.50	34.50	233.40	18.90	587.00	3.00	12.00
BR-41C	Palmas	CX	7.00	1.70	13.90	5.10	16.00	57.00	<20	180.50	154.60	40.80	261.20	21.30	641.00	4.00	11.10
LR-35-A	Palmas	CX	6.60	1.60	14.30	5.30	16.00	93.00	<20	166.70	148.50	38.10	245.70	19.60	666.00	3.00	10.80
LBC-68A	Palmas	CX	6.80	1.60	14.80	4.60	16.00	70.00	3.30	213.70	145.10	36.20	253.40	21.60	687.00	<1	9.40
LBC-68B	Palmas	CX	6.90	1.60	14.40	5.20	17.00	69.00	<20	175.90	149.00	36.00	252.30	19.00	610.00	4.00	10.50
CPM-2-P	Palmas	CX	6.20	1.40	12.50	4.00	17.00	76.00	15.30	169.20	148.20	41.40	227.60	18.30	600.00	1.00	11.90
LBC-31	Palmas	CX	6.70	1.60	13.10	4.00	17.00	110.00	<20	180.50	130.60	41.80	231.20	18.80	641.00	4.00	13.40
Jade 1-P	Palmas	CX	6.40	1.50	13.20	4.10	18.00	86.00	16.20	159.50	149.70	35.90	236.40	18.80	581.00	4.00	12.10
SG-33	Palmas	CX	6.20	1.90	12.30	4.90	16.00	89.00	<20	157.20	142.80	56.00	225.10	18.30	603.00	4.00	15.30
LBC-33B	Palmas	CX	5.80	1.70	13.00	4.40	16.00	86.00	<20	167.90	142.30	34.60	227.50	18.70	574.00	4.00	11.30
GA-03P	Palmas	CX	6.40	1.70	13.90	4.60	-	84.00	20.00	178.50	144.20	45.50	224.20	-	631.00	-	11.30
BR-29B	Palmas	CX	6.80	1.70	13.20	4.60	17.00	70.00	<20	180.90	117.00	38.50	245.60	20.80	577.00	4.00	10.60
LBC-54A	Palmas	CX	7.00	1.60	14.80	4.60	17.00	80.00	2.70	197.90	143.00	40.90	257.00	20.70	853.00	7.00	11.30
SG-121Q	Palmas	CX	7.10	1.60	16.10	4.30	15.00	42.00	3.30	227.30	110.60	31.30	267.80	20.10	711.00	1.00	9.60
BR-20A	Palmas	CX	6.50	1.50	14.40	5.40	16.00	48.00	<20	158.90	121.20	34.40	227.70	19.40	577.00	3.00	9.10
LBC-87B	Palmas	CX	6.60	1.50	14.10	4.90	16.00	54.00	<20	155.90	184.90	37.90	246.90	20.40	739.00	4.00	10.70
CPM-1-P	Palmas	CX	6.10	1.40	13.50	4.70	18.00	83.00	3.40	163.20	147.30	35.50	227.60	18.20	611.00	5.00	11.30
CPM-4-P	Palmas	CX	6.00	1.20	13.40	4.60	18.00	88.00	3.70	170.40	151.30	45.40	233.20	18.40	624.00	4.00	11.00
Jade 10	Palmas	CX	6.10	1.30	13.30	4.30	18.00	77.00	4.90	159.60	148.50	54.10	234.90	17.80	609.00	3.00	12.20
LBC-32A	Palmas	CX	6.50	1.60	13.40	4.40	16.00	103.00	<20	161.20	162.40	43.20	236.70	20.30	626.00	3.00	13.90
Jade 11	Palmas	CX	6.60	1.40	13.60	4.30	18.00	83.00	15.50	164.70	154.10	37.90	244.10	18.80	580.00	5.00	12.00
LBC-54B	Palmas	CX	7.90	1.80	15.40	5.30	17.00	83.00	2.40	194.20	144.20	39.20	264.00	20.90	895.00	4.00	10.80

Amostra	Fm.	Grupo	Hf 0.1	Ta 0.1	Th 0.2	U 0.1	Sc 1	V 8	Ni 20	Rb 0.1	Sr 0.5	Y 0.1	Zr 0.1	Nb 0.1	Ba 1	Be 1	Co 0.2
GA-10	Palmas	CX	7.00	1.60	14.00	4.50	-	71.00	20.00	177.50	147.70	41.10	233.50	-	702.00	-	11.30
LBC-87A	Palmas	CX	7.10	1.50	14.50	5.10	17.00	83.00	<20	192.00	151.90	37.10	251.80	20.30	612.00	5.00	11.20
SM-32	Palmas	CX	7.70	1.60	16.10	3.70	18.00	71.00	2.50	180.50	103.30	42.70	279.30	20.30	639.00	3.00	7.20
CPM-3-B	Palmas	CX	6.60	1.30	13.70	3.60	18.00	77.00	12.30	175.80	138.20	48.80	229.90	17.70	648.00	<1	11.00
LBC-60	Palmas	CX	7.10	1.60	15.10	4.70	17.00	74.00	3.30	175.50	171.50	40.90	260.20	21.80	632.00	6.00	11.70
BR029A	Palmas	CX	6.60	1.70	13.60	5.00	17.00	81.00	24.00	218.60	169.40	39.50	255.30	21.90	643.00	3.00	11.20
GA-04	Palmas	CX	6.90	1.70	15.10	4.70	-	76.00	20.00	187.90	125.10	65.90	248.00	-	669.00	-	10.20
GA-13	Palmas	CX	7.00	1.60	14.50	4.60	-	73.00	20.00	177.60	152.50	36.60	240.90	-	661.00	-	10.90
LR-54B	Palmas	CX	5.80	1.40	13.10	4.20	18.00	95.00	4.50	154.30	139.60	32.60	212.90	16.00	542.00	4.00	11.50
CPM-4-B	Palmas	CX	6.40	1.40	13.10	3.70	18.00	79.00	17.50	184.30	138.60	36.50	234.50	18.50	672.00	1.00	12.10
IT-04	Palmas	CX	6.80	1.40	14.40	4.80	16.00	70.00	2.40	169.50	135.50	37.90	255.50	19.80	602.00	2.00	10.50
SG-34	Palmas	CX	6.90	1.70	14.80	5.00	16.00	73.00	<20	163.00	155.80	38.20	244.80	19.50	627.00	2.00	10.00
LBC-59	Palmas	CX	6.70	1.40	14.80	5.10	17.00	77.00	2.60	166.60	168.00	39.40	258.90	22.10	703.00	<1	11.40
Jade 1-V	Palmas	CX	6.60	1.40	14.30	4.60	18.00	89.00	3.60	157.70	144.40	34.70	231.20	18.00	618.00	3.00	12.60
GA-11	Palmas	CX	6.90	1.70	13.90	5.00	-	72.00	20.00	165.60	141.20	36.90	233.60	-	634.00	-	10.40
LR-54A	Palmas	CX	6.10	1.40	13.30	4.00	18.00	114.00	19.20	142.70	139.60	33.20	213.80	16.60	551.00	4.00	12.10
GA-12	Palmas	CX	6.80	1.50	14.20	4.90	-	74.00	20.00	172.30	137.80	49.50	242.90	-	718.00	-	10.20
GA-16	Palmas	CX	6.90	1.60	14.10	4.60	-	88.00	20.00	185.00	133.00	34.20	238.40	-	628.00	-	11.80
CPM-4-V	Palmas	CX	6.90	1.40	14.20	4.50	18.00	106.00	15.40	177.80	157.00	47.30	250.40	19.30	697.00	2.00	13.10
LR-28-A	Palmas	CX	7.40	1.60	14.30	4.80	17.00	82.00	<20	165.50	152.20	38.30	215.50	18.70	626.00	3.00	12.40
LR-54D	Palmas	CX	5.80	1.30	12.10	3.90	18.00	91.00	3.30	153.20	119.10	31.40	205.60	15.80	506.00	4.00	11.00
IT-01A	Palmas	CX	6.80	1.50	13.90	5.20	17.00	82.00	3.60	161.10	157.30	38.80	254.60	19.80	608.00	5.00	12.50
Jade 12	Palmas	CX	6.60	1.40	14.30	4.50	19.00	93.00	2.90	176.90	158.60	41.30	248.40	19.30	625.00	3.00	12.00
SM-54	Palmas	CX	6.20	1.50	12.50	4.70	18.00	95.00	4.20	193.60	135.70	37.00	239.00	19.30	592.00	3.00	12.30
CPM-2-V	Palmas	CX	6.70	1.60	14.40	4.10	19.00	103.00	4.10	175.60	154.60	49.40	245.30	19.50	705.00	3.00	21.30
GA-37	Palmas	CX	6.20	1.50	13.20	4.50	-	86.00	20.00	149.30	147.00	34.10	222.00	-	553.00	-	12.20
LR-54C	Palmas	CX	6.60	1.50	14.70	5.30	19.00	86.00	10.70	169.10	128.70	34.80	232.40	18.00	605.00	6.00	11.40
LR-33-B	Palmas	CX	6.90	1.70	14.00	4.90	18.00	97.00	<20	186.90	165.40	36.50	244.00	19.60	624.00	3.00	13.50
LR-53B	Palmas	CX	6.40	1.50	14.10	4.40	19.00	81.00	4.70	159.60	118.40	34.30	223.60	16.70	603.00	3.00	11.30
SG35-A	Palmas	CX	6.90	1.80	14.10	4.20	18.00	93.00	<20	157.70	152.40	36.70	247.40	20.10	610.00	3.00	10.70
LR-29-A	Palmas	CX	7.00	1.60	14.40	4.20	18.00	86.00	<20	168.10	156.90	43.50	224.20	20.00	656.00	3.00	13.40
GA-35B	Palmas	CX	6.30	1.50	12.60	4.40	-	89.00	20.00	157.20	143.10	109.50	225.10	-	596.00	-	13.30

			Hf	Ta	Th	U	Sc	V	Ni	Rb	Sr	Y	Zr	Nb	Ba	Be	Co
Amostra	**Fm.**	**Grupo**	0.1	0.1	0.2	0.1	1	8	20	0.1	0.5	0.1	0.1	0.1	1	1	0.2
SM-16A	Palmas	CX	6.30	1.30	12.40	4.10	18.00	107.00	11.90	182.10	125.80	48.90	210.80	16.30	576.00	5.00	15.60
LR-32-A	Palmas	CX	6.90	1.70	14.80	4.70	18.00	100.00	<20	163.90	159.10	36.30	255.20	21.10	619.00	3.00	12.80
LBC-53	Palmas	CX	6.90	1.50	13.50	3.80	18.00	112.00	2.80	190.10	147.20	54.70	258.10	21.20	683.00	3.00	14.30
LBC-61	Palmas	CX	7.30	1.40	13.60	4.20	18.00	67.00	1.40	167.80	169.00	41.90	265.10	19.30	650.00	<1	12.30
SM-16B	Palmas	JC	6.80	1.40	13.10	3.60	19.00	57.00	2.80	136.60	480.00	41.00	227.90	17.30	634.00	4.00	14.50
LBC-32C	Palmas	JC	8.20	1.60	15.40	4.40	20.00	110.00	4.20	141.10	224.60	42.00	268.50	24.00	708.00	7.00	14.70
GA-03V	Palmas	JC	7.20	1.80	16.10	4.60	-	103.00	20.00	197.20	154.50	65.60	259.60	-	721.00	-	13.80
LBC-32B	Palmas	JC	7.30	1.80	15.00	4.00	19.00	117.00	<20	175.70	158.30	40.40	263.00	21.70	754.00	3.00	14.70
GA-34	Palmas	JC	6.50	1.40	13.10	4.20	-	102.00	20.00	149.70	150.00	42.90	234.30	-	715.00	-	15.20
SM-50	Palmas	JC	6.90	1.80	13.80	4.00	17.00	97.00	5.80	167.20	226.70	38.50	276.30	23.50	648.00	6.00	12.50
SM-27	Palmas	JC	6.60	1.40	13.20	4.10	19.00	102.00	2.60	149.80	156.90	35.80	227.50	16.90	588.00	3.00	12.80
LBC-17*	Palmas	JC	7.80	1.70	14.30	3.50	19.00	73.00	<20	163.90	151.20	57.50	300.00	22.40	787.00	2.00	13.60
SM-51	Palmas	JC	6.40	1.60	12.20	4.10	18.00	102.00	10.90	169.10	140.20	53.60	239.40	19.50	681.00	3.00	13.00
LBC-50*	Palmas	AG	6.90	1.50	12.70	4.30	16.00	95.00	2.30	193.30	126.90	151.50	259.60	19.10	637.00	3.00	10.70
LBC-49	Palmas	AG	7.10	1.70	13.80	4.50	17.00	87.00	1.70	169.40	151.90	42.80	271.60	21.20	725.00	4.00	11.40
LBC-40	Palmas	AG	6.30	1.60	12.30	4.10	16.00	80.00	<20	148.60	145.70	40.20	253.70	20.00	571.00	1.00	11.40
LBC-51	Esmeralda	-	2.9	0.5	2.5	0.4	44	423	24	20.8	187.1	30.2	108.0	6.0	191	<1	47.4
LBC-39	Esmeralda	-	2.4	0.4	1.6	0.4	40	400	71	31.3	196.9	25.9	94.1	5.8	157	<1	47.3
LBC-38	Esmeralda	-	5.6	1.1	7.6	1.9	40	462	<20	85.5	170.7	79.6	200.1	15.8	480		38.3
LBC-52	Esmeralda	-	3.7	0.6	5.1	1	38	428	13.7	40.5	215.2	36.7	159.8	10.2	323		42
SG-97Q	High Ti	-	6.20	1.50	3.20	0.60	32.00	474.00	16.10	25.70	441.80	38.10	241.70	20.90	433.00	<1	41.80
SG-98Q	High Ti	-	4.50	0.90	2.50	0.60	40.00	454.00	14.60	48.90	280.90	36.00	170.50	14.20	322.00	<1	41.50
SM-37	High Ti	-	4.20	0.90	2.60	0.50	37.00	446.00	26.70	31.20	360.20	27.00	151.70	12.90	351.00	3.00	38.30
LBC-55	Dike	-	4.10	0.50	3.30	0.60	41.00	398.00	16.60	28.90	224.60	32.20	134.40	8.70	361.00	<1	44.30
IT-2-DQ	Dike	-	4.20	0.50	4.10	0.80	38.00	382.00	15.30	48.00	229.20	34.10	162.70	9.90	356.00	<1	46.20
LR-38-B	Dike	-	4.00	0.70	5.10	1.10	34.00	365.00	43.00	28.40	237.60	28.30	134.80	10.80	324.00	1.00	42.20
LR-50	Dike	-	3.40	0.50	3.00	0.60	42.00	373.00	21.40	25.70	207.10	29.40	119.00	6.80	390.00	<1	42.30
Bas-106	Dike	-	2.50	0.40	2.80	0.60	39.00	241.00	47.00	21.20	234.00	18.20	93.60	7.80	246.00	<1	42.20
SG-13a	Sill	-	3.40	0.40	4.80	0.90	39.00	399.00	22.70	48.60	231.00	25.60	131.30	8.30	341.00	2.00	45.30
Bas-105	Sill	-	5.00	1.00	6.50	1.80	36.00	449.00	11.10	90.60	306.80	35.90	176.80	13.00	697.00	2.00	40.50

	Cu	Pb	Zn	Ga	Mo	Cs	La	Ce	Pr	Nd	Sm	Eu	Gd	Tb	Dy	Ho	Er	Tm	Yb	Lu
Amostra	**0.1**	**0.1**	**0.1**	**0.5**	**0.1**	**0.1**	**0.1**	**0.1**	**0.02**	**0.3**	**0.05**	**0.02**	**0.05**	**0.01**	**0.05**	**0.02**	**0.03**	**0.01**	**0.05**	**0.01**
LBC-1	50.30	4.70	49.00	20.90	0.80	1.60	41.50	80.90	9.77	37.70	7.36	1.74	6.69	1.08	5.86	1.13	3.38	0.47	3.13	0.46
LR-02-A	20.60	1.80	53.00	19.90	0.20	1.60	33.20	67.70	8.39	33.00	6.86	1.64	6.06	1.00	5.50	1.08	3.10	0.45	2.82	0.43
LR-04-A	23.00	3.30	41.00	18.90	0.40	1.30	32.70	68.50	8.36	32.50	6.82	1.63	6.13	1.00	5.69	1.06	3.05	0.46	2.92	0.42
LBC-12	28.20	4.20	43.00	20.80	0.60	1.70	37.70	76.30	8.90	35.00	6.96	1.73	6.15	1.02	5.77	1.08	3.26	0.46	3.04	0.44
SG-124Q	113.00	2.60	61.00	20.20	0.70	0.20	27.90	58.10	6.74	26.20	5.51	1.54	5.80	0.89	5.35	1.07	3.31	0.43	2.82	0.40
LBC-56	46.70	8.30	50.00	19.30	0.30	0.50	35.70	69.70	8.33	30.40	6.69	1.56	6.21	0.93	5.48	1.05	3.09	0.43	2.97	0.44
SG-125Q	75.20	2.70	47.00	20.60	0.40	0.50	25.80	55.30	6.45	26.40	5.51	1.59	5.66	0.87	5.12	1.02	2.99	0.39	2.65	0.38
BR-08	66.00	2.20	43.00	17.60	0.50	0.40	22.90	50.30	5.90	22.80	4.86	1.32	4.91	0.79	4.47	0.99	2.54	0.39	2.34	0.39
LBC-46	55.80	7.80	41.00	18.20	0.70	0.40	30.20	62.80	7.23	26.50	5.90	1.35	5.51	0.91	5.20	1.01	3.04	0.44	2.88	0.44
BR-07	68.70	2.10	37.00	17.60	0.50	0.60	23.40	49.90	5.91	23.90	4.78	1.36	4.85	0.80	4.37	0.98	2.77	0.37	2.44	0.41
SG-6	103.80	1.20	40.00	17.30	1.20	1.30	20.70	42.20	4.92	21.10	4.48	1.30	4.86	0.76	4.45	0.84	2.42	0.34	2.25	0.35
SG-106Q	152.30	2.80	31.00	20.10	0.30	0.20	24.10	48.10	5.66	23.00	4.68	1.28	4.60	0.75	4.58	0.89	2.57	0.37	2.30	0.33
SG-103Q	31.00	3.90	33.00	18.60	0.20	<0.1	22.00	46.30	5.53	21.50	4.50	1.32	4.66	0.76	4.56	0.97	2.62	0.35	2.35	0.33
CT-3	95.70	3.70	30.00	17.60	0.10	0.80	20.50	39.20	5.07	20.20	4.32	1.22	4.64	0.75	4.60	0.84	2.59	0.38	2.14	0.35
SG-102Q	56.80	4.60	42.00	20.40	0.20	0.20	21.80	45.00	5.36	21.50	4.47	1.27	4.71	0.73	4.46	0.91	2.54	0.34	2.50	0.35
LBC-78C	82.50	2.10	40.00	20.60	0.50	0.70	21.20	41.50	5.05	20.20	4.61	1.30	4.97	0.78	4.32	0.92	2.68	0.38	2.49	0.36
CT-1-B	95.00	4.00	33.00	17.40	0.10	1.00	18.50	38.40	4.58	19.40	4.03	1.11	4.44	0.71	4.14	0.78	2.33	0.35	2.12	0.32
LR14-B	94.30	3.00	38.00	18.20	0.20	0.40	17.60	40.70	4.80	19.70	3.97	1.13	4.34	0.68	4.24	0.78	2.28	0.34	2.14	0.31
LR-14A	87.60	3.40	43.00	20.10	0.40	0.20	19.20	40.60	4.82	20.80	4.25	1.26	4.35	0.71	4.26	0.83	2.24	0.34	2.19	0.32
SG-123Q	58.30	2.20	34.00	17.60	0.20	<0.1	18.00	36.80	4.26	17.30	3.57	1.14	3.93	0.63	3.92	0.81	2.29	0.31	2.02	0.30
SM-57	124.70	3.90	44.00	15.60	0.20	1.90	15.70	32.80	4.13	17.30	3.80	1.14	4.12	0.67	4.01	0.87	2.43	0.38	2.24	0.32
LR-15-A	85.20	3.50	32.00	16.90	0.10	1.30	16.00	34.50	4.44	17.70	3.89	1.16	4.06	0.71	4.08	0.83	2.47	0.36	2.29	0.33
SM-55	126.60	4.70	48.00	17.80	0.90	0.40	18.20	36.60	4.54	19.10	4.07	1.12	4.26	0.70	4.34	0.86	2.42	0.37	2.38	0.35
SG-80B	100.80	5.10	51.00	15.80	0.20	<0.1	20.90	42.30	4.96	19.40	4.24	1.22	4.14	0.64	3.99	0.78	2.16	0.29	1.97	0.29
SM-58*	124.00	3.60	52.00	17.30	0.90	0.50	13.40	29.00	3.64	15.80	3.65	1.10	3.74	0.61	3.74	0.82	2.28	0.33	2.07	0.30
LR-7A	81.50	3.60	36.00	17.30	0.20	0.40	17.20	39.30	4.52	18.00	3.94	1.10	4.08	0.69	4.09	0.75	2.07	0.32	2.07	0.33
LR-11-A	129.20	2.40	35.00	16.10	0.30	0.40	16.10	34.50	4.52	16.80	3.96	1.23	4.10	0.74	4.29	0.87	2.48	0.36	2.22	0.35
BR-05B	91.60	2.00	31.00	14.60	0.30	0.10	14.20	31.80	3.81	14.70	3.14	1.00	3.52	0.56	3.37	0.71	1.91	0.30	1.75	0.28
SG-119Q	113.10	2.30	28.00	18.80	0.20	<0.1	15.30	31.60	3.89	15.70	3.28	1.02	3.70	0.58	3.59	0.74	2.23	0.27	1.92	0.28
LR-7B	83.00	2.30	51.00	19.30	0.30	0.10	16.70	34.20	4.10	17.30	3.77	1.08	3.77	0.62	3.75	0.75	2.14	0.30	1.82	0.32
LR-55A	51.90	1.70	26.00	16.30	0.30	0.70	18.10	36.10	4.42	18.10	4.16	1.15	4.32	0.72	4.27	0.88	2.30	0.36	2.29	0.35
BR-05A*	93.70	2.00	34.00	14.10	0.30	<0.1	12.30	26.80	3.20	12.90	2.83	0.89	2.95	0.50	3.11	0.64	1.71	0.25	1.56	0.26

	Cu	Pb	Zn	Ga	Mo	Cs	La	Ce	Pr	Nd	Sm	Eu	Gd	Tb	Dy	Ho	Er	Tm	Yb	Lu
Amostra	**0.1**	**0.1**	**0.1**	**0.5**	**0.1**	**0.1**	**0.1**	**0.1**	**0.02**	**0.3**	**0.05**	**0.02**	**0.05**	**0.01**	**0.05**	**0.02**	**0.03**	**0.01**	**0.05**	**0.01**
LR-55B	85.30	1.60	24.00	18.30	0.30	0.50	14.60	32.40	3.85	16.70	3.24	1.14	3.86	0.65	3.67	0.73	2.02	0.33	1.95	0.32
LR-12-A	76.70	2.10	26.00	15.40	0.20	0.60	14.30	31.00	3.95	16.10	3.63	1.13	3.74	0.63	3.80	0.76	2.22	0.33	2.10	0.32
LR-48*	79.00	2.10	28.00	14.40	0.20	0.70	15.20	32.40	4.04	16.60	3.75	1.07	3.92	0.64	4.02	0.73	2.25	0.30	1.97	0.29
SG-27	194.20	2.40	62.00	20.40	1.20	12.00	26.60	55.70	6.68	28.40	6.42	1.83	6.98	1.13	6.73	1.33	3.80	0.53	3.42	0.53
SG-23	186.00	4.40	59.00	20.80	0.80	2.90	29.20	60.20	7.16	29.10	6.43	1.91	7.44	1.23	7.21	1.37	4.08	0.54	3.62	0.54
SG-26*	206.20	2.80	73.00	20.40	0.90	2.60	27.40	55.10	6.92	27.80	6.53	1.92	7.51	1.20	7.11	1.43	4.09	0.58	3.54	0.54
SG-95Q	142.70	2.70	56.00	24.30	0.20	2.70	26.00	53.90	6.58	27.70	6.45	1.81	7.36	1.18	7.59	1.51	4.61	0.62	4.03	0.59
SG-25	123.80	2.00	35.00	20.70	1.10	2.20	24.00	50.50	5.91	25.00	5.59	1.72	6.40	1.03	6.54	1.22	3.38	0.50	3.21	0.48
SG-96Q	136.30	2.20	56.00	22.60	0.20	1.40	21.20	44.80	5.52	23.30	5.74	1.54	6.45	1.09	6.84	1.49	4.41	0.61	3.79	0.58
SG-7	137.50	1.40	46.00	18.80	1.10	1.20	18.80	39.80	4.64	19.50	4.28	1.17	4.64	0.75	4.36	0.86	2.49	0.36	2.26	0.36
SG-20	97.40	1.90	37.00	18.50	0.80	1.20	16.60	34.00	4.15	17.10	4.13	1.23	4.64	0.76	4.61	0.83	2.44	0.35	2.12	0.34
BR-16B	20.20	4.90	36.00	14.50	<0.1	1.00	18.80	39.80	4.77	18.70	4.07	1.20	4.35	0.74	4.18	0.94	2.44	0.39	2.33	0.38
GA-30	-	2.30	-	18.30	-	0.70	22.30	48.50	5.65	22.70	4.97	1.39	5.07	0.85	5.00	1.01	2.79	0.42	2.77	0.41
BR-16C	87.70	4.70	38.00	20.70	0.50	<0.1	21.30	45.80	5.67	24.00	4.79	1.32	5.09	0.84	5.05	1.03	2.90	0.44	2.75	0.42
BR-15*	76.50	3.80	49.00	17.40	0.50	1.10	19.10	42.00	4.93	19.40	4.51	1.29	4.34	0.73	4.31	0.95	2.58	0.36	2.35	0.38
BR-14	60.10	4.10	34.00	16.90	0.70	0.20	20.00	44.60	5.30	20.40	4.66	1.34	4.80	0.83	4.92	1.06	2.75	0.43	2.64	0.43
LBC-16A	94.80	4.10	39.00	21.60	0.50	0.60	25.70	51.80	6.51	27.80	5.48	1.58	5.51	0.92	5.98	1.18	3.30	0.49	3.04	0.47
SG-108Q	54.40	10.10	42.00	19.00	0.30	0.40	31.20	63.20	7.26	28.40	5.80	1.38	5.61	0.85	5.36	1.05	3.00	0.43	2.74	0.43
BR-10*	32.30	5.60	37.00	16.60	0.50	5.40	33.30	73.50	8.36	31.60	6.49	1.51	6.28	0.99	5.62	1.21	2.99	0.47	2.78	0.47
LR-18-B*	96.70	2.90	51.00	18.80	0.70	1.90	30.30	63.30	7.91	29.60	6.52	1.75	6.63	1.14	6.30	1.29	3.73	0.53	3.27	0.51
LR-16*	124.50	3.30	71.00	15.10	1.20	1.40	21.20	44.30	5.42	21.80	4.86	1.32	5.21	0.88	5.18	1.03	2.83	0.42	2.62	0.43
LBC-19	76.90	3.00	52.00	22.20	0.60	1.10	28.90	62.50	7.50	29.90	6.53	1.71	6.03	1.06	6.42	1.27	3.48	0.53	3.22	0.47
BR-11	143.70	4.20	50.00	18.50	0.40	0.80	23.70	54.40	6.38	25.30	5.34	1.45	5.51	0.93	5.36	1.11	3.01	0.48	2.69	0.45
BR-13A	178.70	8.80	72.00	18.50	0.20	1.70	18.90	43.10	5.16	20.40	4.45	1.26	4.88	0.80	4.47	0.94	2.68	0.40	2.44	0.40
GA-22	-	3.50	-	19.30	-	2.60	21.30	46.10	5.60	24.10	5.22	1.43	5.39	0.88	5.13	1.07	3.01	0.45	2.87	0.44
BR-27B	106.40	7.90	22.00	20.40	0.20	4.80	20.80	45.40	5.42	21.80	5.06	1.38	5.37	0.89	5.08	1.05	2.99	0.43	2.67	0.41
CT-5-A	106.10	6.10	13.00	21.10	0.10	7.30	26.70	48.50	6.10	25.60	5.63	1.58	6.25	1.01	5.71	1.24	3.24	0.49	3.19	0.47
GA-14B	-	7.70	-	19.20	-	3.50	20.00	44.30	5.22	20.90	4.68	1.34	5.19	0.88	5.10	1.04	2.80	0.42	2.72	0.40
BR-25	110.40	3.80	33.00	21.40	0.40	2.90	21.80	47.00	5.69	24.10	5.17	1.37	5.40	0.90	5.12	1.06	3.03	0.45	2.71	0.42
LR-38-A	125.40	3.40	30.00	19.80	0.50	2.50	20.50	43.70	5.47	21.40	5.47	1.48	5.54	0.95	5.73	1.10	3.08	0.48	2.99	0.44
GA-24	-	5.10	-	18.40	-	1.30	23.40	52.70	6.05	25.00	5.36	1.45	5.41	0.94	5.40	1.12	3.02	0.46	3.01	0.43
LBC-71	150.70	5.00	30.00	18.80	0.30	2.60	18.90	39.10	4.90	20.10	4.44	1.30	4.58	0.82	4.91	0.93	2.86	0.44	2.70	0.40

	Cu	Pb	Zn	Ga	Mo	Cs	La	Ce	Pr	Nd	Sm	Eu	Gd	Tb	Dy	Ho	Er	Tm	Yb	Lu
Amostra	**0.1**	**0.1**	**0.1**	**0.5**	**0.1**	**0.1**	**0.1**	**0.1**	**0.02**	**0.3**	**0.05**	**0.02**	**0.05**	**0.01**	**0.05**	**0.02**	**0.03**	**0.01**	**0.05**	**0.01**
SM-23	118.90	5.90	32.00	19.50	0.90	5.90	22.50	44.90	5.49	22.80	5.01	1.42	5.74	0.92	5.15	1.03	2.93	0.44	2.71	0.42
IT-05A	145.70	3.30	50.00	21.30	0.60	1.30	23.30	45.70	5.74	23.10	5.30	1.49	5.53	0.91	5.65	1.14	3.29	0.42	2.93	0.41
LR-23-A	88.30	2.40	36.00	17.90	0.60	0.70	22.20	46.10	5.86	23.00	4.76	1.45	5.03	0.86	5.23	1.04	3.17	0.46	2.83	0.42
SG-8b*	116.80	1.90	42.00	18.60	0.90	1.90	25.10	46.90	5.90	23.20	5.62	1.52	6.08	0.97	5.86	1.11	3.11	0.47	2.76	0.43
LBC-25	96.90	2.30	62.00	20.10	0.40	1.60	21.60	43.40	5.61	24.90	5.49	1.55	5.78	0.98	6.14	1.20	3.58	0.50	3.27	0.48
BR-24	74.10	3.80	34.00	15.40	0.30	2.20	17.20	36.90	4.22	17.50	3.61	1.09	4.16	0.66	3.93	0.86	2.39	0.33	2.10	0.34
BR-21A	151.00	4.00	31.00	17.10	0.30	1.60	17.80	41.40	4.66	19.80	4.52	1.27	4.63	0.78	4.67	0.96	2.65	0.41	2.31	0.39
LBC-97	107.90	4.00	16.00	20.40	0.20	2.00	25.30	49.50	5.80	25.20	5.56	1.47	5.95	0.95	5.20	1.11	3.20	0.47	3.11	0.43
CT-4-B	74.70	3.40	24.00	19.30	0.20	1.70	16.70	34.80	4.27	16.00	4.06	1.19	4.54	0.75	3.86	0.84	2.53	0.35	2.28	0.31
BR-19A	97.70	12.00	73.00	17.50	0.70	3.60	33.20	69.20	8.23	32.70	7.01	1.75	7.41	1.23	7.25	1.52	4.02	0.57	3.79	0.57
IT-08	50.20	5.00	83.00	21.30	0.60	1.10	38.60	76.10	9.09	35.90	7.33	1.84	7.65	1.22	7.14	1.46	4.30	0.58	3.98	0.58
SM-29*	177.00	2.40	72.00	18.70	0.90	6.20	23.90	50.10	6.50	27.20	6.34	1.95	8.03	1.37	7.93	1.72	4.92	0.71	4.62	0.68
LBC-10	207.20	2.40	91.00	21.00	1.00	2.70	35.50	71.40	9.30	36.60	8.49	2.28	8.66	1.57	8.92	1.78	5.31	0.85	5.53	0.79
LBC-8	146.10	3.80	64.00	23.60	0.90	2.00	31.00	63.40	7.67	30.40	6.61	1.72	6.62	1.07	6.51	1.23	3.85	0.53	3.41	0.48
SM-48	165.20	2.70	44.00	18.30	1.00	5.50	23.70	51.20	6.17	26.10	5.98	1.69	6.74	1.18	7.50	1.47	4.25	0.60	3.73	0.58
LBC-9	165.90	4.20	64.00	20.60	0.90	2.90	32.80	67.20	8.20	31.80	7.08	1.72	6.34	1.05	6.22	1.23	3.50	0.53	3.52	0.49
BR-17A	19.80	6.30	61.00	16.00	1.20	2.30	30.30	67.50	7.85	32.40	6.50	1.72	6.72	1.14	6.46	1.39	3.75	0.54	3.59	0.56
SM-49	161.70	2.40	52.00	20.90	0.20	2.20	23.30	49.10	6.27	26.50	6.18	1.69	7.03	1.18	7.50	1.56	4.54	0.63	4.12	0.67
BR-17B	55.40	2.80	73.00	20.70	0.80	1.90	29.90	67.00	7.65	29.50	6.42	1.58	6.48	1.09	6.26	1.32	3.66	0.53	3.49	0.53
LBC-6	157.90	4.80	60.00	19.40	0.40	2.10	39.50	57.00	8.68	36.40	7.85	2.22	10.09	1.61	10.02	2.28	6.57	0.86	4.79	0.85
LBC-82A	63.00	3.70	33.00	17.30	0.50	1.30	32.60	65.60	8.01	30.50	6.79	1.73	7.14	1.14	6.33	1.31	3.74	0.59	3.55	0.53
LBC-81	102.40	2.90	57.00	20.30	0.70	3.20	36.10	71.90	8.52	34.10	7.07	1.74	7.46	1.21	7.00	1.39	4.01	0.60	3.99	0.60
LBC-43	171.60	2.90	53.00	20.50	0.30	3.20	25.50	53.90	6.53	27.20	6.28	1.81	6.57	1.16	6.87	1.37	4.06	0.60	3.82	0.56
IT-2	167.90	7.60	57.00	25.00	0.30	4.20	31.80	62.20	8.16	33.60	8.24	2.20	9.45	1.48	9.13	1.93	5.33	0.73	4.52	0.75
LR-27-B	97.10	4.90	25.00	19.20	0.20	11.00	27.80	46.90	7.24	28.40	6.29	1.81	6.49	1.09	6.52	1.23	3.51	0.51	3.19	0.47
SM-19	168.60	4.10	52.00	18.80	1.50	1.40	26.90	55.20	6.80	27.00	5.83	1.61	6.21	1.03	6.09	1.24	3.51	0.50	3.24	0.45
SG-120	119.50	2.20	55.00	23.60	0.60	0.30	23.80	49.90	6.31	26.50	5.93	1.73	5.89	0.91	5.24	1.04	2.76	0.38	2.49	0.32
SM-38	21.80	3.70	62.00	17.60	1.70	9.20	47.40	89.90	10.87	41.10	8.50	1.72	8.28	1.38	8.09	1.60	4.52	0.67	4.26	0.66
SG-10v	25.90	2.20	40.00	16.80	2.10	10.20	49.40	97.60	11.33	43.40	9.31	1.65	8.87	1.49	8.62	1.63	4.54	0.70	4.41	0.69
SG-94Q	19.50	3.30	55.00	15.90	0.10	8.60	48.20	98.00	11.63	43.60	8.84	1.64	9.05	1.47	8.73	1.84	5.28	0.72	4.84	0.72
SM-39	28.20	6.40	75.00	15.50	0.80	11.40	46.70	94.00	11.01	42.60	9.00	1.56	8.87	1.44	8.51	1.72	4.87	0.71	4.69	0.69
SG-4*	28.00	3.70	77.00	17.60	1.40	11.70	63.40	95.80	18.68	84.20	20.09	3.74	23.99	3.85	23.04	4.62	13.44	1.96	12.73	1.87

	Cu	Pb	Zn	Ga	Mo	Cs	La	Ce	Pr	Nd	Sm	Eu	Gd	Tb	Dy	Ho	Er	Tm	Yb	Lu
Amostra	**0.1**	**0.1**	**0.1**	**0.5**	**0.1**	**0.1**	**0.1**	**0.1**	**0.02**	**0.3**	**0.05**	**0.02**	**0.05**	**0.01**	**0.05**	**0.02**	**0.03**	**0.01**	**0.05**	**0.01**
SG-15	24.60	3.70	65.00	18.30	1.30	9.20	65.20	113.50	16.56	67.10	13.12	2.45	12.75	1.99	11.21	2.15	5.88	0.90	5.75	0.82
SG-18	21.00	1.70	35.00	17.50	1.10	11.50	53.20	104.00	12.46	46.90	9.60	1.71	9.60	1.54	8.99	1.79	4.96	0.74	4.77	0.72
SG-16*	23.10	4.50	59.00	16.70	1.20	10.90	46.50	90.20	10.57	40.90	8.31	1.66	8.08	1.30	8.06	1.55	4.60	0.65	4.31	0.64
SG-93Q	22.80	4.60	59.00	14.90	0.30	9.20	44.80	88.60	10.06	37.20	7.64	1.41	7.34	1.23	7.29	1.47	4.41	0.62	3.99	0.61
SM-42	25.80	4.90	80.00	16.00	0.90	10.70	48.20	99.70	11.52	45.20	9.33	1.68	9.48	1.57	9.21	1.73	5.15	0.77	4.83	0.76
SM-40	26.40	4.40	59.00	16.00	2.60	9.70	50.90	102.90	11.95	46.10	9.71	1.71	9.17	1.59	9.62	1.84	5.27	0.74	4.86	0.76
SG-10p	26.10	3.20	41.00	17.60	2.20	9.90	48.90	99.30	11.47	44.20	9.23	1.68	8.78	1.46	8.61	1.79	5.06	0.73	4.69	0.71
BR-23	14.90	2.80	34.00	14.80	0.30	7.40	36.30	79.80	8.71	34.70	6.54	1.27	6.39	0.99	5.72	1.18	3.25	0.45	3.03	0.48
BR-41B	18.40	5.90	55.00	18.40	0.70	5.90	42.40	89.80	10.53	40.50	7.92	1.51	7.69	1.21	6.86	1.37	3.92	0.58	3.68	0.56
GA-07	-	3.90	-	15.60	-	6.80	36.60	81.00	9.15	35.50	7.08	1.42	6.52	1.08	6.08	1.20	3.41	0.51	3.30	0.48
LBC-33A	42.50	2.60	51.00	16.80	1.50	8.20	40.50	83.30	9.73	36.50	7.71	1.48	6.98	1.15	6.22	1.13	3.73	0.57	3.32	0.47
BR-41C	18.60	1.30	37.00	19.60	0.40	9.10	42.90	93.60	10.72	41.70	8.16	1.54	7.76	1.24	7.03	1.40	3.79	0.59	3.76	0.55
LR-35-A	37.10	3.40	55.00	16.20	1.30	6.90	41.00	82.30	10.20	37.80	8.39	1.63	7.70	1.30	7.36	1.44	4.12	0.59	3.74	0.57
LBC-68A	28.20	2.60	59.00	17.90	0.60	9.40	43.00	83.00	9.76	36.20	7.36	1.42	6.88	1.13	6.02	1.23	3.68	0.52	3.66	0.51
LBC-68B	29.70	2.30	64.00	18.50	0.70	6.70	45.50	91.00	10.59	38.30	8.37	1.50	7.37	1.22	6.67	1.31	3.60	0.58	3.69	0.53
CPM-2-P	72.70	3.60	52.00	15.30	4.70	8.40	39.80	79.40	9.60	35.30	7.54	1.40	7.02	1.14	6.87	1.28	3.48	0.51	3.35	0.51
LBC-31	31.50	4.60	53.00	17.30	1.00	7.50	42.10	87.70	10.36	39.60	8.19	1.60	7.77	1.26	7.56	1.44	4.21	0.59	3.71	0.58
Jade 1-P	60.70	3.70	47.00	15.40	4.70	7.40	41.50	83.60	9.57	36.90	7.40	1.44	7.15	1.19	6.51	1.24	3.53	0.52	3.35	0.51
SG-33	32.00	2.70	80.00	18.10	0.90	8.60	46.30	100.20	11.32	47.00	9.92	1.91	10.43	1.71	9.92	1.92	5.78	0.87	5.84	0.86
LBC-33B	40.20	2.20	46.00	17.60	1.70	8.10	39.70	82.40	9.74	37.10	7.51	1.50	6.75	1.14	7.20	1.22	3.52	0.56	3.58	0.51
GA-03P	-	2.70	-	16.80	-	7.90	39.90	84.20	9.65	37.70	7.51	1.44	7.30	1.17	6.39	1.38	3.79	0.54	3.42	0.51
BR-29B	36.50	5.20	43.00	18.20	0.40	5.30	39.30	87.20	9.84	38.90	7.78	1.46	7.27	1.15	6.54	1.29	3.56	0.53	3.37	0.50
LBC-54A	42.80	4.30	59.00	17.40	0.90	9.70	46.00	92.30	10.74	43.40	8.78	1.68	7.86	1.28	7.13	1.33	3.96	0.60	3.70	0.54
SG-121Q	17.90	9.00	69.00	20.10	0.50	9.40	41.60	76.40	9.67	39.10	7.66	1.54	7.10	1.07	6.40	1.19	3.38	0.43	3.02	0.44
BR-20A	25.20	2.80	74.00	19.50	1.20	6.60	40.50	87.30	9.72	37.60	7.52	1.47	7.14	1.15	6.54	1.37	3.66	0.54	3.41	0.54
LBC-87B	35.70	4.60	39.00	16.20	0.40	2.50	44.00	86.50	10.10	41.80	8.16	1.45	7.94	1.20	6.67	1.32	3.90	0.57	3.42	0.50
CPM-1-P	36.80	2.80	45.00	15.90	0.80	7.80	40.80	81.70	9.65	37.10	7.46	1.44	7.12	1.16	6.51	1.24	3.41	0.51	3.28	0.49
CPM-4-P	37.20	3.50	53.00	15.60	1.00	8.00	42.60	82.90	10.16	40.80	7.85	1.55	7.68	1.25	7.43	1.46	4.15	0.59	3.56	0.55
Jade 10	41.90	3.40	47.00	16.20	1.10	6.00	43.60	85.30	11.19	45.50	9.62	1.88	9.33	1.53	9.18	1.81	5.01	0.75	4.55	0.64
LBC-32A	48.70	2.80	50.00	17.50	1.30	7.20	43.30	85.50	10.52	41.50	8.22	1.65	7.64	1.28	7.62	1.50	4.13	0.61	3.92	0.56
Jade 11	75.30	3.90	48.00	17.00	4.40	7.40	42.60	83.70	9.96	39.00	7.75	1.54	7.58	1.20	6.77	1.31	3.69	0.54	3.55	0.53
LBC-54B	46.60	4.10	51.00	18.00	0.90	7.60	45.20	93.90	10.58	41.10	8.09	1.57	8.13	1.31	7.12	1.45	4.21	0.61	3.95	0.55

	Cu	Pb	Zn	Ga	Mo	Cs	La	Ce	Pr	Nd	Sm	Eu	Gd	Tb	Dy	Ho	Er	Tm	Yb	Lu
Amostra	**0.1**	**0.1**	**0.1**	**0.5**	**0.1**	**0.1**	**0.1**	**0.1**	**0.02**	**0.3**	**0.05**	**0.02**	**0.05**	**0.01**	**0.05**	**0.02**	**0.03**	**0.01**	**0.05**	**0.01**
GA-10	-	3.70	-	17.30	-	6.30	39.80	85.70	9.80	40.20	7.75	1.54	7.35	1.18	6.59	1.36	3.88	0.57	3.60	0.54
LBC-87A	33.50	4.20	47.00	17.30	0.90	8.30	44.90	92.80	10.41	38.80	8.13	1.56	7.44	1.23	6.23	1.33	3.85	0.58	3.67	0.49
SM-32	27.40	6.30	64.00	16.50	0.50	7.80	45.30	82.50	10.70	42.30	8.54	1.81	8.60	1.41	8.34	1.68	4.65	0.71	4.50	0.67
CPM-3-B	65.00	3.30	55.00	15.80	3.90	9.20	44.90	82.60	10.54	41.80	8.52	1.59	8.26	1.36	7.86	1.61	4.43	0.66	4.20	0.60
LBC-60	22.80	3.50	55.00	17.80	0.50	8.30	46.30	94.00	10.71	45.70	8.22	1.59	8.36	1.26	6.90	1.47	4.29	0.59	3.67	0.57
BR029A	34.50	2.40	32.00	18.30	1.90	14.50	41.30	90.20	10.37	41.50	8.03	1.54	7.53	1.20	6.63	1.34	3.77	0.56	3.49	0.53
GA-04	-	4.50	-	17.60	-	6.60	49.90	110.60	12.95	52.00	10.34	2.03	10.57	1.72	9.84	2.04	5.90	0.86	5.42	0.79
GA-13	-	3.50	-	17.30	-	7.50	41.10	89.90	10.24	39.40	7.86	1.50	7.12	1.17	6.70	1.28	3.60	0.55	3.48	0.53
LR-54B	35.80	4.50	50.00	14.90	1.00	6.90	38.00	76.70	9.02	36.20	7.12	1.39	7.03	1.09	6.31	1.22	3.49	0.48	3.25	0.48
CPM-4-B	66.40	4.80	55.00	16.70	5.50	8.40	41.10	88.40	10.24	40.10	7.86	1.56	7.41	1.18	6.88	1.26	3.40	0.54	3.45	0.53
IT-04	48.10	5.70	50.00	18.90	0.60	6.30	46.40	93.70	10.84	41.30	8.40	1.57	7.95	1.26	7.08	1.39	4.15	0.58	3.61	0.51
SG-34	34.50	3.70	45.00	18.30	0.60	6.30	46.90	96.80	10.81	41.10	8.27	1.62	7.96	1.23	7.34	1.33	3.92	0.58	3.62	0.56
LBC-59	30.70	3.00	47.00	18.20	0.60	7.20	45.70	91.10	10.73	42.50	7.84	1.65	7.58	1.24	7.48	1.39	4.00	0.58	3.71	0.57
Jade 1-V	48.30	3.80	56.00	15.70	0.90	7.10	42.10	86.70	10.25	37.70	8.06	1.61	7.40	1.23	7.13	1.36	3.71	0.54	3.38	0.51
GA-11	-	3.00	-	16.70	-	6.20	39.50	85.00	9.75	38.20	7.60	1.47	7.05	1.15	6.41	1.29	3.65	0.55	3.58	0.51
LR-54A	76.60	4.20	50.00	15.00	5.20	6.30	37.30	75.20	8.86	33.50	6.86	1.33	6.88	1.07	6.41	1.17	3.09	0.49	3.20	0.47
GA-12	-	3.30	-	17.50	-	7.30	39.30	82.90	9.75	37.20	7.59	1.54	7.81	1.25	6.90	1.52	4.24	0.61	3.76	0.58
GA-16	-	5.00	-	17.10	-	7.80	38.10	85.10	9.63	37.40	7.28	1.43	6.61	1.09	6.22	1.20	3.20	0.50	3.15	0.47
CPM-4-V	72.20	3.80	61.00	16.90	4.80	8.20	47.80	89.90	11.25	44.10	8.95	1.76	8.88	1.48	8.75	1.65	4.75	0.67	4.27	0.67
LR-28-A	59.40	2.40	52.00	16.30	0.60	6.60	39.90	82.00	9.84	37.40	7.69	1.56	7.42	1.24	7.36	1.37	4.08	0.60	3.70	0.55
LR-54D	43.90	5.70	47.00	14.10	0.90	6.10	36.20	75.70	8.58	33.50	6.49	1.28	6.17	1.05	5.88	1.14	3.18	0.47	3.04	0.45
IT-01A	66.50	3.10	59.00	19.80	1.00	7.70	45.40	89.50	10.51	41.10	8.48	1.63	7.96	1.23	7.17	1.45	4.00	0.57	3.61	0.53
Jade 12	51.00	5.50	47.00	17.70	0.90	7.40	44.30	87.20	10.61	39.90	8.32	1.62	7.60	1.27	7.31	1.49	3.86	0.59	3.71	0.55
SM-54	56.10	3.60	42.00	18.00	0.60	8.50	38.70	80.20	9.37	37.00	7.41	1.50	7.37	1.11	6.62	1.31	3.90	0.56	3.46	0.52
CPM-2-V	54.60	3.90	54.00	17.70	1.00	7.70	46.90	91.90	10.96	41.50	8.50	1.72	8.64	1.39	8.37	1.67	4.83	0.70	4.58	0.70
GA-37	-	0.80	-	16.60	-	8.30	36.20	80.60	9.09	35.00	7.20	1.41	6.69	1.11	6.33	1.21	3.41	0.51	3.36	0.51
LR-54C	80.70	7.10	62.00	15.70	2.80	7.40	41.30	83.90	9.88	36.70	7.63	1.55	7.02	1.16	7.11	1.31	3.69	0.57	3.35	0.50
LR-33-B	62.30	1.40	38.00	18.60	0.40	10.60	39.70	81.80	9.99	39.70	8.25	1.58	7.49	1.26	7.06	1.38	3.91	0.59	3.84	0.54
LR-53B	39.20	4.60	51.00	15.80	0.50	7.10	40.90	79.20	9.68	36.60	7.43	1.50	7.20	1.13	6.43	1.28	3.66	0.52	3.31	0.50
SG35-A	53.30	2.30	63.00	17.80	1.30	6.10	43.80	92.70	10.48	41.00	8.19	1.58	7.80	1.23	7.05	1.33	4.02	0.58	3.75	0.55
LR-29-A	49.30	2.50	50.00	16.90	0.40	8.10	42.10	84.00	10.63	40.70	8.37	1.87	8.39	1.42	8.38	1.62	4.69	0.68	3.96	0.61
GA-35B	-	1.90	-	16.30	-	7.20	47.60	106.30	13.49	58.90	12.93	2.98	15.40	2.58	15.45	3.32	9.65	1.46	9.48	1.42

	Cu	Pb	Zn	Ga	Mo	Cs	La	Ce	Pr	Nd	Sm	Eu	Gd	Tb	Dy	Ho	Er	Tm	Yb	Lu
Amostra	**0.1**	**0.1**	**0.1**	**0.5**	**0.1**	**0.1**	**0.1**	**0.1**	**0.02**	**0.3**	**0.05**	**0.02**	**0.05**	**0.01**	**0.05**	**0.02**	**0.03**	**0.01**	**0.05**	**0.01**
SM-16A	73.10	3.80	81.00	15.20	2.60	7.00	37.50	72.50	9.10	34.80	7.54	1.64	8.23	1.32	7.86	1.52	4.22	0.63	3.76	0.57
LR-32-A	79.20	3.00	49.00	18.10	0.70	6.20	39.90	83.90	10.26	40.10	8.50	1.59	7.46	1.27	7.09	1.36	3.79	0.57	3.71	0.53
LBC-53	62.30	2.50	48.00	18.10	0.60	8.60	63.90	117.10	16.23	66.40	13.37	2.71	12.40	1.99	10.48	2.12	5.57	0.86	5.34	0.79
LBC-61	15.20	7.50	17.00	18.30	0.20	10.10	45.50	93.30	10.82	36.80	8.85	1.66	7.78	1.32	7.49	1.45	4.01	0.62	3.97	0.56
SM-16B	39.80	10.30	54.00	16.60	0.10	10.90	38.40	78.60	9.29	35.60	7.59	1.58	7.83	1.29	7.33	1.40	4.04	0.58	3.69	0.59
LBC-32C	55.00	7.30	57.00	20.40	1.10	4.70	45.30	92.90	10.83	39.90	8.39	1.59	7.74	1.38	7.40	1.52	4.22	0.62	4.06	0.60
GA-03V	-	4.40	-	19.20	-	7.80	48.10	94.10	11.91	46.80	9.56	1.88	10.43	1.72	10.01	2.13	6.29	0.91	5.71	0.88
LBC-32B	55.20	5.00	60.00	18.80	1.20	6.60	46.90	97.00	11.23	43.10	8.52	1.73	7.85	1.34	8.11	1.53	4.30	0.61	3.91	0.58
GA-34	-	2.60	-	18.10	-	6.40	39.90	86.90	9.67	36.80	7.76	1.61	7.59	1.26	7.16	1.45	4.05	0.60	3.76	0.57
SM-50	52.50	2.90	44.00	18.50	1.00	8.70	45.40	94.30	10.50	41.60	8.12	1.69	7.59	1.18	7.00	1.29	3.58	0.54	3.22	0.51
SM-27	67.70	3.00	45.00	16.00	0.70	5.70	37.90	77.60	9.36	35.90	7.40	1.47	7.31	1.18	6.77	1.32	3.76	0.55	3.46	0.52
LBC-17*	22.30	4.30	84.00	19.30	1.00	7.50	57.80	106.30	14.88	57.20	11.64	2.35	10.56	1.73	9.94	1.87	5.49	0.81	4.80	0.70
SM-51	72.40	3.20	71.00	17.10	3.30	6.30	38.30	77.80	9.68	41.00	8.75	1.99	9.91	1.53	9.32	1.94	5.59	0.82	5.41	0.84
LBC-50*	85.00	3.50	62.00	17.80	0.60	10.30	74.20	137.20	22.02	99.80	22.47	5.29	25.73	4.21	25.39	5.16	14.90	2.15	13.07	1.92
LBC-49	95.50	3.80	56.00	17.20	0.70	4.70	45.30	90.50	10.56	41.10	8.51	1.76	8.10	1.38	7.71	1.52	4.54	0.69	4.39	0.63
LBC-40	100.10	2.20	58.00	17.60	0.90	5.70	39.90	84.40	9.94	36.50	8.08	1.74	7.58	1.28	7.91	1.43	4.00	0.60	4.31	0.56
LBC-51	184.1	1.1	49	18.2	0.5	0.5	13.1	27.3	3.62	14.9	3.94	1.33	5.04	0.89	5.43	1.15	3.55	0.49	3.25	0.49
LBC-39	161.7	0.9	45	17.8	0.4	0.8	10.2	21.9	2.92	14.2	3.62	1.22	4.15	0.77	5.00	0.99	2.67	0.42	2.62	0.40
LBC-38		3.6					42.3	59.9	9.61	37.6	8.32	2.36	9.68	1.71	10.92	2.1	6.59	0.93	5.88	0.9
LBC-52		1.5					22.7	48	5.94	25.5	5.88	1.75	6.55	1.13	7.33	1.45	4.24	0.54	3.73	0.56
SG-97Q	229.10	1.40	75.00	24.60	0.70	0.50	33.50	72.10	8.93	38.60	8.29	2.61	8.53	1.27	7.41	1.49	4.02	0.54	3.51	0.52
SG-98Q	272.60	1.00	52.00	21.40	0.20	0.40	23.90	49.20	6.17	25.40	5.73	1.82	6.47	1.07	6.34	1.35	3.89	0.54	3.60	0.55
SM-37	186.60	1.20	68.00	16.70	1.30	0.80	23.30	47.40	6.11	26.10	5.58	1.74	5.85	0.91	5.32	1.06	2.96	0.40	2.54	0.38
LBC-55	159.70	1.40	66.00	18.30	0.50	0.40	18.70	37.60	4.80	20.50	4.87	1.53	5.58	0.99	5.60	1.20	3.65	0.51	3.48	0.48
IT-2-DQ	176.40	1.30	65.00	21.10	0.70	1.60	22.80	48.80	5.92	25.40	5.86	1.65	6.41	1.02	6.51	1.30	3.81	0.54	3.51	0.52
LR-38-B	131.90	4.80	43.00	19.90	0.40	2.80	21.90	44.50	5.31	22.60	4.86	1.45	5.29	0.87	5.32	1.00	3.01	0.44	2.70	0.39
LR-50	143.50	1.80	69.00	16.20	1.30	0.70	16.40	33.50	4.36	19.20	4.26	1.39	5.37	0.88	5.28	1.04	3.03	0.45	2.79	0.43
Bas-106	167.30	3.30	43.00	15.70	2.00	<0.1	15.00	30.40	3.77	15.70	3.35	1.02	3.42	0.56	3.68	0.68	1.92	0.28	1.88	0.28
SG-13a	114.40	2.10	47.00	18.90	1.20	1.80	20.20	41.10	4.84	20.10	4.74	1.25	4.80	0.80	4.70	0.88	2.51	0.38	2.36	0.35
Bas-105	160.00	4.80	83.00	19.80	0.60	1.70	28.30	53.30	7.39	30.50	6.99	1.92	7.35	1.20	7.04	1.38	3.71	0.56	3.51	0.51

Amostra	Rb	Sr	$^{87}Sr/^{86}Sr_m$	Rb/Sr*	$^{87}Sr/^{86}Sr_{134Ma}$	Sm	Nd	$^{143}Nd/^{144}Nd_m$	$^{147}Sm/^{144}Nd$*	$^{143}Nd/^{144}Nd_{134Ma}$	εNd_{134Ma}	$^{208}Pb/^{204}Pb$	$^{207}Pb/^{204}Pb$	$^{206}Pb/^{204}Pb$
LBC.50	167.2	226.7	0.72181	4.41564	0.71365	8.1	41.6	0.51222	0.13596	0.51210	-7.17	38.94362	15.71638	19.12518
LBC.17	163.9	151.2	0.72560	3.14349	0.71979	11.6	57.2	0.51214	0.12288	0.51203	-8.51	38.89893	15.70337	18.96352
SG.4	244.6	77.4	0.73820	9.17560	0.72125	20.1	84.2	0.51216	0.14408	0.51204	-8.49	38.92401	15.70580	19.09352
SG.16	268.7	82.2	0.73899	9.49178	0.72145	8.3	40.9	0.51215	0.12269	0.51204	-8.37	38.91437	15.70957	19.07524
LR.48	27.3	225.3	0.70998	0.35067	0.70933	3.8	16.6	0.51226	0.13642	0.51214	-6.41	39.03660	15.69588	18.63880
BR.5A	17.7	204.8	0.71052	0.25012	0.71006	2.8	12.9	0.51233	0.13248	0.51221	-5.02	38.90470	15.66670	18.60810
SM.58	34.3	214.7	0.71016	0.46234	0.70930	3.7	15.8	0.51234	0.13951	0.51222	-4.90	38.86557	15.65834	18.68140
SG.26	75.4	217	0.71122	1.00556	0.70936	6.5	27.8	0.51238	0.14185	0.51226	-4.12	38.79878	15.69156	18.86359
SG.8B	69	238.8	0.70993	0.83621	0.70838	5.6	23.2	0.51229	0.14629	0.51216	-5.97	39.03008	15.70366	18.70877
BR.10	96.9	239.5	0.71882	1.17089	0.71665	6.5	31.6	0.51210	0.12402	0.51199	-9.37	39.00073	15.71680	18.90043
LR.18B	79.9	214.5	0.71448	1.07800	0.71249	6.5	29.6	0.51223	0.13302	0.51212	-6.87	39.00234	15.69370	18.75605
LR.16	79.4	133.2	0.71465	1.72510	0.71146	4.9	21.8	0.51230	0.13463	0.51218	-5.66	38.97710	15.70560	18.81355
BR.15	81.5	221.6	0.71179	1.06451	0.70983	4.5	19.4	0.51218	0.14039	0.51206	-8.02	38.90000	15.65600	18.44300
SM.29	70.1	161.8	0.71324	1.25383	0.71092	6.3	27.2	0.51234	0.14076	0.51222	-4.93	38.89130	15.67860	18.82556
LBC.51	20.8	187.1	0.70707	0.32180	0.70648	3.9	14.9	0.51239	0.15969	0.51225	-4.26	38.58596	15.56183	18.18771
LBC.39	31.3	196.9	0.70678	0.46013	0.70593	3.6	14.2	0.51250	0.15396	0.51237	-2.06	-	-	-

ANEXO I
Título da Dissertação/Tese:
" LITOESTRATIGRAFIA E GEOQUÍMICA DA PROVINCIA ÍGNEA DO PARANÁ-ETENDEKA E CARACTERIZAÇÃO DOS ASPECTOS PETROFÍSICOS DE SEQUÊNCIAS VULCANO-SEDIMENTARES)"
Área de Concentração: Geoquímica
Autor: **Lucas de Magalhães May Rossetti**
Orientador: Prof. Dr. Evandro Fernandes de Lima
Examinadora: Profa. Dra. Isabela de Oliveira Carmo
Data: 31/07/18
Conceito: A (Excelente)
PARECER:
Conforme documento em anexo.

Isabela de O. Carmo

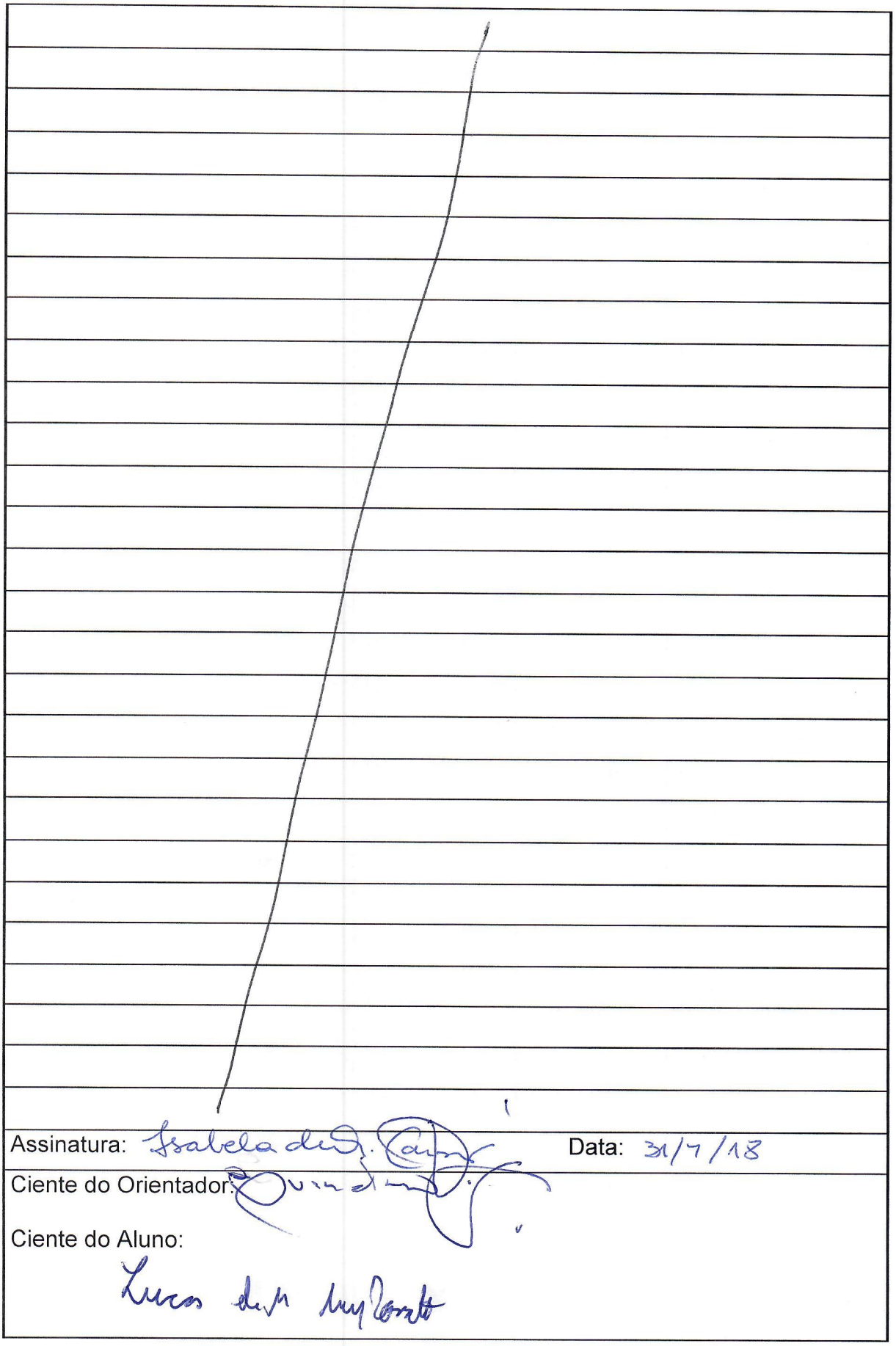

Assinatura: Isabela dos S. Cardoso Data: 31/7/18

Ciente do Orientador:

Ciente do Aluno:

Lucas dos Santos

ANEXO I

Título da Dissertação/Tese:

" *LITOESTRATIGRAFIA E GEOQUÍMICA DA PROVINCIA ÍGNEA DO PARANÁ-ETENDEKA E CARACTERIZAÇÃO DOS ASPECTOS PETROFÍSICOS DE SEQUÊNCIAS VULCANO-SEDIMENTARES* "

Área de Concentração: Geoquímica

Autor: **Lucas De Magalhães Mayrossetti**

Orientador: Prof. Dr. Evandro Fernandes de Lima

Examinador: Prof. Dr. Valdecir de Assis Janasi

Data: 31/07/2018

Conceito: A (EXCELENTE)

PARECER:

A Tese aborda diversos aspectos relacionados ao vulcanismo da Província Magmática Paraná na região da calha de Torres: (1) estratigrafia, baseada em levantamentos estruturais de campo e geoquímica; (2) propriedades petrofísicas através de medidas de laboratório de porosidade, permeabilidade e velocidades acústicas ultrassônicas, e (3) petrofísica com base em geoquímica de rochas e minerais. Todos os aspectos são abordados com extrema finalidade, utilizando métodos modernos e alcançando importantes bem fundamentados a muitas frentes de grande relevância. ~~Para~~ Cumpre destacar a proposta fazendo de divisão do Grupo Serra Geral em 4 formações, já publicada em revista internacional de alto impacto, e que tem, desde então, contribuído uma referência essencial e um estímulo para toda a comunidade científica em prender o desafio de construir uma coluna estratigráfica para a província em toda a sua extensão no Brasil.

Também merece destaque a abordagem petrofísica abordando os processos de evolução em subsuperfície em um sistema de alimentação até complexo utilizando modelamento geofísico e geotermobarometria e, adicionalmente, inferindo as condições de fonte dos magmas no manto, a partir de modelagens

termodinâmica moderna, alcançando resultados bem sustentados. Com consequências importantes para a evolução tectônica da província.

Os dados de química mineral utilizados para os cálculos termobarométricos não foram incorporados, e deverão ser acessados como anexo do terceiro artigo, quando publicado.

Assinatura: [signature] Data: 31/07/2018

Ciente do Orientador: [signature]

Ciente do Aluno: [signature]

Defesa de Tese de Doutorado
Lucas de Magalhães May Rossetti (UFRGS)
31/7/2018 (14 h, UFRGS)
Orientador: Evandro F. Lima

Titulo: LITOESTRATIGRAFIA E GEOQUÍMICA DA PROVINCIA ÍGNEA DO PARANÁ-ETENDEKA E CARACTERIZAÇÃO DOS ASPECTOS PETROFÍSICOS DE SEQUÊNCIAS VULCANO-SEDIMENTARES

Generalidades e Formatacao:

- Tese muito bem escrita, praticamente não ocorrem erros ortográficos ou de digitação, gramaticais ou semânticos.
- Parabens pela consolidacao dos resultados em 3 artigos (1 publicado e 2 submetidos), em temas variados e que se complementam.
- Eh claro que o trabalho ainda pode gerar mais artigos, visto a demonstracao de visao critica do Lucas (qualidade bastante louvavel do candidato, demonstrada durante
    - 4o artigo = "Anatomia de provincias basalticas continentais"
    - 5o artigo = Petrogenese de provincias basalticas continentais em diferentes continentes/contextos geotectonicos
- Otima escolha das figuras (fora dos artigos), boas qualidades de edicao e grafica; no entanto, algumas figuras (com fotos) parecem escuras. E faltaram algumas figuras e tabelas/quadros mostrados na apresentacao.
- Erros de formatacao – se possivel, rever e corrigir (anotados na minha versao impressa)
    - Versao impressa e em PDF com problemas na numeracao das figuras;
    - Citacao bibliografica (&, e, and);
    - Palavras em italico (pahoehoe, aa, rubbly, onshore, offshore etc.);
    - Escrever siglas por extenso (ex., SCLM, AFC) quando aparecem pela primeira vez (mesmo no resumo e *abstract*);
    - Sumario (identacoes);
    - Anexos – colocar a referencia complete dos artigos;
    - Fig. 3 citada como Fig. 4 (p.9);
    - Repeticao de paragrafos (ver partes riscadas no meu volume);
    - Algumas citacoes no texto nao tem o ano;
    - Referencias bibliograficas
        - nome das revistas COM e SEM abreviacoes, ver pequenos erros marcados no meu volume.
        - Falta Murata et al. (1986)

- Descricao dos metodos petrofisicos sao mais detalhados que os geoquimicos.
- Ponto fraco, que deve ser melhor elaborado - item "hipotese" – nao parece uma hipotese, mas uma afirmacao. Apresentar a(s) hipotese(s) (cada artigo/tema pode ter a sua) e informar como o estudo desenvolvido na tese/artigos vai testa-las.
    - Artigo 2 – ex., sabe-se que derrames de lavas X e Y sao compostos por facies porosas e nao porosas e, portanto, as facies porosas tem potencial para ser reservatorios se a porosidade for > XX%. Medidas de porosidade e permeabilidades em diferentes facies de diferentes tipos de derrames devem indicar se as facies primarias (crostas brechadas e porosas) sao as mais promissoras para ser reservatorio; se derrames X ou Y, que tem maior volume de facies porosas devem ser os melhores reservatorios, etc. Os processos de alteracao podem afetar as porosidades primarias positivamente (precipitacao de cimento) e negativamente (dissolucao). Medidas de porosidade/permeabilidade(?) devem diminuir em basaltos alterados.

Artigo 1 (Litoestratigrafia):

- *Interbeds* → sao marcos estratigraficos? Cada unidade litoestratigrafica tem seu padrao de *interbeds*? Se ha diferenca de padrao de uma unidade para outra, qual o significado (imposicao do sistema vulcanico? mudancas ambientais/climaticas?)
- Existem relacoes laterais entre as litounidades ?
- O quadro com espessuras totais e dos depositos unitarios, mostrado na apresentacao, eh importante! Poderia mostrar na tese brasileira tambem. Ou em um futuro artigo sobre a "anatomia" de provincias basalticas.
- Com qual outra LIP a anatomia do vulcanismo na calha de Torres se assemelha?
- Qual a expectativa de estender a estratigrafia reconhecida na calha de Torres para as porcoes centro e norte da Prov. PR? Qual a carencia de dados?
- Como eh possivel fazer a predicao de facies e extrapolar para as bacias onde dados sao indiretos e escassos.
- Qual a relacao da estratigrafica proposta com a paleomagnetoestratigrafia e a geocronologia radioisotopica disponivel? Como voce avalia os dois modelos cronologicos sugeridos para a provincial, S para N (Renne e colaboradores) e N para S (Turner et al., Stewart et al.)
- Com base no padrao de derrames (lavas compostas, simples, etc., suas espessuras individuais e total) eh possivel, por correlacao com exemplos magmaticos ativos, estimar o tempo de formacao de pilhas de diferentes derrames? (como eh feito com as taxas de sedimentacao?)
- Sao citadas referencias diferentes (de artigo para artigo) para a informacao de variação de idades obtidas para a provincia (usar as mesmas referencias e as referencias que definiram estas idades, de preferencia com significado estratigrafico e geografico.

Artigo 2 (Petrofisica):

- As melhores facies reservatorio sao as rochas sedimentares, mas parte delas esta cimentada (silicificada) – as vulcanicas tem algum papel neste processo? Quais as evidencias? Entao as vulcanicas atuaram negativamente na preservacao do sistema poroso?
- Como as rochas vulcanicas, mesmo as facies muito porosas , podem ser bons reservatorios, se as permeabilidades sao muito baixas? Esta afirmacao eh recorrente, mas nao ha uma discussao mais profunda sobre as evidencias de outros elementos que contribuam para a permeabilidade nas unidades vulcanicas.
- Como voce ve a permeabilidade em meso e macro escala?
- Existem zonas estratigraficamente mais ou menos alteradas?
- Qual o controle das zonas de alteracao?
- Nao destacou os metodos usados para caracterizacao petrográfica (microscopia otica?)
- Soterramento – quanto de soterramento existiu nestes basaltos?
- Diagenese x alteracao hidrotermal → isto foi diferenciado? Sao processos precoces (concomitante a atividade vulcanica) ou tardios (>10 Ma)
- Seria interessante um maior detalhamento dos processos de alteracao (diagenese? Alteracao hidrotermal?) (sequencia relativa)
    - Figura com a sequencia de alteracao
    - Quadro com avaliacao das acoes positivas e negativas dos (diferentes) processos ou produtos de alteracao na porosidade

Artigo 3 (Geoquimica):

- Abordagem inovadora, inedita. Importantes informações para estudos e discussoes de modelos geotectonicos.
- Diferentes fontes e diferentes formas de ascencao (mais ou menos polibarica?) → quais as implicacoes para a evolucao tectonica?
- Qual a diferenca para a estratigrafia proposta por Peate? E por Licht (2018)?
- A figura/modelo apresentada com grupos geoquimicos dentro da litoestratigrafia proposta eh fundamental para mostrar a ambiguidade da estratigrafia quimica.

Porto Alegre, 31/7/2018

Isabela O. Carmo

ANEXO I
Título da Dissertação/Tese:
" LITOESTRATIGRAFIA E GEOQUÍMICA DA PROVINCIA ÍGNEA DO PARANÁ-ETENDEKA E CARACTERIZAÇÃO DOS ASPECTOS PETROFÍSICOS DE SEQUÊNCIAS VULCANO-SEDIMENTARES)"
Área de Concentração: Geoquímica
Autor: **Lucas de Magalhães May Rossetti**
Orientador: Prof. Dr. Evandro Fernandes de Lima
Examinador: Prof. Dr. Lauro Valentim Stoll Nardi
Data:
Conceito: A
PARECER:
EM ANEXO

ANEXO I

Título da Tese: **LITOESTRATIGRAFIA E GEOQUÍMICA DA PROVINCIA ÍGNEA DO PARANÁ-ETENDEKA E CARACTERIZAÇÃO DOS ASPECTOS PETROFÍSICOS DE SEQUÊNCIAS VULCANO-SEDIMENTARES**

Área de Concentração: Geoquímica
Autor: **Lucas de Magalhães May Rossetti**
Orientador: Prof. Dr. Evandro Fernandes de Lima
Examinador: Prof. Lauro Valentim Stoll Nardi
Data: 31/07/2018
Conceito: **A**

PARECER

A tese aborda tema de grande relevância científica e tecnológica, com aplicações na exploração de óleo e gás e no estudo de aqüiferos. Capítulos introdutórios muito bem escritos e consistentes. Excelentes ilustrações - esquemas, fotos, diagramas no capítulo do Estado da Arte, e no trabalho como um todo. Os três artigos são de ótimo nível e constituirão, sem dúvida, uma excelente contribuição científica e tecnológica. As anotações a seguir, concentradas no terceiro artigo por este estar submetido e ser de minha área de conhecimento, tem em vista apenas à contribuir com o andamento das publicações.

Correções e comentários

p. 45 ponto decimal em vez de vírgula?
p.142 pequenos erros: faltou a palavra Province, "upper portions of stratigraphy" - a estratigrafia não tem upper portions, a coluna estratigráfica sim. Occurs.
p. 56 Chama a atenção a queda abrupta de Ti e Fe nas rochas acidas ou com MgO< 2%. Qual a explicação? Seria uma origem independente?
Na verdade as rochas com menos de 2% de MgO (> 63% SiO2) parecem não ser comagmáticas, talvez produtos de fusãp crustal ou líquidos com muita ssimilaçào de fusões crustais.
A Fm Torres sem enriquecimento em Fe talvez represente líquidos contaminados.
artigo 1 - p. 111 O que é "low aspect ratio"?

Artigo III

p. 150 - A presença de magnetita e Ti-magnetita indica magmas muito oxidados, o que é mais comum no magmatismo cálcio alcalino. O que explicaria isto neste caso?
p. 153 - o que são os valores entre parênteses?
Group 3 lavas?
p. 156 - 2.5mm is what?
p. 157 - frase incompleta: variations of 2 to 6 wt.% Vale do Sol and have Ni and Cr concentrations
p. 158 - c. 20 higher = 20 times higher
p. 160 - Plagioclase is labradorite and shows just minor chemical variations from core to rims, with anorthite ranging from 55 to 60 (Fig.2C). All phenocrysts are within

equilibrium conditions with whole rock compositions. Labradorita está em equilíbrio com composições dacíticas e riolíticas?
p. 160 - Al/(Na+K) > 1 and Al/(Ca+Na+K) < 1 (following the Shand index). Qual a unidade, átomo grama? O usual é móis dos óxidos!
p. 162 - has or shows compositions . O que são os valores entre parênteses?
p. 164 - composition of the source rock or of the parental magma?
these inputs could be in the mantle source by a previous subdcuction or delamination!
p. 171 - Quais seriam estas evidências em líquidos com MgO próximo de 9%?
p. 175 - Boa discussão de fontes com base em isótopos. Razões entre elementos traços - Zr, Nb, Th, Yb - tem sido utolizadas para investigação de fontes (Weaver 1991, Pearce 2008, Condie 2015).
p. 177 - falta o D na legenda da figura.
p. 179 - Para este tipo de modelamento eu retiraria as amostras do Palmas, *por* representarem líquidos ácidos com comportamento diverso (fig 12 D) dos magmas básicos e intermediários.
p. 185 - in general [La/Yb]N is greater than .... em vez de >.
p. 189 - As rochas do Palmas não foram discutidas, parecem ter sido simplesmente esquecidas depois dos capítulos inicias.

Sobre o Palmas:
Embora não seja tema central dos artigos anexados, os dacitos e riolitos (Fm. Palmas) tem alto Fe/Mg e Na2O + K2O é em torno de 7-8, assemelhando-se aos termos menos diferenciados. O Ti e Fe mostram comportamento distinto dos termos menos diferenciados, mas os elementos traços (Ba, Sr, Nb, Y, ...) mostram comportamento coerente. Nb (15-25) cresce com a diferenciação, Zr (200-350) também cresce.
Os padrões de ETR do Palmas mostram LaN c. 200-300 e YbN 20-35. Anomalias negativas de Eu. Correspondem a rochas do tipo A pelo critério de elementos traços, ferroan, Y/Nb c. 2 isto é, Eby 2006: A2 = tipo A da série toleítica pós-colisional. Magmas graníticos com essas características seriam descritos como diferenciados toleíticos por vários autores (Frost, Carol; Nardi 2016).

Concluímos pela aprovação com conceito máximo (A).

Assinatura: 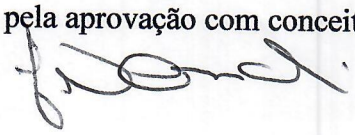 Porto Alegre, 31 de julho de 2018

Ciente do Orientador:

Ciente do Aluno: